TRANSIENT NATURAL CONVECTION OF FLUIDS WITHIN VERTICAL CYLINDERS

by

Elisabeth M. Drake

S.B., Massachusetts Institute of Technology
(1958)

Submitted in Partial Fulfillment

of the Requirements for the

Degree of Doctor of Science

at the

MASSACHUSETTS INSTITUTE OF TECHNOLOGY

May, 1966

Signature of Author: _____

Department of Chemical Engineering, May 13, 1966

Certified by: _____

_____

Thesis Supervisors

Accepted by: _____

Chairman, Departmental Committee on Graduate Theses

TRANSIENT NATURAL CONVECTION OF FLUIDS WITHIN VERTICAL CYLINDERS

by

Elisabeth M. Drake

Submitted to the Department of Chemical Engineering on May 13, 1966, in partial fulfillment of the requirements for the degree of Doctor of Science.

ABSTRACT

Transient natural convection temperature fields and circulation patterns were investigated experimentally for fluids contained in vertical cylindrical tanks and subjected to a uniform wall heat flux. Evaluation of the data, which were obtained for a wide range of conditions,

Prandtl Number $\left(Pr = \frac{\nu}{\alpha}\right)$: 2 to 8000

Grashof Number $\left(Gr = \frac{g\beta(T_w - T_o)L^3}{\nu^2}\right)$: 10^3 to 10^{11} (laminar and turbulent flow regimes)

Aspect ratio $\left(\frac{L}{D}\right)$: 1 to 3

Fourier number $\left(\frac{\alpha t}{ID}\right)$: 0.0002 to 0.08,

led to development of a useful theoretical model for the system.

An 8-in. diameter, Pyrex cylinder, coated with a transparent, electrically-conductive film to permit uniform wall heat generation by resistance heating, was sealed between two insulated end flanges to form the basic experimental enclosure. Temperature data from an internal network of thermocouples and dye tracer observations indicated that the system could be divided into three regions for purposes of analysis: a thin boundary layer region rising along the heated walls, a mixing region located in about the top 10% of the system where the boundary layer is discharged and mixed with upper core fluid, and a main core region with no radial temperature gradients. After an initial period, defined as the time required for the first warm fluid to reach the bottom of the vessel, the axial temperature in the main core was observed to be nearly linear in height. Consequently, a boundary layer analysis was made for the case in which temperature at the outer edge of the boundary layer varies linearly with height. The solution indicated that, for a given outer edge temperature gradient, a limiting value of boundary layer energy and momentum occurred. A theoretical model to describe the transient temperature distributions within the enclosure was developed, based on the analytical expression for the limiting boundary layer energy, an energy balance around the mixing region and a radially-mixed, plug flow model for the main core. The model predicts that:

1. The core temperature is a linear function of axial distance, x, with a constant gradient which varies as:

$$\underline{\text{laminar}} \quad \frac{k}{q}\frac{dT}{dx} = 4(Fo)^{4/9}/(RaNu)^{1/9}$$

$$\underline{\text{turbulent}} \quad \frac{k}{q}\frac{dT}{dx} = 11.5(Pr)^{7/45}(Fo)^{8/15}/(RaNu)^{2/15}$$

$$\text{where } RaNu = \frac{g\beta q L^4}{k\nu^2}$$

2. The temperature of the core fluid at the midplane of the cylinder is equal to the mixed mean fluid temperature.

Experimental data agreed closely with this model, except during an initial period when the core temperature is not a linear function of axial distance. A method is presented for computing the temperature distribution during this period by means of an iterative technique. Initial temperature distributions may also be estimated from curves representing the experimental data in which dimensionless temperature is presented as a function of dimensionless time and height.

Methods for extending the boundary layer model analysis to constant wall temperature systems and to systems with cooling at the walls are indicated. Also, it is shown analytically that the dependence of the Nusselt number on the Rayleigh number for laminar flow changes from a 1/4-power to a 1/3-power relationship in the presence of a constant core temperature gradient.

Thesis Supervisors: Robert C. Reid , Lawrence B. Evans
Titles: Prof. of Chem. Eng., Asst. Prof. of Chem. Eng.

Department of Chemical Engineering
Massachusetts Institute of Technology
Cambridge 39, Massachusetts
May 13, 1966

Professor William Greene
Secretary of the Faculty
Massachusetts Institute of Technology
Cambridge 39, Massachusetts

Dear Professor Greene:

In accordance with the regulations of the Faculty, I herewith submit a thesis, entitled "Transient Natural Convection of Fluids within Vertical Cylinders", in partial fulfillment of the requirements for the degree of Doctor of Science in Chemical Engineering at the Massachusetts Institute of Technology.

Respectfully submitted,

Elisabeth M. Drake

cc: Harold L. Hazen, Dean of the Graduate School
Robert C. Reid, Professor of Chemical Engineering
Lawrence B. Evans, Assistant Professor of Chemical Engineering
Glenn C. Williams, Professor of Chemical Engineering and
Chairman, Department Committee on Graduate Students

ACKNOWLEDGEMENT

The author sincerely appreciates the guidance and encouragement given generously throughout the course of this project by both Professor Robert C. Reid and Professor Lawrence B. Evans.

In addition, special thanks go to:

Professor Kenneth A. Smith for suggesting the use of the von Kármán-Pohlhausen analytical technique,

The Sloan Basic Research Program for providing funds for experimental equipment and materials,

The National Science Foundation for fellowship aid during most of the program and The Sun Oil Company for a Summer Term scholarship,

The Computation Center of the Massachusetts Institute of Technology for its donation of services and IBM 7094 computer time,

Mr. Schuyler M. Holbrook for many helpful suggestions during the design and fabrication of experimental apparatus.

TABLE OF CONTENTS

Page

LIST OF FIGURES

Page

Page

Page

LIST OF TABLES

I. SUMMARY

A. Background

This study was directed toward obtaining an improved quantitative understanding of transient natural convection within enclosed fluids. Such phenomena play an important role in a number of diverse engineering applications, including thermal stratification of cryogenic fluids, emergency cooling of nuclear reactors, and heating of buildings or storage vessels filled with fluid on hot days.

The specific system selected for study consists of a vertical cylindrical tank, partially filled with liquid, as shown in Figure 1-1. Initially the fluid is isothermal and motionless. At some specified time, a uniform constant heat flux, q_w, is suddenly imposed at the side walls. The resulting natural convection circulations are completely characterized by the transient temperature and velocity fields within the fluid. These fields depend on the fluid properties, the body force field (gravity, in most cases, but any body force field, e.g. centrifugal, may be considered), the system geometry and the manner in which heat is supplied to the fluid boundaries.

The constant wall heat flux case, which is studied in detail in this work, is often encountered for tanks of stored liquids in which heat transfer from the surroundings is limited by the outside heat transfer coefficient and the temperature difference between the surroundings and the wall is large relative to internal fluid temperature variations. The constant wall heat flux case is often encountered in the storage of cryogenic fluids. A constant wall temperature, on the other hand, is a common thermal boundary condition for systems in isothermal environments with high outside heat transfer coefficients. Since heat transfer

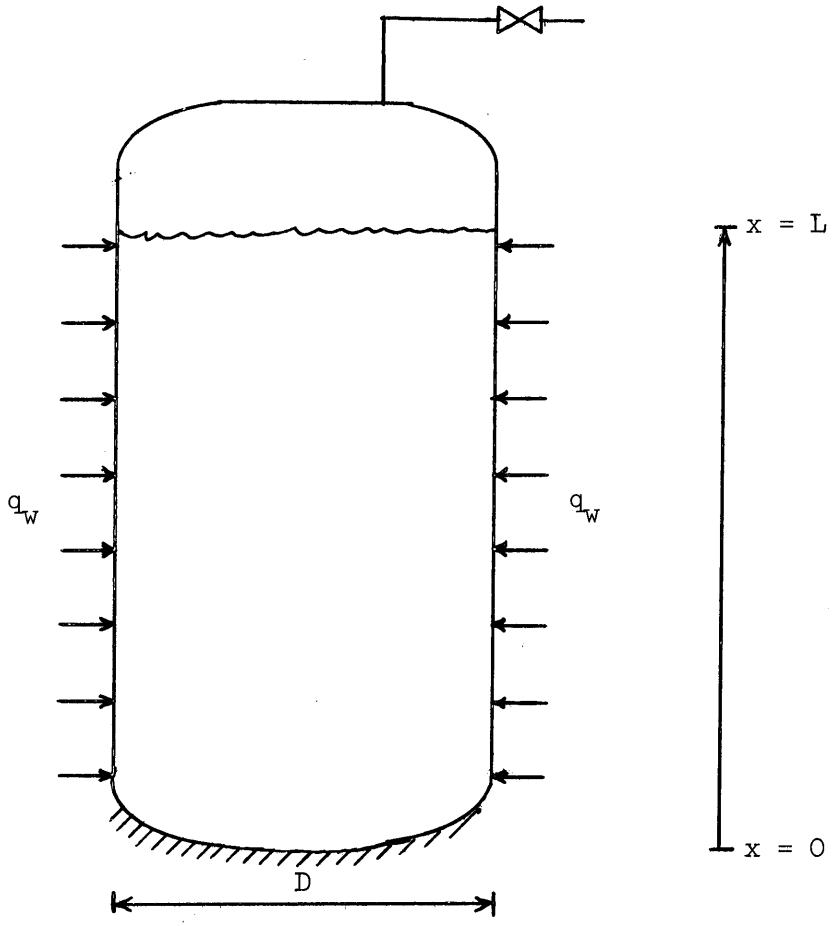

FIGURE 1-1

A Sketch of the System

through the bottom of vertical storage tanks is, in many cases, very much less than that through the sidewalls, bottom heating was considered negligible for the purposes of this study.

A group of dimensionless parameters, which are important in transient natural convection systems, may be found by the techniques of dimensional analysis (54) or by consideration of the dimensionless form of the partial differential equations describing the system behavior. These groups are:

$$\text{Gr, Grashof Number} = \frac{g\beta(T_w - T_o)L^3}{\nu^2}$$

$$\text{Pr, Prandtl Number} = \frac{\nu}{a}$$

$$\text{Nu, Nusselt Number} = \frac{hL}{k} \qquad (1\text{-}1)$$

$$\text{Fo, Fourier Number} = \frac{at}{ID}$$

Geometric Factors ($\frac{L}{D}$, for example, for a vertical, cylindrical enclosure)

In problems for which wall heat flux, q_w, is specified rather than wall temperature, T_w, the value of the Grashof number is not known directly. For these systems a modified Grashof number may be used, which is

$$\text{GrNu} = \frac{g\beta(T_w - T_o)L^3}{\nu^2}\ \frac{hL}{k} = \frac{g\beta q_w L^4}{k\nu^2} \qquad (1\text{-}2)$$

In addition, the product of the Grashof and Prandtl numbers,

$$\text{Ra, Rayleigh Number} = (\text{Gr})(\text{Pr})$$

is significant as an index of natural convection intensity. The

Rayleigh number may be considered as a ratio between the product of the buoyant and inertial forces driving the flow and the viscous forces tending to retard the flow.

For a heated or cooled vertical flat plate in an isothermal medium, conduction predominates over convection below Rayleigh numbers of about 10^3. Between Rayleigh numbers of 10^3 and about 10^8 to 10^9, the natural convection flows are laminar. At still higher Rayleigh numbers, the convective flow near the plate becomes turbulent.

Although bulk average temperatures can be computed from an energy balance if the wall heat flux is known, this technique does not provide any idea of detailed internal temperature distributions. In the case of a vertical cylindrical tank, there has been no general reliable method for predicting temperature as a function of radius, height and time from known system parameters. As examples of systems requiring a detailed knowledge of natural convection temperature fields, one might include thermally stratified cryogenic propellant tanks, liquid-cooled nuclear reactors (in case of coolant pump failure), tanks of petroleum crude products kept from solidifying by wall heating, and systems in which boiling (freezing) is initiated at some local "hot" ("cold") spot. In addition, a knowledge of transient temperature distributions could lead to a better understanding of the general mechanisms controlling natural convection within enclosed fluids.

This thesis was therefore concerned with an analytical and experimental study of transient natural convection temperature fields. A detailed experimental study, including mapping of temperature fields and qualitative observation of flow patterns, was conducted for one special group of systems: liquids contained in vertical cylindrical tanks and

subjected to a constant side-wall heat flux. Heating levels, fluid properties and tank height-to-diameter ratio were varied; effects such as heat transfer at the bottom surface, vaporization at the upper liquid surface and boiling were minimized or eliminated. Evaluation of the experimental data for this particular case provided a basis for developing a useful system model. Theoretical analysis of the model then led to analytical techniques for correlating the data. The results can be extended with little difficulty to include systems with other thermal boundary conditions.

B. Prior Work

The most general theoretical approach for determining natural convection temperature and velocity distributions within enclosed fluids is to formulate and solve the three-dimensional partial differential equations for conservation of mass, energy and momentum for specified boundary conditions. Unfortunately, this approach leads to formidable mathematical problems and attempts to solve the equations by numerical techniques have met with only limited success as extremely large amounts of computation are required.

Intuitively, actual problems can often be reduced to two dimensions because of symmetry. Hellums (36), Wilkes (103), and Barakat (4) have obtained numerical solutions to the two-dimensional natural convection equations for certain limited cases. Hellums and Wilkes considered systems with one hot and one cold wall, and solved the transient equations to find the steady-state temperature and velocity distributions. Hellums found computation times in the order of an hour (IBM 704) were necessary to reach steady-state even for gases at very low Grashof numbers. At higher Grashof and Prandtl numbers, computation times would be in considerable excess of one hour. Wilkes' method, again applied at the Prandtl number for air, became unstable at Rayleigh numbers above 200,000.

Barakat considered a vertical heated cylinder filled with liquid and was able to achieve stable solutions at very much higher Rayleigh numbers. However, the required computation times were again very long and convergence was not achieved in regions where temperature and velocity gradients were steep, that is, near the walls, in the corners, and just below the upper liquid surface. Barakat (5) noted that compu-

tation times required to obtain an accurate and reasonably complete solution by this method would be exhorbitant on any present day computer. Noble (60) has recently made further improvements in numerical methods for treating two-dimensional natural convection problems, but the solution times for high Grashof number cases still appear excessive.

The complexity of the analytical problem has led to the formulation of several greatly simplified models for natural convection stratification phenomena, especially in relation to cryogenic tank systems. Bailey (3) has suggested a two-temperature level model for the central region of a vertical cylindrical tank. The lower region remains at the initial fluid temperature while the upper warm stratified layer gradually grows in depth as the energy of the system increases. The temperature level and the rate of growth of the warm upper layer is determined by use of the boundary layer equations for flow along an infinite, heated vertical plate in an infinite, isothermal fluid medium. His model does not correspond well to temperature data taken in cryogenic tanks which generally show linear axial temperature profiles and negligible radial temperature gradients. Neff (59) and Ruder (75) assume a model in which the axial temperature gradient is described by an error function dependence. Their model agrees better with data than the simpler model suggested by Bailey, but it is empirical and depends on knowledge of the surface temperature. For cryogens, the surface temperature is often the saturation temperature corresponding to the tank pressure level; in general, however, the surface temperature can not be accurately estimated. Both of these models are also limited to a rather short time in that they apply only to the period before the first warmed fluid has reached the bottom of the system.

Maahs (50) has made a thorough experimental study of the temperature fields for natural convection within horizontal cylinders subjected to a constant wall heat flux. An empirical correlation was developed for estimating transient heat transfer coefficients. Maahs also evaluated several finite difference schemes in an attempt to obtain a numerical solution to his problem, but concluded that computation times would be excessive without computers significantly faster than the IBM 709.

The classical boundary layer problem of natural convection flow along a heated (cooled) infinite vertical plate immersed in an infinite fluid medium has been treated extensively in the literature. Although the solutions for temperature and velocity fields near the plate in this classical case would be modified if, as would be expected for enclosed fluid systems, a non-uniform temperature were present outside the boundary, the boundary layer analytical techniques are valid for more complex cases. Laminar natural convection solutions for the classical problem have been obtained by Ostrach (65) and Sparrow and Gregg (96, 98) for various thermal boundary conditions at the wall. Turbulent flow along a constant temperature wall was analyzed by Eckert and Jackson (17).

C. Experimental

Natural convective flow was induced in a fluid contained in a vertical cylinder as a result of a constant wall heat flux. The experimental enclosure (Figure 1-2) consisted of an 8-in. diameter Pyrex cylinder held by tie rods between two gasketed-end flanges. A thin-film, transparent, electrically-conductive coating (E-C coating, Corning Glass Works) had been deposited on the outside of the cylinder to allow resistance heating of the walls while also permitting visual observation of flow tracers. The two-foot long cylinder was subdivided into three 8-in. long cylindrical sections by circumferential silver bands deposited over the E-C coating. Electrical contact to the heating film was made by copper straps fastened over the silver bands. Since each section could be heated independently, the system could be used to provide a constant wall heat flux to liquids at depths of 8-, 16-, and 24-in., i.e., $\frac{L}{D}$ ratios of 1 to 3 were possible. A Variac controller was used to vary the input power. Heating rates ranged from 20 to 2000 BTU/hr ft^2. The bottom and top of the vessel were insulated with glass wool. A free liquid surface was present in all tests. A surfactant film of stearic acid was used to retard surface vaporization when necessary.

The test fluids, glycerin, water, and an 85 weight per cent mixture of glycerin in water were used to provide a wide range of physical properties. The fluid was not agitated or stirred in any way for at least 24 hours before any run was started. It was, therefore, isothermal and quiescent. A test was started by switching a specified voltage across each of the heating sections which was filled with liquid. The test was continued until boiling started or system tem-

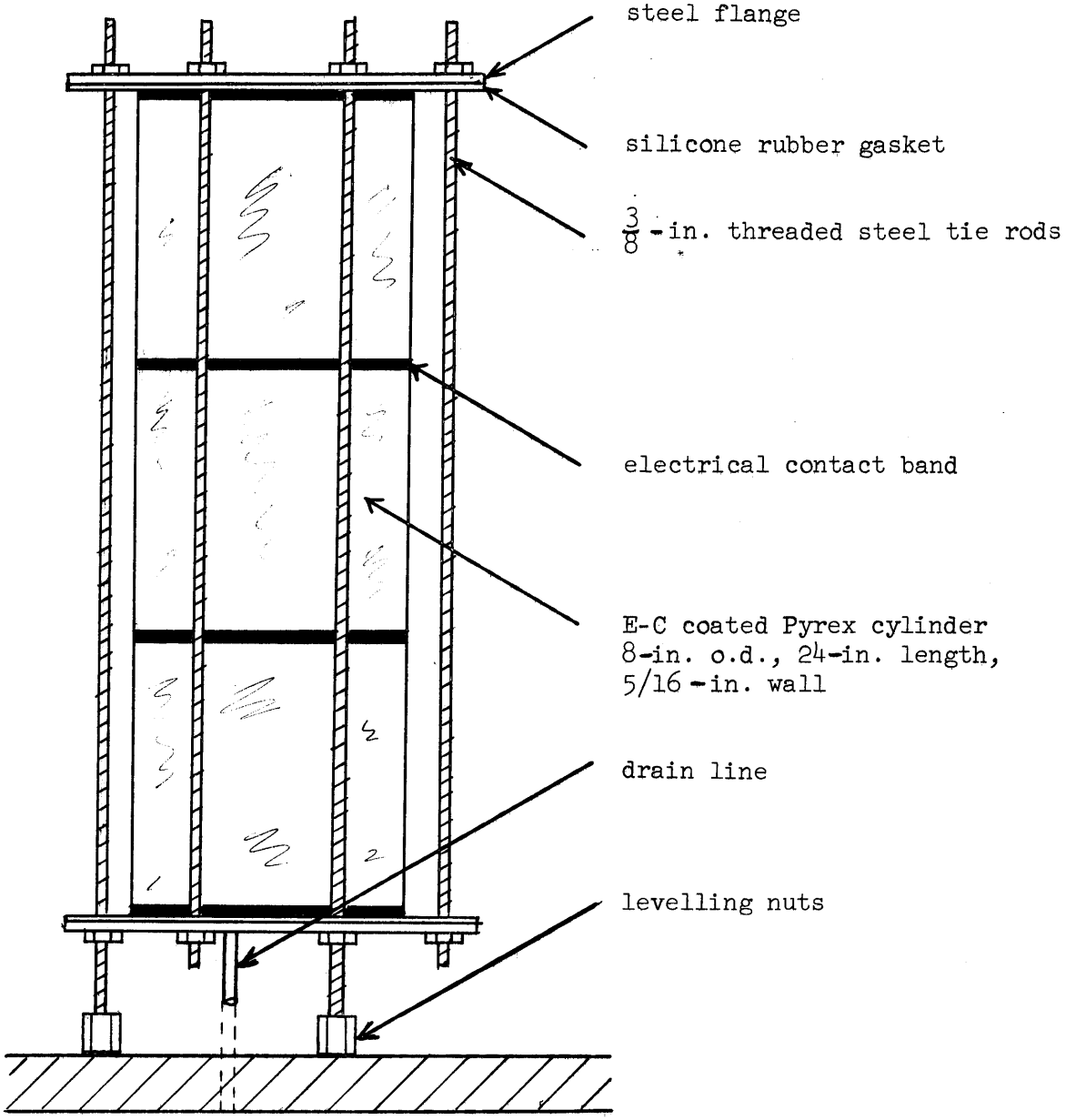

FIGURE 1-2

Experimental Enclosure

perature approached a temperature of 250°F. Typical test durations ranged from one-half to six hours.

During an experiment, temperature measurements were recorded and when desired visual and/or photographic observations of flow tracers were made. Preliminary tests had indicated that no discernible azimuthal in temperature gradient existed. Consequently, most of the temperature measurements were made over a single radial plane.

The thermocouples were made of 3-mil copper-constantan wire and the beads were approximately 10-mil diameter spheres. Thirty-eight were used. The wires were threaded on a vertical support ladder but extended away from the ladder to preclude any flow disturbance. The positioning of thermocouples in the measurement matrix (Fig. 1-3) was such that an arithmetic average of the readings along a horizontal row would represent a volume average fluid temperature at that particular height. In any test, data were recorded from about twenty-five locations which were selected to give good coverage for the particular liquid depth being studied. Using an adjustable probe, liquid surface temperatures were also measured. The probe was raised to keep the bead of the surface thermocouple just submerged as the liquid expanded slightly during the course of a run. A few additional temperature measurements were made outside of the data plane to check the assumption of symmetry, to measure wall temperatures, and to obtain an independent temperature reference. The last determination was made with an accurate thermometer which had a calibration thermocouple bonded to its bulb.

Dye was injected into various parts of the system through a long, 22-gauge hypodermic needle. Injection near the bottom corner of the vessel permitted observation of flow up the wall. The streaklines were

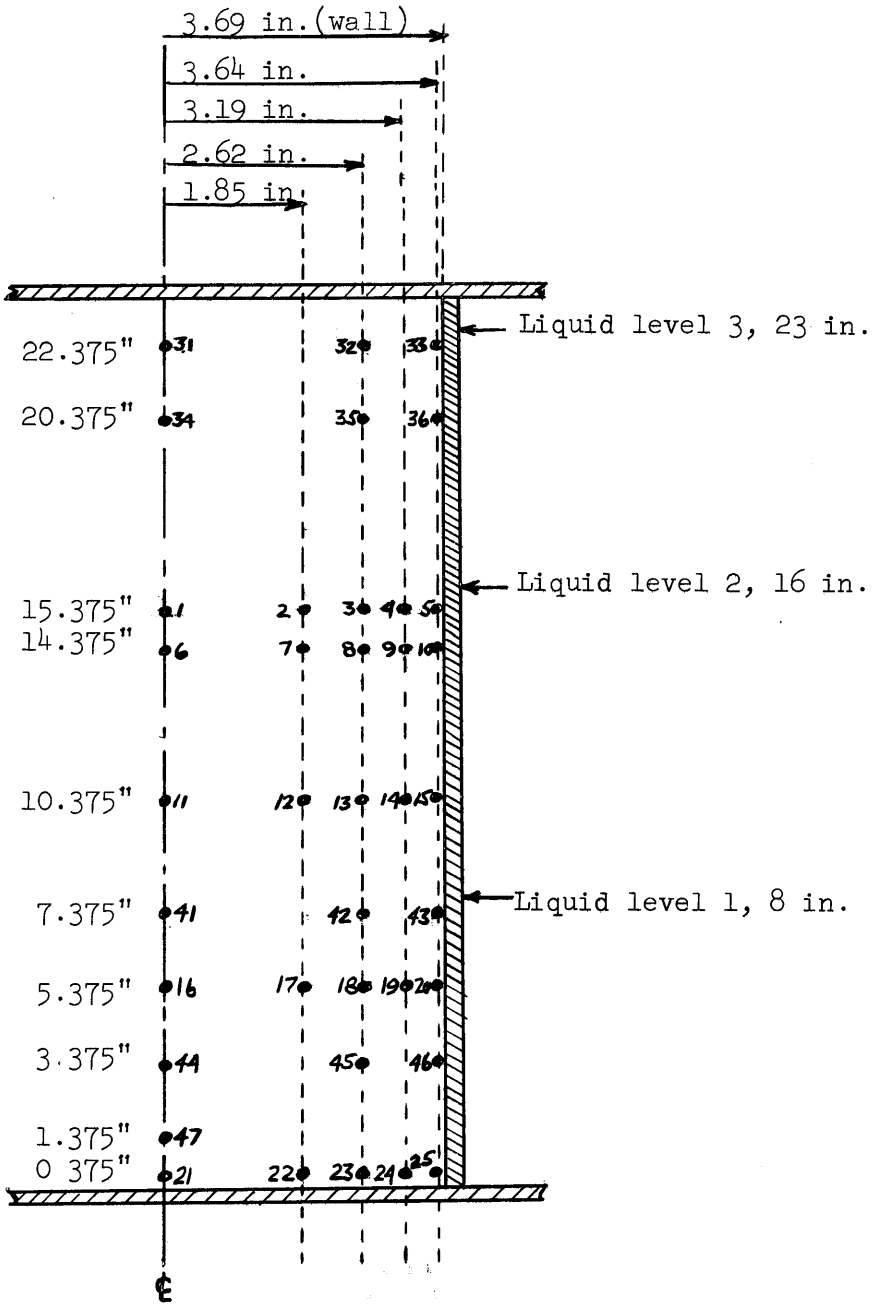

FIGURE 1-3

Temperature Measurement Locations

photographed at various times after injection. A second hypodermic needle was used to inject dye into the region just below the surface.

Typical temperature data are shown in Figure 1-4 and sketches made from photographs of tracer movements are presented in Figure 1-5. The temperature plot presents profiles showing the increase in temperature, relative to the initial fluid temperature, as a function of dimensionless fluid height at particular times after the start of heating. The solid line represents an average fluid temperature; the dotted and dashed lines indicate the axial temperature profiles at the center line and at a radial point only 0.05-in. from the wall.

FIGURE I-4
AXIAL CORE TEMPERATURE PROFILES

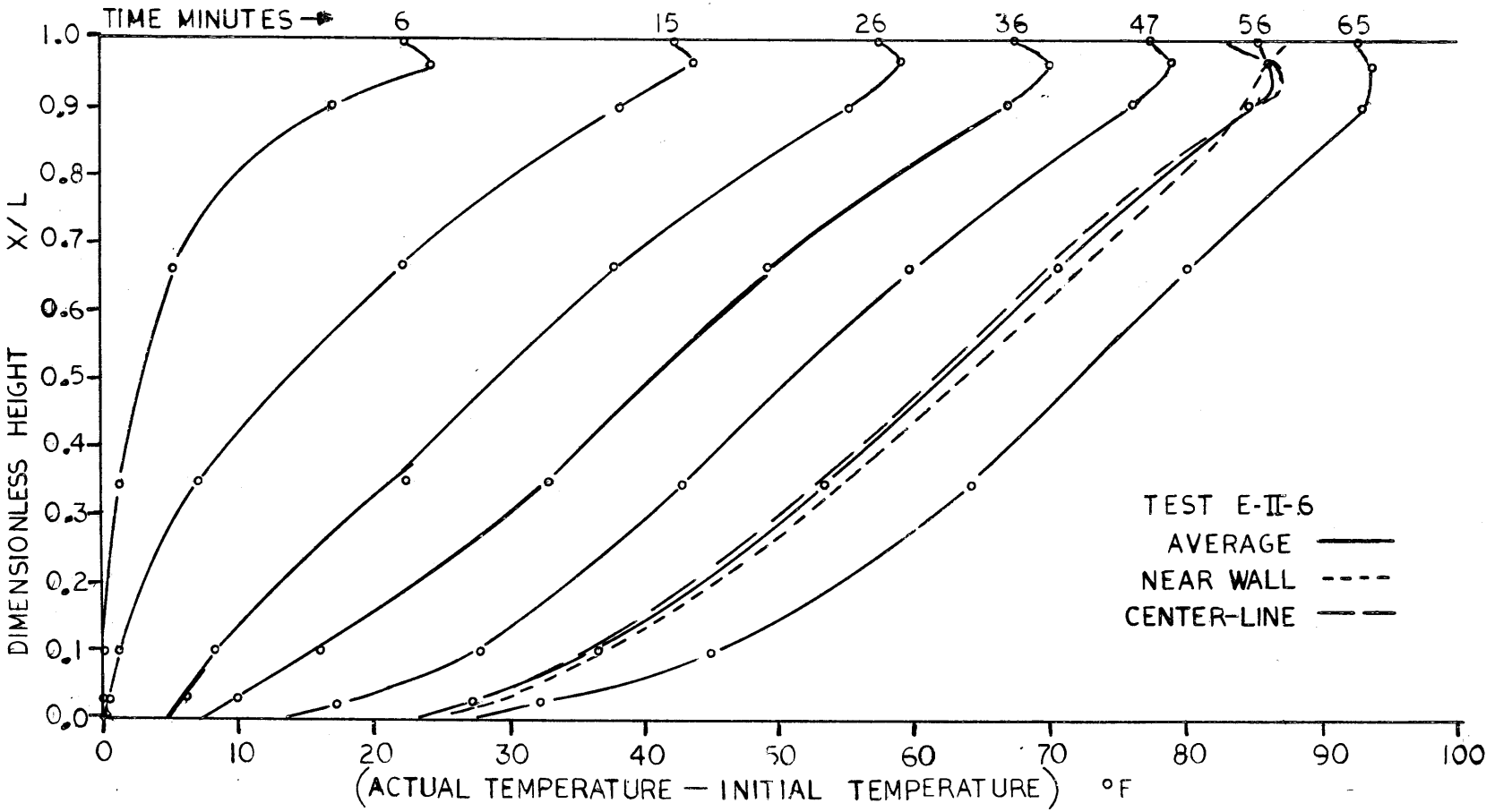

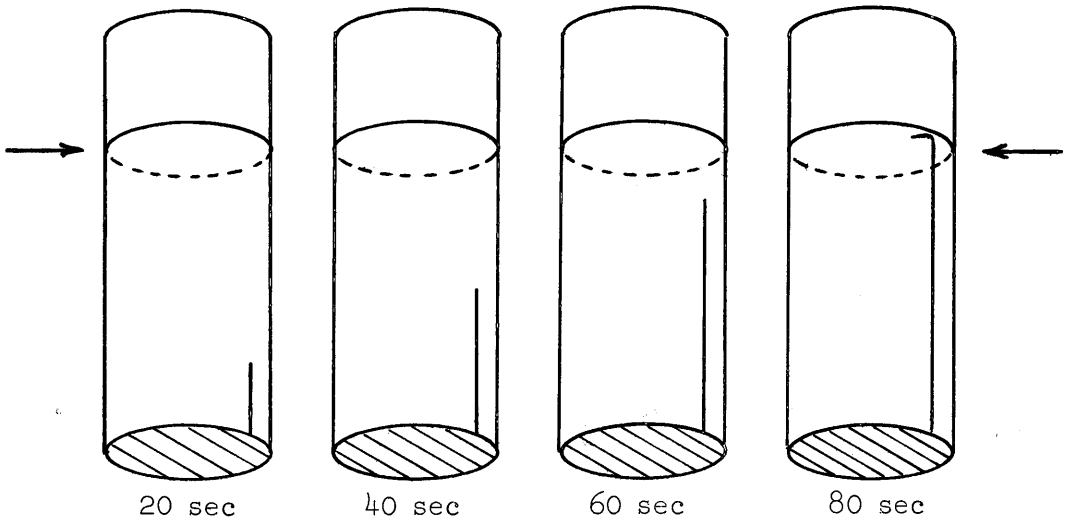

Times (sec) after dye injection in bottom corner
Arrows indicate liquid level

FIGURE 1-5

Typical Flow Pattern Observations

(Test E-2-6, 85% glycerine, L=1.33 ft, q_w = 500 BTU/hr,ft^2 (nominal))

D. Formulation of Model

Analysis of temperature data and observation of dye tracer paths from about thirty tests covering a wide range of experimental conditions led to a number of important conclusions which allow a visualization of the process.

1. Side-wall heating results in a thin boundary-layer type of flow up the walls. For most tests, the boundary layer was not sufficiently thick to encompass the thermocouple located only 0.05-in. from the wall. The maximum thickness of about 0.5-in. was obtained only for the high viscosity glycerine test fluid near the top of the $\frac{L}{D} = 3$ configuration.

2. Boundary layer fluid is discharged radially inward slightly below the liquid surface. Figure 1-5 indicates the type of mixing observed near the top of the cylindrical core region. Although the mixing behavior was complex and varied in detail from test to test, it was generally confined to about the upper 10% of the core region.

3. Below the mixing region, radial temperature gradients in the fluid are small. The warm core fluid settles gradually as cooler fluid from lower regions in the core feed the boundary layer. Still warmer fluid is deposited near the surface by the exit boundary layer flow. A plug flow model appears reasonable for this region.

4. Below the mixing region and after an initial period of time, the axial core temperature is essentially linear with height. The value of the core temperature gradient varies with time, fluid properties and wall heat flux level.

On the basis of these observations, the system was divided, for analytical purposes, into three regions: a boundary layer, a mixing

region, and a main core region as shown in Figure 1-6. Radial temperature gradients were assumed negligible in the main core and, after an initial period corresponding to the time required for the first warm fluid to sink to the bottom of the core, the axial core temperature distribution was assumed to be linear with respect to height.

If, in fact, the core temperature distribution is linear, then for the cylindrical system used here, the temperature at a dimensionless height of $\frac{X}{L} = 0.5$ should be equal to the bulk average temperature of the fluid. Since the energy input to the fluid was known as a function of time, the bulk fluid temperature could be computed by an energy balance by assuming that average fluid property values, based on the bulk temperature, could be used. The mid-plane temperature measurement was read directly from temperature profile curves similar to the ones shown in Figure 1-4.

Experimental data obtained for the entire range of conditions studied were used to test the hypothesis that the midplane temperature rise is equal to the bulk average temperature rise. Figure 1-7 shows that the results obtained from plotting the observed midplane temperature rise against the computed bulk temperature rise. Above about 10°F, the agreement is good. The discrepancy at lower temperatures is due to the start-up effect mentioned previously. At the start of heating, the average fluid temperature begins to rise immediately. However, the midplane core temperature does not begin to change until warm core fluid sinks to its level. The midplane temperature represents an average temperature only after a linear temperature gradient is established throughout the core.

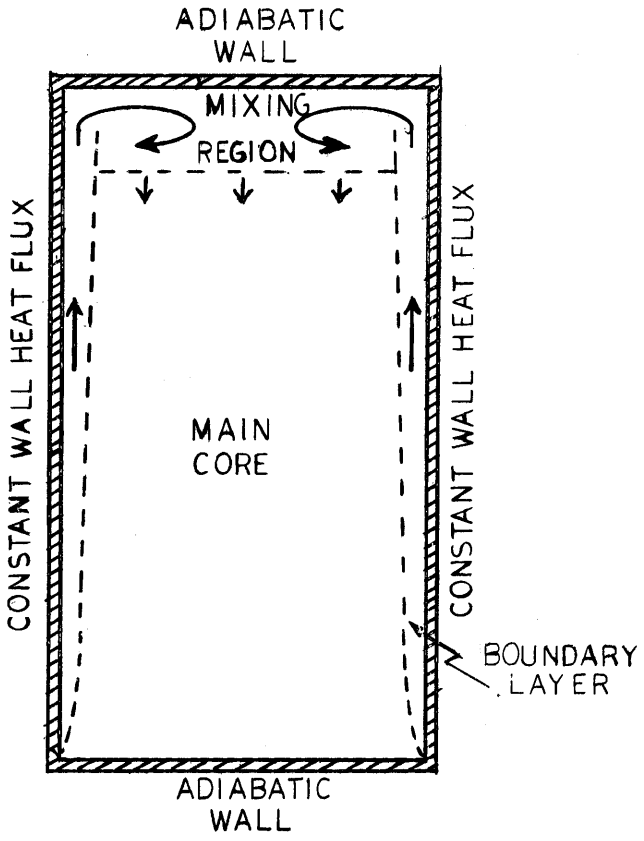

FIGURE 1-6

MODEL FOR NATURAL CONVECTION
WITHIN A VERTICAL CYLINDER
FOR CONSTANT WALL HEAT FLUX

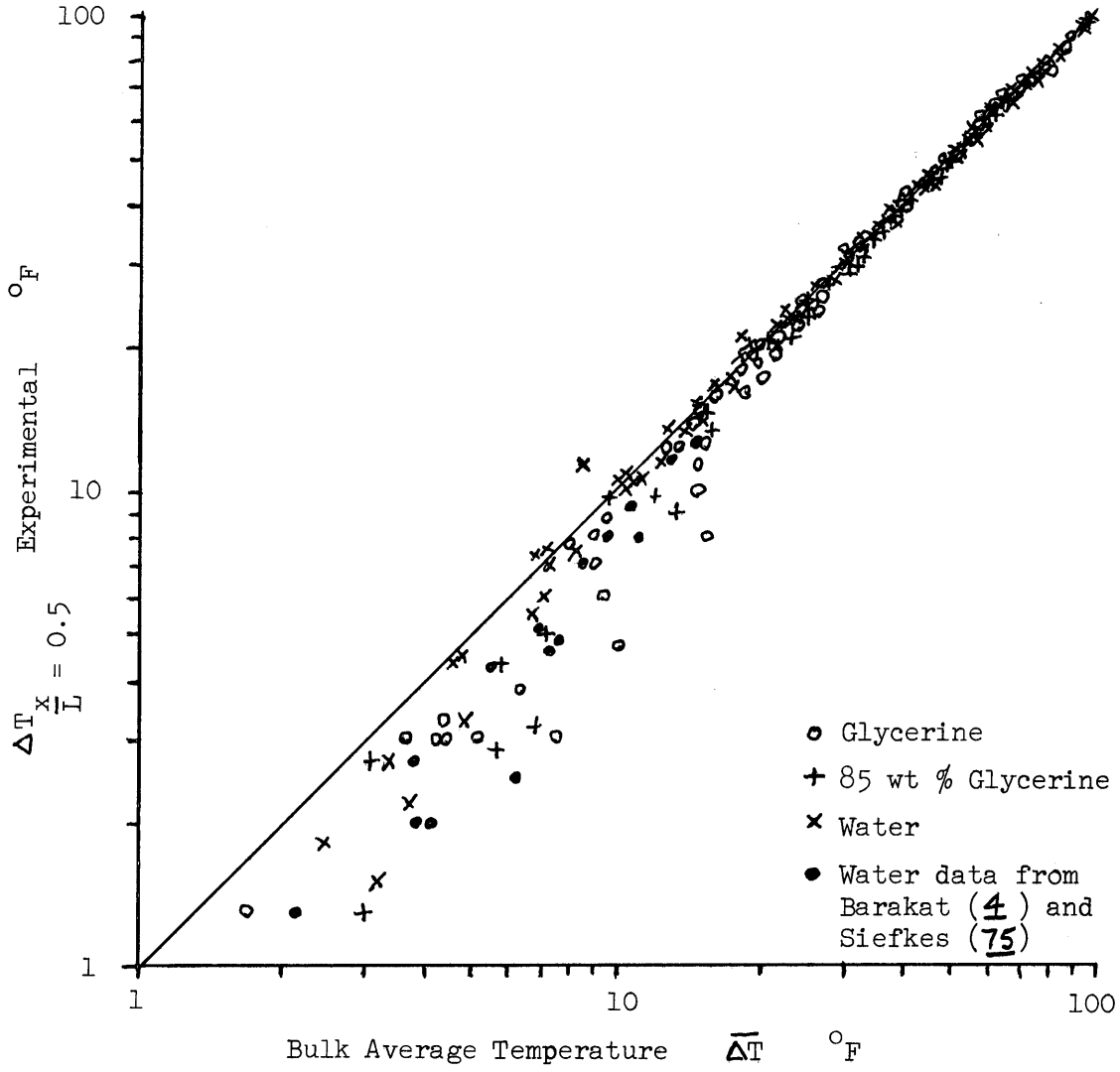

FIGURE 1-7

Comparison of Mid-plane and Bulk Average Temperature Increases

$$\overline{\Delta T} = \frac{4}{\rho C_p D} \int_0^t q_w dt$$

E. Analysis of the Model

1. Boundary Layer Region

Assuming that the fluid is initially isothermal and quiescent, a step change in the wall heat flux to a finite value results in the initiation of a boundary layer flow. The time to establish a fully developed natural convection boundary layer flow is small (typical durations for the starting transient are 1-5 sec) and during this time, the bulk is essentially not affected. In fact, for a period thereafter, since the boundary layer flow rate is small, the heat transfer may be modelled by assuming an isothermal bulk fluid feeds this boundary layer. Since the boundary layer thickness is small relative to the tank radius, the cylinder wall may be treated as a vertical flat plate.

The integral form of the momentum and energy equations for boundary layer flow are

$$\frac{\partial}{\partial x}\int_0^\infty u(T - T_\infty)dy = \frac{q}{\rho C_p} - \int_0^\infty u\frac{\partial T_\infty}{\partial x}dy \qquad (1\text{-}3)$$

$$\frac{\partial}{\partial x}\int_0^\infty u^2 dy = \beta g\int_0^\infty (T - T_\infty)dy - \frac{\tau_w}{\rho} \qquad (1\text{-}4)$$

where

x = distance measured up from start of vertical plate

ρ = fluid density

C_p = fluid heat capacity

β = fluid thermal expansion coefficient

g = gravitational acceleration

τ_w = wall shear stress

y = distance from the plate in the normal direction

T_∞ = temperature at $y = \infty$

u = fluid velocity

T = fluid temperature

To solve these equations, it is necessary to assume a functional form for the velocity and temperature profiles. Profiles of the type used previously by others (17, 65, 96, 98) for the case of T_∞ = constant, were chosen.

$$\left.\begin{aligned} T - T_\infty &= \frac{q}{2k}\,\delta\left[1 - \frac{y}{\delta}\right]^2 \\ u &= \omega\,\frac{y}{\delta}\left[1 - \frac{y}{\delta}\right]^2 \end{aligned}\right\} \text{Laminar Flow} \qquad (1\text{-}5)$$

$$\left.\begin{aligned} \frac{T - T_\infty}{T_w - T_\infty} &= \left[1 - \left(\frac{y}{\delta}\right)^{1/7}\right] \\ u &= \omega\left(\frac{y}{\delta}\right)^{1/7}\left[1 - \frac{y}{\delta}\right]^4 \end{aligned}\right\} \text{Turbulent Flow} \qquad (1\text{-}6)$$

where

δ = boundary layer thickness

T = temperature at point y inside the boundary layer (y varies from zero at the wall to δ at the edge of the boundary layer)

T_w = wall temperature

T_∞ = temperature outside boundary layer (at $y > \delta$)

u = fluid velocity

ω = characteristic fluid velocity

q = wall heat flux

k = thermal conductivity

When these profiles are substituted into Eqs. 1-3 and 1-4, a pair of simultaneous ordinary differential equations are obtained which give $\delta(x)$ and $\omega(x)$, for specified fluid properties. The boundary layer flow rate is proportional to $(\omega\delta)$ and the thermal energy flow rate is proportional to $(\omega\delta^2)$.

In an enclosed system, as heating progresses, warm fluid is deposited in the core region and the boundary layer solutions based on a constant temperature everywhere outside the boundary layer are not applicable. However, the last term in Eq. 1-3 describes the effect of core temperature distribution on the boundary layer region. Therefore the same profiles assumed for the constant core temperature case may be substituted into the more general form of the energy equation to give a solution for a varying core temperature distribution.

For convenience and generality, dimensionless momentum and energy variables are used in the analysis:

$$E \propto \int_0^\infty u(T - T_\infty)dy \tag{1-7}$$

$$M \propto \int_0^\infty u^2\, dy \tag{1-8}$$

Noting that (Eq. 1-2),

$$(GrNu)_x = \frac{g\beta q x^4}{k\nu^2} \tag{1-9}$$

and defining

$$C = \left[\frac{g\beta q}{k\nu^2}\right]^{1/4} \tag{1-10}$$

and $$X = Cx = (GrNu)_x^{1/4}\,, \tag{1-11}$$

the energy and momentum variables for the isothermal core case become:

$$\left.\begin{aligned} E_o &= C_E X \\ M_o &= C_M X^{7/5} \end{aligned}\right\} \quad \text{Laminar} \tag{1-12}$$

$$\left.\begin{aligned} E_o &= C_E X \\ M_o &= C_M X^{11/7} \end{aligned}\right\} \quad \text{Turbulent} \tag{1-13}$$

The coefficients C_E and C_M are known functions of only the Prandtl number but they are, of course, different for the laminar and turbulent cases. Consequently, new normalized variables are defined:

$$E^* = \frac{E}{C_E} \tag{1-14}$$

$$M^* = \frac{M}{C_M} \tag{1-15}$$

These definitions lead to simple relationships for the isothermal core case:

$$E_o^* = X = (GrNu)_x^{1/4} \tag{1-16}$$

$$M_o^* = \begin{cases} X^{7/5} & \text{laminar} \\ X^{11/7} & \text{turbulent} \end{cases} \tag{1-17}$$

The original energy and momentum equations 1-3 and 1-4 may now be transformed into equations of the form:

$$\text{Let} \quad \frac{d\theta_{\infty}}{dX} = \frac{k}{q}\frac{dT_{\infty}}{dx} = \text{dimensionless core temperature gradient} \tag{1-18}$$

$$\left.\begin{aligned} \text{Laminar:} \quad \frac{dE^*}{dX} &= 1 - \left[f_1(Pr)\right]\left[E^*M^*\right]^{1/3}\frac{d\theta_{\infty}}{dX} \\ \frac{dM^*}{dX} &= \left[f_2(Pr)\right]\frac{E^{*4/3}}{M^{*2/3}} - \left[f_3(Pr)\right]\frac{M^*}{E^*} \end{aligned}\right\} \tag{1-19}$$

$$\left.\begin{aligned} \text{Turbulent:} \quad \frac{dE^*}{dX} &= 1 - \left[f_4(Pr)\right]\left[E^*M^*\right]^{4/9}\frac{d\theta_{\infty}}{dX} \\ \frac{dM^*}{dX} &= \left[f_5(P_r)\right]\frac{E^{*13/9}}{M^{*5/9}} - \left[f_6(Pr)\right]\frac{M^*}{E^*} \end{aligned}\right\} \tag{1-20}$$

The functions of Prandtl number in the above equations depend only on the Prandtl number and constants obtained from integration over the assumed forms of the boundary layer temperature and velocity profiles.

It is interesting to note that although T_{∞} may be an arbitrary function of x, only the derivative, $\frac{dT_{\infty}}{dx}$ or $\frac{d\theta_{\infty}}{dX}$, appears in the above energy and momentum equations for the constant wall heat flux case.

These equations were solved numerically for the important case of $\frac{d\theta_{\infty}}{dX}$ = constant which corresponds to the linear axial temperature distribution case observed experimentally. Typical results of these computations for various values of Prandtl number and core temperature gradient are shown in Figures 1-8 and 1-9 for the laminar and turbulent models respectively. In the computation, a finite X starting point was chosen to avoid difficulties in evaluating the derivatives at X = 0.

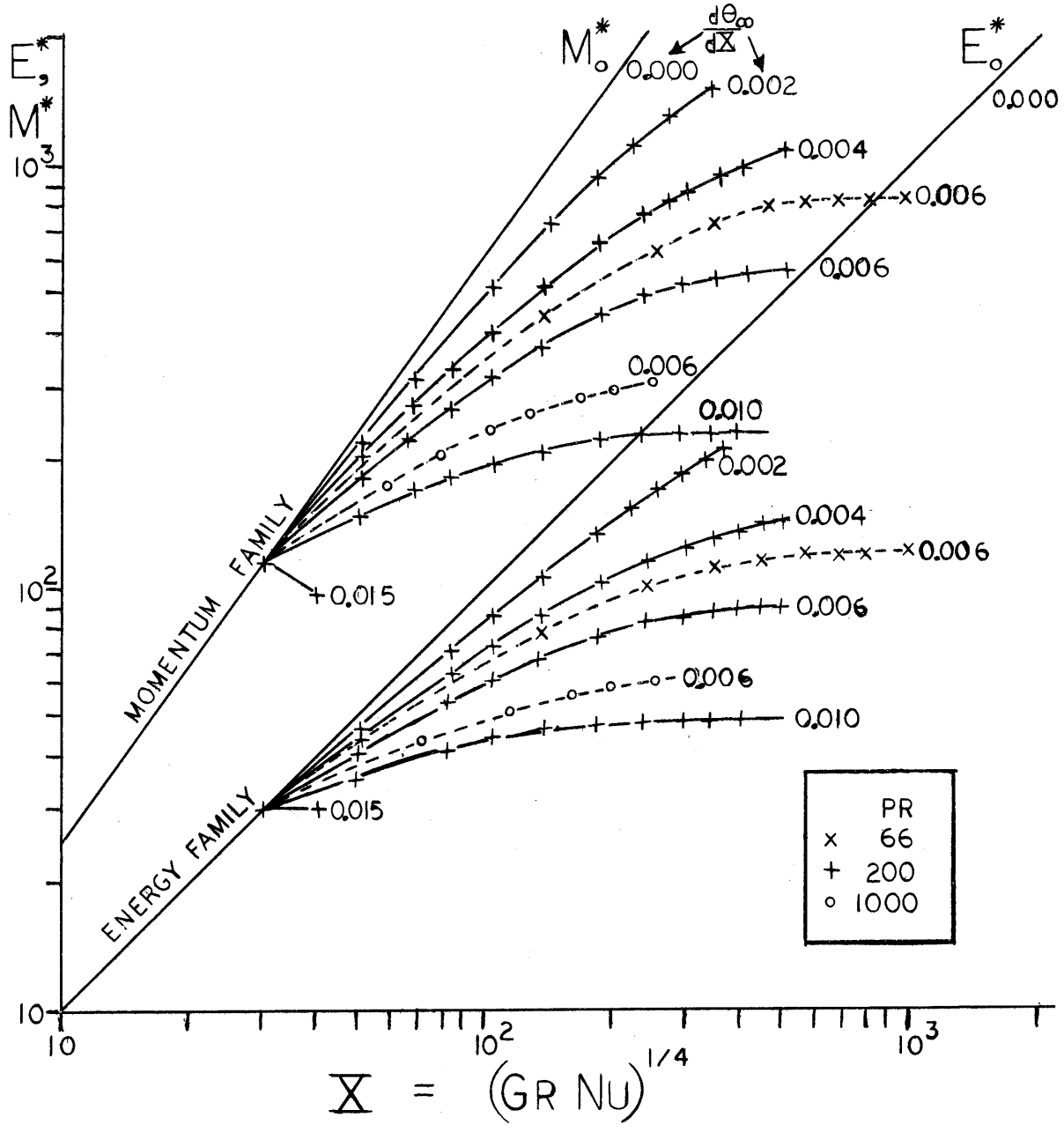

FIGURE 1-8

DIMENSIONLESS BOUNDARY LAYER ENERGY AND MOMENTUM FUNCTIONS
LAMINAR MODEL WITH CONSTANT CORE TEMPERATURE GRADIENT

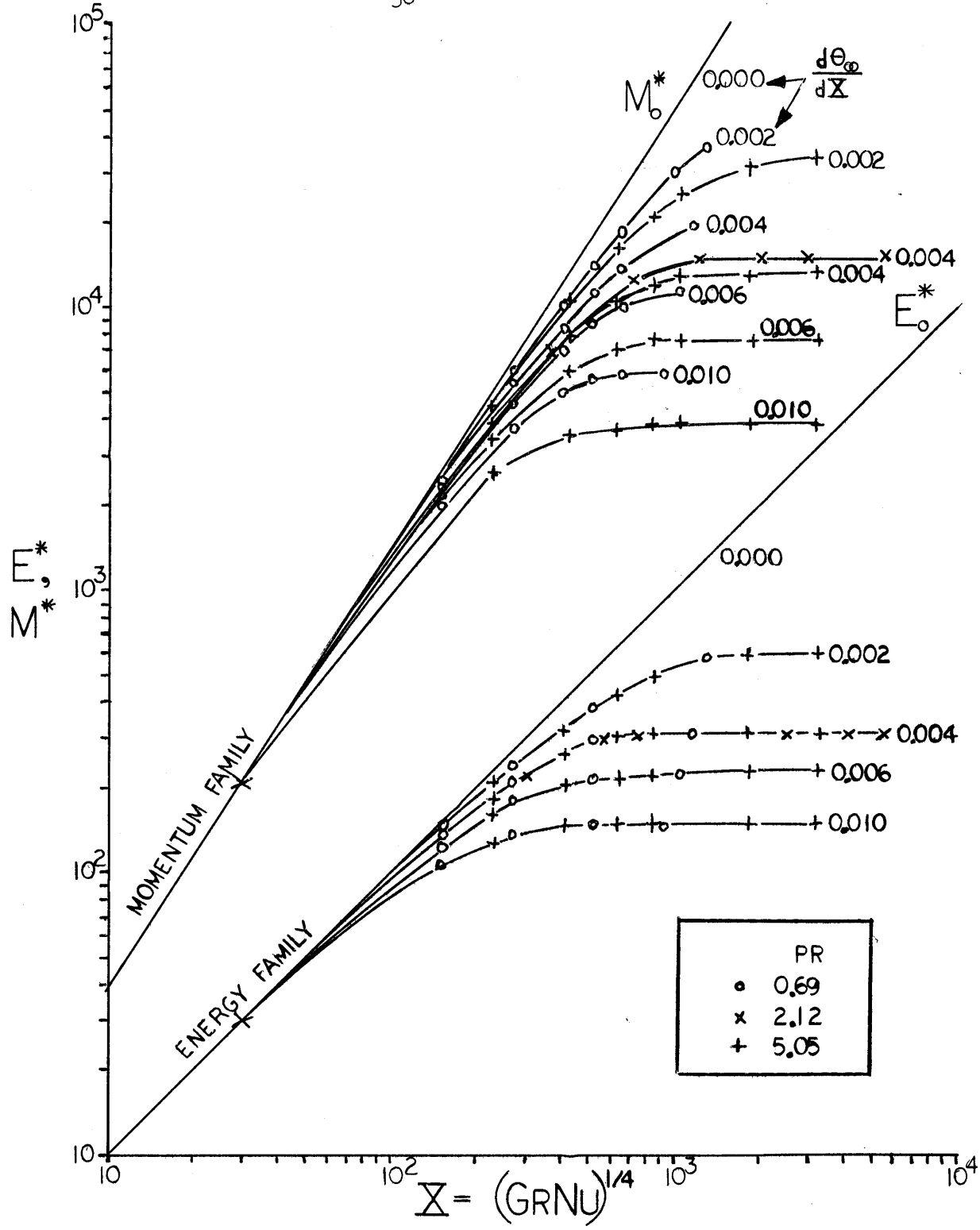

FIGURE 1-9

DIMENSIONLESS BOUNDARY LAYER ENERGY AND MOMENTUM FUNCTIONS
TURBULENT MODEL WITH CONSTANT CORE TEMPERATURE GRADIENT

As long as the starting point value was less than about 10% to 20% of the dimensionless height at which the variables were to be evaluated, the error introduced by use of a finite starting point was found to be negligible.

With no core temperature variation, both the boundary layer thermal energy and momentum increase with distance up the wall. However, if a positive core temperature gradient is present, the boundary layer energy and momentum variables reach limiting values. A physical interpretation is that, assuming the fluid volumetric heat capacity (ρC_p) remains constant, at some height the boundary layer will have grown large enough so the total energy input from the wall is required to keep its average temperature level increasing at the same rate as the core temperature is increasing. Beyond this point, no energy is available for additional growth or acceleration of the boundary layer.

The limiting values, E_a^* and M_a^*, may be found by setting the derivatives in equations 1-19 and 1-20 equal to zero, then, assuming that E_a^* and M_a^* are constant, and solving the equations simultaneously to obtain

$$\left.\begin{matrix} E_a^* \\ M_a^* \end{matrix}\right\} = f\left(Pr, \frac{d\theta_\infty}{dX}\right) \qquad (1\text{-}21)$$

2. The Mixing Region

Although the mixing region flow patterns and temperature distributions were found to be complex in the experimental portion of this study, the mixing region was confined only to about the upper 10 percent of the core and served the purpose of mixing hot boundary layer fluid with surface core fluid to produce well-mixed fluid feeding the main core. Consequently a simplified model was proposed for the mixing region. Assume that the mixing region is of depth Δx and at some uniform temperature, T_L. The rate of change of T_L with time can be found from an energy balance if the boundary layer temperature and flow rate are known and if the inflow from the boundary layer equals to outflow to the main core region.

Choose an energy datum level at T_L. An analysis of the mixing region model shows

$$\text{Energy in:} \qquad \rho C_p \pi D \int_0^\infty u(T - T_L)dy\, dt \tag{1-22}$$

$$\text{Energy out:} \qquad 0 \quad \text{(Fluid at } T_L\text{)} \tag{1-23}$$

$$\text{Energy change:} \qquad \rho C_p \frac{\pi D^2 \Delta x}{4} dT_L \tag{1-24}$$

These lead to,

$$\frac{dT_L}{dt} = \frac{4}{D\Delta x} \int_0^\infty u(T - T_L)dy \tag{1-25}$$

Note that $\int_0^\infty u(T - T_L)dy$ (or in other nomenclature $\int_0^\infty u(T - T_\infty)dy$, since $T_\infty = T_L$ at $x = L$) is proportional to E^*, the boundary layer energy parameter. (Eqn. 1-7)

3. Main Core Region

The model is based on a radially-well-mixed core with an axial temperature variation which varies linearly with height. Assume that the rate of change of core temperature gradient is due to the variation in T_L of the mixing region.

$$\frac{d}{dt}\left[\frac{d\theta_\infty}{dX}\right] = \frac{k}{q}\,\frac{1}{(L - \Delta x)}\,\frac{dT_L}{dt} \tag{1-26}$$

Using equations 1-26, 1-25 and the asymptotic energy parameter (eqn. 1-21), an expression for the core temperature gradient can be obtained. This solution should apply whenever the axial core gradient is essentially constant throughout the main core and when the boundary layer energy has reached a limiting value with respect to the core temperature level.

$$\underline{\text{Laminar}} \quad \left[\frac{d\theta_\infty}{dX}\right]_a = 1.454\,\frac{Fo^{4/9}}{\left[\frac{\Delta x}{L}\left(1 - \frac{\Delta x}{L}\right)\right]^{4/9}}\,\frac{1}{(RaNu)^{1/9}} \tag{1-27}$$

$$\underline{\text{Turbulent}} \quad \left[\frac{d\theta_\infty}{dX}\right]_a = 3.46\,\frac{Fo^{8/15}}{\left[\frac{\Delta x}{L}\left(1 - \frac{\Delta x}{L}\right)\right]^{8/15}}\,\frac{Pr^{7/45}}{(RaNu)^{2/15}} \tag{1-28}$$

F. Discussion of Model

In Figures 1-10 to 1-12, experimental values of the dimensionless core temperature gradient are plotted against the appropriate function of Fo, RaNu and Pr for the laminar and turbulent cases (eqns. 1-27 and 1-28) respectively. Using the Ra $\backsimeq 10^8 - 10^9$ criterion for transition to turbulence, the glycerin test data should be only in the laminar regime, the 85 weight percent glycerine data should be laminar except at some of the higher values of wall heat flux which give Rayleigh numbers in the transition region, and the water data should correspond to the transition range and fully developed turbulence.

In Figure 1-10, the "laminar" core temperature gradient data are plotted against $\left[Fo^{4/9}/(RaNu)^{1/9}\right]$. The resulting line has a slope of unity thus verifying the parametric dependence predicted by the laminar model. The correlating line has the equation

$$\frac{d\theta_{oo}}{dX} = 4\, Fo^{4/9}(RaNu)^{-1/9} \qquad (1\text{-}29)$$

Comparison with equation 1-27 indicates that

$$\frac{\Delta x}{L}\left(1 - \frac{\Delta x}{L}\right) = \left(\frac{1.456}{4.0}\right)^{9/4} = 0.104 \qquad (1\text{-}30)$$

or that $\frac{\Delta x}{L} \backsimeq 0.12$. The 12% mixing region agrees well with the experimental observation of about a 10% mixing region. (A 10% mixing region would give a constant of 4.24 in eqn. 1-29; a 15% mixing region, a constant of 3.64.)

Before checking the turbulent model, it is interesting to note from Figure 1-10 that the "turbulent" water data are also correlated by the laminar correlation, eq. 1-29. Any scatter in points is random and

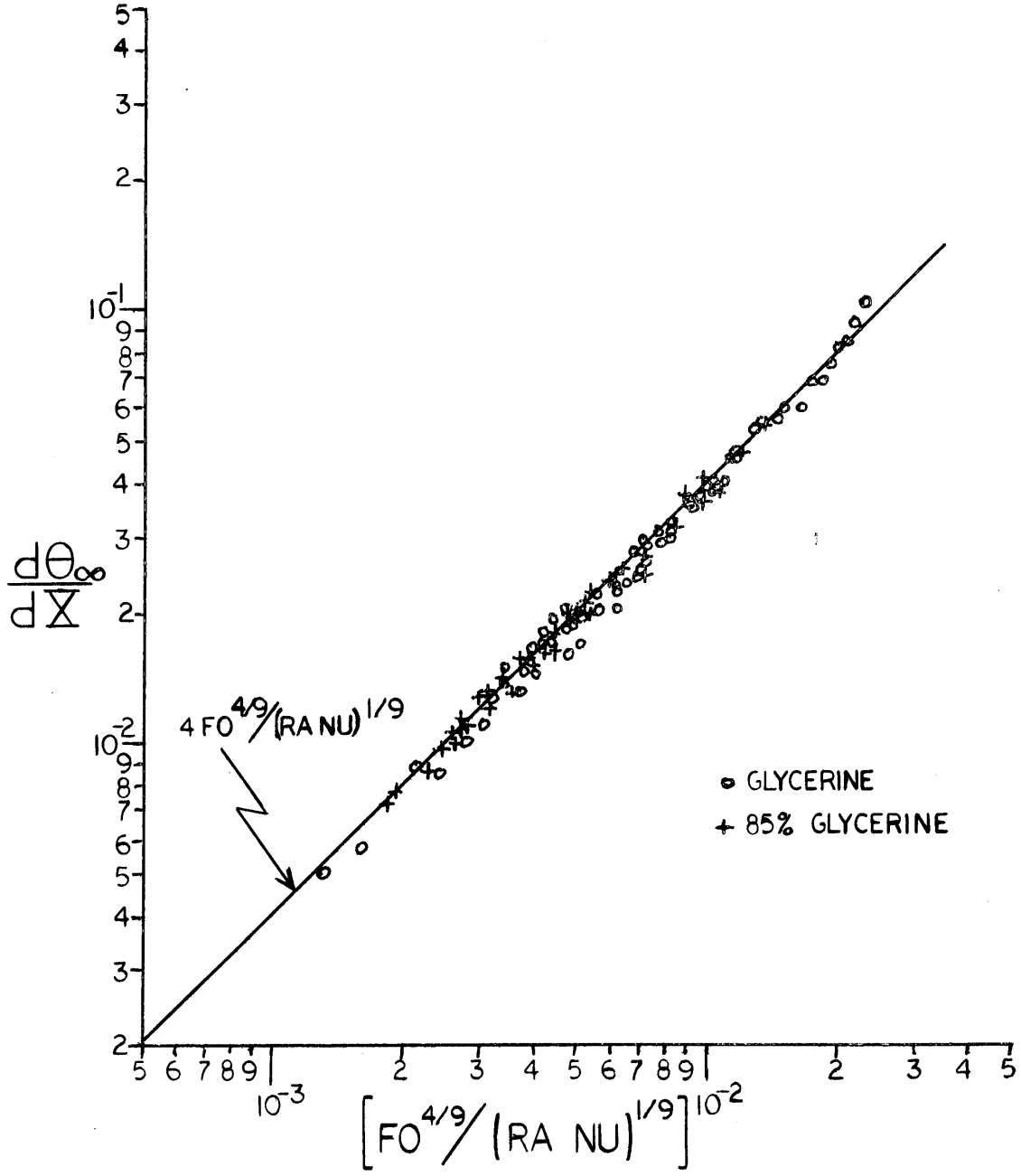

FIGURE 1-10

AXIAL CORE TEMPERATURE GRADIENT

COMPARISON OF GLYCERINE AND 85% GLYCERINE DATA WITH LAMINAR MODEL

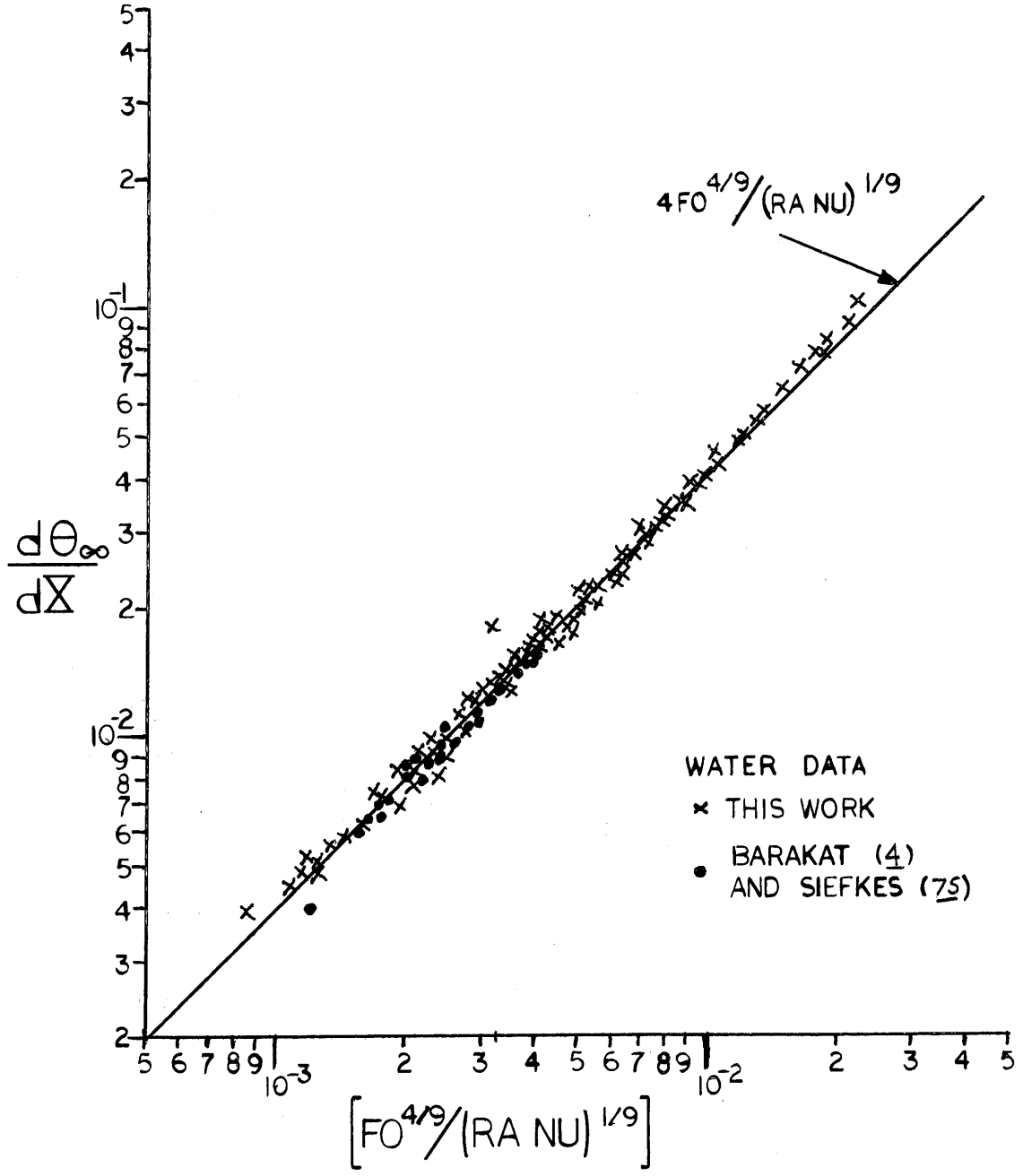

FIGURE 1-11

AXIAL CORE TEMPERATURE GRADIENT

COMPARISON OF WATER DATA WITH LAMINAR MODEL

there is no detectable shift in position or slope between results from tests at different Rayleigh number levels. The data of Barakat (4) and Seifkes (91), shown as solid dots, correspond to Rayleigh numbers of 10^9 - 10^{10}. Barakat's data were obtained in a 4-in. diameter cylinder; Siefkes' system consisted of an 8-in. enclosure, the same nominal size for the cylinder used in this study. Barakat's data were obtained only for times up to four minutes after the start of heating. Siefkes' data were taken at a single wall heat flux level.

When all the data are plotted against the turbulent model parameter $\left[Fo^{8/15}\ Pr^{7/45}\ (RaNu)^{-2/15}\right]$, the results shown in Figure 1-12 are obtained. The "laminar" glycerin and 85 weight per cent glycerin data are poorly correlated by the turbulent model, as would be expected. More surprising, however, is that the supposedly turbulent water data do not exhibit a slope of unity at the higher experimental values of $\frac{d\theta_\infty}{dX}$. Examination of Figure 1-13 will provide an explanation for this apparent discrepancy. Boundary layer analysis for the constant wall heat flux case indicated, as discussed previously, that boundary layer energy and momentum were limited by the presence of a constant core temperature gradient. The limiting values for E_a^* are plotted as functions of the core temperature gradient and the Prandtl number in Figure 1-13. The energy limitation may, in certain cases, prevent a transition to turbulence. Recalling that $E_o^* = X = (GrNu)^{1/4}$ for $\frac{d\theta_\infty}{dX} = 0$, it is reasonable to suggest that E_a^* is related to the limiting value of the actual Grashof or Rayleigh number for a system. A conservative estimate for the transition point is given in equation 1-31.

$$(Ra)_{transition} = GrPr = 10^8 \qquad (1\text{-}31)$$

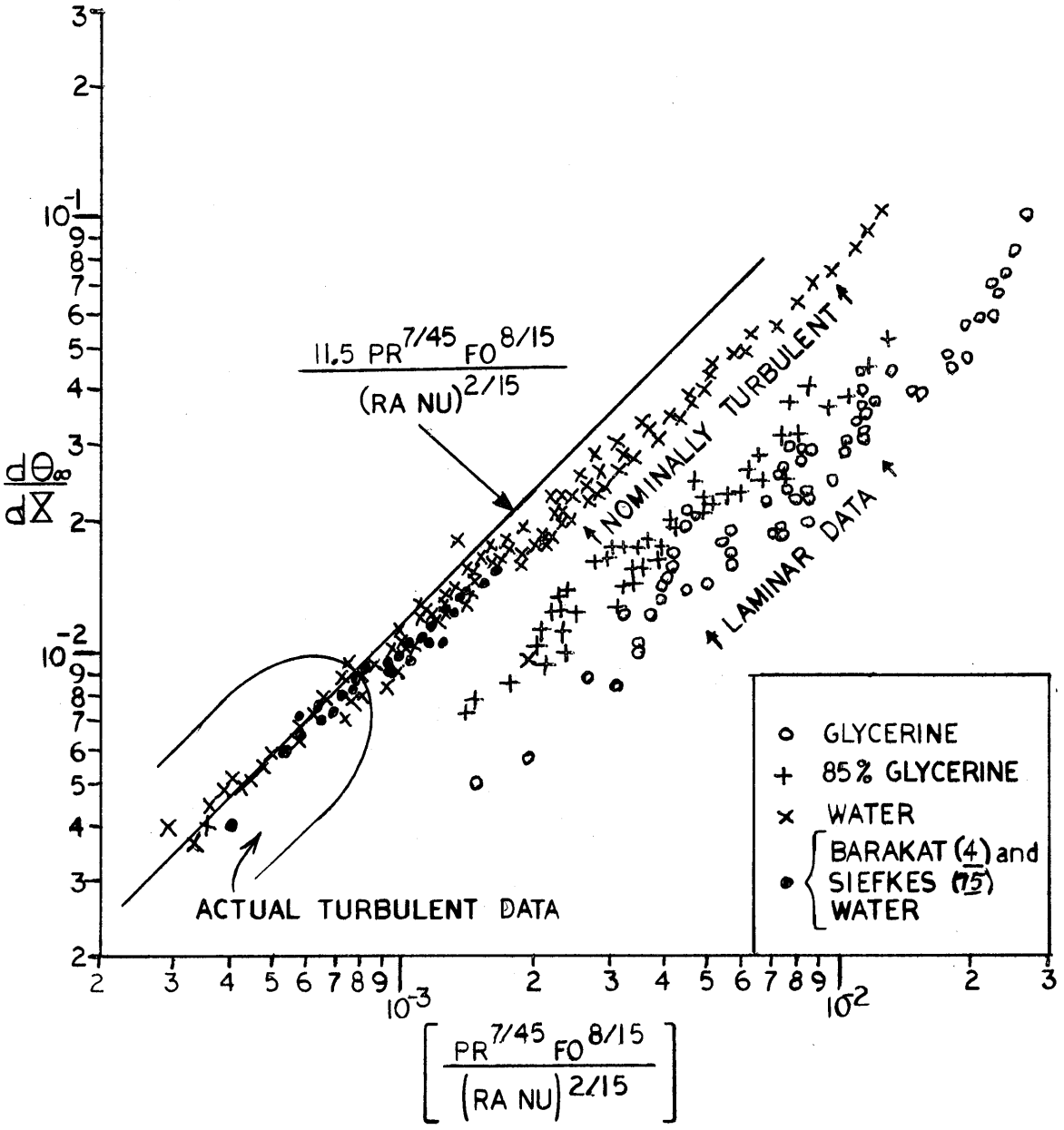

FIGURE 1-12

AXIAL CORE TEMPERATURE GRADIENT

COMPARISON OF
ALL DATA
WITH TURBULENT MODEL

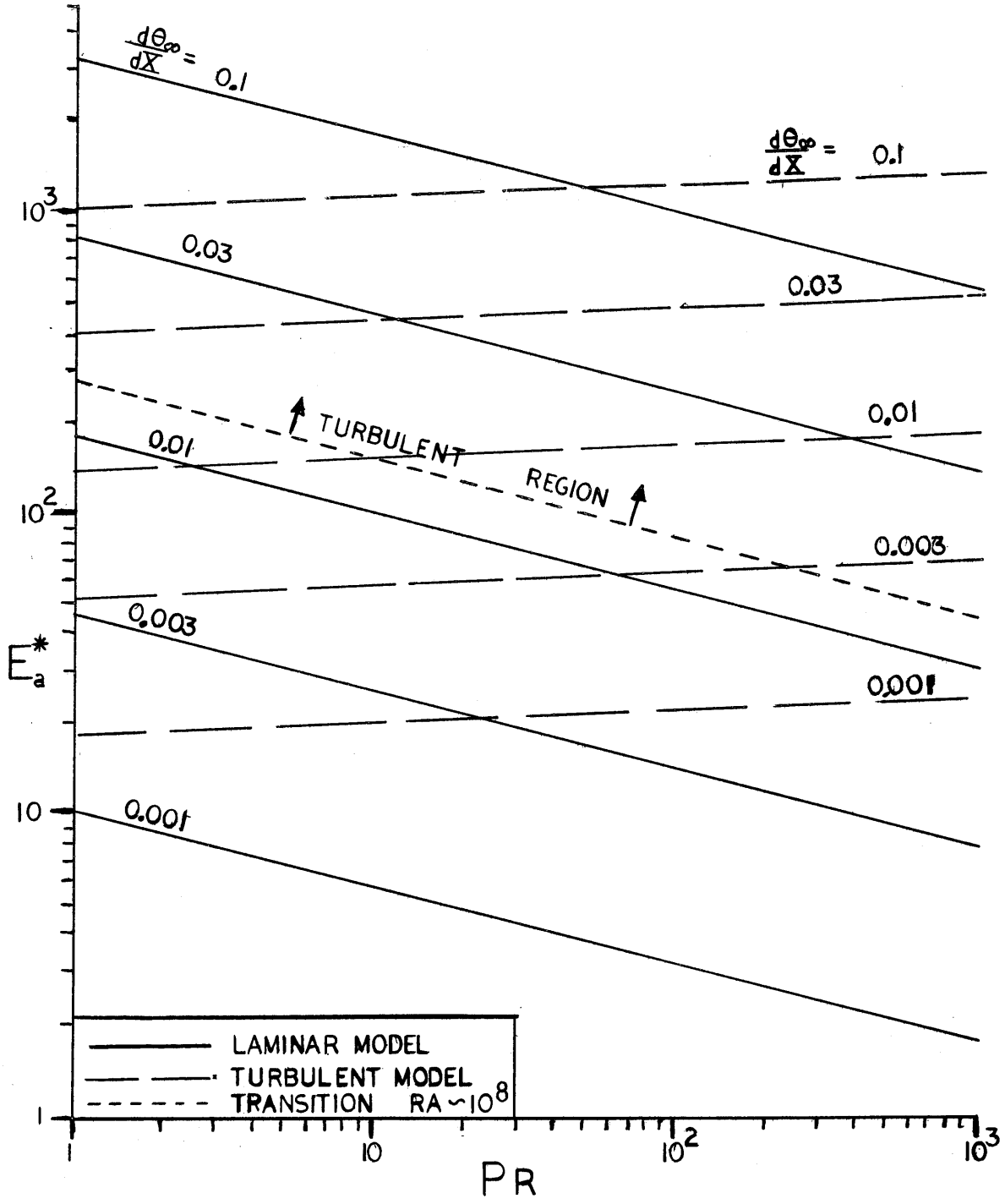

FIGURE 1-13

ASYMPTOTIC VALUES FOR
BOUNDARY LAYER ENERGY FUNCTION

Then with the usual correlation for laminar natural convection heat transfer to a vertical plate with constant temperature at infinity (54),

$$Nu = 0.56(Ra)^{1/4} \tag{1-32}$$

One obtains,

$$(GrNu)_{transition} = \frac{10^8}{Pr} \quad (0.56 \times 10^2) \tag{1-33}$$

$$E^*_{transition} = (GrNu)^{1/4}_{transition} = \frac{274}{Pr^{1/4}} \tag{1-34}$$

Using the limiting values of boundary layer energy, the dotted line in Figure 1-13 shows the predicted transition region. The limiting values predicted by the laminar model are shown as solid lines; the turbulent, as dashed lines. All the water data correspond to Prandtl numbers below ten, and, from the limiting energy analysis, no transition would be expected to occur if the dimensionless core gradient were greater than 0.01. If data points for $\frac{d\theta_\infty}{dX}$ greater than 0.01 are eliminated from consideration in Figure 1-12 on the basis that turbulent transition is prevented by the energy limitation, then the remaining data are well correlated by a turbulent model of the form

$$\frac{d\theta_\infty}{dX} = 11.5Fo^{8/15}\ Pr^{7/45}\ (RaNu)^{-2/15} \tag{1-35}$$

Comparison of equation 1-35 with equation 1-28 again indicates about a 12% mixing region.

Even though there is good agreement between the turbulent model and the data which should be turbulent on the basis of the limiting energy analysis, there is no reason why both the laminar and turbulent models

should not correlate these data. Because of the energy limitation, these turbulent data probably correspond to the transitional range rather than the highly turbulent conditions predicted by the large Rayleigh numbers which extend up to 10^{13}. However, for still higher Rayleigh numbers, the turbulent model would be expected to give better results than the laminar model.

Figure 1-14 shows a comparison between axial temperature profiles computed from the model and actual axial temperature profiles measured for equivalent conditions. Agreement is good except for the initial period mentioned previously. Before the first warm fluid reaches the bottom of the core, the axial temperature profile is not linear and the use of a bulk average temperature as a midpoint temperature is not acceptable. During this period, accurate temperature profiles could be estimated by numerical integration of the simultaneous first order nonlinear differential equations (1-19 and 1-20) for boundary layer energy and momentum. The same general model could be used for a mixing region, but core temperature distribution would be found by combining the mixing region temperature variation with a plug flow model for the core. The variation in core temperature distribution would be accounted for when integrating the energy equation along the boundary layer.

Temperature distributions may also be estimated during the initial period using the data presented in Figures 1-15 and 1-16. Although there is considerable scatter in the normalized temperatures (based on the bulk average) for various dimensionless heights as functions of dimensionless time, a consistent picture of the core temperature distribution transient is given. At the time when the temperature

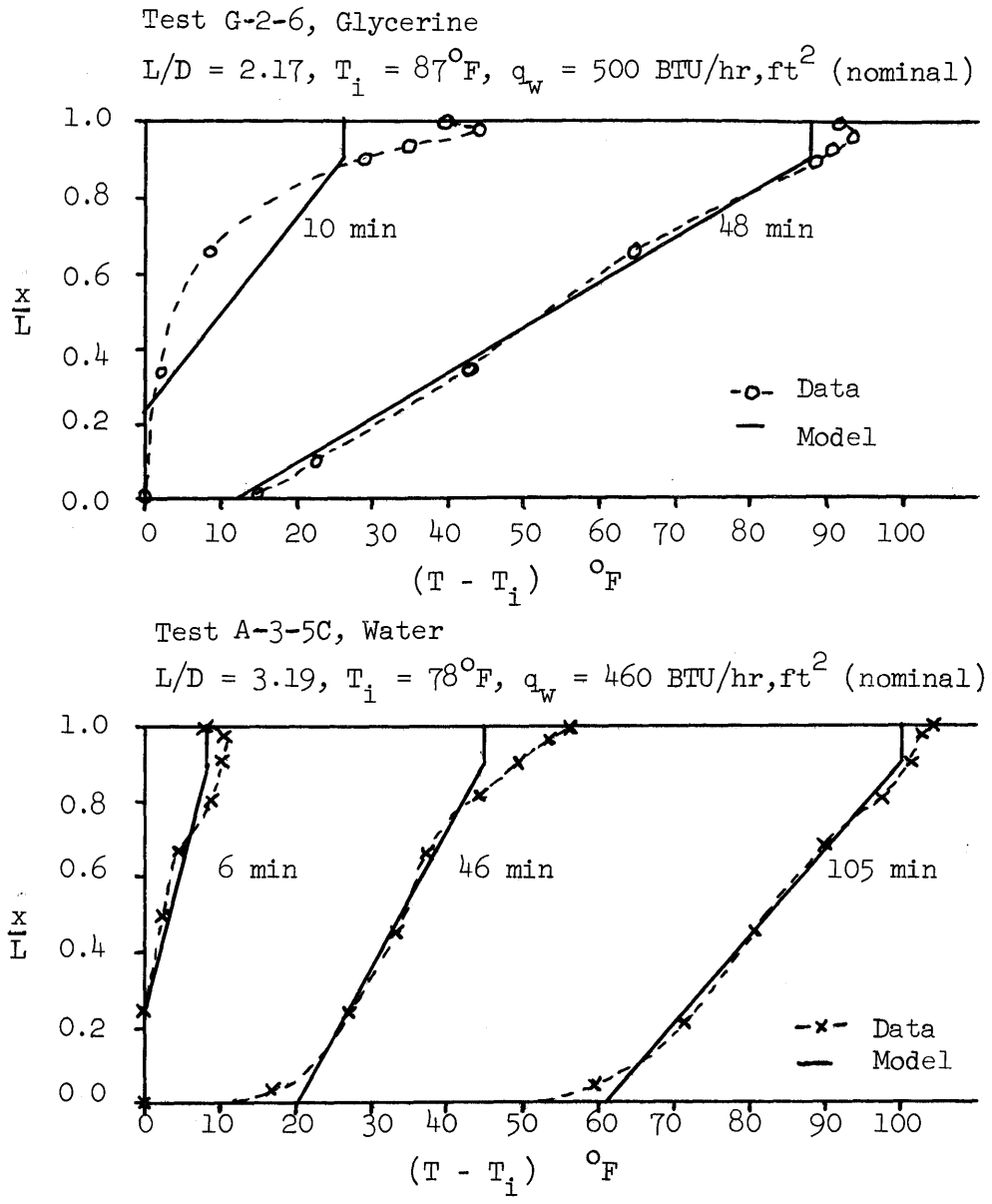

FIGURE 1-14

Comparison between Predicted and Observed
Axial Core Temperature Profiles
Limiting Boundary Layer Energy Model

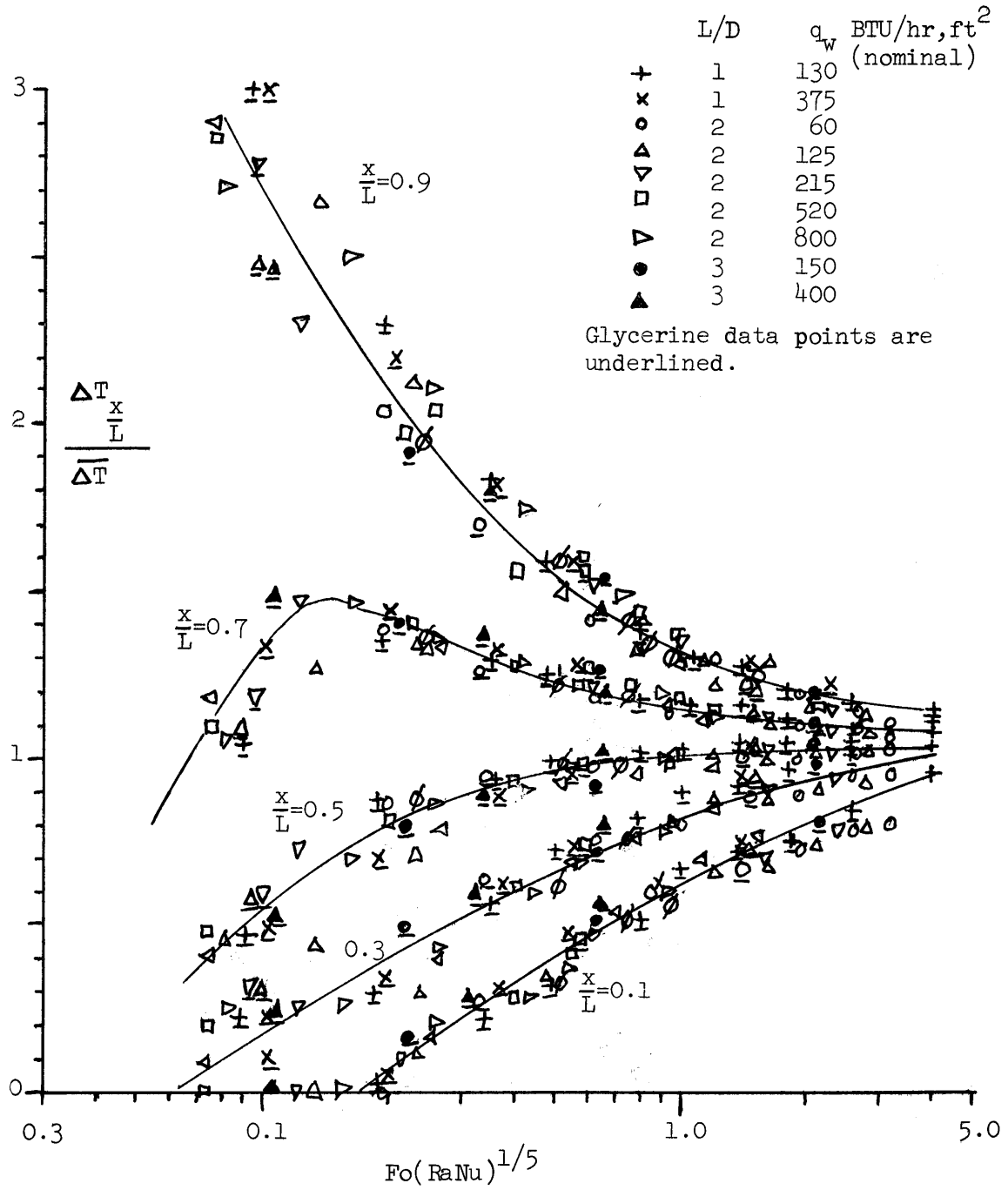

FIGURE 1-15

Normalized Transient Temperature Distribution for Fluid in a Vertical Cylinder with Constant Wall Heat Flux

Glycerine and 85% Glycerine Data

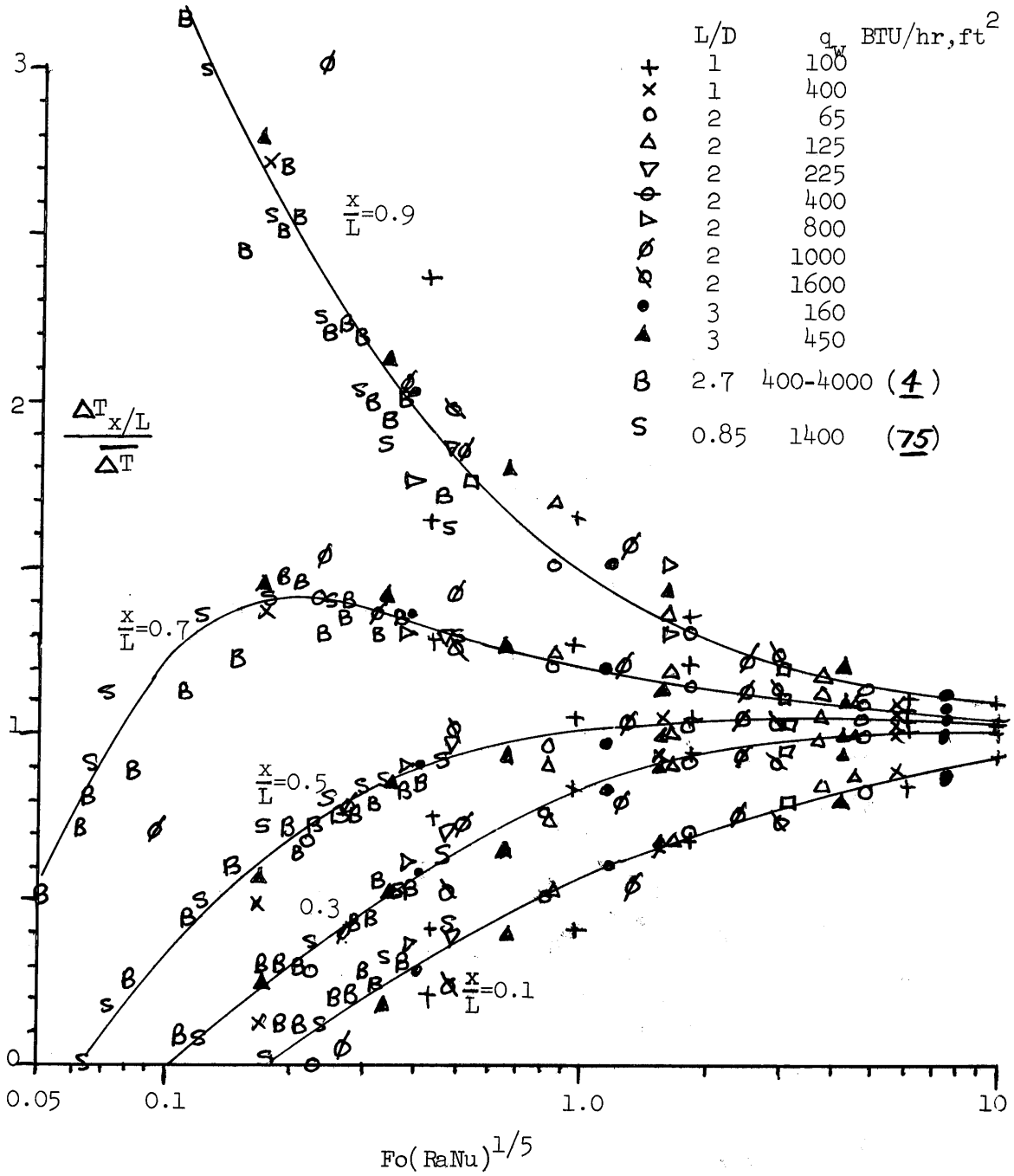

FIGURE 1-16

Normalized Transient Temperature Distributions for
Fluid in a Vertical Cylinder
with Constant Wall Heat Flux

Water Data

at $\frac{X}{L} = 0.1$ begins to rise, the constant core temperature gradient model, that was previously developed, becomes valid. Prior to this time, the temperature values are described by the fairly complicated differential equations for the boundary layer and the interaction between local core temperature gradients and the boundary layer energy variation.

A further result of interest is the behavior of the Nusselt number when a linear core temperature distribution is present. Using the values for limiting boundary layer energy,

$$\underline{\text{Laminar}} \quad (Nu)_a = 0.605\ (Ra)^{1/3} \quad \frac{d\theta_\infty}{dX}^{1/3} \tag{1-36}$$

As $\frac{d\theta_\infty}{dX}$ becomes small the limiting energy is achieved at distances further and further up the plate. This equation, therefore, becomes meaningless as $\frac{d\theta_\infty}{dX} \rightarrow 0$, since the boundary layer fluid never reaches a height great enough for the limiting solution to apply. However, for finite values of $\frac{d\theta_\infty}{dX}$, eq. 1-36 becomes valid at some finite height.

The one-third power dependence on the Rayleigh number is generally considered a characteristic of turbulent natural convection. However, this dependence evidently can occur for laminar natural convection if a core temperature distribution is present.

The model developed in detail and verified experimentally in this study is for the constant wall heat flux case. However, the equations for the boundary layer energy and momentum have also been developed, in differential form, for the constant wall temperature case. Because the core temperature behavior would be somewhat different in a constant wall temperature system, modification of the core model would be necessary before a simplified solution of the type presented for the constant wall heat flux case could be obtained. In such a system, the upper

region of the core would tend to fill with fluid at the wall temperature and limit the convective circulations to lower portions of the core. Finally the whole system would reach a final isothermal state in equilibrium with the wall temperature. However, numerical solution of the constant wall temperature equations in the manner suggested for computing initial temperature distributions for the constant wall flux case would also provide results for the constant wall temperature case.

G. Conclusions

Temperature distributions within fluids enclosed in vertical cylinders and subjected to a uniform side-wall heat flux may be estimated during the period shortly after the start of heating using Figures 1-15 and 1-16. A more accurate model involving numerical solution of two differential equations by successive iterations in space and time is suggested in part F. This more complex procedure might be justified for a particular system in which initial temperature distributions were of primary concern.

After the initial period, a model assuming a radially, well-mixed core with a linear axial temperature distribution permits use of the equation shown in Figure 1-7 to estimate the axial midpoint core temperature. Solution of the boundary layer equations for a heated-vertical plate with a core temperature variation, led to development of equations 1-29 and 1-35 for predicting axial core temperature gradients as functions of Prandtl, Fourier and Rayleigh-Nusselt numbers only.

H. Recommendations for Future Work

Further investigation of the mixing region below the surface, especially for various controlled surface conditions, would be useful. The effect of mass transfer at the interface is of particular interest in practical applications such as those involving boiling systems or self-pressurization of stored saturated liquid.

The boundary layer analysis conducted for the constant wall heat flux case and formulated for the constant wall temperature case in this study could be further developed for the latter case and extended to other systems. Solution of the boundary layer equations for various non-linear core temperature distributions would yield results which could be applied to other geometries such as spherical or conical tanks or even horizontal cylinders.

II. INTRODUCTION

A. Statement of the Problem

Transient natural convection circulations, occurring within vertical cylindrical tanks of fluid as a result of heat transfer through the side walls, often produce thermal stratification effects within the bulk fluid. The primary object of this study was to develop a model which would permit prediction of such temperature distributions as a function of known system parameters: fluid properties, tank size and geometry, and the variation in wall heat flux or temperature distribution as a function of time.

The results are applicable to a broad class of natural convection problems involving the heating and cooling of fluids, although for purposes of detailed analysis attention was concentrated on the system shown in Figure 2-1. Consider a vertical cylindrical vessel of diameter, D, and height, L, containing a fluid which is initially isothermal and motionless. At time, $t = 0$, a known heat flux or temperature distribution is suddenly imposed on the system boundaries.

In a cylindrical coordinate system, (r, θ, x), with the origin located at the center of the bottom surface of the enclosure, and with a gravitational force in the negative x-direction, the problem can be stated as:

Given: 1. Geometry L, D

2. Fluid properties μ, ρ, C_p, k, β

3. Initial Conditions

for $t = 0$, $0 \leq r \leq \frac{D}{2}$, $0 \leq x \leq L$, $0 \leq \theta \leq 2\pi$

$T = T_i = \text{constant}$

$\bar{V} = 0$

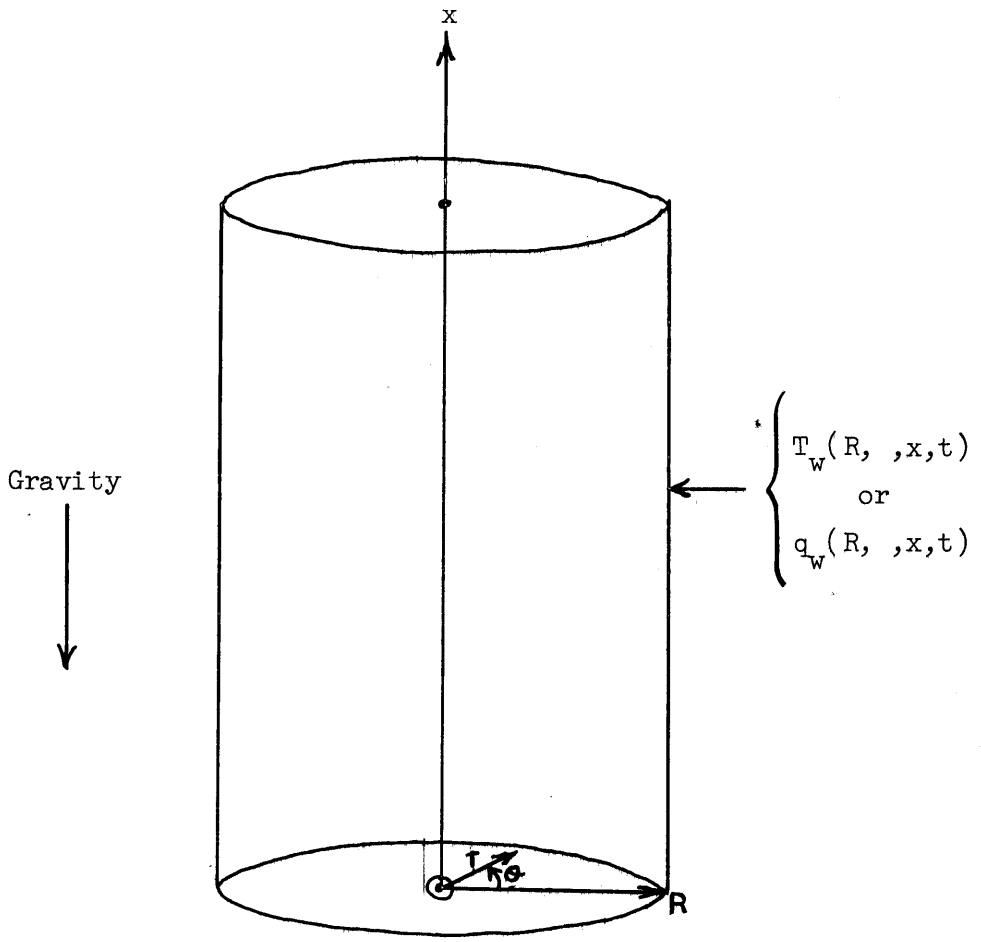

FIGURE 2-1

General Co-ordinate System for Analysis of

Natural Convection within a Vertical Cylinder

4. Thermal Boundary Conditions

for $t > 0$, $r = \frac{D}{2}$, $0 \leq x \leq L$, $0 \leq \theta \leq 2\pi$

$t > 0$, $0 \leq r \leq \frac{D}{2}$, $\begin{cases} x = 0 \\ x = L \end{cases}$, $0 \leq \theta \leq 2\pi$

Specify T_w or $\frac{dT_w}{dn}$ where n is the normal to the surface

5. Velocity Boundary Conditions

for $t > 0$, $r = \frac{D}{2}$, $0 \leq x \leq L$, $0 \leq \theta \leq 2\pi$

$0 \leq r \leq \frac{D}{2}$, $x = 0$, $0 \leq \theta \leq 2\pi$

$\bar{V} = 0$ (no slip at walls)

for $t > 0$, $0 \leq r \leq \frac{D}{2}$, $x = L$, $0 \leq \theta \leq 2\pi$

$\bar{V} = 0$ for bounded surface

$V_x = \frac{\partial V_r}{\partial x} = \frac{\partial V_\theta}{\partial x} = 0$ for free surface

Find: $T(r, \theta, x, t)$

$\bar{V}(r, \theta, x, t)$

Typical thermal boundary conditions are a specified constant wall temperature, a specified constant wall heat flux, or an adiabatic surface. The constant wall heat flux condition is often encountered for stored liquids when an outside heat transfer coefficient is controlling the energy flux to the system.

Based on a dimensional analysis using the Pi theorem (53) or from analysis of the differential equations for natural convection (Section II.C.3) using a method similar to that suggested by Hellums and Churchill (38), the important dimensionless groups which would appear in the general temperature and velocity field solutions are:

Grashof Number (Gr): $\frac{g\beta(\Delta T)L^3}{\nu^2}$

Prandtl Number (Pr): $\frac{\nu}{a}$

Fourier Number (Fo): $\frac{at}{ID}$

Aspect Ratio: $\frac{L}{D}$

Nusselt Number (Nu): $\frac{hL}{k}$

A remaining group, the thermal expansion modulus $(1 + \beta\Delta T)$, can usually be neglected since $\beta\Delta T \ll 1$ for most common natural convection systems.

The (ΔT) in the Grashof number and the above group is a characteristic temperature difference for the system. If wall temperature is specified, $\Delta T = T_w - T_i$; if wall heat flux is specified, the equivalent temperature difference is not known directly from the problem statement. However, since $q_w = h(T_w - T_i)$, the ΔT factor can be multiplied by the Nusselt number to give, $(\Delta T)(Nu) = \frac{q_w L}{k}$, which contains the known q_w boundary condition. This group can then be used as a characteristic system temperature in describing the system. (Note that it is not numerically equal to the actual overall temperature driving force but rather to the product of this difference and the Nusselt number.)

The Grashof number may be considered as an index of the natural convection intensity since it is a ratio of the buoyant and inertial forces driving the flow to the square of the viscous forces tending to retard the flow. The Prandtl number, a ratio of momentum diffusivity to thermal diffusivity, serves as a link between the temperature and velocity fields in the system.

Well established correlations for predicting steady-state natural

convection heat transfer coefficients (54) are of the form:

$$Nu = a(GrPr)^b. \qquad (2\text{-}1)$$

The product of the Grashof and Prandtl numbers, which appears frequently in natural convection analyses, is known as the Rayleigh number (Ra). The magnitude of the Rayleigh number has been found to be an index for the type of natural convection flow regime in a particular system. (54)

$\underline{Ra < 10^3}$

Conduction is the primary mode of heat transfer and convective effects are either very weak or even may be totally supressed in the case of fluid above a heated, infinite horizontal plate. (64, 68, 74)

$\underline{10^3 < Ra < 10^8 \text{ to } 10^9}$

The flow is laminar.

$\underline{Ra > 10^8 \text{ to } 10^9}$

In this range, the flow becomes sufficiently strong to undergo a transition to turbulence.

For fluids near a phase transition temperature, the problem may be further complicated by phenomena such as boiling, freezing or condensation.

Experimental and analytical studies of natural convection phenomena are numerous, especially for predicting over-all heat transfer coefficients; some works present temperature distributions for steady-state conditions and for a number of special configurations such as vertical and horizontal flat plates and long, narrow vertical slots. However a general model to describe natural convection within a completely enclosed fluid has apparently not been developed previously for any geometry.

Although the relationships between the dependent temperature and velocity variables may be expressed in partial differential form using equations for conservation of energy, mass and momentum, the resulting system of nonlinear partial differential equations is too complex to be solved in closed analytical form except for a few special cases, in which major simplifications can be made. Even for very simple geometries, direct numerical solution of the general equations has been found by Hellums (36), Wilkes (103), Barakat (5) and Maahs (50) to require excessive amounts of computation time in terms of present day computers and meaningful solutions have been obtained only for very low energy input levels. Therefore, the approach to the problem was to conduct an extensive experimental program in which detailed temperature field measurements were obtained and qualitative flow patterns were observed for a wide range of conditions. Evaluation of these experimental results would be used to indicate certain simplifications which could reduce the general partial differential equations describing energy and momentum transfer in the system to forms allowing development of a theoretical solution for the transient temperature field.

The aim of this study was to develop such a model, covering a broad range of fluid properties and thermal perturbations at the wall and including both the laminar and turbulent flow regimes. The resulting model would be in a form of use to an engineer confronted with a practical application for which the localized temperature distribution in an enclosed fluid must be delineated.

B. Important Applications

Many engineering problems in natural convection involve only the prediction of over-all heating (or cooling) rates for a stored fluid. For practical design purposes, natural convection heat transfer coefficients may be estimated reasonably well using existing correlations. However, there are a number of more complex problems in which actual internal temperature distributions must be known.

A typical application, which has recently aroused much interest, is the problem of thermal stratification within cryogenic propellant storage tanks as a result of ambient heat leak, produced by outside conditions ranging from still air surroundings to aerodynamic heating. Since the cryogen is usually stored at or slightly below its boiling point, the temperature of the surface layer of liquid has a strong effect on the system pressure. Also, the surface temperature is a major factor in estimating amounts of external pressurizing gas required for pressurized transfer of liquid from the vessel. For pump transfer systems, the liquid must be subcooled (at the tank pressure) to prevent cavitation in the pump. Regions of warm fluid in the storage vessel may easily lead to vapor binding and failure of the pumping system. Since most of these problems are associated with airborne systems, the penalties for over-design are such that it is necessary to determine actual transient temperature distributions in the liquid.

Similar to the cryogen storage problem is the more general problem of boiling (or freezing, if the cooling case is considered) a liquid by heating at the walls. The temperature distribution in the liquid just before the onset of phase change will determine the regions where boiling will begin. In many cases, this region will be adjacent to the

boundary where the external heat transfer occurs. However, natural convection may carry the warm boundary fluid to another portion of the system where bulk boiling may occur. The location of the region of maximum temperature in the bulk is important in determining the degree of superheating before boiling occurs; the original natural convection circulation may be strongly related to the circulation in the presence of boiling. Although phase changes are not included in the scope of this study, the quantitative description of temperature and velocity fields at incipient phase change is a major and necessary step in the solution of the general problem.

Natural convection is used for mixing in certain processes such as maintaining stored crude petroleum products in a liquid state by localized heating.

Still another area of interest in detailed natural convection circulations has grown out of problems associated with convective cooling in nuclear reactors. In mobile fuel reactors, convection in liquid metals is of concern. In other systems, convection cooling of cores is accomplished with more conventional fluids. Since natural convection cooling may be the only means of emergency cooling in case of pump failure, a detailed knowledge of temperature fields and especially of "hot spots" is required. In many of the nuclear reactor systems, internal heat generation in the fluid must also be considered.

C. General Theoretical Basis

1. Energy and Momentum Equations

A general description of a natural convection system behavior is given by the energy equation, the continuity equation, the three-dimensional momentum equations and appropriate initial and boundary conditions. The Navier-Stokes equations, presented in complete form by Schlicting (83) and others, express the balance on the rate of change of momentum in a fluid system. Consider again a velocity vector, $\bar{V}(r, \theta, x, t)$, and a scalar temperature field, $T(r, \theta, x, t)$, inside a cylinder of fluid as shown in Fig. 2-1. The velocity vector has components V_r, V_θ and V_x in the r-, θ-, and x-directions respectively. Based on the a priori knowledge of experimental observations showing that the flow is radially symmetrical in the vertical cylindrical configuration studied, angular variation is neglected and the two-dimensional system equations may be written as:

$$\text{Continuity} \qquad \frac{\partial \rho}{\partial t} = \nabla \cdot \rho \bar{V} \tag{2-2}$$

$$\text{Energy} \qquad \frac{DT}{Dt} = \alpha \nabla^2 T \tag{2-3}$$

$$\text{Momentum} \qquad \frac{DV_r}{Dt} = -\frac{1}{\rho}\frac{\partial P}{\partial r} + \nu \nabla^2 V_r \tag{2-4}$$

$$\frac{DV_x}{Dt} = g - \frac{1}{\rho}\frac{\partial P}{\partial x} + \nu \nabla^2 V_x \tag{2-5}$$

$$\text{where} \quad \frac{D}{Dt} = \frac{\partial}{\partial t} + V_r \frac{\partial}{\partial r} + V_x \frac{\partial}{\partial x}$$

$$\text{and} \quad \nabla^2 = \frac{\partial^2}{\partial r^2} + \frac{1}{r}\frac{\partial}{\partial r} + \frac{\partial^2}{\partial x^2}$$

The pressure variation in the x-direction is assumed equal to the initial

hydrostatic pressure distribution and small pressure variations due to convective phenomena are neglected.

$$\frac{\partial P}{\partial x} = g\rho_o \tag{2-6}$$

$$\frac{\partial P}{\partial r} = 0 \tag{2-7}$$

The variation of fluid density with temperature can be approximated by

$$\rho = \frac{\rho_o}{1 + \beta(T - T_o)} \quad . \tag{2-8}$$

Fluid viscosity has been assumed constant in equations 2-4 and 2-5, since momentum changes due to viscosity variation are negligible in comparison with changes produced by variations in the velocity field. By similar reasoning, density variations can be neglected <u>except</u> in the body force term which provides the basic convective driving force. Consequently, the fundamental equations commonly used to describe a radially symmetrical, natural convective flow are:

<u>Continuity</u>: $$\nabla \cdot \bar{V} = 0 \tag{2-9}$$

<u>Energy</u> $$\frac{DT}{Dt} = \alpha_o \nabla^2 T \tag{2-10}$$

<u>Momentum</u> $$\frac{DV_r}{Dt} = \nu_o \nabla^2 V_r \tag{2-11}$$

$$\frac{DV_x}{Dt} = g\beta_o(T - T_o) = \nu_o \nabla^2 V_x \tag{2-12}$$

These equations are valid for laminar flows, but not necessarily for turbulent flows. Unless the turbulence is essentially isotropic, the three-dimensional coordinate system analysis must be used. In

addition, the equations must either be applied within the turbulent micro-scale considering the distribution of eddy sizes and the turbulent frequency spectrum or else they must be interpreted in terms of averages taken over the turbulent fluctuations. Average field values might be predicted by the latter method if suitable momentum and thermal diffusivity parameters, which include eddy transport effects, can be specified.

Further modifications are required for special problems such as those involving additional body forces (MHD flows, for example, or systems in which there is an acceleration field other than normal gravity), internal heat generation (fluids undergoing nuclear or chemical reaction), or "non-thermal" density variations (reacting fluids or systems involving mass transfer effects).

2. Boundary Conditions

Initial Conditions: Temperature and velocity fields are completely specified at time t = 0. Usually the condition of interest is that the fluid is initially isothermal and motionless.

Velocity Boundary Conditions: Fluid velocity is zero at the surface of all bounding walls. This is the familiar "no-slip" condition. In a liquid system a free surface may be present. For a free surface the shear stress is assumed negligible along the boundary and there is no flow across the boundary. The boundary conditions, in the previously defined coordinate system (Fig. 2-1), are $V_x = 0 = \frac{dV_r}{dx}$.

Thermal Boundary Conditions: Either the temperature or the temperature gradient normal to the surface, or some relation between the two, must be specified along all system boundaries. No temperature discontinuity is permitted across the wall-fluid interface if only conductive and

convective heat transfer modes are present. Examples of commonly encountered boundary conditions are a constant wall temperature, a constant wall heat flux $q_w = k \left.\frac{dT}{dr}\right|_{r = \frac{D}{2}}$, or a perfectly insulated surface.

3. Dimensionless Equations

A convenient non-dimensional form of the equations results from substitution of a new set of variables following a technique used by Hellums and Churchill (38), Wilkes (103) and others:

$$X = \frac{x}{L} \qquad R = \frac{r}{L}$$

$$V_R = \frac{V_r L}{\nu_o} \qquad V_X = \frac{V_x L}{\nu_o} \tag{2-13}$$

$$\tau = \frac{\alpha_o t}{L^2} \qquad \theta = \frac{g\beta_o (T - T_o) L^3}{\nu_o \alpha_o}$$

The dimensionless equations are:

Continuity: $$\frac{\partial V_R}{\partial R} + \frac{V_R}{R} + \frac{\partial V_X}{\partial X} = 0 \tag{2-14}$$

Energy: $$\frac{D\theta}{D\tau} = \nabla^2 \theta \tag{2-15}$$

Momentum: $$\frac{DV_R}{D\tau} = Pr \nabla^2 V_R \tag{2-16}$$

$$\frac{DV_X}{D\tau} = \theta + Pr \nabla^2 V_X \tag{2-17}$$

The formulation of the problem for a constant wall heat flux case would involve multiplying the temperature parameter, θ, by the Nusselt number. If all terms in equations 2-15 to 2-17 are multiplied by the Nusselt number, note that the natural temperature parameter for the constant wall heat flux is $Nu\theta$ or the Rayleigh-Nusselt number (RaNu).

The initial and boundary conditions for a constant wall heat flux, q_w, an insulated bottom, and a free surface at x = L become, in dimensionless form:

$$\underline{\text{Initial}}: \quad \tau = 0, \quad 0 \le R \le \frac{D}{2L}, \quad 0 \le X \le 1$$

$$\theta = 0 \quad \text{isothermal}$$

$$\left.\begin{aligned} V_r &= 0 \\ V_x &= 0 \end{aligned}\right\} \quad \text{motionless} \tag{2-18}$$

$$\underline{\text{Thermal}}: \quad \tau > 0, \quad R = \frac{D}{2L}, \quad 0 \le X \le 1$$

$$\frac{\partial \theta}{\partial R} = -(RaNu) \quad \text{specified wall heat flux} \tag{2-19}$$

$$\tau > 0, \quad 0 \le R \le \frac{D}{2L}, \quad X = \begin{cases} 0 \\ 1 \end{cases}$$

$$\frac{\partial \theta}{\partial X} = 0 \quad \text{adiabatic}$$

$$\underline{\text{Velocity}}: \quad \tau > 0, \quad R = \frac{D}{2L}, \quad 0 \le X \le 1$$

$$\tau > 0, \quad 0 \le R \le \frac{D}{2L}, \quad X = 0$$

$$V_X = V_R = 0 \quad \text{(no slip)}$$

$$\tau > 0, \quad 0 \le R \le \frac{D}{2L}, \quad X = 1 \tag{2-20}$$

$$V_X = 0 \quad \text{(no flow)}$$

$$\frac{\partial V_R}{\partial X} = 0 \quad \text{(no shear)}$$

Examination of the non-dimensional equations and boundary conditions shows that they contain the important natural convection parameters mentioned in Part II.A.1, namely:

θ = dimensionless temperature = GrPr

τ = dimensionless time = Fo $(\frac{D}{L})$

Pr = Prandtl number

Had the system been analyzed using dimensional analysis, the same result would be obtained, namely that the solution to the constant wall heat flux case should be of the form $\theta = f(\tau, R, X)$ with parameters Pr, $\frac{L}{D}$, and (RaNu).

4. Transient Solutions

The natural convection system equations 2-15 through 2-17 describe the transient behavior of the temperature and velocity fields. Consider the case of an isothermal, stagnant fluid in a tank suddenly subjected to a wall heat flux. Since $\overline{V} = 0$ at time $t = 0$, at this instant the fluid has no momentum and heat is transferred to the fluid by thermal conduction. There is an initial transient interval, which will be referred to as the starting transient, that exists briefly until the fluid inertia is overcome and convective flow is established as a result of unstable density gradients produced by the initial conductive heat transfer. For the range of conditions investigated, starting transients of about one to five seconds duration would be anticipated.

Long-term transients produced by time and spatial variation in convective temperature and velocity fields, by variation of fluid properties with temperature, or by variation in thermal boundary conditions are of primary concern in this study. For an enclosed system perturbed by a step change in wall temperature, the transient would consist of the development and eventual decay of a convective circulation until the

fluid approached a final isothermal state with a uniform temperature equal to the imposed wall temperature. If the initial thermal perturbation is a step change in wall heat flux, the system temperature will continue to rise indefinitely. An ideal "quasi-steady-state" for such a system would be development of a steady-state velocity field and of a temperature field increasing linearly with time. Since real fluids have properties which vary with temperature and heated liquids eventually reach their boiling point, such an ideal quasi-steady-state is never achieved in practice although it may be approximated if the time scale of the transients becomes long compared to the time scale of interest to the observer.

D. Previous Approaches to Solution

1. Direct Solution by Finite Difference Approximation

The partial differential equations for two-dimensional natural convection may be transformed into a set of finite difference equations. In order to obtain a valid numerical solution to the difference equations, certain conditions must be satisfied. First, the time and space grids used for the stepwise numerical calculation must be of sufficiently fine grain to give results which converge toward the exact solution of the differential equations. In other words, further reduction of the calculational grid size should not produce major changes in the calculated values of the dependent variables. In addition, certain stability criteria must be satisfied to ensure against amplification of errors which are inherent in any approximate solutions.

Hellums (36) succeeded in obtaining a numerical solution for convection along a constant temperature vertical plate and for inside a horizontal cylinder with the opposite halves of the cylindrical walls maintained at different temperatures. Computations were performed for a Prandtl number corresponding to that of air. Even at low values of Prandtl number and Grashof number, his numerical computation time required (on an IBM 704 computer) to reach a steady-state solution was much longer than the real transient period in the corresponding physical system. Also, although his computed steady-state temperature fields compared quite well with some experimental data (53), there was enough uncertainty in the experimental thermal boundary conditions and velocity measurements to prevent a critical comparison of the data with Hellum's computed results.

Wilkes (103) numerically solved the problem of natural convection in a rectangular box with one vertical wall hot and the other cold.

Using a formulation with the stream function and vorticity as flow variables, he successfully computed transient temperature fields and streamlines. The steady-state solution compared closely with that predicted by Poots (72) who used the method of orthogonal polynomials to find a steady state solution for the same system. Poots' method failed above $Ra = 10^4$; Wilkes' computation became unstable above Ra = 200,000.

Deardorff (12) considered transient energy and vorticity transport between two parallel plates for a number of different boundary conditions using a numerical iterative involving three time levels. Computation times to obtain meaningful solutions were excessive except for very slow convective flows.

Barakat (4), using the same basic formulation and combinations of forward and backwards differences depending on the sign of the velocity components, was able to achieve stable solutions for convection inside a heated vertical cylinder at very high Rayleigh numbers (into the turbulent regime), but computation times were very long and convergence was not achieved in regions where temperature and velocity gradients were steep, i.e. near the walls, in the upper and lower corners. In order to obtain an accurate solution, computation times would be exhorbitant on any present day computer as Barakat himself noted (5).

Maahs (50), in a study of convection in horizontal cylinders, carefully evaluated several different finite difference schemes and concluded that the general two-dimensional transient natural convection problem could probably not be solved satisfactorily without computers significantly faster than the IBM 709.

Noble (60) has contributed a number of improvements to numerical solution of the energy and vorticity transport equations, but computation

times for high Grashof and Prandtl number cases still appear to be excessive.

Fromm (34), using a "particle-in-cell" method has demonstrated the potential of numerical solution of the Navier-Stokes equations by the computation of Kármán vortex streets using a Stretch computer. However, until improved methods and faster computers are developed, direct numerical solution of the natural convection equations even in two-dimensions appears to be of very limited practical usefulness.

2. Transforms and Series Solutions

A number of other solution techniques for the natural convection equations have been suggested. Bhutani (7) treated the problem of a vertical cylinder with a constant wall temperature (with no radial momentum transfer) using Laplace transforms and obtained a solution in terms of Mathieu functions. Liu (49) used the method of orthogonal polynomials to obtain a steady-state solution to the problem of convection in an annulus. Poots (72) also used this method, but was able to get satisfactory results only at such low heat fluxes that conduction rather than convection was controlling. Sugawara (100) used a successive approximation method to solve the two-dimensional equations for a vertical wall. His initial approximation was the known solution to the Fourier heat conduction equation. However, Siegel (92) questions these results on the basis that it is not certain that the second approximation converges to the steady-state solution at long times.

Siegel (92) approached the same "heated vertical wall in an infinite fluid" problem using a boundary layer formulation which he solved for the starting transient and the steady-state by the method of characteristics.

Illingworth (40) obtained a solution to the same problem in terms of Bessel functions. Schetz and Eichhorn (82) and Menold and Yang (56) used Laplace transforms in similar independent analyses of the problem.

3. Boundary Layer Solutions

a. Creeping Flow

Further simplification of the natural convection equations is possible if boundary layer flow is assumed. Schmidt and Beckmann (85), using Pohlhausen's (71) approach, suggested a model for natural convection flow along a heated vertical element (Figure 2-2) in which it is assumed that:

1. There is no momentum transfer in the y-direction
2. Flow is steady
3. Flow is slow enough so that $\frac{\partial^2 u}{\partial x^2}$, $\frac{\partial^2 T}{\partial x^2}$ and $\frac{\partial P}{\partial x}$ may be neglected (creeping flow)

These assumptions yield a set of ordinary differential equations:

$$\frac{du}{dx} + \frac{dv}{dy} = 0 \tag{2-21}$$

$$\alpha \frac{d^2T}{dy^2} = 0 \tag{2-22}$$

$$\frac{d^2u}{dy^2} = -g\beta(T - T_o) \tag{2-23}$$

From the nature of the assumptions, it is evident that this model is not suitable as a description of two-dimensional flows, such as at the leading edge of a vertical plate. It also proves to be inaccurate at distances far from the plate in the y-direction and for rapid flows. The solution is, however, fairly good for viscous fluids, since they exhibit creeping flow behavior over a wide range of convective conditions.

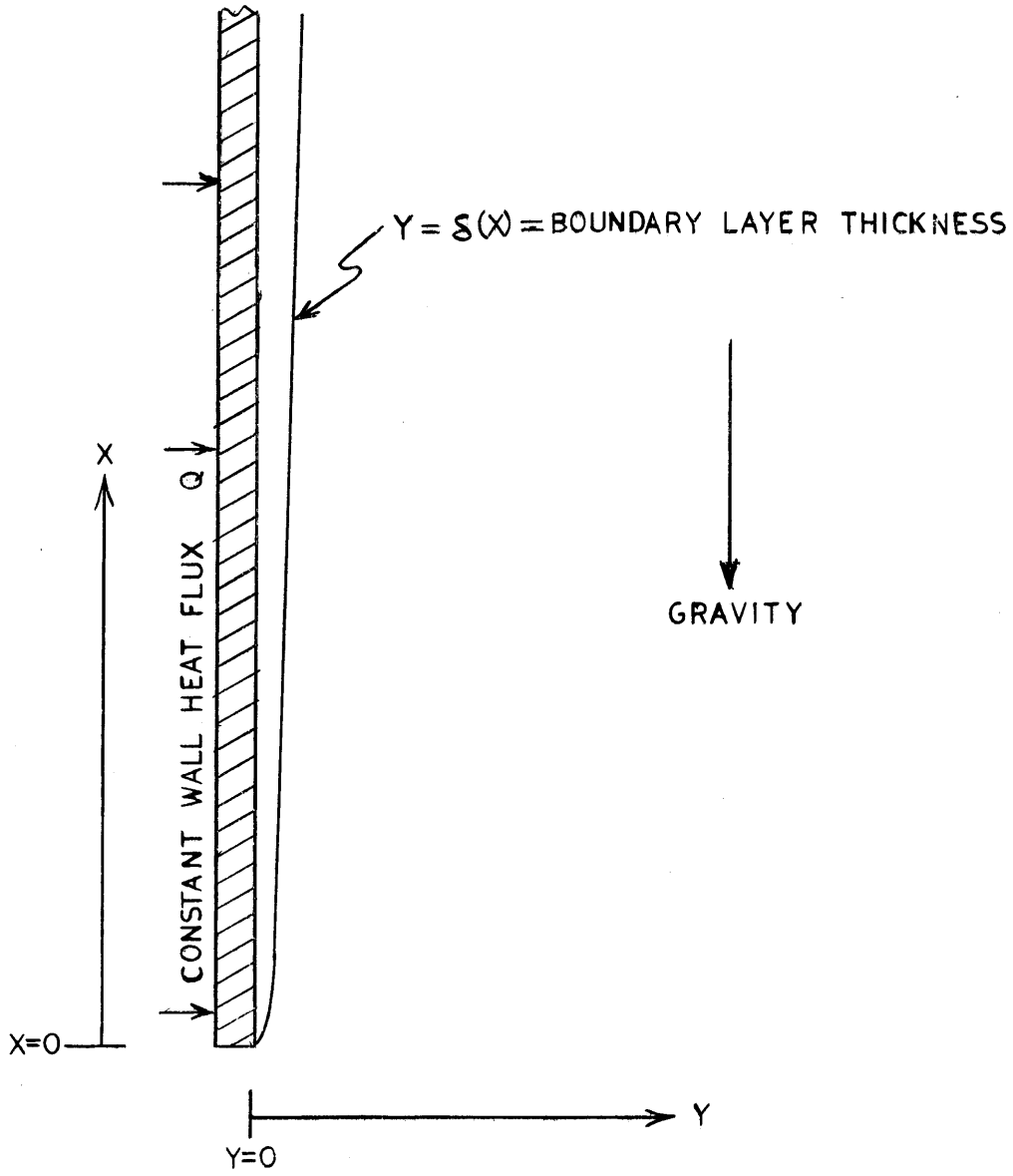

FIGURE 2-2
MODEL FOR BOUNDARY LAYER FLOW
ALONG VERTICAL HEATED PLATE

The original solution to this set of equations was made by a series approximation.

b. Kármán-Pohlhausen and Similarity Solutions

A more general boundary layer solution, without the assumption of creeping motion, can be obtained if a boundary layer temperature and velocity profile are assumed. Pohlhausen (71, 83) applied this technique to the case of forced convection past a flat plate. He assumed a boundary layer thickness, δ, and expressed the velocity profile as a fourth order power series in $(\frac{y}{\delta})$. The four arbitrary constants in the power series were found by specifying four boundary conditions and an integrated continuity equation was used to estimate δ. The profile was assumed constant and only δ varied with distance. Consequently, the integrated velocity profile was expressed as the product of a constant and a function of δ in the momentum equation.

Lighthill (47) extended this technique to natural convection problems by assuming an appropriate boundary layer temperature profile and using its integrated value in the energy equation.

A further refinement is merely to assume that, with a choice of "similar" co-ordinates, a constant profile does exist. Pohlhausen also showed that the boundary layer equations for steady-state natural convection near a vertical flat plate at constant temperature

$$\frac{\partial u}{\partial x} + \frac{\partial v}{\partial y} = 0 \tag{2-24}$$

$$u \frac{\partial u}{\partial x} + v \frac{\partial u}{\partial y} = \nu \frac{\partial^2 u}{\partial y^2} + g\beta(T - T_o) \tag{2-25}$$

$$u \frac{\partial T}{\partial x} + v \frac{\partial T}{\partial y} = \alpha \frac{\partial^2 T}{\partial y^2} \tag{2-26}$$

can be transformed by assuming

$$\eta = c\,\frac{y}{\sqrt[4]{x}}\,, \qquad = 4\nu c\, x^{3/4}\, \xi(\eta) \tag{2-27}$$

where $c = \sqrt[4]{\dfrac{g\beta(T - T_o)}{4\nu^2}}$

to differential equations in η, $\xi(\eta)$, and $\theta_s(\eta)$ where $\theta_s = (T - T_o)/(T_w - T_o)$.

$$\xi''' + 3\xi\xi'' - 2(\xi')^2 + \theta_s = 0 \tag{2-28}$$

$$\theta_s'' + 3(Pr)\,\xi\,\theta_s' = 0 \tag{2-29}$$

with boundary conditions

$$\left.\begin{matrix}\xi = \xi' = 0 \\ \theta_s = 1\end{matrix}\right\}\ \eta = 0 \quad \text{and} \quad \left.\begin{matrix}\xi' = 0 \\ \theta_s = 0\end{matrix}\right\}\ \eta = \infty . \tag{2-30}$$

The profiles can be computed at a given value of Prandtl number by various iterative methods which allow selection of values of $\xi''(0)$ and $\theta_s'(0)$ that produce results satisfying the boundary conditions at $\eta = \infty$. Smith (93) has recently developed interpolation schemes which permit estimation of $\xi''(0)$ and $\theta'(0)$ for any Prandtl number.

Similarity velocity and temperature profiles for low Prandtl number fluids, namely liquid metals, were recently published by Chang (9).

4. Experimental Analyses

a. Vertical Flat Plate

The case of convection from a heated, semi-infinite plate immersed in an infinite fluid has also been thoroughly investigated in the

laboratory. In 1930, Schmidt and Beckmann (85) published their experimental results and compared them with the "creeping-flow" boundary layer model they also developed. The model proved to give accurate estimates of heat transfer coefficients along the plate, although it was poor in the vicinity of the leading edge of the plate.

Jakob (42) used data obtained by Mull and Reiher (58) and others to test the simplified relationships:

$$Nu = a(Ra)^b \tag{2-31}$$

$$\text{laminar:} \quad b = \frac{1}{4}$$

$$\text{turbulent:} \quad b = \frac{1}{3}$$

for parallel, vertical plates which were spaced far enough apart to prevent interaction of their boundary layers. Saunders (78, 79) obtained heat transfer coefficients for water, mercury and high pressure air which agreed with the empirical relationship (2-31). Transition to turbulence was observed at about $Ra = 10^9$. Klei (45) measured transient heat transfer coefficients along a flat vertical plate. Systems of parallel vertical plates also were studied experimentally by Schwind and Vliet (86), and by Elenbaas (22), whose results were analyzed by Bodoia and Osterle (8) using a boundary layer model. Eckert and Carlson (16) studied convection between one heated and one cooled vertical wall. They measured a linear vertical temperature distribution in the mid-region and found that, even for an observed laminar flow, the Nusselt number varied with the 0.3 power of the Rayleigh number. The authors attributed the unusual dependence to the non uniform core temperature distribution. Elder (20, 21) conducted an extensive experimental and theoretical study of convection in a long, narrow vertical slot. He presents interesting

photographs of tracers which show a main boundary layer circulation and superimposed secondary cellular circulations. Other velocity studies were made by Goldstein (29) who used an interferometer to study the boundary layer on a uniformly heated vertical plate and by Eichhorn (19) who used a tellurium dye method to observe boundary layer flow along a heated cylinder submerged in water. These studies all indicate the presence of a natural convection boundary layer and in many cases give results which may be predicted from a boundary-layer analysis.

b. Heated Vertical Cylinder Open at Top to Reservoir of Cooled Fluid

This system, Figure 8-2, has been studied in detail because of its applicability to the convective cooling of turbine blades. As mentioned in Part 3b. of this section, Lighthill (47) used a von Kármán-Pohlhausen method to analyze the system. Qualitatively he found that a boundary layer model applies until the system height and heating rate are large enough to give a boundary layer thickness equal to the cylinder radius at the entrance to the reservoir. At this point, cool fluid from the reservoir cannot flow freely into the core of the tube. Experimental measurements of heat transfer coefficients for this system by Martin and Cohen (52) indicated that Lighthill's laminar models were reasonably valid for predicting heat transfer rates to air, water, and high viscosity fluids such as glycerin. They observed a temporary decrease in heat transfer coefficient with increasing Rayleigh number in a range close to that at which the model boundary layer would fill the tube.

Hartnett and Welsh (35) also studied this system. They obtained data for the constant wall heat flux case and presented arguments ex-

plaining why the Nusselt numbers for the constant heat flux case should be about the same as those for the constant wall temperature case at equivalent Rayleigh numbers. It was shown analytically that this result would be anticipated for all fluids except those having very small Prandtl numbers, e.g. liquid metals.

Larson and Hartnett (46) subsequently obtained data for mercury in the same system. Their Nusselt number data were not correlated by the usual Rayleigh number relationship, as previously anticipated for a low Prandtl number fluid which would tend to have a thin thermal boundary layer limiting development of a normally thicker momentum boundary layer.

c. Totally Enclosed Cylinder

Convection inside long, narrow heated vertical tubes (L/D = 12) was investigated by Foster (25) who measured heat transfer coefficients higher than those reported by Martin and Cohen (52) for an equivalent system fed at the top with cool fluid. The discrepancy probably can be attributed to a difference in core temperature distributions in the two systems. Pchelkin (70) also obtained heat transfer coefficients for a long vertical tube containing fluid subjected to a constant heat flux. Ostroumov (67) studied this system in terms of the Rayleigh number required to initiate over-all convective flows in both vertical and slanted configurations.

Studies at lower aspect ratios, which are in the same range as those considered in the present work and which correspond to tank configurations with boundary layers much thinner than tank radius, have been considered by several investigators at M.I.T. Evans and Stefany (23, 99) measured transient over-all heat transfer coefficients using a fluid expansion technique for horizontal and vertical cylinders filled completely with liquid and subjected to a step change in wall temperature. They observed that the heat transfer coefficient remained essentially constant during most of the transient period and data from both heating and cooling tests were described by the usual empirical relationship for laminar natural convection: $Nu = .55(Ra)^{1/4}$.

Siefkes (91) obtained some temperature measurements in a constant wall heat flux system. His data, for water and ethylene glycol at a single heat flux level in each case, have been evaluated along with the more extensive data obtained in this study and are presented in Chapter IV.

In student laboratory projects, Sandel (77) observed boundary layer

flow and found no radial temperature gradients in a similar liquid system; Cooper (10) obtained some additional heat transfer coefficient data. Another project by Dickey (14) involved the use of circumferential baffles to interrupt liquid boundary layer flow up the walls of a heated vessel. The idea was to reduce stratification by diverting the boundary layer into lower regions of the core fluid. The baffles, in the form of flat annular rings (Figure 2-3) wer cemented to the tank walls. The baffles, which extended distances of $\frac{1}{8}$ -, $\frac{1}{4}$ -, and $\frac{7}{8}$ - of the radius of the cylinder, were studied sequentially and were located midway up the vertical wall. The boundary layer flow merely was diverted around the smallest baffle. With the medium baffle, the temperature differential between the top and bottom of the core was reduced by 14%; with the large baffle, by 30%. Still larger reduction (34%) was obtained using two baffles in the system at the same time. The use of baffles to reduce stratification appears reasonable, but it is significant that a fairly wide baffle (filling about the outer one-quarter of the system radius) is required to divert the boundary layer sufficiently to cause mixing with core fluid.

Some additional temperature data in a system corresponding to the one studied by the author were obtained by Barakat (4) at the University of Michigan to complement an attempt to solve the two-dimensional natural convection equations numerically. His data are for only about the first four minutes after the start of heating, since this was the maximum time scale of his computed results. His data are evaluated in Chapter IV, along with the data from this study. Barakat used a 4-in. diameter vessel which provides an additional check on diameter effects since both Seifkes (91) and the author studied systems nominally 8-in. in diameter.

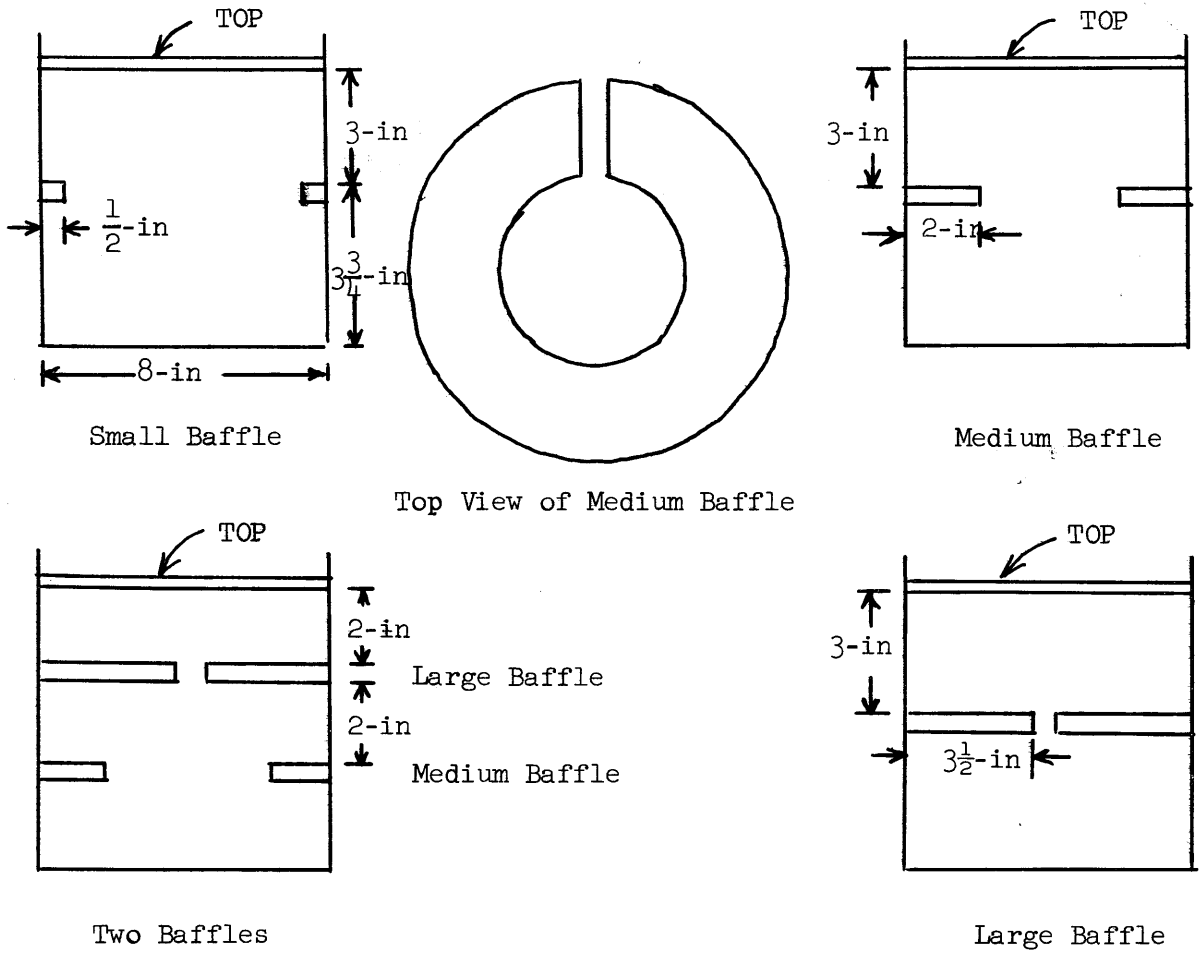

FIGURE 2-3

Baffle Arrangements in Boundary Layer Diversion Experiments

(Dickey et al, 14)

The problem of stratification in cryogenic storage vessels has prompted a number of studies in which limited center-line temperature measurements from large-scale systems have been evaluated.

Bailey (3) proposed a model based on an upper isothermal stratified layer which increased in thickness with time. He notes that experimental data indicate a nearly linear variation in core temperature with depth rather than the step change in temperature at the bottom of the stratified layer, predicted by his model. Neff (59) and Ruder (72) consider a model in which a Gaussian type core temperature distribution is assumed. This model provides better qualitative agreement with data than the step-change model of Bailey but is again empirical and is conveniently applicable only during the period before warm fluid reaches the bottom of the vessel. Arnett (1) recently has presented a model in which a vertical tank with a conical upper section is analyzed using a vertical plate boundary layer model and assuming a stratified region in the upper conical section. Numerical solution of the equations is required and the model is based on the assumption that the boundary layer decays completely in traversing the layer. Since the analysis is completely theoretical, the validity of the various assumptions in the model apparently remains unchecked by experimental observations.

Most available data obtained from measurements of center-line temperature in large cryogenic propellant tanks are only semi-quantitative because of uncertainties in actual wall heat flux and major effects due to unknown surface conditions produced by boiling of saturated surface fluid or by possible condensation of vapor in suddenly pressurized systems. One carefully controlled experimental study has been reported by Segel (87) who conducted careful experiments with liquid hydrogen.

Although boiling occurred in his system, boiloff gases were metered so that the effect of surface boiling can be quantitatively evaluated. His results will be discussed further in Chapter V in terms of the convection model developed in the present work.

E. Theory for Classical Vertical Plate Boundary Layer Model

Natural convection boundary layer flow up a semi-infinite heated vertical flat plate immersed in an infinite fluid is one of the classical problems in fluid mechanics. (Figure 2-2) Sparrow (96) has presented an extensive analysis of the problem for laminar boundary layer flow including both variable temperature and heat flux distributions along the plate in the vertical direction. He obtained approximate solutions to the boundary layer equations by utilizing the von Kármán-Pohlhausen (71) integral technique discussed in Section IIE. Subsequently, Sparrow and Gregg (98) re-solved the constant wall heat flux case, obtaining exact solutions to the boundary layer equations by using a similarity transform (Section II.D.3).

Of particular interest was their conclusion that this "exact" solution gave results only slightly different from the approximate von Kármán solution which Sparrow had developed previously.

A similarity solution for laminar natural convection along an isothermal heated plate was obtained by Ostrach (61). His results also may be approximated by a von Kármán solution using the same type of velocity and temperature profiles which were assumed by Sparrow.

Also of interest is the solution to the same problem for turbulent natural convection. Starting with the same set of boundary layer equations, Eckert and Jackson (18) assumed velocity and temperature profiles appropriate to a turbulent boundary layer. In addition, they used an empirical relation for the turbulent shear stress along the plate. The Reynolds analogy, which couples the turbulent momentum and heat transfer rates, permits the wall heat flux to be computed for a specified value of wall temperature.

To gain insight into natural convection boundary layer flow, consideration of the von Kármán integral method solutions for the various cases is helpful. Although a general treatment of the problem would allow an arbitrary wall temperature distribution (63, 96) , for sake of comparison only four specific cases are considered:

a. Laminar Flow, constant plate temperature

b. Laminar Flow, constant plate heat flux

c. Turbulent Flow, constant plate temperature

d. Turbulent Flow, constant plate heat flux

For the system shown in Figure 2-2, the boundary layer equations in integral form are:

$$\underline{\text{Energy}} \qquad \frac{\partial}{\partial x}\int_0^\infty u(T - T_\infty)dy = \frac{q}{\rho c_p} \tag{2-32}$$

$$\underline{\text{Momentum}} \qquad \frac{\partial}{\partial x}\int_0^\infty u^2 dy = \beta g\int_0^\infty (T - T_\infty)dy - \frac{\tau_w}{\rho} \tag{2-33}$$

For all cases, the fluid velocity at the wall and at infinity is zero and the temperature at infinity remains constant at a specified value.

Table I summarizes the assumed velocity and temperature profiles for each of the four cases. The shape of the profiles is specified by the assumed functional form. The actual magnitudes of the velocity and temperature are introduced as two scale factors, δ (boundary layer thickness) and ω (boundary layer reference velocity), which are functions of x but independent with respect to y. The solution of the problem consists of finding ω and δ as functions of x, physical properties of the fluid, and the thermal boundary condition. For convenience, equivalent dimensionless variables are used. Table I presents the dimensionless

TABLE I

Boundary Layer Solutions to the Classical Problem of Natural Convection Flow along a Heated, Semi-infinite, Vertical Flat Plate Immersed in an Infinite Fluid

Part A. Constant Plate Heat Flux

	Laminar (98)	Turbulent
$T - T_\infty$ =	$\frac{q}{2k}\,\delta\left[1-\frac{y}{\delta}\right]^2$	$\frac{q}{\rho C_p}\,Pr^{2/3}\,\frac{1}{0.0225\,\omega}\left(\frac{\omega\delta}{\nu}\right)^{1/4}\left[1-\left(\frac{y}{\delta}\right)^{1/7}\right]$
u =	$\omega\,\frac{y}{\delta}\left[1-\frac{y}{\delta}\right]^2$	$\omega\left(\frac{y}{\delta}\right)^{1/7}\left[1-\frac{y}{\delta}\right]^4$
τ_w/ρ =	$\frac{\nu\omega}{\delta}$	$0.0225\,\omega^2\left(\frac{\nu}{\omega\delta}\right)^{1/4}$
C =	$\left[g\beta q/k\nu^2\right]^{1/4}$	$\left[g\beta q/k\nu^2\right]^{1/4}$
$X = Cx,\ \Delta = C\delta,\ \Omega = \frac{\omega}{\nu C}$		
Ω =	$C_\Omega X^{3/5}$	$C_\Omega X^{3/7}$
Δ =	$C_\Delta X^{1/5}$	$C_\Delta X^{5/7}$
C_Ω =	$\left(\frac{60}{Pr}\right)^{1/5}\left(\frac{10}{Pr}\right)^{2/5}\left[\frac{4}{5}\frac{1}{Pr}+1\right]^{-2/5}$	$\left(\frac{0.615}{Pr^{2/3}}\right)^{3/7}\left(\frac{106}{Pr^{1/3}}\right)^{5/14}\left[\frac{2.24}{Pr^{2/3}}+1\right]^{-5/14}$
C_Δ =	$\left(\frac{360}{Pr}\right)^{1/5}\left[\frac{4}{5}\frac{1}{Pr}+1\right]^{1/5}$	$\left(\frac{0.615}{Pr^{2/3}}\right)^{5/7}\left(\frac{Pr^{1/3}}{106}\right)^{1/14}\left[\frac{2.24}{Pr^{2/3}}+1\right]^{1/14}$
Nu =	$0.55\,(Gr\,Pr)^{1/4}\left[\frac{4}{5}\frac{1}{Pr}+1\right]^{-1/4}$	$0.0403\,Pr^{1/5}\,Gr^{2/5}\left[\frac{2.24}{Pr^{2/3}}+1\right]^{-2/5}$

TABLE I Cont'd

Part B. Constant Plate Temperature

	Laminar (96, 63)	Turbulent (18)
$T - T_\infty$ =	$(T_w - T_\infty)\left[1 - \frac{y}{\delta}\right]^2$	$(T_w - T_\infty)\left[1 - \left(\frac{y}{\delta}\right)^{1/7}\right]$
u =	$\omega \frac{y}{\delta}\left[1 - \frac{y}{\delta}\right]^2$	$\omega \left(\frac{y}{\delta}\right)^{1/7}\left[1 - \frac{y}{\delta}\right]^4$
τ_w/ρ =	$\frac{\nu\omega}{\delta}$	$0.0225\ \omega^2 \left(\frac{\nu}{\omega\delta}\right)^{1/4}$
C =	$\left[g\beta(T_w - T_\infty)/\nu^2\right]^{1/3}$	$\left[g\beta(T_w - T_\infty)/\nu^2\right]^{1/3}$
$X = Cx$, $\Delta = C\delta$		
$\Omega = \omega/\nu C$		
Ω =	$C_\Omega X^{1/2}$	$C_\Omega X^{1/2}$
Δ =	$C_\Delta X^{1/4}$	$C_\Delta X^{7/10}$
C_Ω =	$\left(\frac{80}{3 P_r}\right)^{1/2}\left[\frac{20}{21}\frac{1}{P_r} + 1\right]^{-1/2}$	$\left(\frac{2.84}{P_r^{2/3}}\right)^{1/2}\left[\frac{2.02}{P_r^{2/3}} + 1\right]^{-1/2}$
C_Δ =	$\left(\frac{80}{P_r}\right)^{1/4}\left[\frac{20}{21}\frac{1}{P_r} + 1\right]^{1/4}$	$0.842\left(\frac{0.512}{P_r^{2/3}}\right)^{7/10}\left[\frac{2.02}{P_r^{2/3}} + 1\right]^{1/10}$
Nu =	$0.51\,(G_r P_r)^{1/4}\left[\frac{20}{21}\frac{1}{P_r} + 1\right]^{-1/4}$	$0.0392\ P_r^{1/5}\ G_r^{2/5}\left[\frac{2.02}{P_r^{2/3}} + 1\right]^{-2/5}$

solutions for each case.

Obviously, the solutions depend upon the validity of the assumed profiles. One check is to compare the profiles with actual measurements made within the boundary layer. Such data are sparse, but Eckert and Jackson (18), for example, show that data of Griffiths and Davis (30) agree reasonably well with the assumed turbulent profiles. In the laminar cases, comparison with the profiles obtained from the more rigorous similarity solution of the differential boundary layer equations provides a reasonable check. A more definitive evaluation of the error introduced by the approximate method, is to compare the Nusselt number computed using the von Kármán method to the well-established empirical values for the Nusselt number.

Table I also shows the derived expressions for the Nusselt number in each case. The most common empirical correlations are:

$$\underline{\text{Laminar}} \qquad Nu = .56\ (GrPr)^{1/4} \tag{2-34}$$

$$\underline{\text{Turbulent}} \qquad Nu = .13\ (GrPr)^{1/3}. \tag{2-35}$$

The laminar results are in good agreement. Although the turbulent Nusselt number predicted by the model differs from the common empirical form, Eckert and Jackson (18) show that flat plate data are also well correlated in the turbulent range by:

$$Nu = .0210\ (GrPr)^{2/5}. \tag{2-36}$$

This is in exact agreement with the derived value at Pr = 0.72 and within experimental scatter for values of the Prandtl number from about 0.5 to 10.0. Also, Eckert and Jackson studied the effect of assuming a different velocity profile on the Nusselt number. For

$$u = \omega \left(\frac{y}{\delta}\right)\left(1 - \frac{y}{\delta}\right)^{2} , \qquad (2\text{-}37)$$

the predicted values of Nusselt number were about 17% lower than measured values. This profile also agreed poorly with experimental boundary layer profiles.

In summary, the von Kármán approximation to the solution of the boundary layer equations provides good agreement with data for the case of a heated, vertical flat plate immersed in an infinite fluid if reasonable velocity and temperature profiles are assumed. In particular, the assumed profiles presented in Table I give good agreement with observations.

III. THEORETICAL ANALYSIS

A. Formulation of Enclosed System Boundary Layer Model

A mathematical model describing the natural convection boundary layer produced within large vertical cylindrical tanks as a result of heat transfer at the walls will be developed in this chapter. For vessels with diameters very much greater than the thickness of the convective boundary layer, the curvature of the wall can be neglected. Further, if the tank height is orders of magnitude greater than the boundary layer width, end effects due to termination of the boundary layer flow in a bounded system may be neglected. These simplifications reduce the problem to that of boundary layer flow along a semi-infinite heated (or cooled) vertical flat plate. To facilitate the discussion, only the case of heat transfer from the wall to the fluid will be considered although the same solution is applicable to the analogous cooling problem by the mathematical expedient of reversing the direction of gravity. Consequently, the only major difference between the formulation of a boundary layer model for an enclosed system and the classical problem of flow up a vertical heated plate immersed in an infinite fluid is easy to describe. In the classical problem, the fluid infinitely far from the plate is at some constant temperature as a consequence of the assumption of an isothermal, stagnant fluid medium prior to the start of plate heating. On the other hand, in a confined system, the bulk fluid in the central regions of the vessel does not remain at constant temperature even if the fluid is initially isothermal and stagnant. It is evident that the boundary layer fluid discharged into the bulk regions near the upper boundary of the system will be warmer than the bulk fluid. As the boundary layer is fed with fluid from lower regions of the core, the warm

surface fluid will gradually sink and cause a core temperature distribution.

The type of temperature distribution within the core may be quite complex. Certain simplifying assumptions about the core can be made, but a meaningful model can be obtained only if it is in agreement with actual physical phenomena. On the basis of extensive experimental observations which are presented in Section IV, the following conclusions are helpful in developing a mathematical model:

1. A boundary layer flow is produced along the walls.
2. The discharge of the boundary layer into the core at the top of the system produces complex mixing phenomena in about the upper 10% of the core region.
3. Below the top mixing region, radial temperature gradients are small. For practical purposes, the core may be considered isothermal in the radial direction.
4. Core fluid sinks gradually in a manner approximating plug flow.
5. The vertical temperature gradient produced in the core, after a certain period of time, is nearly linear with respect to vertical distance in the lower 90% of the system.

Consideration of these observations indicates that a first step in formulating a mathematical model would be to solve the vertical, heated flat plate problem allowing a variation in the vertical temperature distribution infinitely far from the plate, i.e., at the edge of the boundary layer (Section B). Subsequently a model could be developed to couple the boundary layer flow to the particular core temperature distribution which it produces. (Section C).

B. Vertical Plate Boundary Layer Flow with Core Temperature Variation

1. Description of the System

The natural convection boundary layer flow along a semi-infinite, vertical, heated flat plate will be treated in the same manner as in the classical problem, except that the temperature, T_∞, infinitely far from the plate (or at the outer edge of the boundary layer) will be permitted to vary arbitrarily with height.

2. Derivation for Laminar, Constant Wall Heat Flux Case

The basic equations are developed from the differential forms:

Energy $$u\frac{\partial T}{\partial x} + v\frac{\partial T}{\partial y} = \alpha\frac{\partial^2 T}{\partial y^2} \tag{3-1}$$

Momentum $$u\frac{\partial u}{\partial x} + v\frac{\partial u}{\partial y} = +\beta(T - T_\infty)g + \frac{\mu}{\rho_o}\frac{\partial^2 u}{\partial y^2} \tag{3-2}$$

and a continuity relationship:

$$v = -\int \frac{\partial u}{\partial x}\,dy\ . \tag{3-3}$$

The equations in the von-Kármán integral form become:

Energy $$\frac{\partial}{\partial x}\int_0^\infty u(T - T_\infty)dy = \frac{q}{\rho C_p} - \underline{\int_0^\infty u\frac{\partial T_\infty}{\partial x}\,dy} \tag{3-4}$$

Momentum $$\frac{\partial}{\partial x}\int_0^\infty u^2 dy = \beta g\int_0^\infty (T - T_\infty)dy - \frac{\tau_\omega}{\rho} \tag{3-5}$$

These equations differ from the classical problem only in the addition of the underlined term in the energy equation and in the fact that T_∞

is an arbitrary function of x, rather than a constant.

The derivation will be presented for the laminar, constant wall heat flux case in the following paragraphs. A comparison between the case described in detail here and the other three cases studied--turbulent flow with constant wall heat flux and both laminar and turbulent flow with constant wall temperature--is presented in Table II.

For the laminar flow case, the velocity and temperature profiles which have been shown to give good results in analyzing the classical problem will be used.

$$\underline{\text{Temperature}} \qquad T - T_\infty = \frac{q}{2k}\,\delta\left[1 - \frac{y}{\delta}\right]^2 \tag{3-6}$$

$$\underline{\text{Velocity}} \qquad u = \omega\,\frac{y}{\delta}\left[1 - \frac{y}{\delta}\right]^2 \tag{3-7}$$

The temperature profile satisfies the constant heat flux boundary condition at the wall, since

$$\left.\frac{dT}{dy}\right|_{y=0} = -\frac{q}{k} \quad . \tag{3-8}$$

The laminar wall shear stress is

$$\frac{\tau_w}{\rho} = \nu \left.\frac{\partial u}{\partial y}\right|_{y=0} = \frac{\nu\omega}{\delta} \quad . \tag{3-9}$$

The velocity profile satisfies the requirements of "no slip" at the wall and also of zero velocity at the outer edge of the boundary where $y = \delta$.

The integrals in the boundary layer equations may now be evaluated.

$$\int_0^\infty u(T - T_\infty)\,dy = \frac{q}{2k}\,\delta^2\omega \int_0^1 \left(\frac{y}{\delta}\right)\left(1 - \frac{y}{\delta}\right)^4 d\left(\frac{y}{\delta}\right)$$

$$= \frac{q}{2k}\,\delta^2\omega\,\left(\frac{1}{30}\right) = A_1\,\frac{q}{2k}\,\delta^2\omega \tag{3-10}$$

TABLE II

Boundary Layer Solutions to the Modified Problem of Natural Convection Flow along a Heated, Semi Infinite, Vertical Flat Plate Immersed in an Infinite Fluid with Core Temperature Variation

Part A. Constant Plate Heat Flux	Laminar	Turbulent
A_N $N=1,2,3\ldots$	$\frac{1}{30}, \frac{1}{12}, \frac{1}{105}, \frac{1}{3}$	$0.036631, 0.146351, 0.52315, 0.125, 0.0225$
E =	$\Omega\Delta^2$	$\Omega^{1/4}\,\Delta^{5/4}$
M =	$\Omega^2\Delta$	$\Omega^2\,\Delta$
C_E =	$2/A_1 P_r$	$A_5/A_1 P_r^{2/3}$
C_M =	$\left\{\frac{A_4}{A_1 P_r}\left[\frac{14}{5}\frac{A_3}{A_1 P_r}+1\right]^{-1}\right\}^{3/5}\left[\frac{2}{A_1 P_r}\right]^{4/5}$	$\left\{\frac{A_4}{A_5 A_1 P_r}\left[\frac{11}{7}\frac{A_3}{A_1 P_r^{2/3}}+1\right]^{-1}\right\}^{9/14}\left[\frac{A_5}{A_1 P_r^{2/3}}\right]^{13/14}$
E_o^* =	$\frac{X}{X^{7/5}}$	$\frac{X}{X^{11/7}}$
M_o^* =		
$\frac{dE^*}{dX}$ =	$1-\frac{2A_2}{A_1}\left\{\frac{A_1 P_r}{2}\right\}^{2/5}\left\{\frac{A_4}{A_1 P_r}\left[\frac{14}{5}\frac{A_3}{A_1 P_r}+1\right]^{-1}\right\}^{1/5}(E^*M^*)^{1/3}\frac{d\theta_\infty}{dX}$	$1-A_2 P_r\left\{\frac{A_5}{A_1 P_r^{2/3}}\right\}^{8/7}\left\{\frac{A_4}{A_5 A_1 P_r}\left[\frac{11}{7}\frac{A_3}{A_1 P_r^{2/3}}+1\right]^{-1}\right\}^{2/7}(E^*M^*)^{4/9}\frac{d\theta_\infty}{dX}$
$\frac{dM^*}{dX}$ =	$\left[\frac{7}{5}+\frac{A_1}{2A_3}P_r\right]\frac{E^{*4/3}}{M^{*2/3}}-\frac{A_1}{2A_3}P_r\frac{M^*}{E^*}$	$\left[\frac{11}{7}+\frac{A_1}{A_3}P_r^{2/3}\right]\frac{E^{*13/9}}{M^{*5/9}}-\frac{A_1}{A_3}P_r^{2/3}\frac{M^*}{E^*}$
for $\frac{d\theta_\infty}{dX}=$ const, $\frac{dE^*}{dX}=0$:		
E_a^* =	$\left\{\frac{A_1}{A_2^{5/4}A_4^{1/4}2^{3/4}}\right\}\frac{1}{P_r^{1/4}}\left(\frac{dX}{d\theta_\infty}\right)^{5/4}$	$\left\{\frac{A_1^{5/4}}{A_2^{7/8}A_5^{3/4}A_4^{1/4}}\right\}P_r^{1/24}\left(\frac{dX}{d\theta_\infty}\right)^{7/8}$
Nu_a =	$2\left\{A_2 A_4 Gr\, P_r\frac{d\theta_\infty}{dX}\right\}^{1/3}$	$\left\{\frac{A_1^{31/27}A_4^{31/63}A_5^{491/567}}{A_2^{1/6}}\right\}(P_r Gr)^{1/3}\frac{1}{P_r^{1/126}}\left(\frac{dX}{d\theta_\infty}\right)^{1/6}$

TABLE II

Part B. Constant Plate Temperature

Note: Values of A_n's are the same as in the same flow regime in Part A

	Laminar	Turbulent
$E =$	$\Omega\Delta$	$\Omega\Delta$
$M =$	$\Omega^2\Delta$	$\Omega^2\Delta$
$C_E =$	$\left\{\frac{8}{3}\frac{1}{A_1 P_r} C_M\right\}^{1/3}$	$\left\{\frac{5}{6}\frac{A_5}{A_1}\frac{1}{P_r^{2/3}} C_M\right\}^{4/9}$
$C_M =$	$\left\{\frac{8}{3 A_1 P_r}\right\}^{1/2}\left\{\frac{A_4}{A_3}\left[\frac{5}{4}+\frac{3}{8}\frac{A_1}{A_3}P_r\right]^{-1}\right\}^{3/4}$	$\left\{\frac{5}{6}\frac{A_5}{A_1}\frac{1}{P_r^{2/3}}\right\}^{4/5}\left\{\frac{A_4}{A_3}\left[\frac{17}{10}+\frac{6}{5}\frac{A_1}{A_3}P_r^{2/3}\right]^{-1}\right\}^{9/10}$
$E^* =$	$\Sigma^{3/4}$	$\Sigma^{6/5}$
$M^* =$	$\Sigma^{5/4}$	$\Sigma^{17/10}$
For $\frac{d\theta_\infty}{d\Sigma} =$ constant (Otherwise need to integrate $d\theta_\infty/d\Sigma$)		
$dE^*/d\Sigma =$	$\frac{3}{4}\frac{M^*}{E^{*2}} - \left[\frac{A_2}{A_1}-1\right]\left\{1-\frac{d\theta_\infty}{d\Sigma}\Sigma\right\}^{-1} E^* \frac{d\theta_\infty}{d\Sigma}$	$\frac{6}{5}\frac{M^*}{E^{*5/4}} - \left[\frac{A_2}{A_1}-1\right]\left\{1-\frac{d\theta_\infty}{d\Sigma}\Sigma\right\}^{-1} E^* \frac{d\theta_\infty}{d\Sigma}$
$dM^*/d\Sigma =$	$\left[\frac{5}{4}+\frac{3}{8}\frac{A_1}{A_3}P_r\right]\frac{E^{*2}}{M^*}\left\{1-\frac{d\theta_\infty}{d\Sigma}\Sigma\right\} - \frac{3}{8}\frac{A_1}{A_3}P_r\frac{M^{*2}}{E^{*3}}$	$\left[\frac{17}{10}+\frac{6}{5}\frac{A_1}{A_3}P_r^{2/3}\right]\frac{E^{*2}}{M^*}\left\{1-\frac{d\theta_\infty}{d\Sigma}\Sigma\right\} - \frac{6}{5}\frac{A_1}{A_3}P_r^{2/3}\frac{M^{*2}}{E^{*9/4}}$

$$\int_0^\infty u\,dy = \omega\delta \int_0^1 \left(\frac{y}{\delta}\right)\left(1 - \frac{y}{\delta}\right)^2 d\left(\frac{y}{\delta}\right)$$

$$= \omega\delta \left(\frac{1}{12}\right) = A_2\,\omega\delta \tag{3-11}$$

$$\int_0^\infty u^2 dy = \omega^2\delta \int_0^1 \left(\frac{y}{\delta}\right)^2 \left(1 - \frac{y}{\delta}\right)^4 d\left(\frac{y}{\delta}\right)$$

$$= \omega^2\delta \left(\frac{1}{105}\right) = A_3\,\omega^2\delta \tag{3-12}$$

$$\int_0^\infty (T - T_\infty)dy = \frac{q}{2k}\,\delta^2 \int_0^1 \left(1 - \frac{y}{\delta}\right)^2 d\left(\frac{y}{\delta}\right)$$

$$= \frac{q}{2k}\,\delta^2 \left(\frac{1}{3}\right) = A_4\,\frac{q}{2k}\,\delta^2 \tag{3-13}$$

The numerical values resulting from integration of the velocity and temperature profiles are indicated in parentheses. These values will be carried through the analysis as arbitrary constants, A_1, A_2, A_3 and A_4, so that the source of coefficients in the final results will be clear. Also, should other assumptions be made for the profiles or should the "exact" profiles be determined, the results can be readily modified by simply changing the set of numerical constants accordingly.

Upon substitution of the integrated terms, the boundary layer equations become:

Energy $$\frac{\partial}{\partial x}\left[\delta^2\omega\right] = \frac{2\alpha}{A_1} - \frac{A_2}{A_1}\,\frac{dT_\infty}{dx}\,\omega\delta\,\frac{2k}{q} \tag{3-14}$$

Momentum $$\frac{\partial}{\partial x}\left[\omega^2\delta\right] = \frac{A_4}{2A_3}\,\frac{\beta g\, q}{k}\,\delta^2 - \frac{1}{A_3}\,\frac{\nu\omega}{\delta} \tag{3-15}$$

It is interesting to note that although $T_\infty = T_\infty(x)$ was allowed to be an arbitrary function of x, only the derivative, $\frac{dT_\infty}{dx}$, appears in the resulting equations for the case of a constant wall heat flux.

A set of dimensionless variables can now be defined:

$$\Omega = \frac{\omega}{\nu C} \tag{3-16}$$

$$\Delta = C\delta \tag{3-17}$$

$$X = Cx \tag{3-18}$$

$$\frac{d\theta_\infty}{dX} = \frac{k}{q}\frac{dT_\infty}{dx} \tag{3-19}$$

where $C = \left[\frac{g\beta q}{k\nu^2}\right]^{1/4}$ and has units of inverse length. It is evident that when C is multiplied by a length such as x, the resulting group is the one-fourth root of the Grashof number-Nusselt number product based on x . In terms of the new variables, the equations become:

Energy
$$\frac{\partial}{\partial X}\left[\Delta^2\Omega\right] = \frac{2}{A_1}\frac{1}{Pr} - \frac{2A_2}{A_1}\Omega\Delta\frac{d\theta_\infty}{dX} \tag{3-20}$$

Momentum
$$\frac{\partial}{\partial X}\left[\Omega^2\Delta\right] = \frac{A_4}{2A_3}\Delta^2 - \frac{1}{A_3}\frac{\Omega}{\Delta} \tag{3-21}$$

For $T_\infty(x)$ = constant, i.e. $\frac{dT_\infty}{dx} = 0$, as discussed in Section IIE, the equations have been solved by Sparrow (96) to give

$$\Omega = C_\Omega X^{3/5} \tag{3-22}$$

$$\Delta = C_\Delta X^{1/5} \tag{3-23}$$

where $C_\Omega = \left(\frac{6000}{Pr}\right)^{1/5}\left(\frac{4}{5} + Pr\right)^{-2/5}$

and $$C_{\Delta} = (360)^{1/5} \, Pr^{-2/5} \, (\tfrac{4}{5} + Pr)^{1/5}.$$

Such a solution obviously does not satisfy the problem when a core temperature gradient is specified. However, a numerical integration technique may be used to solve equations (3-20) and 3-21) for various values of the Prandtl number and a specified variation of the dimensionless core temperature gradient.

To simplify the computational procedure, further modification of the equations was made.

Let: $$E = \Omega \Delta^2 = C_E E^* \tag{3-24}$$

$$M = \Omega^2 \Delta = C_M M^* \tag{3-25}$$

Since the product, $\Omega\Delta$, is a dimensionless flow rate the new variables E and M may be interpreted as a dimensionless convective thermal energy flux (Δ is related to temperature level) and a dimensionless convective momentum flux (Ω is a dimensionless velocity) respectively, in the boundary layer. C_E and C_M are normalizing factors depending only on Prandtl number and the assumed boundary layer temperature and velocity profiles. The factors are defined in terms of the results for the isothermal core case, in which the dimensionless energy and momentum fluxes, denoted with a subscript o, are

$$E_o = C_E X , \qquad E_o^* = X \tag{3-26}$$

$$M_o = C_M X^{7/5} , \qquad M_o^* = X^{7/5} \tag{3-27}$$

By comparison with equations (3-22) and (3-23) and the definitions of E and M (3-24, 3-25), the normalizing factors in the above equations are:

$$C_E = \frac{2}{A_1} \, \frac{1}{Pr} \tag{3-28}$$

$$C_M = \left\{ \frac{A_4}{A_1 Pr} \frac{1}{\left[\frac{14}{5} \frac{A_3}{A_1 Pr} + 1 \right]} \right\}^{3/5} \left[\frac{2}{A_1 Pr} \right]^{4/5} \qquad (3\text{-}29)$$

and the differential equations are:

$$\underline{\text{Energy}} \quad \frac{dE^*}{dX} = 1 - \frac{2A_2}{A_1} \left[\frac{A_1 Pr}{2} \right]^{2/5} \left\{ \frac{A_4}{A_1 Pr} \frac{1}{\left[\frac{14}{5} \frac{A_3}{A_1 Pr} + 1 \right]} \right\}^{1/5} E^{*1/3} M^{*1/3} \frac{d\theta_\infty}{dX} \qquad (3\text{-}30)$$

$$\underline{\text{Momentum}} \quad \frac{dM^*}{dX} = \frac{A_1 Pr}{2A_3} \left[\frac{14}{5} \frac{A_3}{A_1 Pr} + 1 \right] \frac{E^{*4/3}}{M^{*2/3}} - \frac{A_1 Pr}{2A_3} \frac{M^*}{E^*} . \qquad (3\text{-}31)$$

Numerical solutions to equations (3-30) and (3-31) were obtained for the important case of $\frac{d\theta_\infty}{dX}$ constant, i.e., for a linear temperature distribution at infinity. Observations of transient core temperature distributions in the experimental phase of this work indicated that numerical solutions for various constant gradients would be valuable in developing a model for the transient core temperature distributions.

The computer program used for evaluating E^* and M^*, at constant values of $\frac{d\theta_\infty}{dX}$, is presented in VIII.Appendix H.

3. Leading Edge Singularity

A brief look at the properties of these equations leads to some interesting observations. First of all, at X = 0, the original variables, ω and δ, are equal to zero which means that, at the leading edge of the plate, the boundary layer thickness and velocity are zero. Consequently, the energy and momentum variables are also zero at this point. As a consequence of boundary layer simplifications which are not physically valid at the leading edge, both Ω and Ω have infinite slopes at

X = 0. As discussed in Part 7, Section IIIB, computational difficulties were avoided by starting the numerical integration a finite distance away from the origin. The initial values of the variables at the starting point were computed from the analytical solution for the isothermal core case. As will be evident from the computed results, the effect of this arbitrary choice of starting point becomes negligible at reasonable distances away from the start. This is similar to the behavior of the boundary layer equations themselves; the inaccuracies due to the singularity at the leading edge rapidly disappear as distance from the origin increases. Extensive analysis of leading edge effects is presented by Scherberg (81). A further justification of using the isothermal core solution to start the iteration is that, if the model is to be used for an enclosed system with an insulated bottom, the temperature gradient at the bottom would actually approach zero for perfect insulation.

4. Energy and Momentum Parameters

Both the boundary layer energy and momentum tend to increase as fluid flows up the heated wall. If no core temperature gradient were present, the normalized energy variable, E_o^* would increase linearly with X and correspondingly, M_o^* with $X^{7/5}$. However, assuming the core temperature matches the boundary layer temperature at X = 0, the presence of a positive core temperature gradient tends to decrease the energy and momentum in the boundary layer at a given height. This is clearly evident from Equation (3-30), which determines the rate of increase of E^*. The term involving the core temperature gradient is subtracted from the "isothermal core case" growth rate of unity.

The physical implications may be better understood by considering

a simple model. In the "isothermal core case", the velocity and temperature profiles are specified for a boundary layer of width δ_o. If, now, a core temperature gradient is imposed at the outer edge of the boundary layer, the boundary layer base temperature level must match the core temperature level which is increasing with height. Consequently, a fraction of the wall heat flux is used to raise the base temperature level of the boundary layer fluid and only the remaining energy input, the difference between the wall heat flux and the heat required to compensate for the increased thermal energy of the core at greater height, is available for boundary layer growth and acceleration. So, in the presence of a positive core temperature gradient, the boundary layer growth and acceleration are retarded relative to the isothermal core case with the same temperature at $x = 0$.

5. Limiting Solutions: Laminar, Constant Wall Heat Flux Case

Continuing the argument presented in the previous section, the conclusion that limiting values of boundary layer energy and momentum occur for the constant wall heat flux, constant core temperature gradient case becomes evident. Assume that the fluid volumetric specific heat capacity (ρC_p) remains constant. At some height the boundary layer will have grown to the point where the total energy input from the wall is required to keep the boundary layer base temperature level increasing at the same rate as the core temperature is increasing. Beyond this point no energy is available for additional growth or acceleration of the boundary layer. When this occurs, E^* and M^* approach limiting values and their derivatives become zero. The limiting condition occurs when:

$$\frac{dE^*}{dX} = 0 = 1 - \frac{2A_2}{A_1}\left(\frac{A_1 Pr}{2}\right)^{2/5}\left\{\frac{A_4}{A_1 Pr}\,\frac{1}{\left[\frac{14}{5}\frac{A_3}{A_1 Pr}+1\right]}\right\}^{1/5} E^{*1/3} M^{*1/3}\,\frac{d\theta_\infty}{dx}. \quad (3\text{-}32)$$

At the asymptote:

$$E_a^* = \left[\frac{A_1}{A_2^{5/4}A_4^{1/4}2^{3/4}}\right]\frac{1}{Pr^{1/4}}\left[\frac{dX}{d\theta_\infty}\right]^{5/4} \approx \frac{0.583}{Pr^{1/4}}\left[\frac{dX}{d\theta_\infty}\right]^{5/4} \quad (3\text{-}33)$$

$$M_a^* = \left[\frac{A_1^{7/5}}{A_2^{7/4}A_4^{7/20}2^{21/20}}\right]\left[\frac{14}{5}\frac{A_3}{A_1 Pr}+1\right]^{3/5}\frac{1}{Pr^{7/20}}\left[\frac{dX}{d\theta_\infty}\right]^{7/4} \quad (3\text{-}34)$$

$$\approx 0.466\left[\frac{4}{5}\frac{1}{Pr}+1\right]\frac{1}{Pr^{7/20}}\left[\frac{dX}{d\theta_\infty}\right]^{7/4}$$

The numerical values correspond to the values of A_1, A_2, A_3 and A_4 for the profiles chosen in equations (3-10) to (3-13). From these limiting solutions, it is possible to estimate the limiting values of a number of pertinent parameters.

Boundary layer flow

$$\frac{\int_0^\infty u\,dy}{\nu} = A_2\,\Omega\,\Delta = A_2\,E^{1/3}\,M^{1/3} \quad (3\text{-}35)$$

Boundary layer average temperature relative to core temperature

$$\frac{kC}{q\nu}\,\frac{\int_0^\infty u(T - T_\infty)\,dy}{\int_0^\infty u\,dy} = \frac{A_1}{2A_2}\,\frac{E^{2/3}}{M^{1/3}} \quad (3\text{-}36)$$

Thermal Energy in Boundary Layer

$$\frac{kC}{q\nu}\int_0^\infty u(T - T_\infty)dy = \frac{A_1}{2}E \tag{3-37}$$

and finally,

Nusselt number

$$Nu = \frac{q}{(T_w - T_\infty)}\quad \frac{L}{k} = \frac{2CL}{\Delta} = 2CL\ \frac{E^{2/3}}{M^{1/3}} \tag{3-38}$$

When the limiting values for E and M are substituted into the equation for Nusselt number an intriguing result is obtained.

$$Nu_a = 2\left[A_2A_4\ Gr\ Pr\ \frac{d\theta_\infty}{dX}\right]^{1/3}$$

$$\backsimeq 0.605\ (GrPr)^{1/3}\quad \frac{d\theta_\infty}{dX}^{1/3} \tag{3-39}$$

The limiting value for the laminar Nusselt number, given a linear core temperature gradient, $\frac{d\theta_\infty}{dX}$, depends on the one-third power of the Grashof-Prandtl product. This functional dependence, in the absence of a core gradient, is characteristic of turbulent flow. This perhaps is an explanation for the reported results of Eckert (16), who found experimentally a 0.30 power dependence between the Nusselt and Grashof numbers, but found no evidence of boundary layer turbulence in Zehnder-Mach interferometric photographs of the enclosed system which he studied.

6. Other Cases

At this point, the mathematical development for the laminar case is essentially complete. The corresponding assumptions, procedures, and results for the turbulent case and the constant wall temperature cases are shown in Table II. For the turbulent case, the use of an empirical wall shear stress and the Reynolds analogy to relate wall heat flux to wall shear, permit the use of temperature and velocity profiles which are realistic for turbulent flow, but which inherently do not satisfy boundary conditions at the wall. Although the equations become somewhat complex, an obvious difference between the turbulent and laminar cases is the definition of the variable E. This is only a superficial difference if the physical meaning of E is recalled. Since E is a convective thermal energy flux, it is related to the flow, $\Omega\Delta$, and the temperature. In the laminar case, the temperature was determined by the temperature profile and was proportional to Δ , giving $E = \Omega\Delta^2$. In the turbulent case, the temperature is determined by the turbulent heat transport at the wall and is proportional to $\frac{(\Omega\Delta)^{1/4}}{\Omega}$. The interpretation of E is the same as in the laminar case although now $E = \Omega^{1/4}\Delta^{5/4}$.

Attention is also called to the limiting Nusselt number for turbulent flow which is also essentially equal to the one-third power of the Grashof-Prandtl product.

7. Computed Values of Energy and Momentum Variables

Although an analytic solution to equations (3-30) and (3-31), for the boundary layer energy and momentum variables in the presence of a linear core temperature gradient, has not been found, the derivatives

of these variables can be expressed for each specific case in the form:

$$\frac{dE^*}{dX} = f(E^*, M^*, Pr, \frac{d\theta_\infty}{dX}) \tag{3-40}$$

$$\frac{dM^*}{dX} = g(E^*, M^*, Pr, \frac{d\theta_\infty}{dX}) . \tag{3-41}$$

Therefore, E^* and M^* may be computed as functions of X by numerical integration if the model, Pr, and $\frac{d\theta_\infty}{dX}$ are specified. Because of computational problems encountered as $X \rightarrow 0$, a finite starting value of X was used. This value, designated X_{INIT}, was also studied as a parameter to see whether it exerted any long range influence on the primary variables. The computer program is given in VIII.Appendix H.

Detailed computations were made for two cases: laminar and turbulent boundary layer flow with constant wall heat flux. Values of Prandtl number were chosen to correspond to various experimental fluids and temperature levels. The results of these computations are shown in Figs. 3-1 and 3-2. For no temperature gradient in the core, E_o^* is equal to X for both the laminar and turbulent cases. M_o^* is equal to $X^{7/5}$ for the laminar case and equal to $X^{11/7}$ for the turbulent model.

Both energy and momentum are reduced, at any particular value of X, by the presence of a positive core temperature gradient. The larger the core gradient, the greater the reduction in E^* and M^*. For each core gradient, at a given fluid Prandtl number, there is a limiting value of E^* and M^* which is approached in an asymptotic manner as X increases. These are the values predicted by the asymptotic solutions presented in Table II. The approach occurs at lower values of X for higher values of $\frac{d\theta_\infty}{dX}$.

Before discussing the results further, the importance of the choice

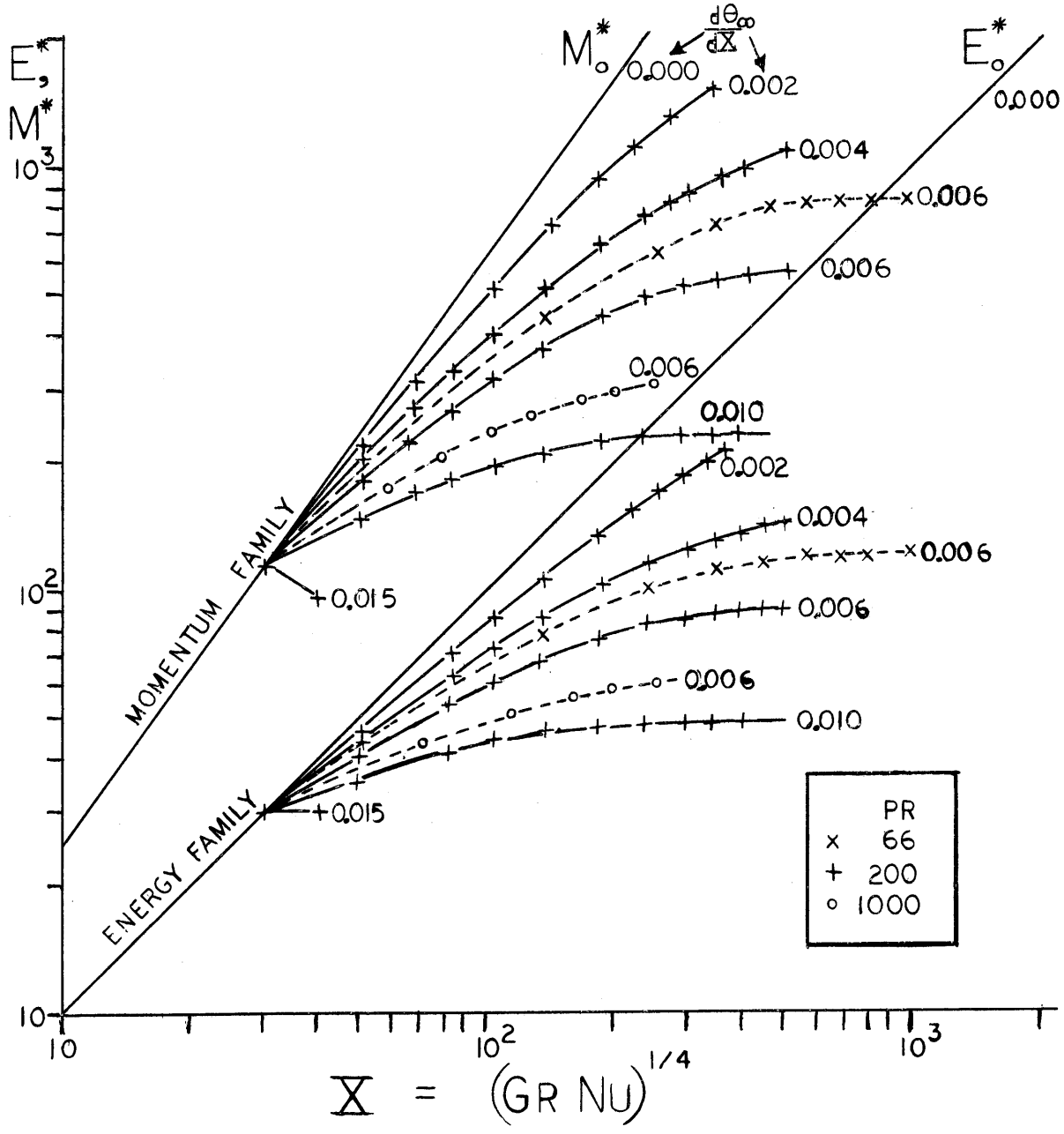

FIGURE 3-1

DIMENSIONLESS BOUNDARY LAYER ENERGY AND MOMENTUM FUNCTIONS
LAMINAR MODEL WITH CONSTANT CORE TEMPERATURE GRADIENT

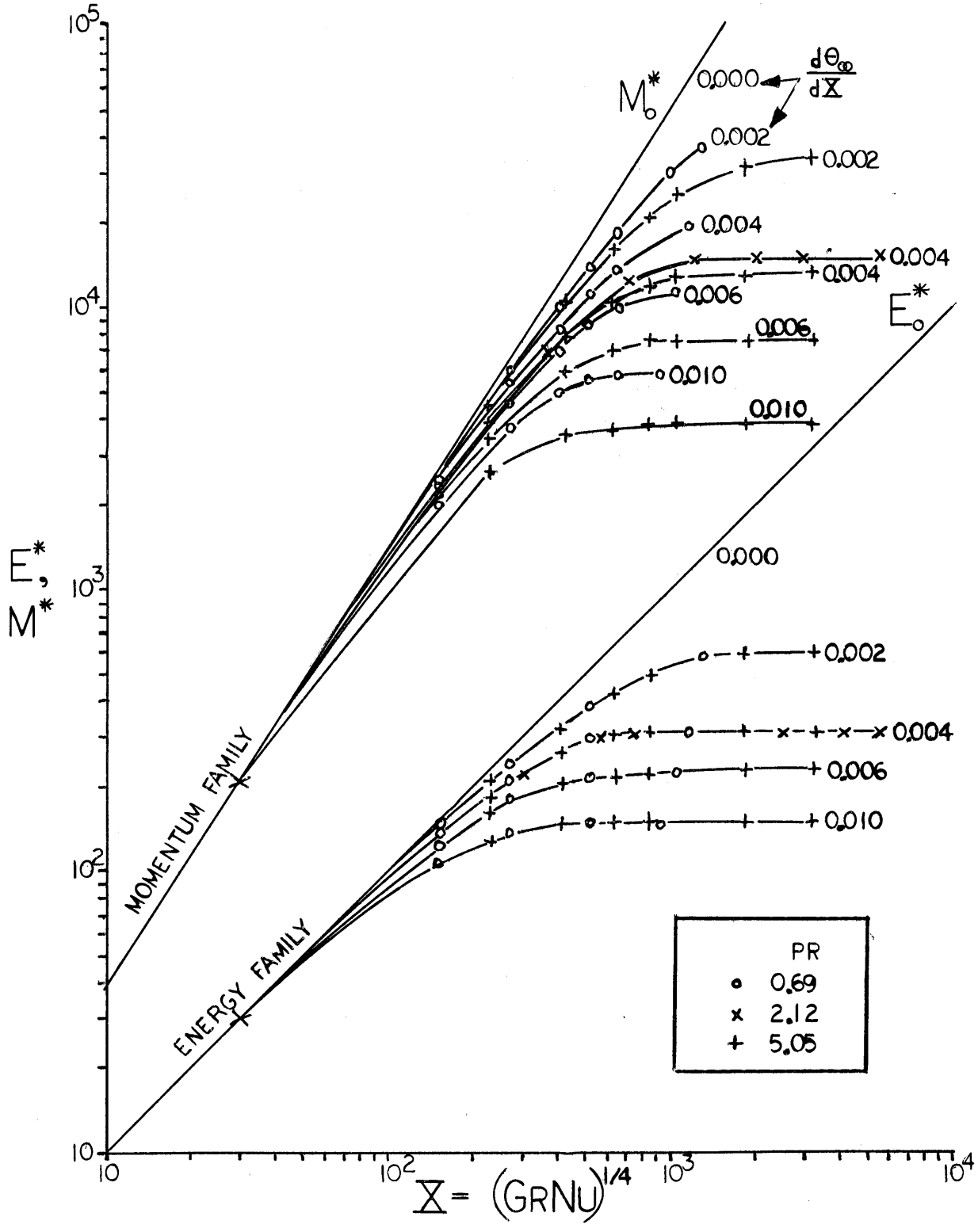

FIGURE 3-2

DIMENSIONLESS BOUNDARY LAYER ENERGY AND MOMENTUM FUNCTIONS
TURBULENT MODEL WITH CONSTANT CORE TEMPERATURE GRADIENT

of starting point should be ascertained. From Figures 3-3 and 3-4, it is clear that the starting point does not affect the eventual asymptotic values of E^* and M^*. In addition to this expected observation, it is encouraging to note that curves with the same $\frac{d\theta_\infty}{dx}$ and Pr parameters, rapidly approach a single curve in spite of variation in starting point. Although a detailed analysis of the effect of starting point has not been made, evaluation of the results of Figures 3-3 and 3-4, and of additional similar computations, indicates that reliable values of E^* and M^* are obtained as long as the starting point is less than about one-fifth of the value of X at the point of interest. This is not a serious limitation except at very high Prandtl numbers where the limitation on the size of X increments is most severe and most stringent at the starting point. This problem could probably be remedied by transformation of X to a new variable, such as $\ln X$. This modification was not made in the present study, since at Pr = 1000 the maximum computation time was only slightly more than one minute of IBM 7094 time, and only a few such runs were made. For Pr = 200, computation times were down to about 0.2 minutes.

Returning to the original discussion of the behavior of E^* and M^*, one may now consider the main parameters of the problem without worrying about start-up effects. The parameters of interest are:

$$\text{Pr} = \text{Prandtl number} = \frac{\nu}{\alpha}$$

$$\frac{d\theta_\infty}{dX} = \text{Core temperature gradient} = \frac{k}{q}\,\frac{dT_\infty}{dx}\,.$$

In both the laminar and turbulent constant wall heat flux cases, the independent variable, X is $(Gr_x Nu_x)^{1/4}$. Dependent variables E^* and M^*

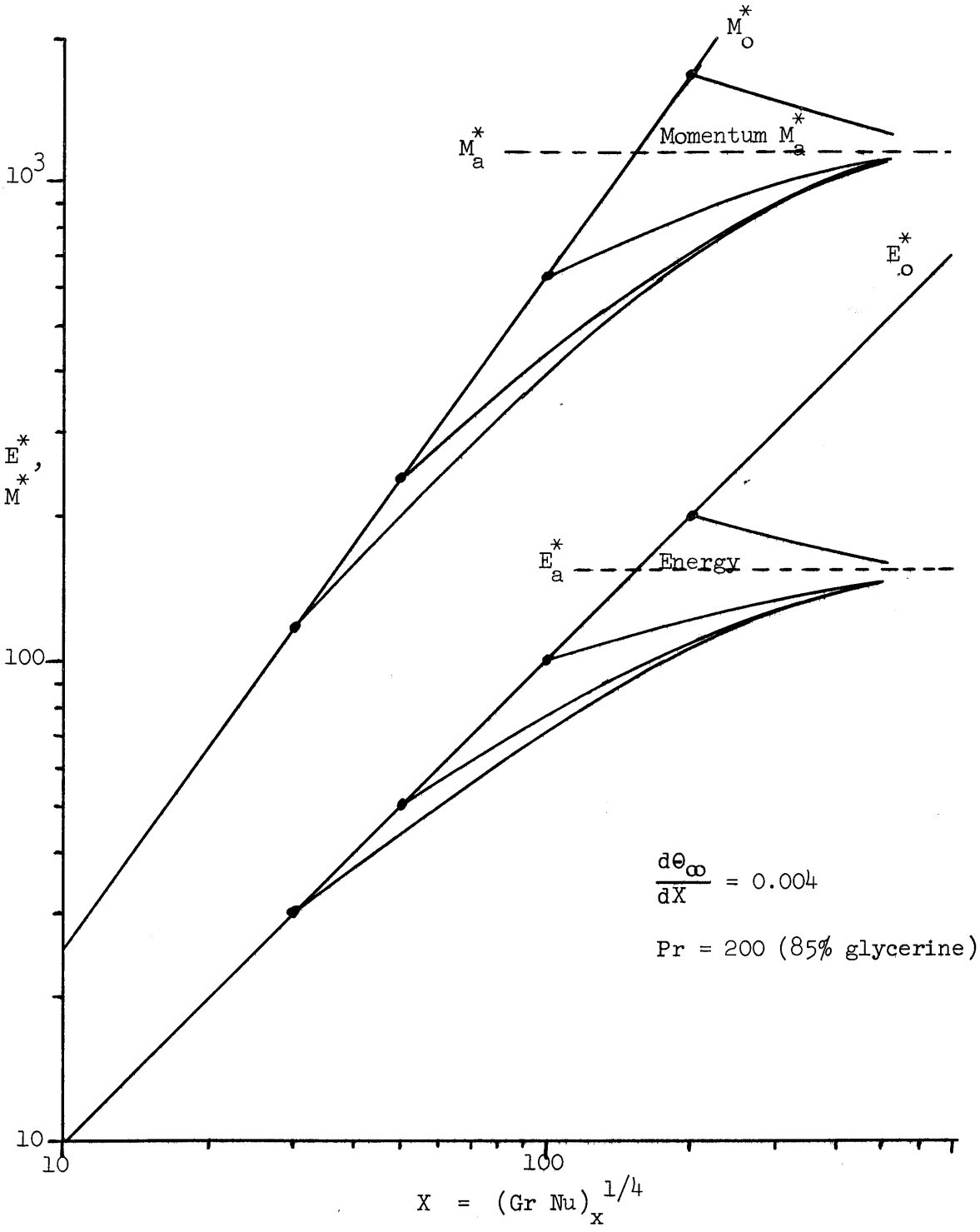

FIGURE 3-3

Effect of Starting Point on Energy and Momentum

Solutions: Laminar

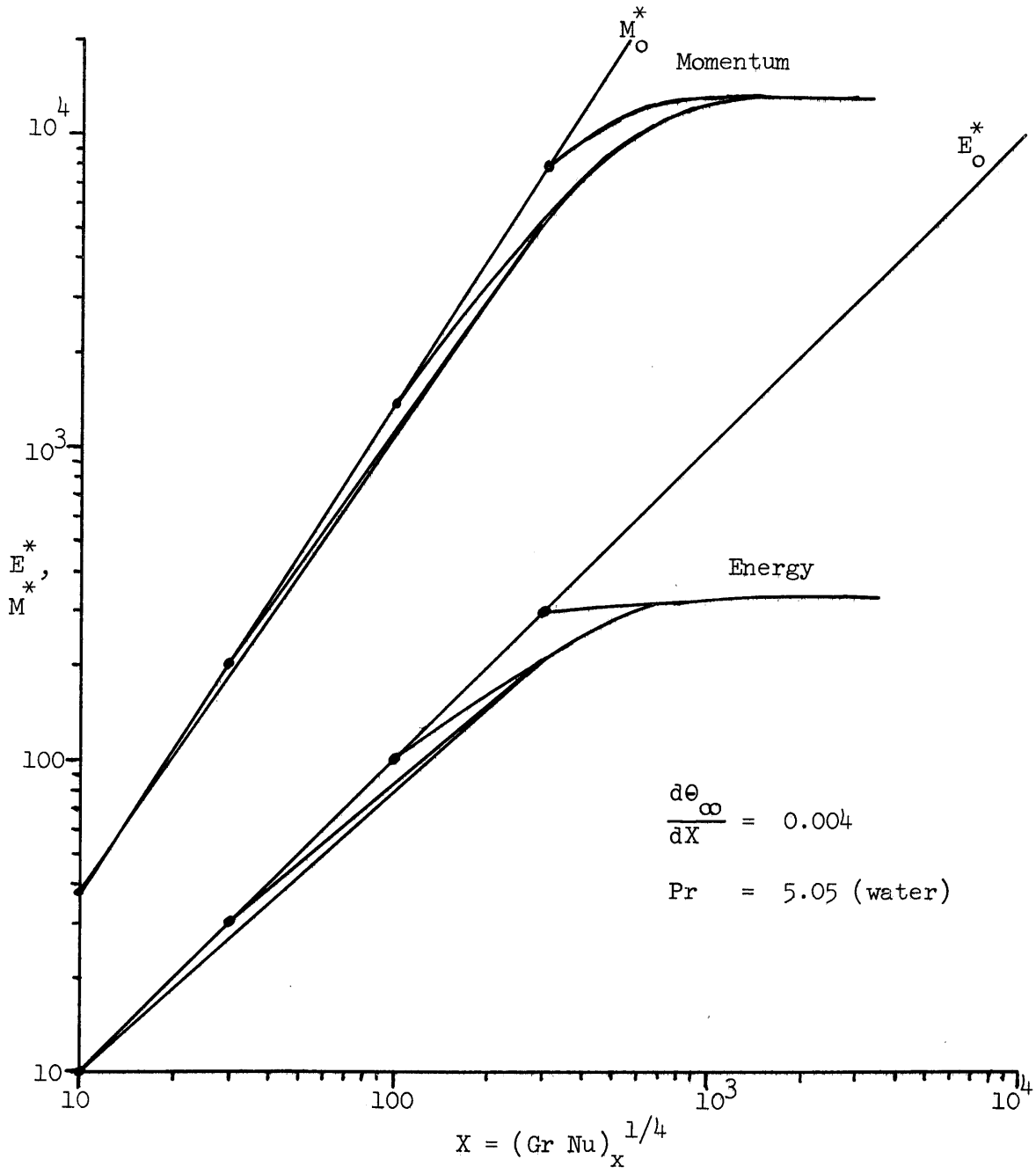

FIGURE 3-4

Effect of Starting Point on Energy and Momentum

Solutions: Turbulent

are to be evaluated and used, in turn, to estimate other items of interest, namely: Nusselt number, average temperature of boundary layer fluid, boundary layer flow rate, wall temperature, boundary layer energy flux.

a. Laminar, Q_w Case

Examination of Figure 3-1 shows the effect that a constant core temperature gradient has on reducing boundary layer energy and momentum, as discussed previously. However, some further qualitative observations can be made. First, increases in Prandtl number cause the same type of decrease in E^* and M^* as do increases in core temperature gradient. Perhaps a single parameter of the form $\left[Pr^a \left(\frac{d\theta_\infty}{dx} \right)^b \right]$ actually determines the curve position. Second, the similarity between the E^* and M^* family of curves is apparent both in terms of the spread produced by varying the parameters, Pr and $\frac{d\theta_\infty}{dX}$, and in terms of the degree of approach to the steady-state asymptote at particular values of the parameters and of X.

A brief analysis sheds light on the relation between E^* and M^* for the laminar model.

Ratio of variables for $\frac{d\theta_\infty}{dX} = 0$:

$$\frac{E_o^*}{(M_o^*)^{5/7}} = \frac{X}{(X^{7/5})^{5/7}} = 1 \qquad (3\text{-}42)$$

Ratio of variables at Asymptote:

$$\frac{E_a^*}{(M_a^*)^{5/7}} = \frac{1}{\left[\frac{14}{5} \frac{A_3}{A_1 Pr} + 1 \right]^{3/7}} = \frac{1}{\left[\frac{4}{5} \frac{1}{Pr} + 1 \right]^{3/7}} \qquad (3\text{-}43)$$

Using the laminar model for $Pr > 10$, $1 < \left[E_a^*/(M_a^*)^{5/7}\right] < .97$. Therefore, with less than 3% error, it may be assumed that

$$M_a^* = E_a^{*7/5} \qquad \text{for } Pr > 10. \tag{3-44}$$

The validity of the approximation may also be checked at intermediate values of X for finite values of core temperature gradient by plotting computed values of M^* versus E^* at various mutual values of X. Again, a single curve results which has the same slope as indicated by both the isothermal core and asymptotic solution analyses.

Using this approximation, a single differential equation for E^* is obtained: $(Pr > 10)$

$$\frac{dE^*}{dX} = 1 - A_2 \left[\frac{2}{A_1}\right]^{4/5} \left[\frac{A_4}{2}\right]^{1/5} Pr^{1/5} \; E^{*4/5} \; \frac{d\theta_\infty}{dX} . \tag{3-45}$$

or for the profiles used:

$$\frac{dE^*}{dX} = 1 - 1.543 \; Pr^{1/5} \; \frac{d\theta_\infty}{dX} E^{*4/5} \tag{3-46}$$

A similar expression in M^* only could be written, but since E^* and M^* are directly related, this is not required for solution of the problem. As suggested by qualitative observation, the curves should be determined by a single parameter, $Pr^{1/5} \frac{d\theta_\infty}{dX}$. Figure 3-5 presents a simplified version of Figure 3-1, which is valid for $Pr > 10$. E^* is plotted versus X as a function of a single parameter, Υ where

$$\Upsilon = 1.543 \; Pr^{1/5} \; \frac{d\theta_\infty}{dX} . \tag{3-47}$$

Figure 3-6 uses the approximate form of the laminar model to show the variation in Nusselt number with (RaNu), or in the present nomenclature,

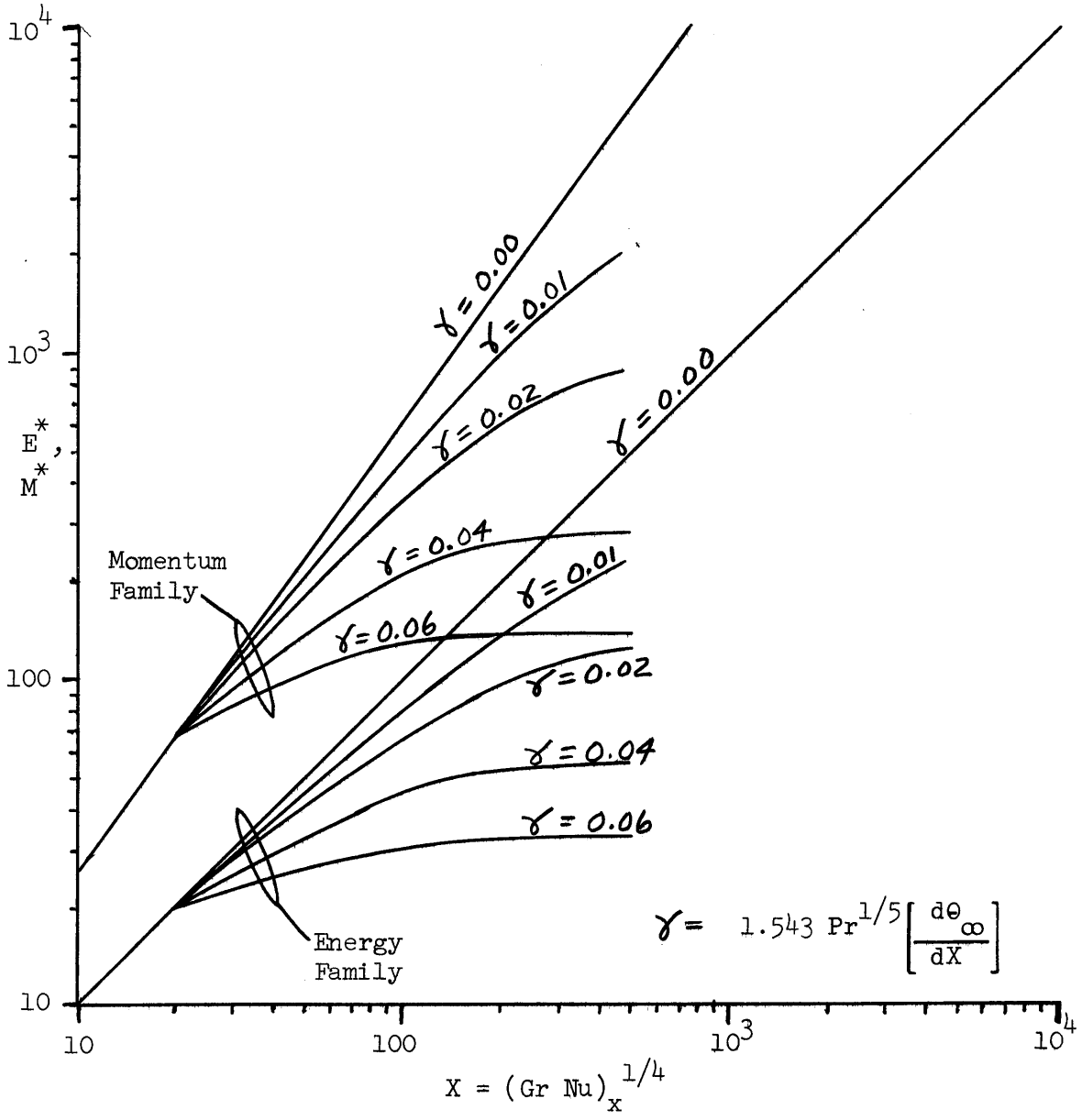

FIGURE 3-5

Dimensionless Boundary Layer Energy and Momentum Functions

Laminar Model with General Prandtl Number and Core Temperature Gradient Parameter

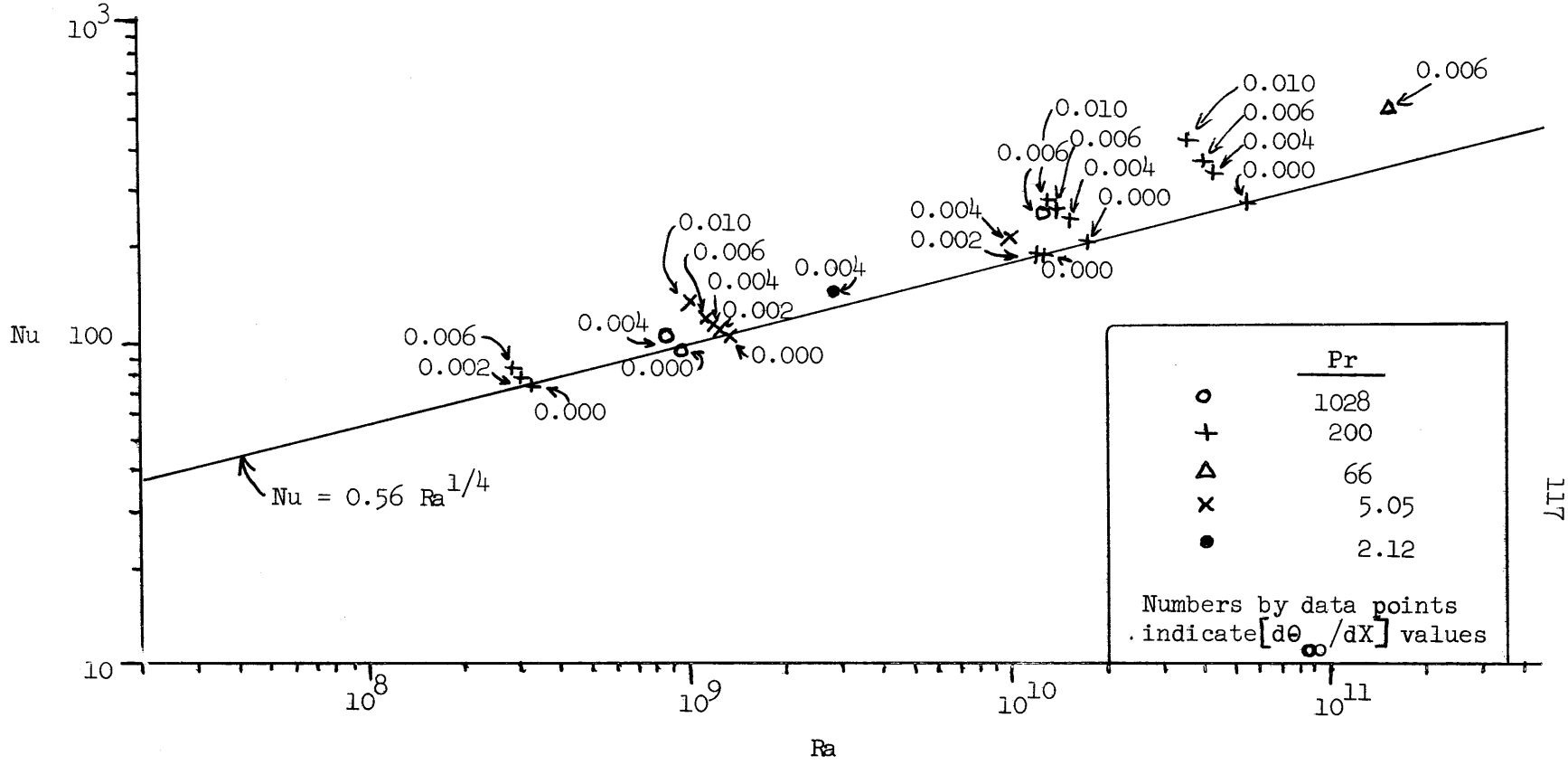

FIGURE 3-6

Effect of Core Temperature Gradient on

Nusselt Number: Laminar

$(\mathrm{Pr}\ X^4)$, as a result of changes in Υ. At $\Upsilon = 0$, the Nusselt number agrees well with the normal empirical correlation (54).

Although the results for Figures 3-5 and 3-6 came from numerical integrations, it is possible to integrate equation 3-46 directly using the method of partial fractions. The result is:

$$\frac{X}{5} + \frac{E^{*1/5}}{\Upsilon} = \frac{1}{4\Upsilon} \ln\left\{\frac{E^{*2/5} - \sqrt{\frac{1}{\Upsilon}}}{E^{*2/5} + \sqrt{\frac{1}{\Upsilon}}}\right\} + \frac{1}{\Upsilon^{3/2}} \ln\left[E^{*2/5} + \sqrt{\frac{1}{\Upsilon}}\right] \quad (3\text{-}47)$$

Unfortunately, although it is interesting to observe the functional relationships in the analytical solution, the expression is sufficiently complex to prevent solving for Υ as a simple function of E^* and X. Such a relation would be useful in the development of a model linking the boundary layer and core regions (Section C).

For the laminar flow, constant wall flux case, the properties of the boundary layer flow, in the presence of a positive core temperature gradient, are determined by numerical integration of equations 3-30 and 3-31. For fluids having $\mathrm{Pr} > 10$, a further simplification is possible involving the approximation that $M^* = E^{*7/5}$ and leading to a single first order, non-linear ordinary differential equation relating E^* and X for values of a single parameter, Υ, which includes the effect of both Prandtl number and core temperature gradient variation.

b. Turbulent, Constant Wall Heat Flux Case

In Figure 3-2, the E^* and M^* variables do not show the same similarity of behavior that was evident for the laminar case, although E^* and M^* do still approach their steady-state values at about the same rate with respect to X. It is immediately evident that variation in Pr

produces significant variation in M^* values while values of E^* are nearly unaffected by changes in Prandtl number.

Two factors must be considered. First, in considering turbulent boundary layer flow conditions, most physically meaningful cases involve values of Prandtl number near unity. In other words, highly viscous fluids become turbulent only at unusually high values of heat flux. Therefore, the restriction of $Pr > 10$ which led to meaningful simplifications in the laminar case has little application to the study of physically occurring turbulent boundary layers.

Second, because of differences in the turbulent and laminar models, the significant influence of Prandtl number persists to higher values than for the laminar case. The significant ratios are

for $\frac{d\theta_{oo}}{dX} = 0$,

$$\frac{E_o^*}{M_o^{*7/11}} = 1 \qquad (3\text{-}48)$$

and for the asymptotic solution:

$$\frac{E_a^*}{M_a^{*7/11}} = \frac{1}{\left[\frac{11}{7}\frac{A_3}{A_1 Pr^{2/3}} + 1\right]^{9/22}} \simeq \frac{1}{\left[\frac{2.242}{Pr^{2/3}} + 1\right]^{9/22}} \qquad (3\text{-}49)$$

At Pr = 10, the second ratio is 15% lower than the first (instead of 3% for the laminar case). At Pr = 2, it is 30% lower, at Pr = .7, 42% lower. Since water, which has values of Prandtl number less than ten, was used as the principal fluid for experimentally studying the turbulent boundary layers and since other fluids of primary interest in turbulent flow--namely low viscosity organics, cryogenic fluids, and

gases--also have low Prandtl numbers, there is little point in developing a simplified solution valid only at much higher Prandtl numbers.

Consequently, E^* and M^* must be found by integration of the two differential equations in Table II as functions of two separate parameters, Pr and $\frac{d\theta_\infty}{dX}$. The Nusselt number which depends on E^* and M^* also is a function of these two parameters. Computed values of Nusselt number for some typical cases are plotted in Figure 3-7. Again, agreement with the empirical relationship is good at $\frac{d\theta_\infty}{dX} = 0$.

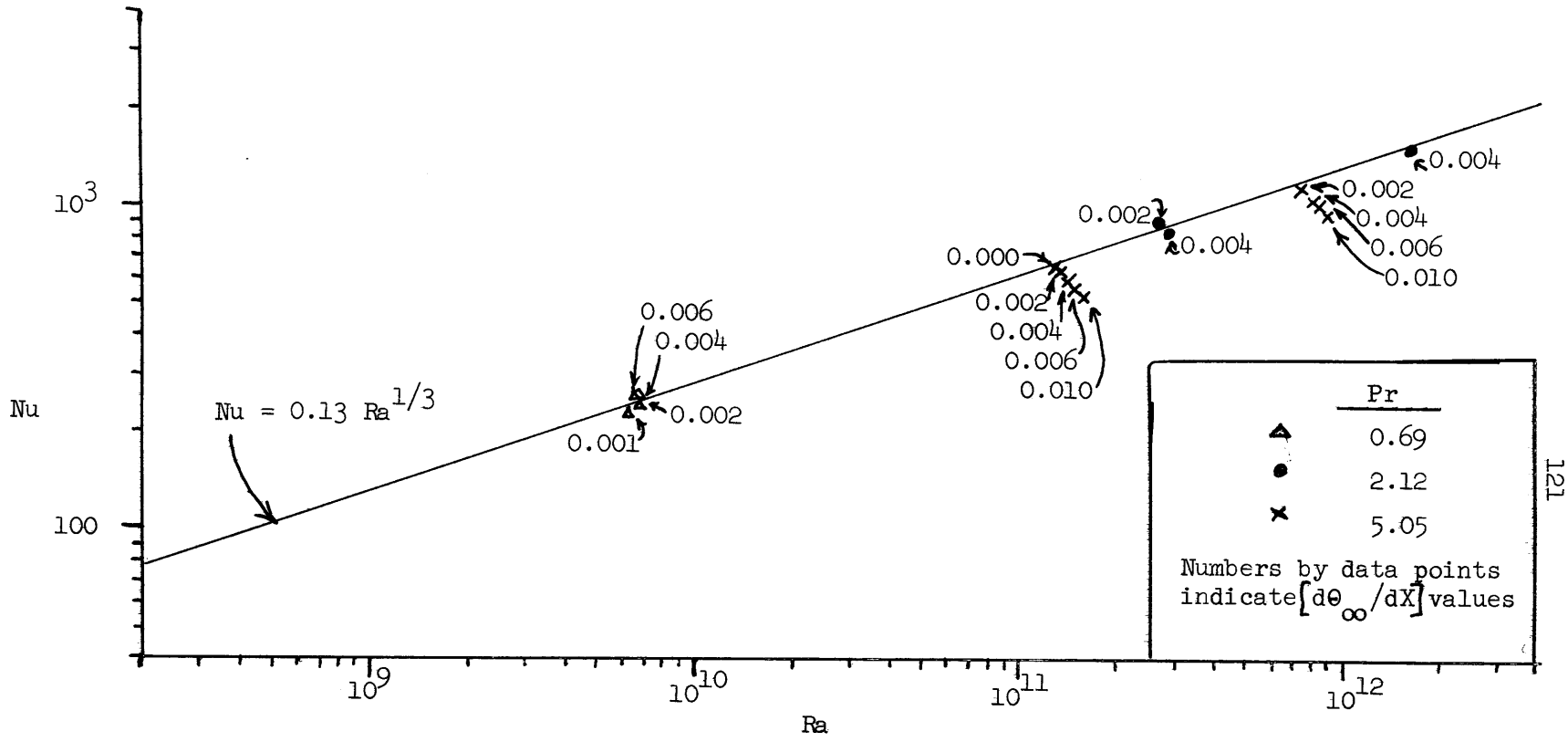

FIGURE 3-7

Effect of Core Temperature Gradient on Nusselt Number: Turbulent

C. Combined Boundary Layer and Core Model

In many enclosed systems, stratification of fluid in the central regions is a consequence of the movement of heated (or cooled) boundary layer fluid into the core at specific locations. From five experimental conclusions presented in Part A of this Section, a model for the core is suggested. Limiting consideration to the heating case for simplicity in discussion, the following model appears valid for describing natural convection within vertical tanks. First, from analysis of boundary layer behavior in the presence of a linear core temperature gradient, the boundary layer volumetric flow rate and the volume-mean temperature can be estimated.

Consider the case of a large vertical cylindrical tank of diameter D and height L. (Figure 3-8) In agreement with experimental observation, the model considers that the boundary layer flow is discharged just below the liquid surface (or the container lid, for completely enclosed liquids or gases) and enters a mixing region which forms the topmost region of the core. The region extends from L to $(L - \Delta x)$, where Δx is the finite thickness of the mixing region. Below the mixing region, no radial core temperature gradients exist and the axial temperature variation is essentially linear in x.

Some simplifying assumptions are now useful. Assume that the mixing region is at a constant temperature, T_L. The rate of change of T_L with time can be found if the temperature and flow rate of boundary layer fluid are known and if the flow from the mixing region to the top of the core is assumed equal to the boundary layer inflow to the mixing region. The mixing region energy balance is, for an energy level assumed equal to zero at T_L and an increment of time, dt:

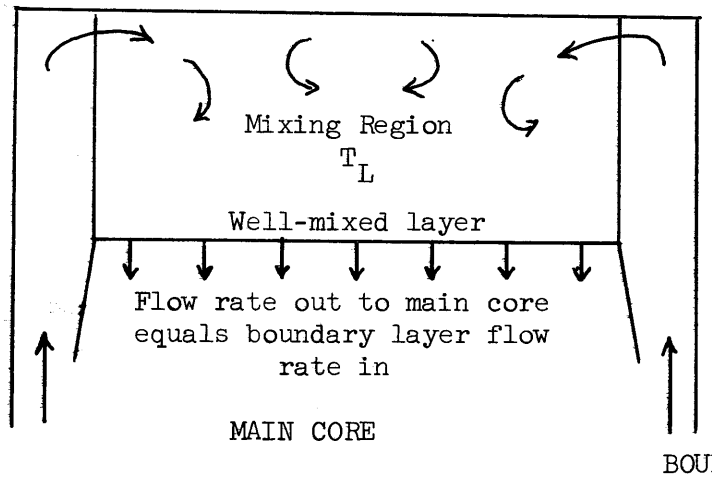

Boundary Layer at x=L:

$$\text{Flow Rate} = \pi D \int_0^\infty u\,dy$$

$$\text{Energy Flux} = \rho C_p \pi D \int_0^\infty u(T-T_L)\,dy$$

FIGURE 3-8

Mixing Region Model

Energy in: $$\left[\rho C_p \pi D \int_0^{y=\infty} u(T - T_L)dy\right] dt \tag{3-50}$$

Energy out: $$0 \quad \text{(Fluid at } T_L\text{)} \tag{3-51}$$

Energy change: $$\rho C_p \frac{\pi D^2 \Delta x}{4} dT_L \tag{3-52}$$

Giving: $$\frac{dT_L}{dt} = \frac{4}{D\,\Delta x} \int_0^{\infty} u(T - T_\infty)dy \tag{3-53}$$

Finally, assume that the rate of change of core temperature gradient is due to the rate of change of T_L:

$$\frac{d}{dt}\left[\frac{d\theta_\infty}{dX}\right] = \frac{k}{q\,(L - \Delta x)} \frac{dT_L}{dt} \tag{3-54}$$

Therefore,

$$\frac{d}{dt}\left[\frac{d\theta_\infty}{dX}\right] = \frac{k}{q\,(L - x)} \frac{4}{D\,\Delta x} \int_0^{\infty} u(T - T_\infty)dy \tag{3-55}$$

Case 1. Laminar, q_w

$$\int_0^{\infty} u(T - T_\infty)dy = \frac{q\nu}{kC} \frac{A_1}{2} E \tag{3-56}$$

where $A_1 = \frac{1}{30}$ for model

$$\frac{d}{dt}\left[\frac{d\theta_\infty}{dX}\right] = \frac{4}{(L - \Delta x)D} \frac{L}{\Delta x} \frac{1}{CL} \frac{1}{Pr} E^* \tag{3-57}$$

since $E = \frac{2}{A_1} \frac{1}{Pr} E^*$.

$$\frac{d}{dt}\left[\frac{d\theta_\infty}{dX}\right] = \frac{4a}{(L - \Delta x)D} \frac{L}{\Delta x} \frac{1}{(GrNu)^{1/4}} E^* \tag{3-58}$$

Although E^* is a known function of L, Pr and $\frac{d\theta_\infty}{dX}$, the above relationship must be solved numerically to find $\frac{d\theta_\infty}{dX} = f(Pr, GrNu, Fo, \frac{\Delta x}{L})$ However, the limiting value of E^* is

$$E_a^* = \frac{.583}{Pr^{1/4}} \left[\frac{dX}{d\theta_\infty}\right]^{5/4} . \tag{3-59}$$

Therefore, as E^* approaches its limiting value, the core temperature gradient should vary as:

$$\frac{d}{dt}\left[\frac{d\theta_\infty}{dt}\right] = \frac{4}{(1 - \frac{\Delta x}{L})} \frac{\alpha}{ID} \frac{L}{\Delta x} \frac{.583}{(GrNuPr)^{1/4}} \left[\frac{dX}{d\theta_\infty}\right]^{5/4} \tag{3-60}$$

Separating variables and integrating:

$$\left[\frac{d\theta}{dX}\right]_a = 1.456 \left[\frac{1}{\frac{\Delta x}{L}(1 - \frac{\Delta x}{L})}\right]^{4/9} \left[\frac{\alpha t}{ID}\right]^{4/9} \frac{1}{(RaNu)^{1/9}} \tag{3-61}$$

Case 2. Turbulent, q_w

$$\int_o^\infty u(T - T_\infty)dy = \frac{q\nu}{kC} \frac{1}{Pr} E^* \tag{3-62}$$

$$\frac{d}{dt}\left[\frac{d\theta_\infty}{dX}\right] = \frac{4 \frac{L}{\Delta x}}{1 - \frac{\Delta x}{L}} \frac{\alpha}{ID} \frac{1}{(GrNu)^{1/4}} E^* \tag{3-63}$$

At the Limiting Value:

$$\frac{d}{dt}\left[\frac{d\theta_\infty}{dX}\right] = \frac{4(2.48) \frac{L}{\Delta x}}{\left[1 - \frac{\Delta x}{L}\right]} \frac{\alpha}{ID} \frac{1}{(GrNu)^{1/4}} Pr^{1/24} \left[\frac{dx}{d\theta_\infty}\right]^{7/8} \tag{3-64}$$

$$\left[\frac{d\theta_\infty}{dX}\right]_a = 3.4 \left[\frac{1}{\frac{\Delta x}{L}(1 - \frac{\Delta x}{L})}\right]^{8/15} Fo^{8/15} \frac{Pr^{7/45}}{(RaNu)^{2/15}} \tag{3-65}$$

The validity of these derived relationships will be tested against experimental data in Chapter IV. They will be shown to be useful for a wide range of conditions. Experimental results will be used to find values of $\Delta x/L$.

IV. EXPERIMENTAL ANALYSIS

A. Scope of Experimental Investigation

Although the particular system studied was a vertical cylinder filled with liquid and subjected to a uniform wall heat flux, the range of system parameters considered was extensive. In addition, use was made of all related data that could be found in the literature. The corresponding case for a horizontal cylinder was treated extensively by Maahs (50), and his results bear some interesting relationships to the present study. A further broadening of the applicability of results to include cooling cases and cases of specified constant wall temperature is probably justified on the basis of the successful use of boundary layer models for the actual problem considered.

The experimental apparatus consisted of a vertical Pyrex cylinder, with 8-in. o.d. and $\frac{5}{16}$ -in. walls. (Figure 4-1) The outside of the cylinder was coated with a uniform, transparent, electrically-conducting coating (Corning E-C coating) which permitted resistance heating of the cylinder walls. In the vertical direction, the cylinder was 24-in. high. However, the coating was divided by circumferential contact bands into three cylindrical sections, each 8-in. high. Consequently, nominal cylinder aspect ratios of one, two and three could be studied by filling and heating only the desired number of sections. The coating resistance was about 8 ohms per section and the practical range of electrical input was from one to ten amperes per section. Since data were recorded on a sixteen point recorder with an eight minute print cycle, meaningful data were not obtained for times less than about two to five minutes. Some runs lasted as long as six hours. The actual experimental fluids were glycerin, water and an 85 wt. % glycerine in water mixture.

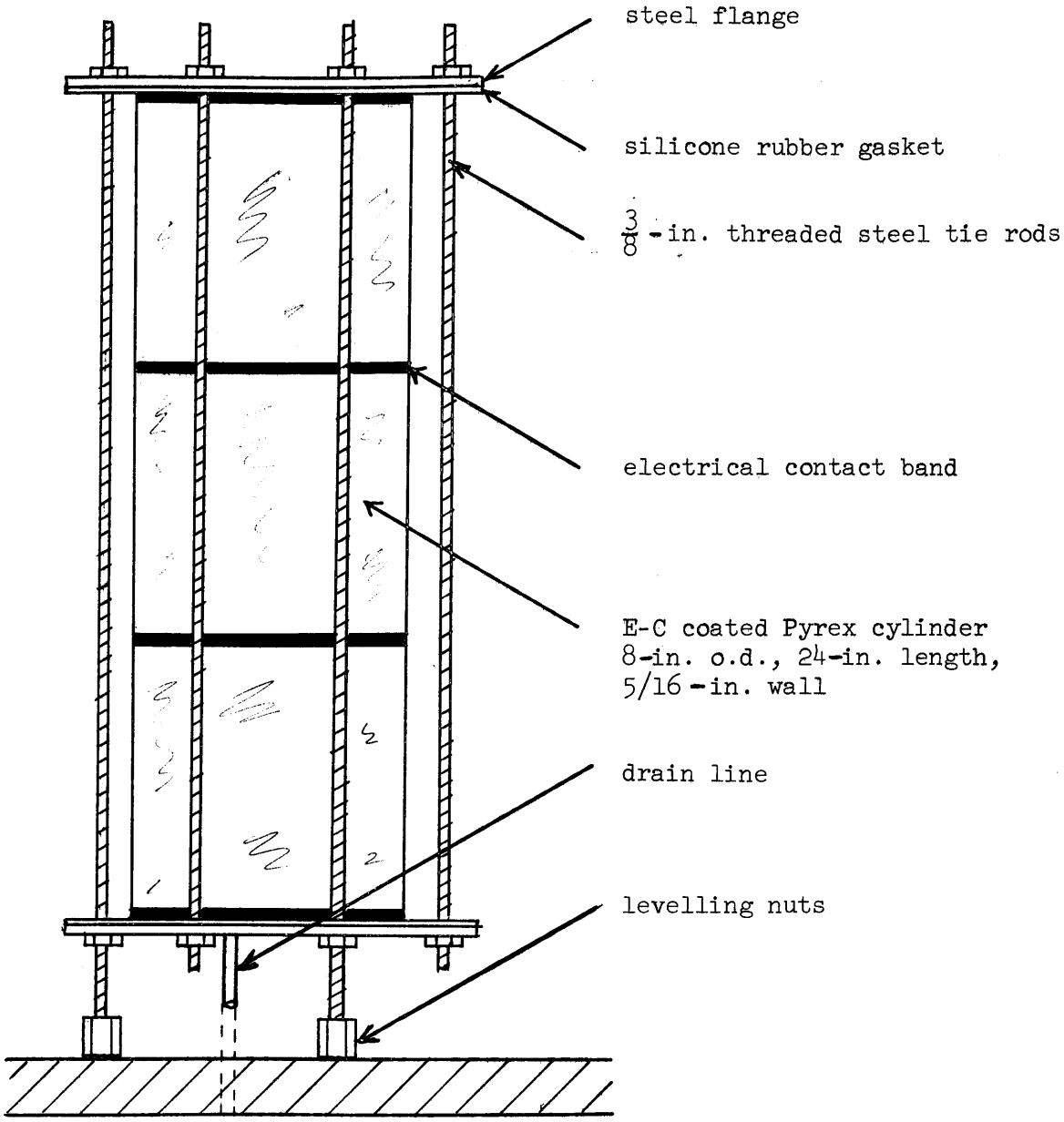

FIGURE 4-1

Experimental Enclosure

The resulting range of experimental parameters, in terms of the dimensionless groups important in natural convection, are:

Dimension held constant:	Diameter = 0.614 ft.
Aspect ratios $(\frac{L}{D})$:	1.09, 2.12, 3.18
Prandtl numbers:	2.2 to 8000
Grashof numbers:	10^3 to 10^{11}
Fourier numbers:	.0002 to .08

In addition, data reported by Barakat (4) for a 0.278 ft. diameter cylinder with an aspect ratio of 2.70 were included in the study. His data which were taken in support of a predominantly theoretical study consisted of temperature readings taken during the first four minutes after a step change in wall heat flux. Therefore, although these measurements do not extend the range of Fourier number they provide additional information in a region where the accuracy of data in the present study is least accurate and complete. Data reported by Siefkes (91) in a 0.667 ft. diameter cylinder with an aspect ratio of 0.845 were also evaluated. His temperature data are only for the first ten minutes after the start of heating and for two specific values of wall heat flux, but he does use a different fluid--ethylene glycol--for one test. Ethylene glycol has properties similar but not identical to the 85% glycerin - water mixture used in this work.

B. Experimental System

1. Test Enclosure

The selection of an 8-in. Pyrex vertical cylinder for the test enclosure was based on several factors. First, the vertical cylindrical tank is a common configuration, especially for cryogenic propellant tanks in which stratification problems are troublesome. Secondly, the diameter was selected as the largest convenient size compatible with accessory laboratory equipment. The height chosen was sufficient to include $\frac{L}{D}$ ratios between one and three, the most common range for industrial tanks. Figure 4-1 is a sketch of the enclosure; additional details are presented in Section VIII Appendix A. Since flow visualization was an important part of the study, the cylindrical portion of the enclosure was made of Pyrex, coated with a transparent, conductive film to permit ohmic heating of the walls. Two 1/4-in. steel end flanges, cushioned from the glass by 1/8-in. silicone rubber gaskets, completed the enclosure and were sealed to the glass by the pressure exerted by a ring of longitudinal tie rods. Fill and drain line and instrumentation connections were made through the flanges.

2. Thermal Boundary Condition Control

The experimental boundary conditions should be selected to match the theoretical boundary conditions as closely as possible to facilitate interpretation of results. The ideal system for this study would undergo a step change in wall heat flux at the start of the experiment and the wall heat flux would remain uniform and constant thereafter. The top and bottom of the enclosure would be perfectly insulated; furthermore, at the free liquid surface, no heat or mass interchange with the vapor

phase would occur.

In the implementation of an ideal system, some compromise is inevitable. The degree of deviation from the ideal will be discussed as part of the physical description of the thermal boundary condition control systems.

Resistance heating is an easy way to obtain a uniform and controllable constant heat flux. The thin-film, electrically-conductive, transparent coating on the Pyrex cylinder wall was remarkably uniform. Since the resistance of all surface squares, when measured between opposite sides, should be the same, the uniformity could be checked by comparing resistance measurements for numerous arbitrary square areas, both large and small (down to about one centimeter square), on the coated surface. Within the accuracy of the ohmmeter (±2%), all readings were identical.

The enclosure was designed so that it could be used at three different liquid depths and the heating system was designed so that only the portion of system containing liquid would be heated. The "E-C" (electrically-conductive) coating was divided into three equal cylindrical sections by four circumferential bands of silver which were deposited on top of the coating. (Figure 4-1) External contact was made by using copper straps held tightly on top of the silver bands by means of a clip arrangement. Power was supplied to each section through separate Variacs with individual current and voltage metering systems. Further details are given in Appendix A.

Several problems result from practical considerations which prevent the application of the E-C coating on the inner surface of the Pyrex cylinder. Although the heat generation is quite uniform at the film, the thermal resistance and capacity of the wall is appreciable. At

start-up, nearly one minute is required to establish a temperature gradient across the wall sufficient to allow full heat flux at the fluid-wall interface. Since investigation of the starting transient was not part of the present study, the error introduced by the initial time lag was small. In a few runs, data were taken as soon as three minutes after start-up; generally, the first data were recorded about ten minutes after start-up. Although the effect of the initial lag might be significant in a few of the very early readings, for the great majority of the data, the effect was negligible.

Two other thermal effects complicate the boundary heat transfer after the effect of the starting transient has died out. First, the wall has sufficient thermal capacity, relative to the contained fluid, to intercept about 10% of the total energy flux. For a given fluid and enclosure, this loss remains nearly constant and can be calculated accurately. Somewhat harder to estimate accurately is the loss from the hot outer wall of the vessel to the surroundings. Standard correlations, given in McAdams (54), were used to estimate natural convection heat transfer coefficients for the air outside the heated vertical cylinder. Since the losses to the surroundings become progressively greater as the system temperature level increases, the amount of energy reaching the fluid inside the cylinder would decrease during the course of a run if the power input to the E-C film remained constant. Consequently, two operational modes were used. One group of tests were run at a constant power input level; another series was run with gradual small increases in the electrical input just sufficient to compensate for the increased heat losses to the ambient.

The remaining boundaries, the bottom flange and the liquid surface,

should be adiabatic to match the mathematical model. Although the bottom flange was insulated to prevent losses to the surroundings, the rubber gasket actually in contact with the liquid was a good enough conductor to cause the bottom flange temperature to follow the temperature level of the bottommost fluid in the enclosure. The system heat loss to the bottom flange was about 5% in most cases. Losses to the upper portion of the enclosure were small due to the low conductivity of the Pyrex wall. In addition, the vapor space was enclosed, so that only a negligible amount of energy (order of less than 0.1%) was required to maintain saturation pressure over the liquid. However, for tests with pure water, the vapor would condense on cooler parts of the system--the upper flange and walls. Since energy losses were increased orders of magnitude by condensation, a surface surfactant film was used to reduce vaporization in water tests.

In spite of the various heat losses, an estimate of the amount of energy reaching the fluid could be made by computing the magnitude of each loss and deducting the sum from the measured electrical energy input. Since extensive temperature measurements were made within the fluid, the total energy input to the fluid could also be estimated by spatial integration of the temperature field and multiplication of the result by the fluid volumetric enthalpy. A sample calculation is given in Appendix D. The instantaneous heat flux is related to the time derivative of the total energy level of the fluid. In Appendix F, energy balances of this sort are shown. The rate of change of fluid enthalpy plus the various heat loss rate estimates generally agree with the electrical power level to within $\pm 5\%$, except for the period immediately after start-up.

3. Temperature Measurements

A network of fine-wire thermocouples was used to obtain temperature measurements during the natural convection experiments. In the design of the thermocouple and thermocouple support systems, results of a series of preliminary tests were considered. Most important was the observation that flows were radially symmetric. In preliminary tests, both temperature measurements and dye tracer observations indicated no detectable differences due to angular position around a number of circles of specified radius and height within the system. Some qualification of this statement is necessary, since the cylinder itself was slightly elliptical in cross-section due to fabrication difficulties (3/8-in. out-of-round). However, if radial distances were measured inward from the wall, rather than outward from a common center, the statement about radial symmetry is valid. Since the natural convection flows studied always consisted of a fairly narrow boundary-layer type flow along the wall, it is easy to see why distance from the wall should be the primary factor in determining symmetry. In the central regions, radial temperature variations are generally small and exact radial position (whether measured from the wall or from the center) is far less critical. To check this hypothesis, measurements were made along the major axis ($7-\frac{11}{16}$ in. diameter) and the minor axis ($7-\frac{5}{16}$ in diameter) of the enclosed fluid. In about the outer 10% of the system, temperature readings agreed only if distances were measured from the wall; in the central regions, differences due to radial position variation between the wall and center-line reference point systems were negligible.

Consequently, the decision to locate nearly all the thermocouples in a single radial plane was made. In Figure 4-2, all of the fluid

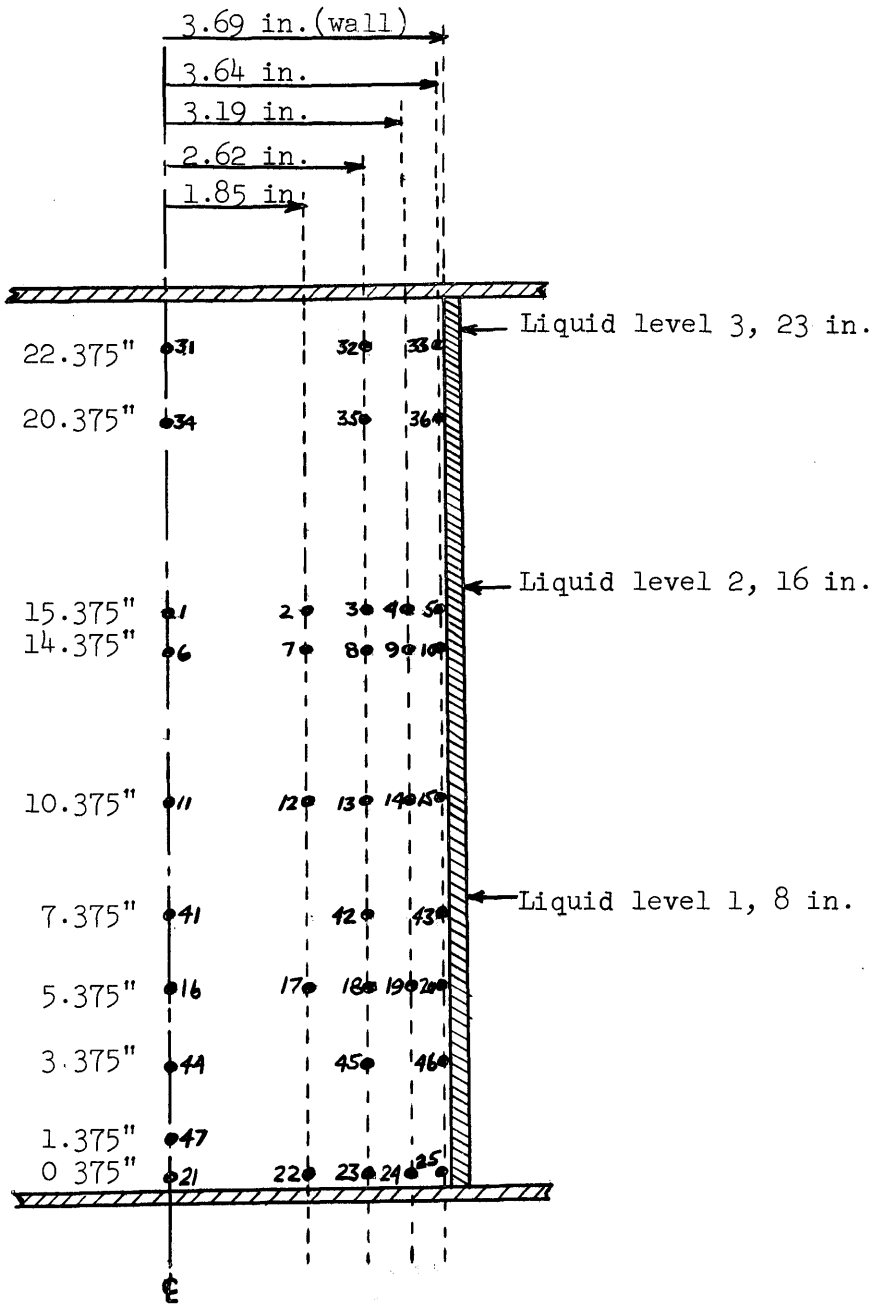

FIGURE 4-2

Temperature Measurement Locations

thermocouple locations which were used in the course of the experimental work are shown with the exception of two thermocouples which were used for recorder calibration and an additional check on the assumption of symmetry. Not all thermocouples were used in every run. Depending on the liquid depth, a group of twenty-five thermocouples, suitably spread throughout the radial plane were selected for data locations. Fifteen thermocouples in locations near the wall and near the liquid surface were connected to a 16-point automatic Brown recorder. The remaining ten thermocouples, at central locations where temperature variation is gradual, were connected to a multiple switch and periodic readings were taken manually by using a precision potentiometer.

Additional thermocouples consisted of a pair of calibration thermocouples attached to the bulb of an accurate thermometer with a thin epoxy film. One of these thermocouples was connected to the Brown recorder; the other, to a position on the multiple switch. Consequently their readings could be compared with each other and with the temperature level registered by the thermometer. The thermometer was located 60° away from the main data plane so that it could also be used to check symmetry. In addition, similar tests were run--one with only the thermometer assembly, another with only the main thermocouple assembly, and one with both--to see whether the presence of the instrumentation was altering the measured temperature field. Although dye tracers indicated local disturbances due to the thermometer and the main thermocouple support structure, no general alteration of the convective circulations was observed.

The thermocouple support structure consisted of a ladder arrangement set 3/4-in. in back of and parallel to the data plane. The main

support rods were 3/8-in. nylon and the cross rods were 1/8-in. (Figure 4-3). Three-mil copper-constantan thermocouples were inserted through holes drilled in the cross rods and cemented so that the 0.01-in. beads were in the desired location in the data plane. The thermocouple wire was electrically insulated with a thin silicone coating to prevent electrical shorts to the weakly conductive test fluids. The radial spacing of the thermocouples was chosen so that an arithmetic average of their readings would represent a volume-average temperature at the particular axial location. The center of the thermocouple beads nearest the wall were located only 0.05-in. out from the glass. Such a spacing corresponds to about five times the width of a thermocouple bead. In general, however, these thermocouples were still outside of the convection boundary layer except for some of the high viscosity fluid tests. Even in these tests, though, such readings can not be interpreted as meaningful point temperatures within the boundary layer.

Thermocouples were also cemented to the inner wall of the enclosure. However, since their beads protruded into the boundary layer, they registered some sort of average fluid-wall temperature which could not be interpreted meaningfully. Outside wall thermocouples were more accurate but were used mainly to guard against overheating of the E-C film.

Surface temperatures were also measured in a number of tests. Since the surface position moves as a result of fluid expansion, a movable probe was used to locate the surface thermocouple bead in the proper radial position just below the surface, i.e., the bead was fully submerged.

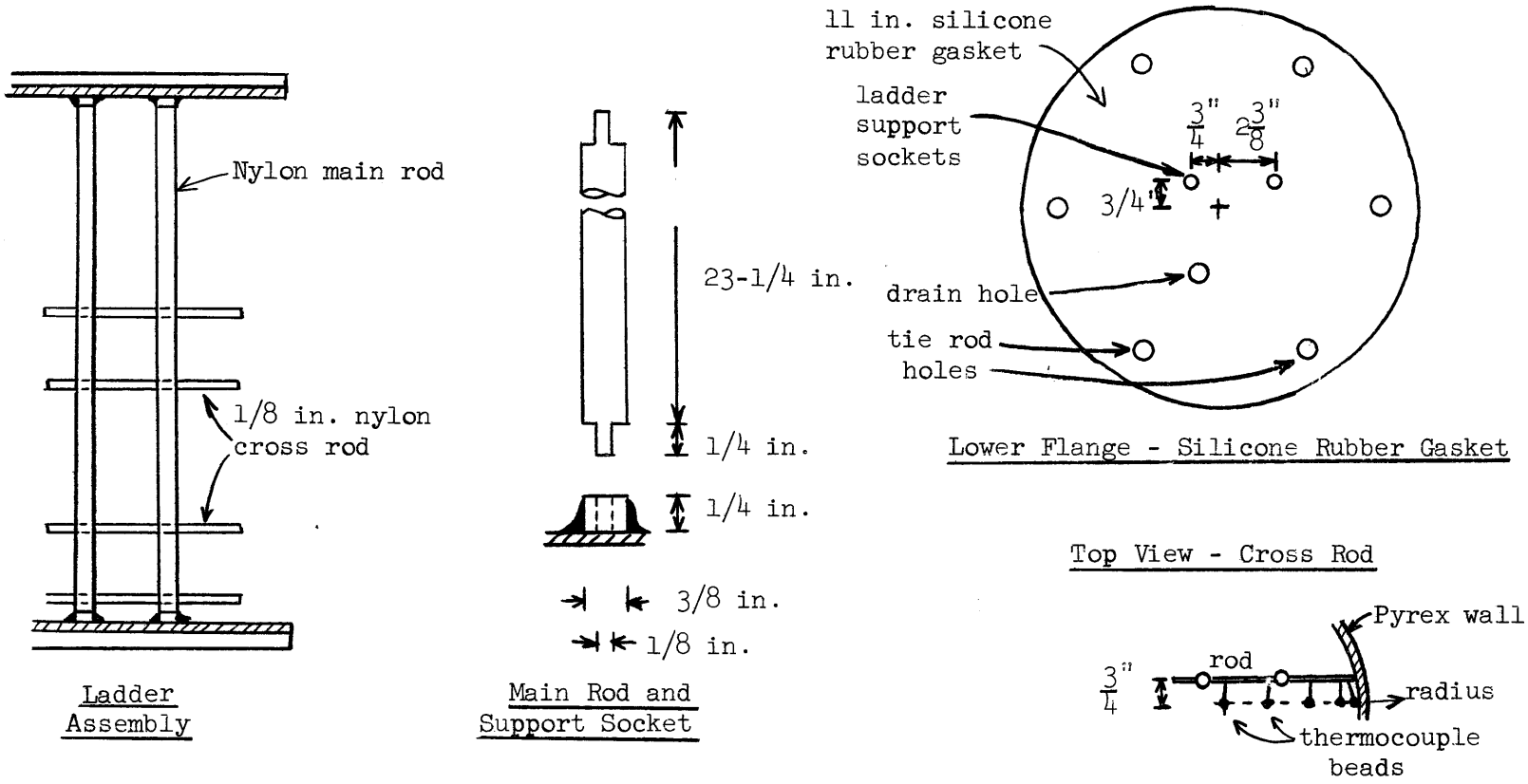

FIGURE 4-3

Thermocouple Support Ladder Assembly

4. Flow Visualization

An original objective of the experimental program was to obtain quantitative velocity field data for the system. A number of problems prevented realization of this goal; however, qualitative observations of dye tracers gave good indications of the nature of the convective circulations and gave additional validity to the theoretical model which was developed mainly from temperature data.

The dye system finally used consisted of two long hypodermic syringes, supported by an assembly which rested on the top flange and which permitted positioning of the injection point at any location within the liquid. The assembly also included a tightly-threaded screw control to allow injection of minute amounts of dye and to prevent flow disturbance as a result of injection.

The dye finally used was a dark blue ink dissolved in a sample of test fluid to match tracer and test fluid densities as closely as possible. The most interesting injection points were at the bottom corners of the system and in the region below the liquid surface. In the first case, distinct boundary layer flow was observed; near the surface, fairly complex circulations, including cell formation, were evident. These phenomena near the surface produced sufficient mixing so that the lower 90% of the core liquid was quite homogeneous radially throughout the entire central region of the vessel. In other words, although axial temperature variation was important, radial variations were negligible as a result of surface mixing.

Drawings of tracer path lines made from photographs taken during actual tests are presented in Figures 4-4 through 4-7.

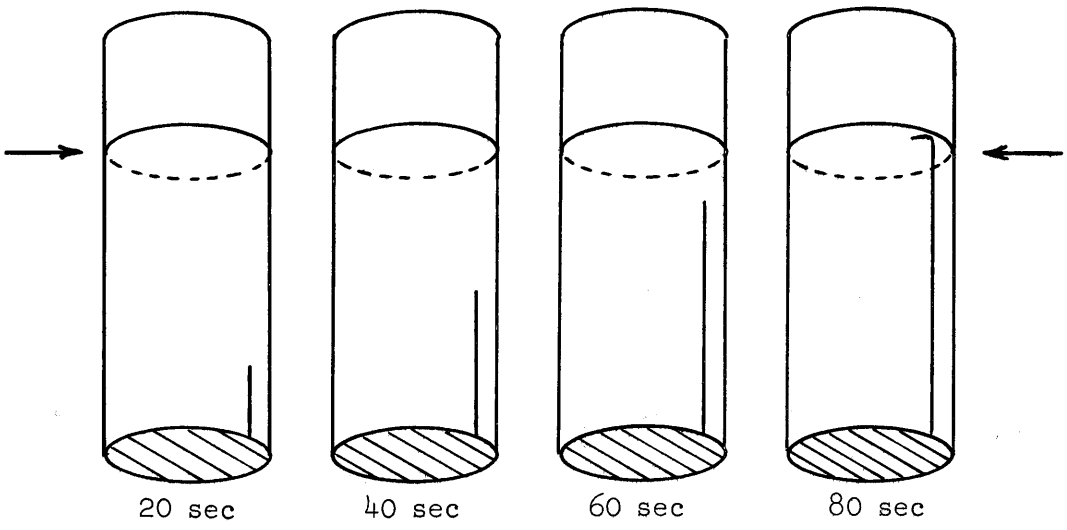

Times (sec) after dye injection in bottom corner
Arrows indicate liquid level

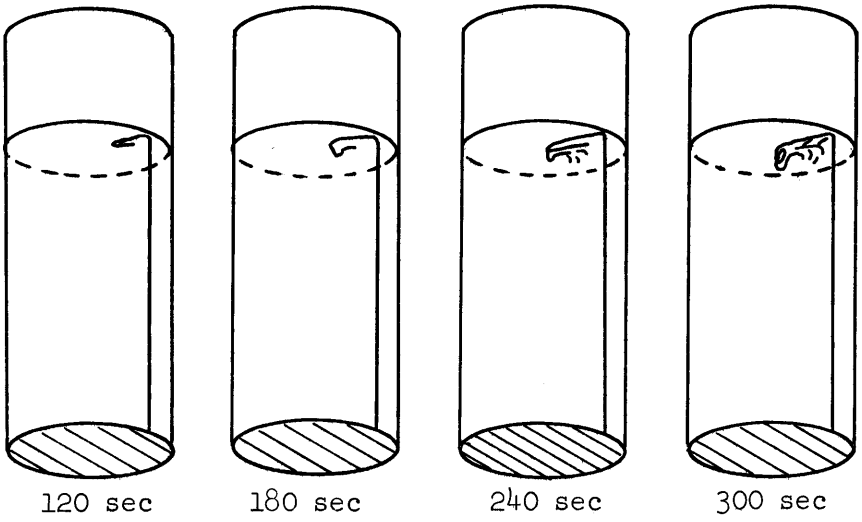

FIGURE 4-4

Typical Flow Pattern Observations

(Test E-2-6, 85% glycerine, L=1.33 ft, q_w = 500 BTU/hr,ft^2 (nominal))

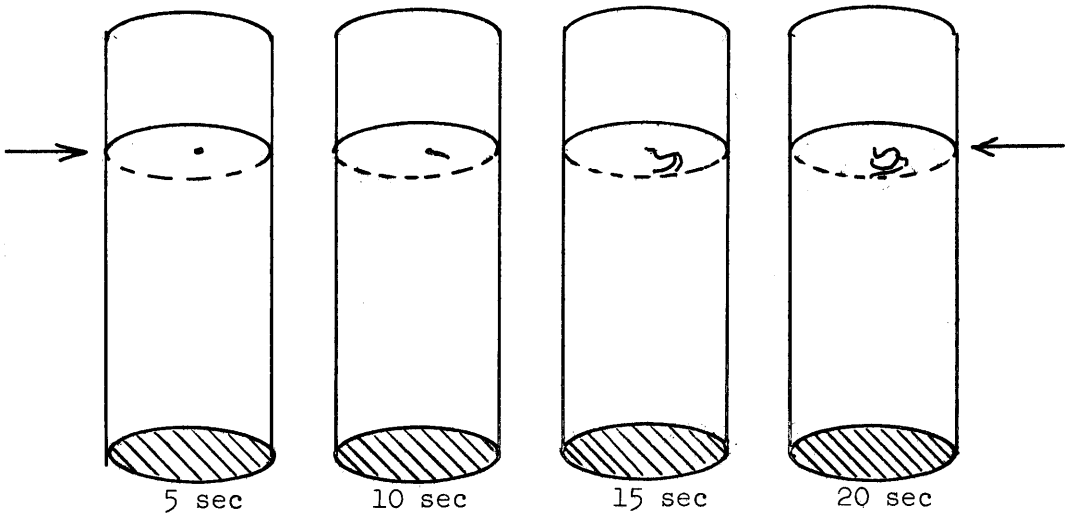

Dye injected just to right of the center of the surface.
Times denote time after injection. Arrows show liquid level.

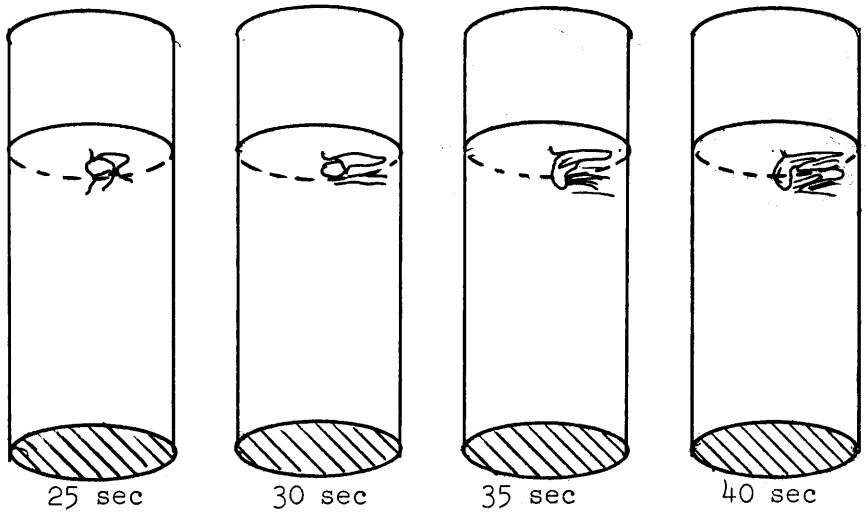

FIGURE 4-5

Typical Flow Pattern Observations

Test E-2-6 85 weight percent glycerine
L = 1.33 ft, q_w = 500 BTU/hr,ft^2 (nominal)

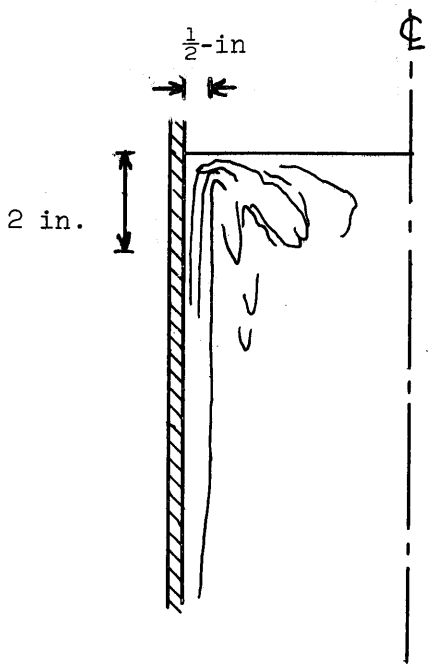

Test G-2-2
Glycerine
L = 1.33 ft
q_w = 60 BTU/hr,ft^2
(nominal)

Dye injected in bottom corner

215 min. - Initial trace rises in 30 sec. Tracer at outer edge of boundary layer has lower velocity of about 3 in/min.

FIGURE 4-6
Typical Flow Pattern Observations

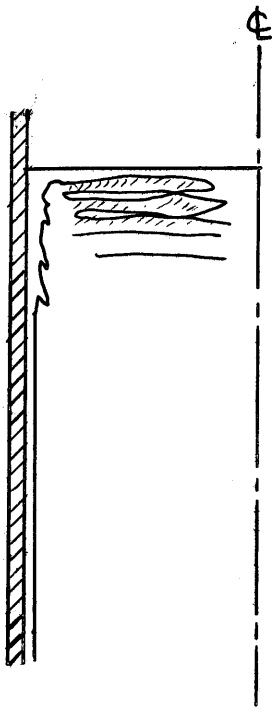

Test A-2-7V
Water
L = 1.33 ft
q_w = 800 BTU/hr,ft^2
(nominal)

Dye injected in bottom corner

2 min. - Dye rises 1 in/sec straight up the wall. Three inches below top surface, flow streaks start to curl over irregularly as shown above. This may be a transition to turbulence. Dye streaks in core sink to bottom in about 20 min.

28 min. - Dye rises straight to top surface with no curling at a velocity of about 0.4 in/sec (turbulence surpressed by core temperature distribution?).

FIGURE 4-7

Typical Flow Pattern Observations

C. Experimental Data

The raw experimental data consisted of visual and photographic observation of dye tracer pathlines and measurement of the temperature field within a radial plane in the system at specific times during an experiment. In addition, the power input to the heating film on the walls was observed by measuring current and voltage across each section. Ambient and initial conditions were also recorded.

The sketches from photographs, Figures 4-4 through 4-7, are typical of the flow visualization data. For the range of conditions studied, the existence of both a distinct boundary layer flow and a mixing region below the surface are evident. Further, the boundary layer behavior is qualitatively consistent with theory. That is, the boundary layer width increases with Prandtl number and with system height, at least near the bottom of the system where initial boundary layer growth occurs. Whether or not an asymptotic boundary layer thickness occurs can not be determined from the visual and photographic observations. Photographs taken at spaced time intervals of dye in the boundary layer indicated that the flow initially accelerated significantly and then tended to reach a fairly constant velocity. However, since the radial diffusion of dye in the boundary layer could affect apparent velocity measurements, these indications are only qualitative. One other qualitative observation, which may be particularly significant, is the fact that a streak of dye remained parallel to main dye flow path in the upper regions of the system long after the main portion of dyed fluid had reached the surface. Perhaps this supports the model that no new fluid is being brought into the boundary layer when an axial core gradient is present. Diffusion of dye is again a possible explanation, but the computed diffusion rates

appear too small to account for this effect. Also the dye line remains intact for a long period after the initial injection and gradually drifts a small distance inward (order of 1/4-in.) from the wall. This may be due to the slow gradual increase of the core temperature gradient. At steeper core gradients, the limiting boundary layer flow rate is somewhat reduced and is achieved in a shorter distance up the wall. Consequently, during the course of time, at a point in the region where boundary layer flow has become constant, the boundary layer flow gradually decreases. This decrease may result in a small amount of fluid being rejected from the outer edge of the boundary layer and may account for the slight inward movement of the dye line.

Stefany (23, 99), who studied natural convection heat transfer coefficients in a constant wall temperature cylinder, also observed dye tracers in the boundary layer. He also noted tracer lines which moved radially inward, but his observations indicated both that the inward movement was considerable (up to about one-third of the radial distance) and that the tracer lines tended to bow toward the center of the cylinder.

For the constant wall temperature system, one might imagine that fluid at the wall temperature would tend to form an upper stratified layer which would grow in depth with time. Below this layer, an axial core temperature variation would occur. In the constant wall temperature case, a positive core temperature gradient could result in fluid being rejected from the boundary layer as it moves up the wall (since the decreasing energy input at the wall might be insufficient to raise the temperature level of all the boundary layer fluid to match the increase in core temperature level). This would explain the more rapid inward movement of the tracer lines in Stefany's system. The bowing of the

lines is probably related to the presence of an upper isothermal strata which would be present in a constant wall temperature system. Rigorous solution of the boundary layer equations for the constant wall temperature case with core temperature variation, as formulated in Table II, would permit further evaluation of the model in light of Stefany's results.

Other dye observations were made in the present system. The precise point of transition to turbulent boundary layer flow was hard to observe although the angular dispersion of dye in some of the highest heat flux tests with water strongly suggested turbulent behavior. These tests were at Rayleigh numbers considerably higher (10^{10}-10^{11}) than the normally cited transition point of 10^{9}.

The over-all behavior of the system was not significantly changed by the transition. Residual dye streaks were still observed. Of course, the deposition of turbulent flow near the surface should affect the surface mixing mechanism. However the model was based on a well-mixed surface region and did not depend on details of the mixing process.

Temperature data at each thermocouple position were recorded as functions of time. In the initial data reduction, specific times were selected and temperatures at the designated times read from smooth curves through the individual time points recorded for each thermocouple location. The initial isothermal temperature of the system was subtracted from all the readings. Consequently the basic temperature data for each run were organized as a two-dimensional spatial matrix of point-temperature increases in the fluid within the radial plane. Time provided a third dimension, generating a series of these data matrices for each experiment. Data in this form is presented in Appendix C.

Further treatment of the data included the plotting of axial temperature variation as a function of specific radial locations and specific times. Figures 4-8 through 4-12 illustrate the results of this procedure. The solid lines represent the average temperature rise (based on averaging radial thermocouple readings at a particular height and time) profile; dotted and dashed lines represent the axial profiles at the center line and at the thermocouple positions nearest the wall (dimensionless radius = 0.985) respectively.

These curves have several useful properties. First of all, qualitatively they lead to the conclusion that, with the exception of surface phenomena in the upper 10% of the system and some start-up phenomena, radial temperature gradients in the core region are so small that the hypothesis of a well-mixed core in the radial direction is substantiated.

Next, by graphical integration of the radial average profile over the axial dimension, these curves can be used to obtain the total enthalpy of the system at particular times. Sample calculations illustrating this and other procedures described in this section are presented in Appendix D. In effect, this graphical integration allows computation of a volume-average temperature for the system as a function of time. Variation in fluid properties are considered only in the sense of variation of the average system temperature level. That is, at a specific time, all properties are assumed constant at their values corresponding to the average system temperature. Spatial variation in fluid properties as a result of the internal temperature field is not considered. This simplification is justified on the basis that the volume average temperature represents a reasonable average temperature level for both the

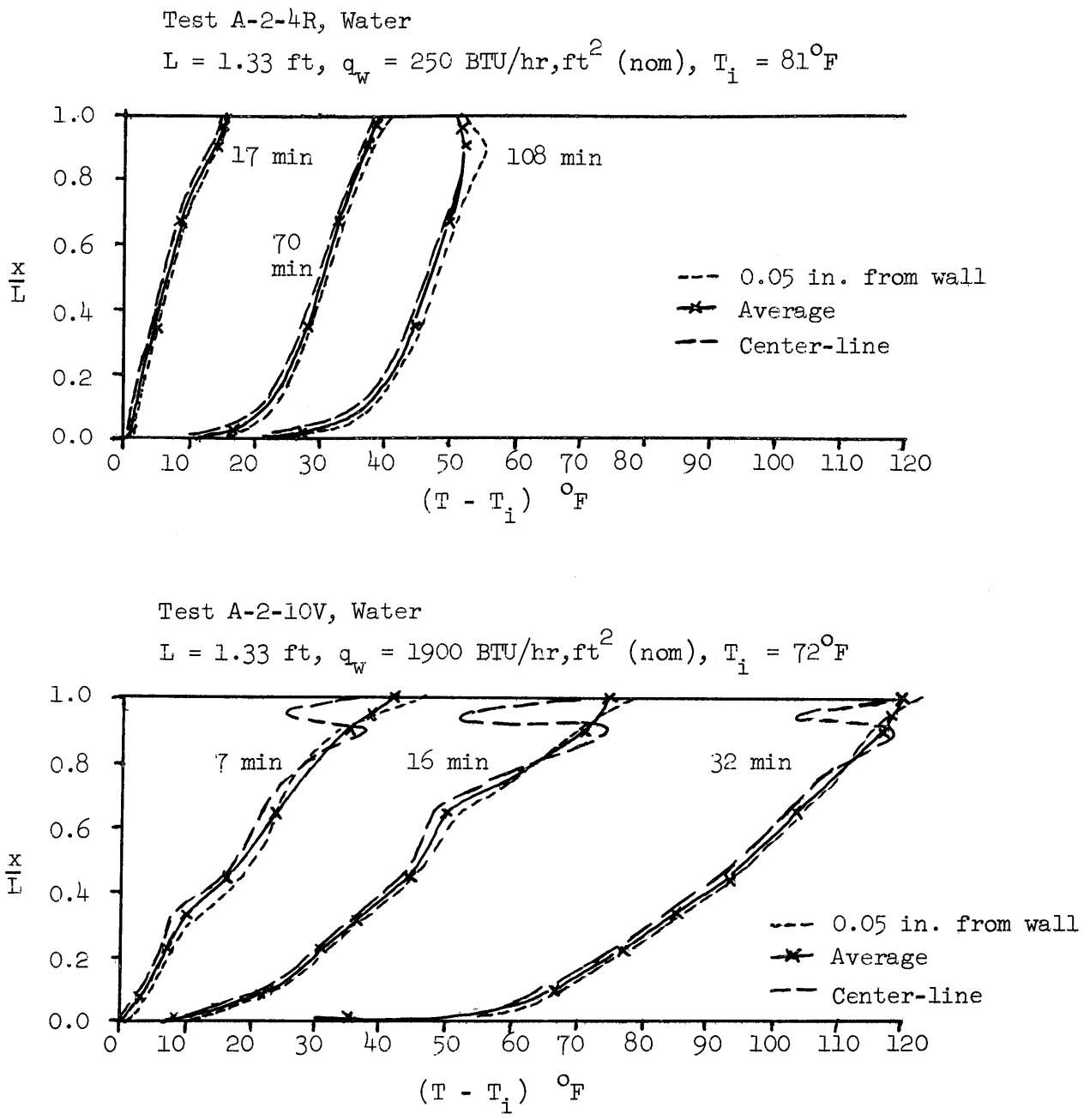

FIGURE 4-8

Axial Core Temperature Profiles

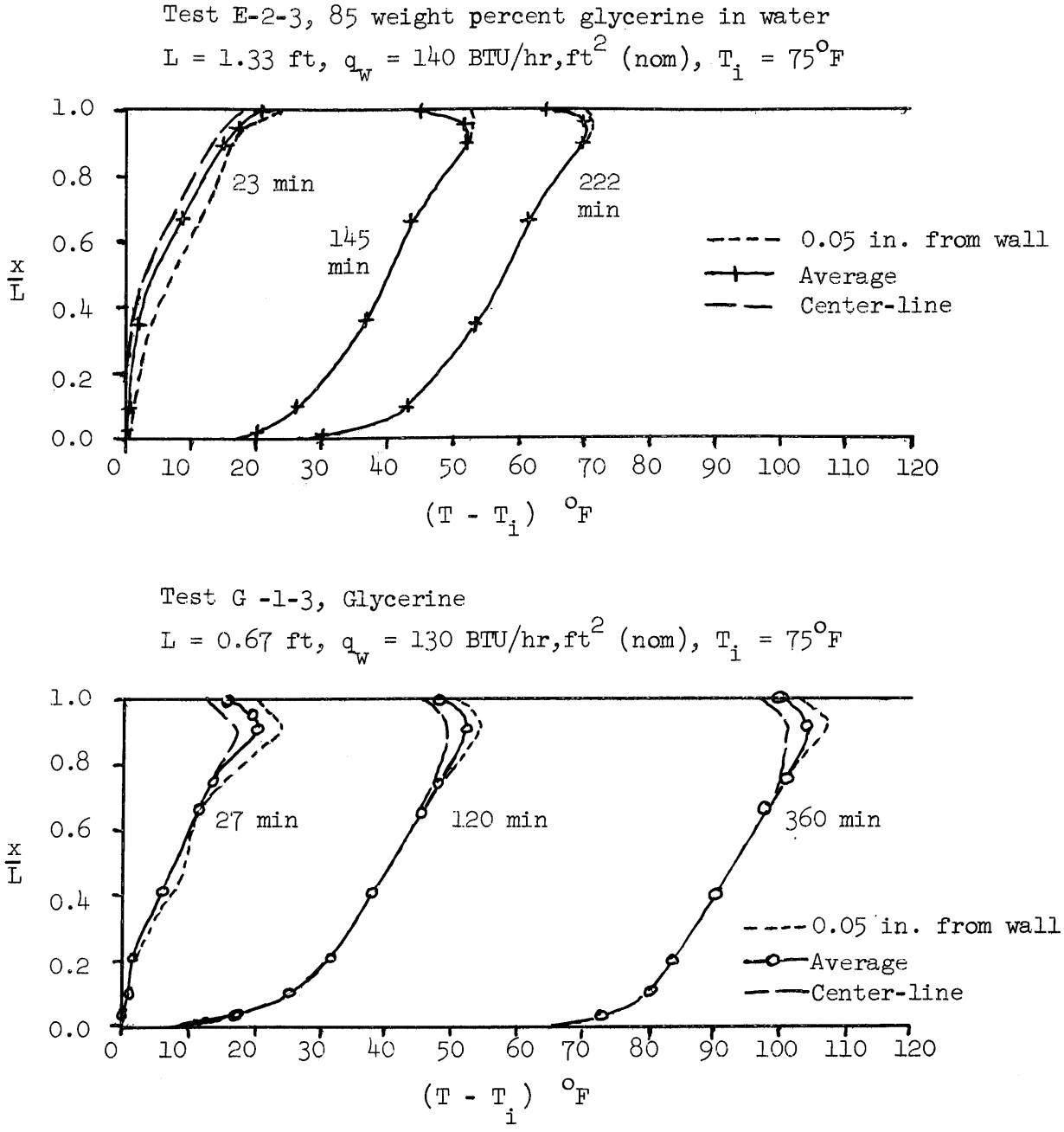

FIGURE 4-9

Axial Core Temperature Profiles

Test A-3-5C, Water

L = 1.96 ft, q_w = 460 BTU/hr,ft^2 (nom), T_i = 78°F

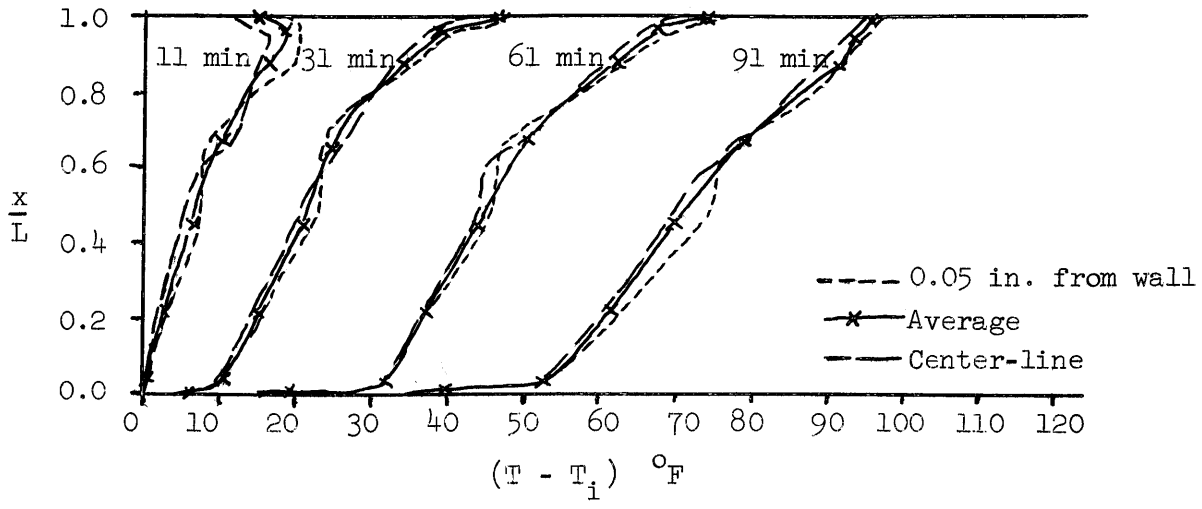

Test G-2-6, Glycerine

L = 1.33 ft, q_w = 500 BTU/hr,ft^2 (nom), T_i = 87°F

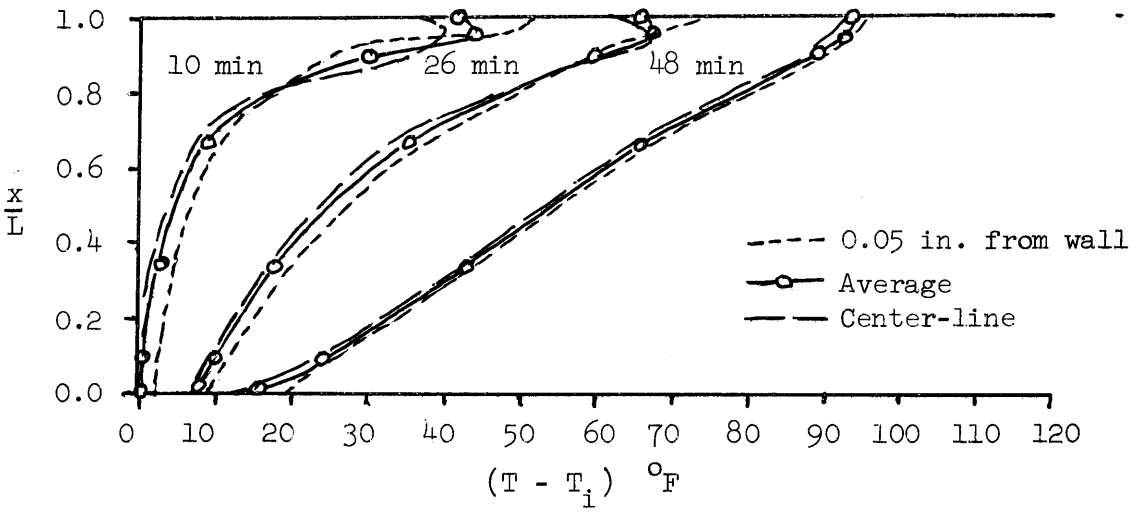

FIGURE 4-10

Axial Core Temperature Profiles

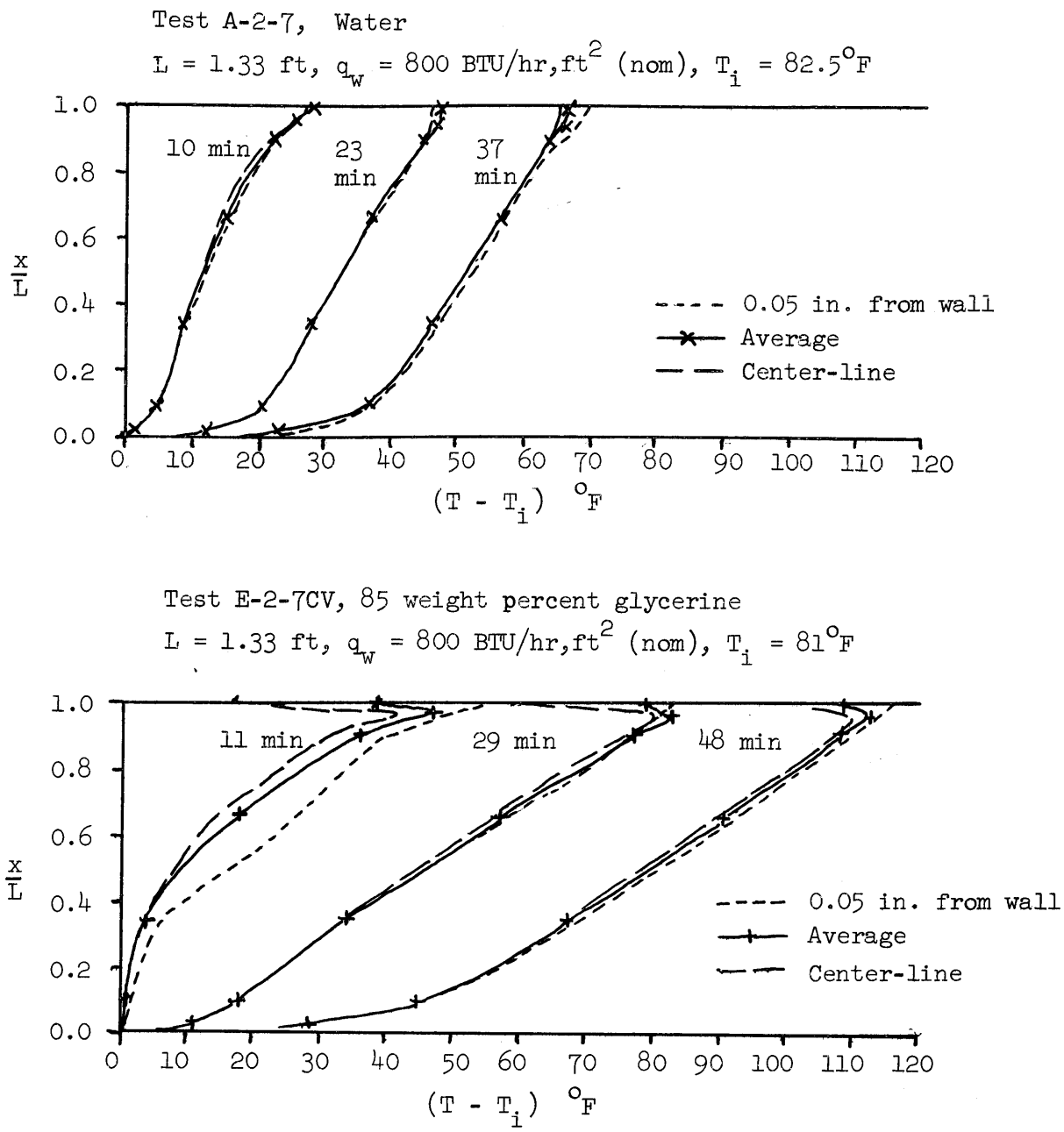

FIGURE 4-11

Axial Core Temperature Profiles

Test E-2-3-5CV, 85 weight percent glycerine in water

$$L = 1.33\text{ft},\quad q = \begin{cases} 150\ \text{BTU/hr,ft}^2 & 0 < t < 90\ \text{min} \\ 400\ \text{BTU/hr,ft}^2 & 90 < t < 150\ \text{min} \end{cases} \text{(nom)},\quad T_i = 75^\circ\text{F}$$

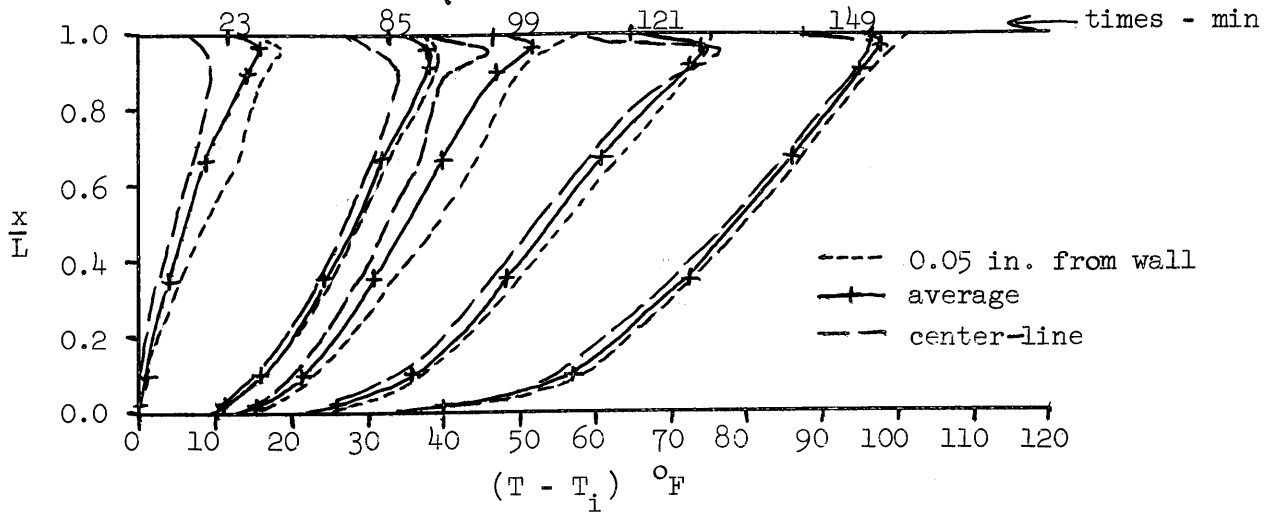

Test G-2-3, Glycerine

$L = 1.33$ ft, $q = 125$ BTU/hr,Ft^2, $T_i = 85^\circ$F

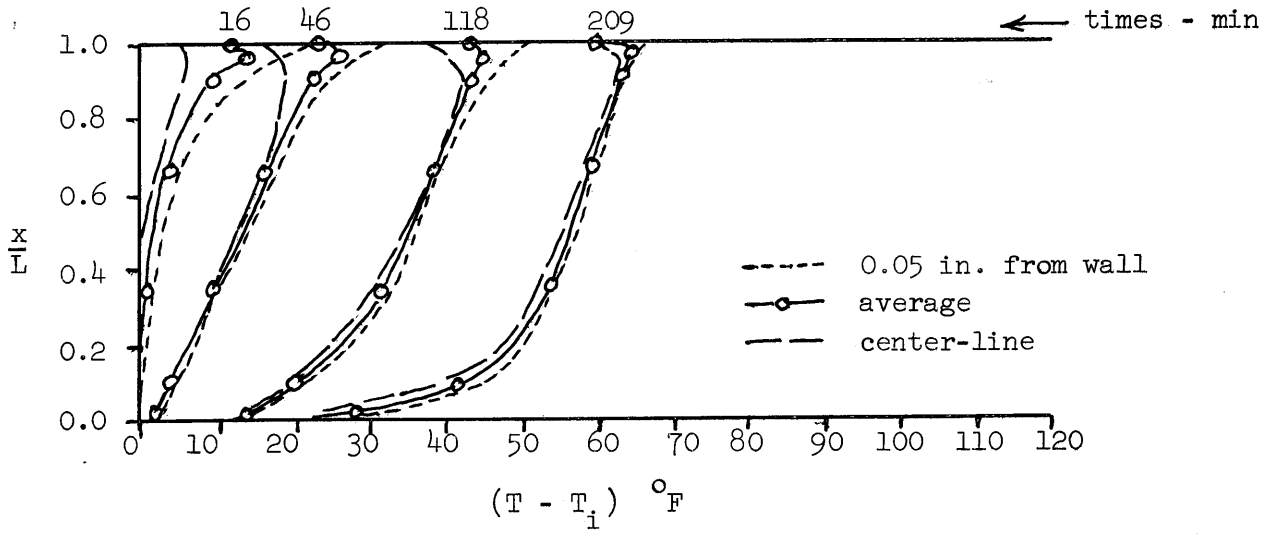

FIGURE 4-12

Axial Core Temperature Profiles

boundary layer and core fluid. Furthermore, Sparrow and Gregg (92) have made a boundary layer analysis including variable fluid properties and have concluded that use of an average value does not significantly affect the results.

From the derivative of the average enthalpy-time curves, the value of the average heat flux to the system can be computed as a function of time. Actually, since the measured temperature field represents only the energy in the core region, the amount of energy in the boundary layer is not included in this average. The effect is to introduce a time lag in the results equivalent to the mean residence time of fluid in the boundary layer. Typical values of this time lag are about one minute. No correction was made since this effect tends to compensate for the physical time lag introduced by the initial transient heating of the wall. (Section IV.B.2.)

Another important observation is that after an initial period, which is interpreted physically as the time required for the first warm fluid to reach the bottom of the core or as the time required to establish an axial temperature gradient throughout the core, the axial core temperature gradients can be well represented by constants. In determining the slope of the axial temperature lines, the top and bottom 10% of the system were not included. The exclusion of the surface region was based on the presence of complex mixing phenomena discussed previously; the bottom portion was excluded because of heat losses to the bottom flange which existed in the experimental system, but which would not occur in the ideal system having an adiabatic bottom surface.

The tabulation of reduced data for each run includes computed

values of wall heat flux, average system temperature, and a set of dimensionless groups based on these values and appropriate system geometry:

Prandtl number, $\frac{\nu}{\alpha}$

Fourier number, $\frac{\alpha t}{L D}$

Grashof-Nusselt number, $\frac{g\beta q L^4}{k\nu^2}$

Rayleigh-Nusselt number, GrNuPr

Dimensionless Core Temperature Gradient, $\frac{d\theta_\infty}{dX} = \frac{k}{q} \left.\frac{\Delta T}{\Delta x}\right|_{\substack{\text{axial} \\ \text{between } \frac{x}{L} = 0.1 \\ \text{and } \frac{x}{L} = 0.9}}$

In addition, the conventional Nusselt number was computed using the familiar empirical correlations given in McAdams (53) and modified for the constant wall heat flux case.

$$\text{Laminar:} \quad Nu = .56(Ra)^{1/4} = (.56)^{4/5}(RaNu)^{1/5} \tag{4-1}$$

$$\text{Turbulent:} \quad Nu = 0.13(Ra)^{1/3} = (.13)^{3/4}(RaNu)^{1/4}. \tag{4-2}$$

Using these estimated values for Nusselt number, the Rayleigh and Grashof numbers could be evaluated. In addition, the effective $(T_w - T_\infty)$ could be computed and compared with experimental data. Since a true wall temperature was not measured due to protrusion of the wall thermocouple bead into the liquid, it is not surprising that the experimental values were consistently lower by about 30%-50%. However, correction for the temperature gradient across the thermocouple bead based on boundary layer theory indicates that discrepancies of this order are indeed possible. There is no reason to doubt the values predicted

empirically, especially in view of the mass of data presented in the literature supporting their validity. The reduced data are tabulated in Appendix E.

One other method of presenting the temperature data was used to provide information about the time variation of average liquid temperatures at specified levels within the core. These data were obtained from average temperature increases as determined from the core axial temperature profile curves at dimensionless heights of 0.1, 0.3, 0.5, 0.7, and 0.9. The temperature rise values were normalized by dividing them by the mixed-mean system temperature increase at the same point in time. These data are plotted as functions of a dimensionless time parameter in Figures 4-13 and 4-14. If the fluid were perfectly mixed, the temperature ratios would all be unity. The deviation from unity indicates the distribution of thermal energy within the system.

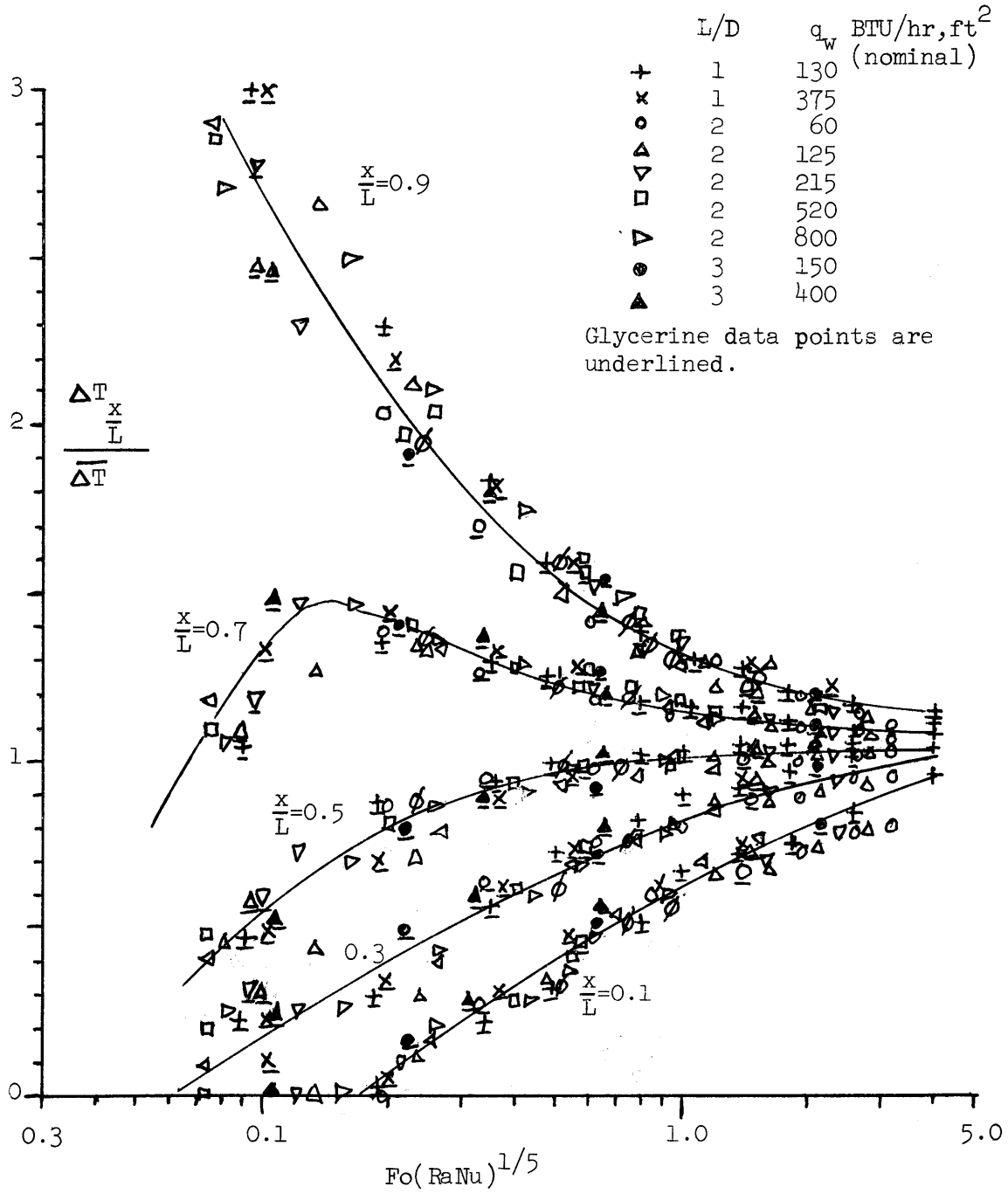

FIGURE 4-13

Normalized Transient Temperature Distribution for Fluid in a Vertical Cylinder with Constant Wall Heat Flux

Glycerine and 85% Glycerine Data

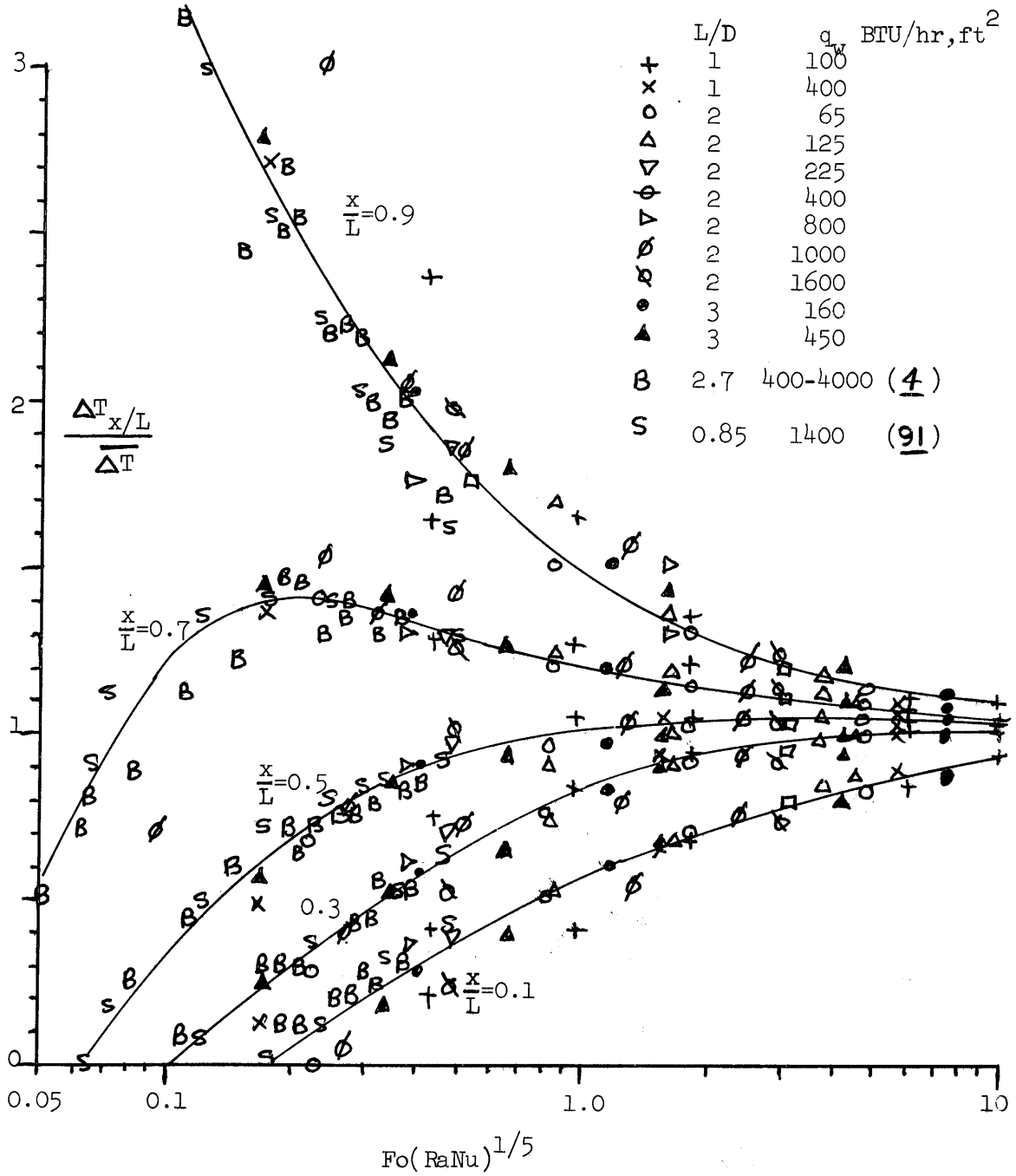

FIGURE 4-14

Normalized Transient Temperature Distributions for
Fluid in a Vertical Cylinder
with Constant Wall Heat Flux

Water Data

D. Interpretation and Correlation of Results

Experimental observations indicated that the natural convection flow within a vertical cylindrical enclosure, as a result of wall heat flux, was of a boundary layer type. When the boundary layer approaches the liquid surface, it turns rapidly and flows radially inward, spreading over the core region. As a result of the sharp turning of the rapid boundary layer flow, rather complex flow circulations occur just below the surface. However, the net effect appears to be good mixing of the fluid in about the upper 10% of the system. Below the mixing region, the core is essentially isothermal in the radial direction and has a nearly linear temperature variation in the axial direction.

These experimental observations were utilized in development of a boundary layer model in which the temperature at the outer edge of the boundary layer was specified as a linear function of height. On the basis of this boundary layer model and a model for the core which incorporated a mixing region of depth Δx in the upper part of the system (Section IIIC), the theoretical results are:

Laminar:
$$\frac{d\theta_\infty}{dX} = 1.456 \left[\frac{1}{\frac{\Delta x}{L}\left(1 - \frac{\Delta x}{L}\right)} \right]^{4/9} (Fo)^{4/9} \frac{1}{(RaNu)^{1/9}} \qquad (3\text{-}61)$$

Turbulent:
$$\frac{d\theta_\infty}{dX} = 3.4 \left[\frac{1}{\frac{\Delta x}{L}\left(1 - \frac{\Delta x}{L}\right)} \right]^{8/15} (Fo)^{8/15} Pr^{7/45} \frac{1}{(RaNu)^{2/15}} \qquad (3\text{-}65)$$

The experimental values for $\frac{d\theta_\infty}{dX}$ are plotted against $(Fo)^{4/9} \frac{1}{(RaNu)^{1/9}}$ for laminar data on log-log paper in Figure 4-15. The slope of the curve is unity which indicates that the parametric dependence predicted by theory is valid. At $Fo^{4/9}/(RaNu)^{1/9} = 0.01$,

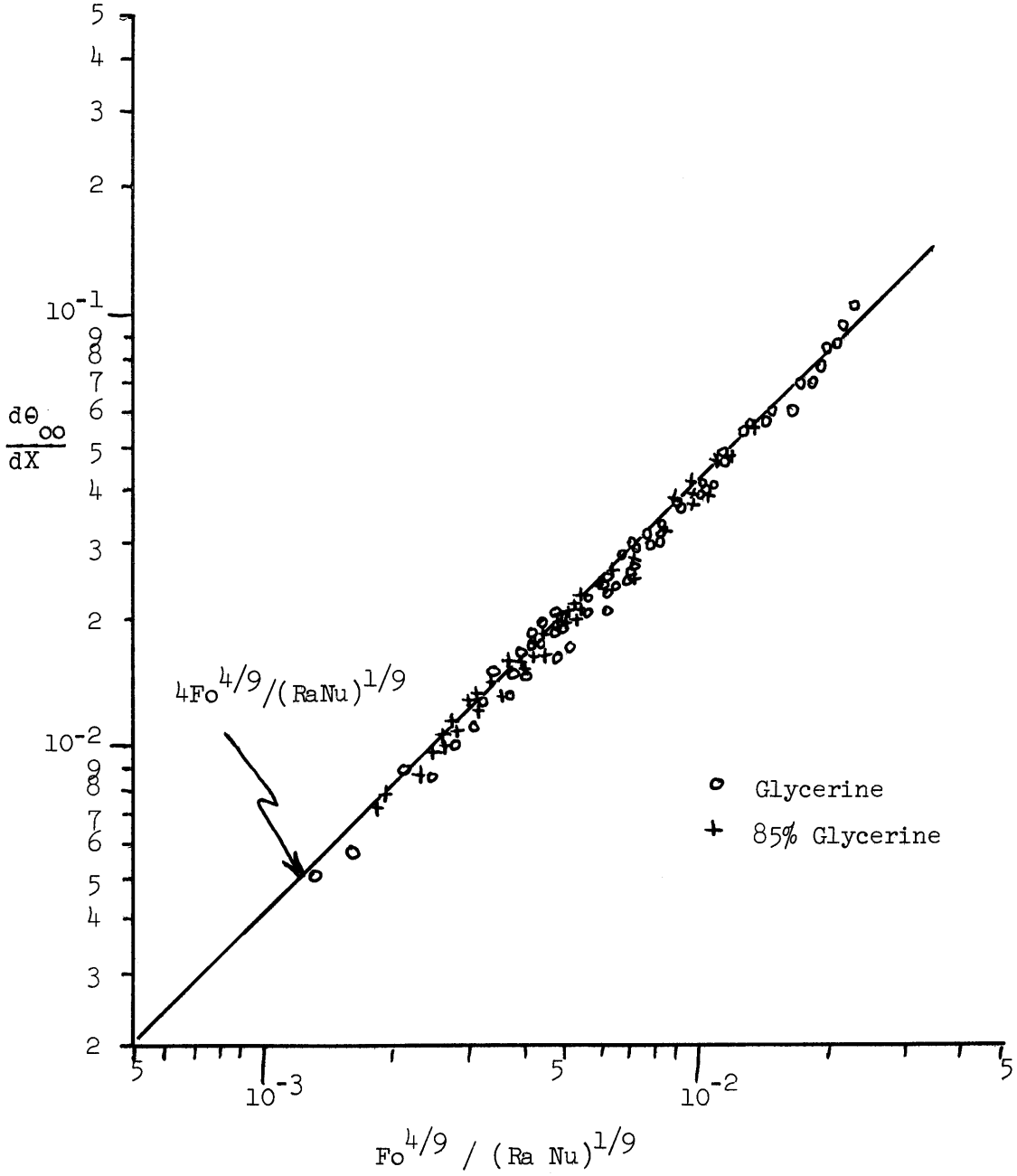

FIGURE 4-15

Axial Core Temperature Gradient

Comparison of Glycerine and 85% Glycerine Data with

Laminar Model

the value of $\frac{d\theta_\infty}{dX}$ is about 0.04 which gives a constant in eq. 3-61 of 4.0 or a value for:

$$\frac{d\theta_\infty}{dX} = 4Fo^{4/9}/(RaNu)^{1/9} \qquad (4\text{-}3)$$

with $\frac{\Delta x}{L}\left(1 - \frac{\Delta x}{L}\right) = \left[\frac{1.456}{4.0}\right]^{9/4} = 0.104$

Solving for $\frac{\Delta x}{L}$ shows that about a 12% mixing region is predicted (a 10% mixing region would give a constant of 0.09 in eq. 4-3; a 15% mixing region, a constant of 0.1275).

Before checking the turbulent correlation, it is interesting to see how well the water data points, which correspond to test conditions at or above the transitional Rayleigh number range, are correlated by the laminar model. From Figure 4-16, it is evident that even the "turbulent" water data fit the laminar correlation very well. Although the plotted points in Fig. 4-16 are not identified in terms of Rayleigh number, if this distinction is made the conclusion remains the same. Any scatter in points is random and there is no detectable shift in position or in slope between results from tests at different Rayleigh number levels. The data of Barakat (4) and Seifkes (91), shown as solid dots, correspond to high Rayleigh number conditions (10^9-10^{10}).

The evaluation of the theoretical turbulent correlation is made by plotting experimental values of $\frac{d\theta_\infty}{dX}$ against the analytically derived parameter, $Fo^{8/15}\ Pr^{7/45}/(RaNu)^{2/15}$. Both laminar and turbulent data are plotted in this manner in Figure 4-17. The glycerin and 85% glycerin data are poorly correlated, as would be expected, since they do not correspond to the flow model on which the turbulent analysis is based. More surprising, however, is the fact that the

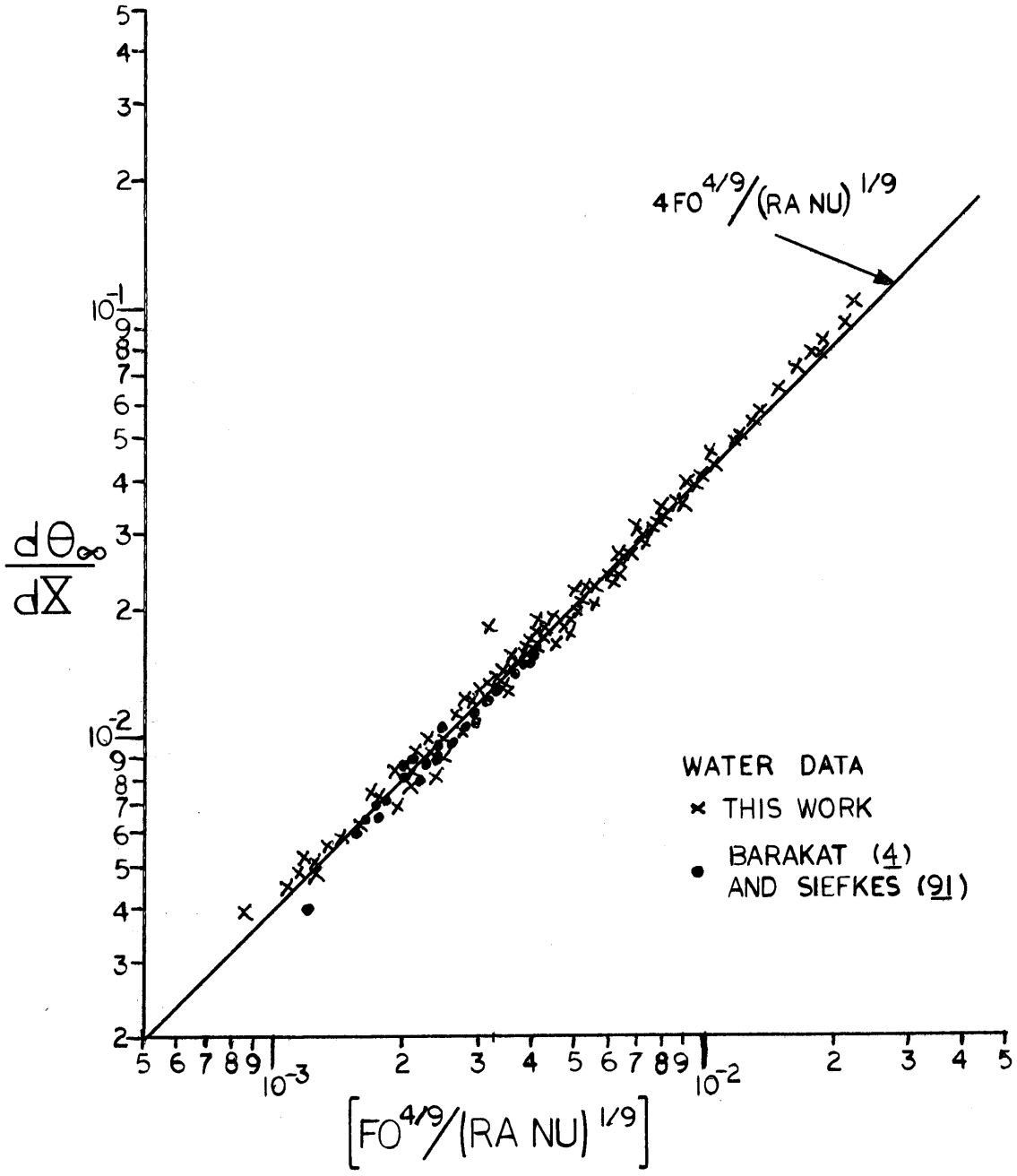

FIGURE 4-16

AXIAL CORE TEMPERATURE GRADIENT

COMPARISON OF WATER DATA WITH LAMINAR MODEL

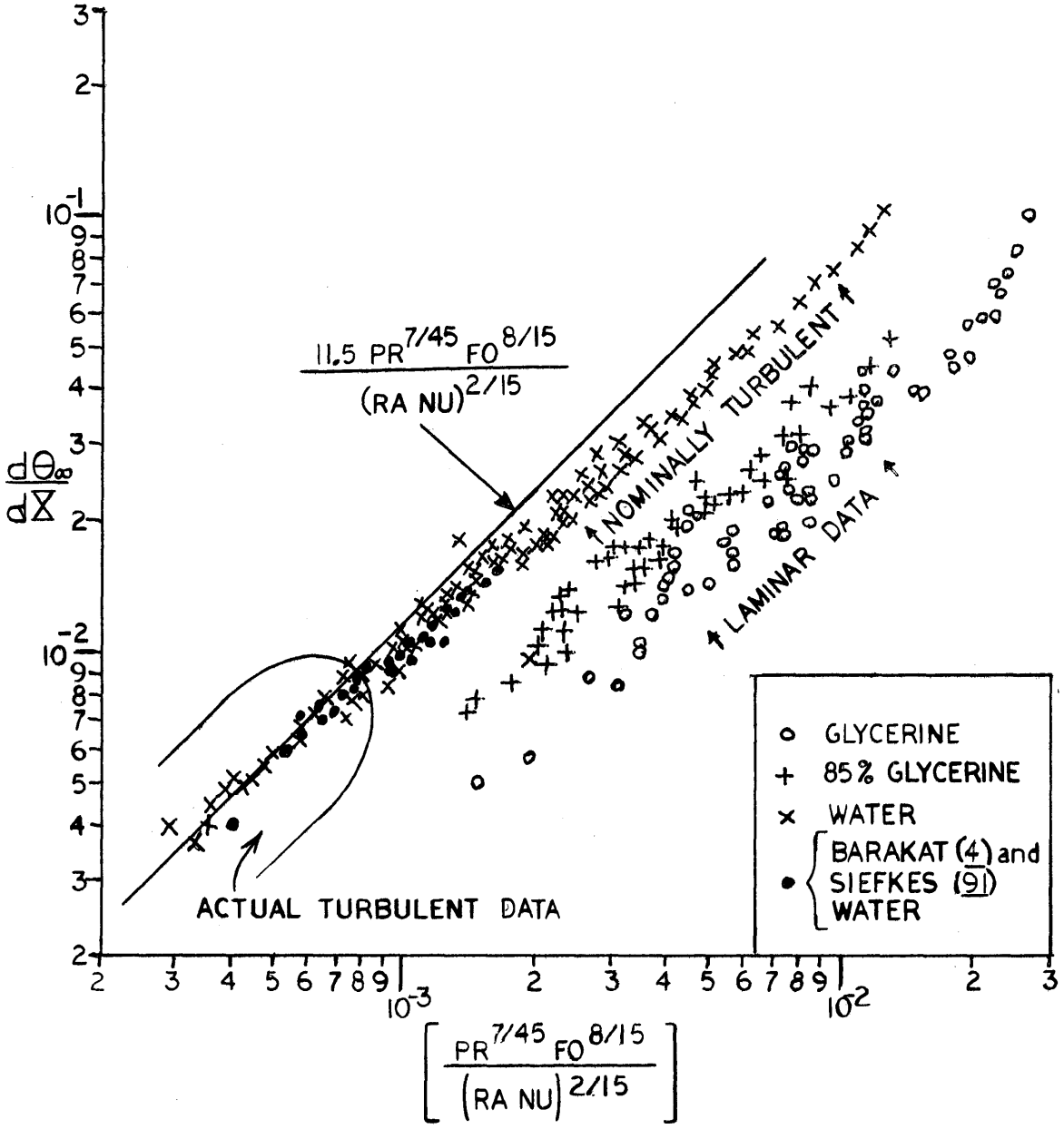

FIGURE 4-17

AXIAL CORE TEMPERATURE GRADIENT

COMPARISON OF
ALL DATA
WITH TURBULENT MODEL

supposedly turbulent water data do not exhibit a slope of unity at the higher experimental values of $\frac{d\theta_\infty}{dX}$. A reason for this apparent discrepancy may be found by considering Figure 4-18. In Chapter III, boundary layer analysis indicated that the presence of a core temperature gradient limited the amount of energy and momentum in the flow up the heated wall. An energy parameter, E^*, was used in the analysis which showed what the limiting energy, E_a^*, was for a particular core temperature gradient. (Table II) Since with no core temperature gradient, $E_o^* = X = (GrNu)^{1/4}$ by definition, the energy limitation can be considered as a limitation on the (GrNu) group and, consequently, on the Rayleigh number. So the flow intensity in an actual situation, would be characterized by a Rayleigh Number reduced by the ratio $(E_a^*/E_o^*)^4$. The limiting values, E_a^*, are presented in Fig. 4-18 for both the laminar (solid lines) and turbulent (dashed lines) boundary layer solutions. The dotted line corresponds to the nominal transition point estimated on the basis:

$$Ra_{transit.} = GrPr \backsim 10^8 \tag{4-4}$$

$$Nu = .56(Ra)^{1/4} \tag{4-5}$$

$$GrNu = \frac{10^8}{Pr} (.56)(100) \tag{4-6}$$

$$E^*_{transit.} = (GrNu)^{1/4} = \frac{274}{Pr^{1/4}} \tag{4-7}$$

The water data all correspond to Prandtl numbers below ten, so, from the limiting energy analysis, no transition would be expected to occur if the dimensionless core gradient were greater than 0.01. If data points, for $\frac{d\theta_\infty}{dX}$ greater than 0.01, are eliminated from consideration

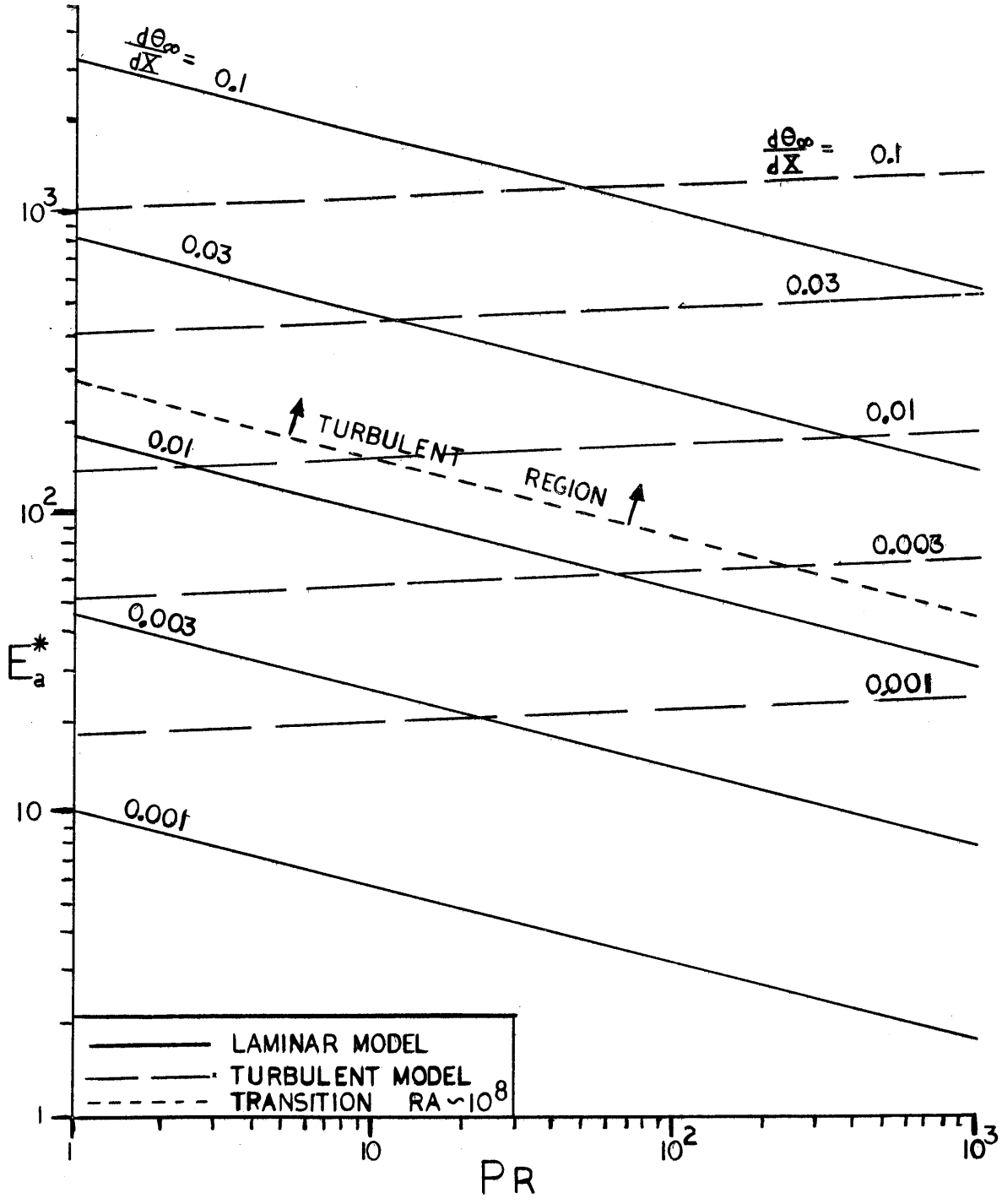

FIGURE 4-18

ASYMPTOTIC VALUES FOR
BOUNDARY LAYER ENERGY FUNCTION

in Fig. 4-17 on the basis that the presence of the core gradient limits the energy sufficiently to prevent turbulent transition, then the remaining water data do fit a turbulent model correlation:

$$\frac{d\theta_{\infty}}{dX} = 11.5\ Fo^{8/15}\ Pr^{7/45}/(RaNu)^{2/15} \qquad (4\text{-}8)$$

very well. Comparison of the experimental constant with the theoretical expression (eq. 3-65), gives

$$\frac{\Delta x}{L}\left[1 - \frac{\Delta x}{L}\right] = \left[\frac{3.4}{11.5}\right]^{15/8} = 0.102 \qquad (4\text{-}9)$$

again corresponding to about a 12% mixing zone.

Even though there is good agreement between the turbulent model and the actually (rather than nominally) turbulent data, there is no reason why both the laminar and turbulent models should not correlate these data. Because of the energy limitation, these data correspond to the transitional turbulent range rather than the highly turbulent conditions indicated by their nominal Rayleigh numbers of up to 10^{13}. However, for still higher Rayleigh numbers, the turbulent model would be expected to give better results than the laminar model.

These correlations give the slope of a linear temperature gradient in the core as a function of known system parameters. However, the system temperature level must be known if actual temperatures are to be predicted. If the core gradient is actually linear, it follows that the temperature at the 50% level should be equal to the mixed-mean temperature of the system, computed on the basis of total energy input to the fluid. Figure 4-19 is a plot of measured temperatures at the 50% dimensionless height level versus mixed-mean temperatures computed on the basis of energy input to the system. Good agreement is obtained

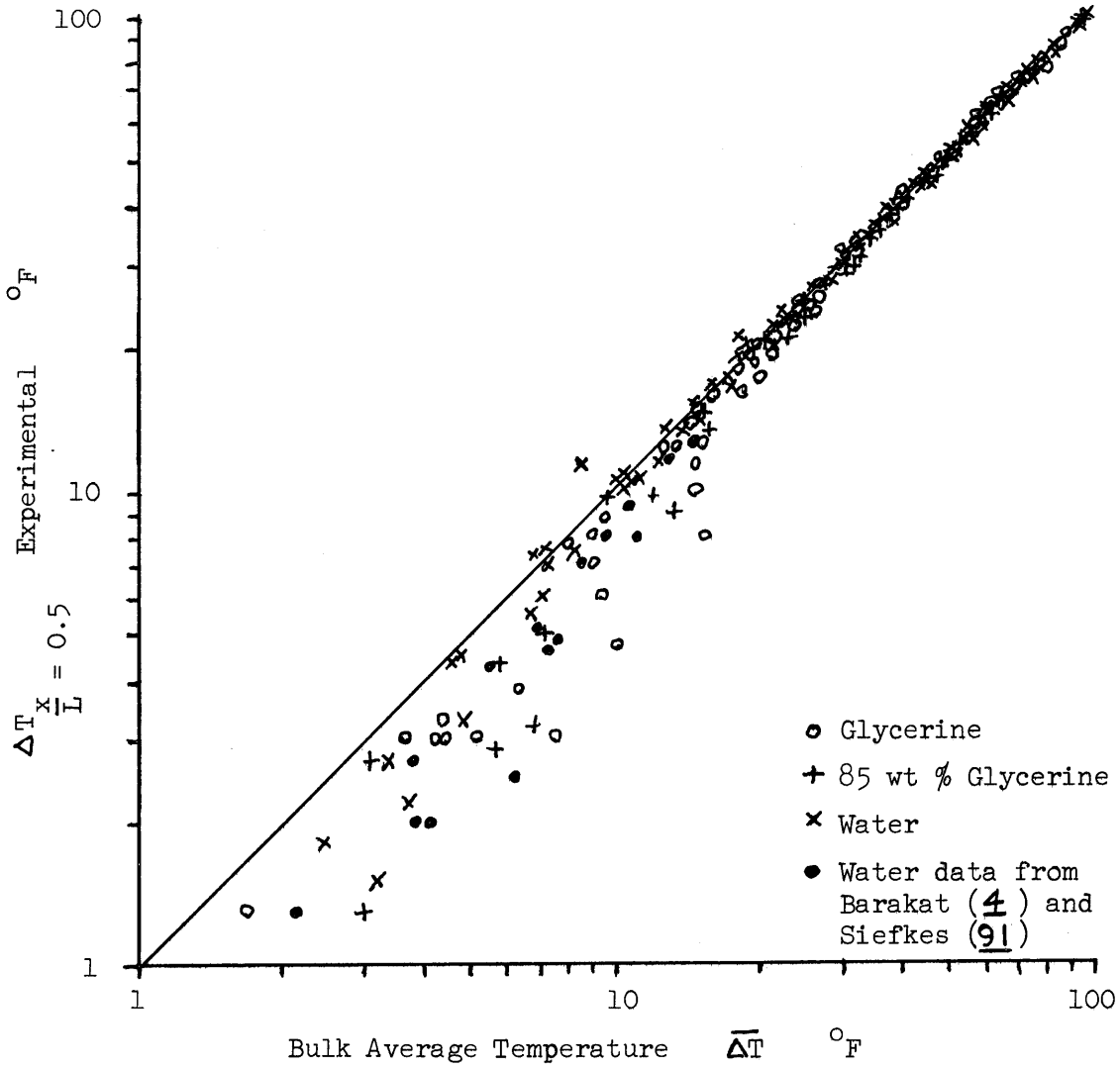

FIGURE 4-19

Comparison of Mid-plane and Bulk Average Temperature Increases

$$\overline{\Delta T} = \frac{4}{\rho C_p D} \int_0^t q_w dt$$

except at very low values of temperature rise. In the latter region the linear core gradient assumption is not valid at the beginning of the natural convection circulation, since a finite time is required for warm fluid to reach lower regions of the core. With the exception of this initial period, which will be discussed subsequently, the mixed-mean temperature rise (or temperature, if the initial system temperature is added to the rise) is very nearly equal to the temperature at the axial midplane of the system.

Starting with the model and a set of parameters corresponding to a specific experiment at a specific time, a theoretical axial profile may be computed and compared with the measured experimental profile. Figures 4-20 to 4-22 show the results of this computation and comparison with experimental data. Accurate estimates of core temperature distribution are obtained over the entire range of parameters investigated except for the initial period.

Figure 4-22 illustrates the weakness of the theoretical linear core temperature model when applied to the initial period. The profile actually is not linear and the use of a mixed-mean temperature as a midpoint temperature is not valid before warm fluid has reached the lower regions of the core.

An empirical representation of the core temperature distribution suggested by Neff (59) and demonstrated by Ruder (75) utilizes the error function in computing initial temperature profiles. This model assumes a temperature distribution:

$$\frac{T - T_b}{T_s - T_b} = e^{-cy^2} \qquad (4\text{-}10)$$

Test A-2-4R, Water

L = 1.33 ft, q = 250 BTU/hr,ft^2 (nom), T_i = 81°F

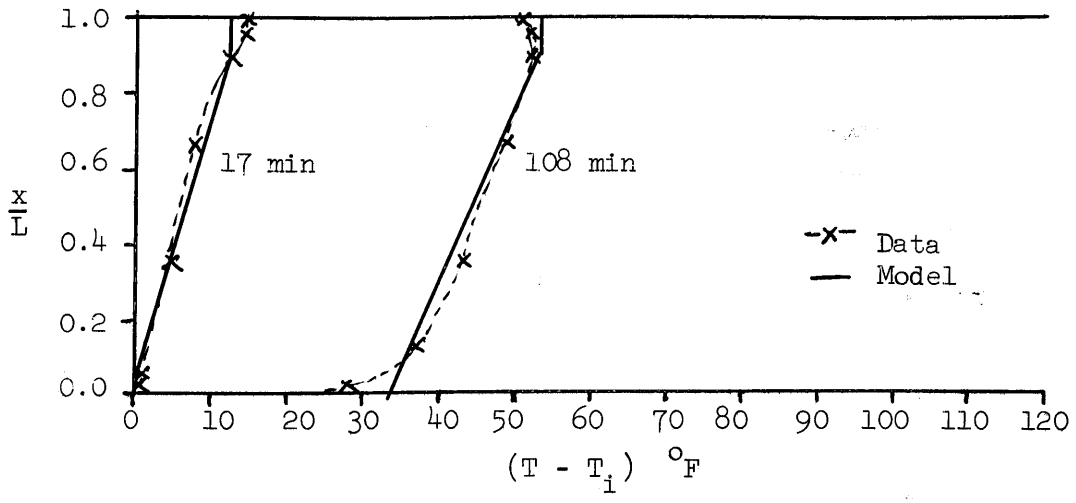

Test A-2-10V, Water

L = 1.33 ft, q = 1900 BTU/hr,ft^2 (nom), T_i = 72°F

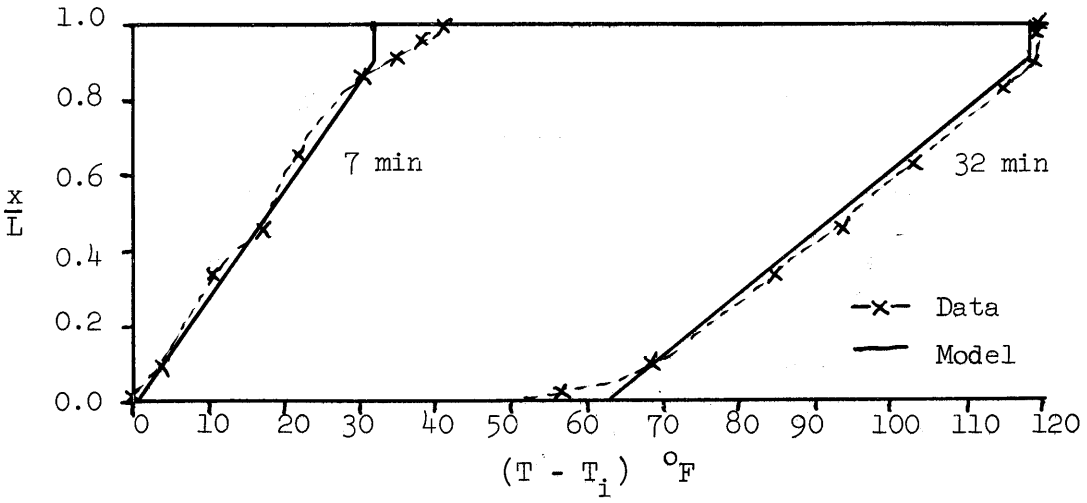

FIGURE 4-20

Comparison between Observed and Predicted

Axial Core Temperature Profiles

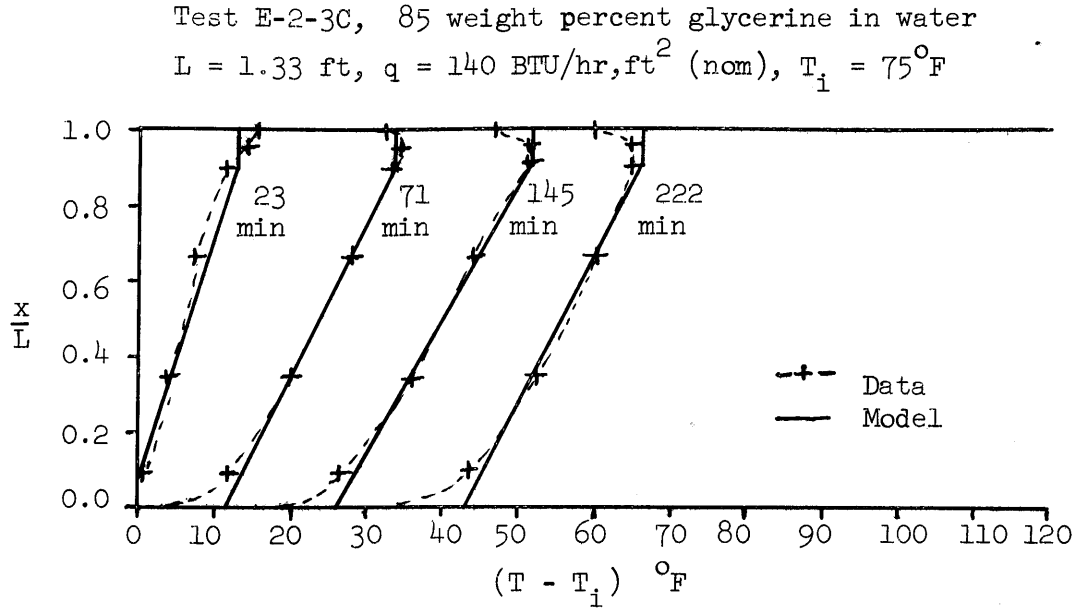

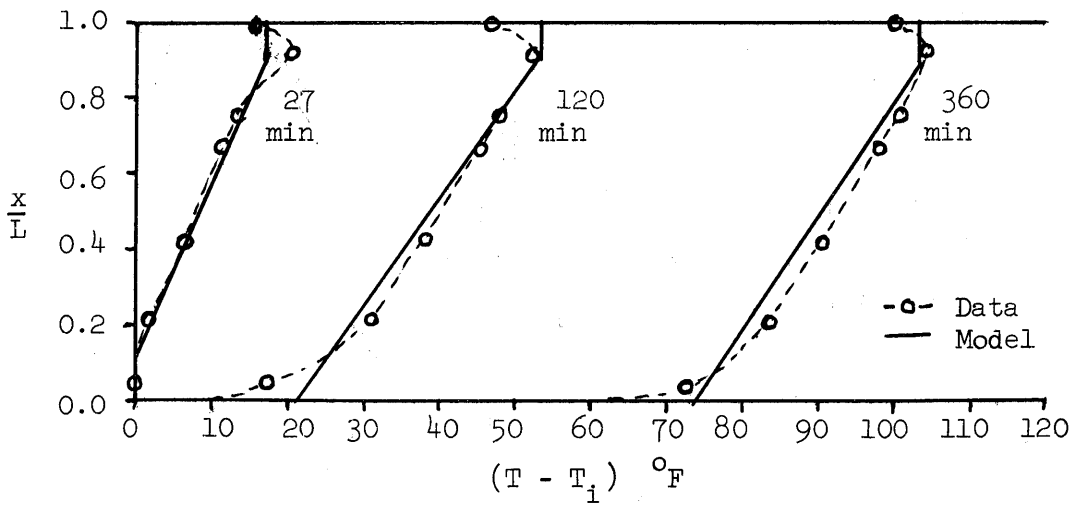

FIGURE 4-21

Comparison between Observed and Predicted

Axial Core Temperature Profiles

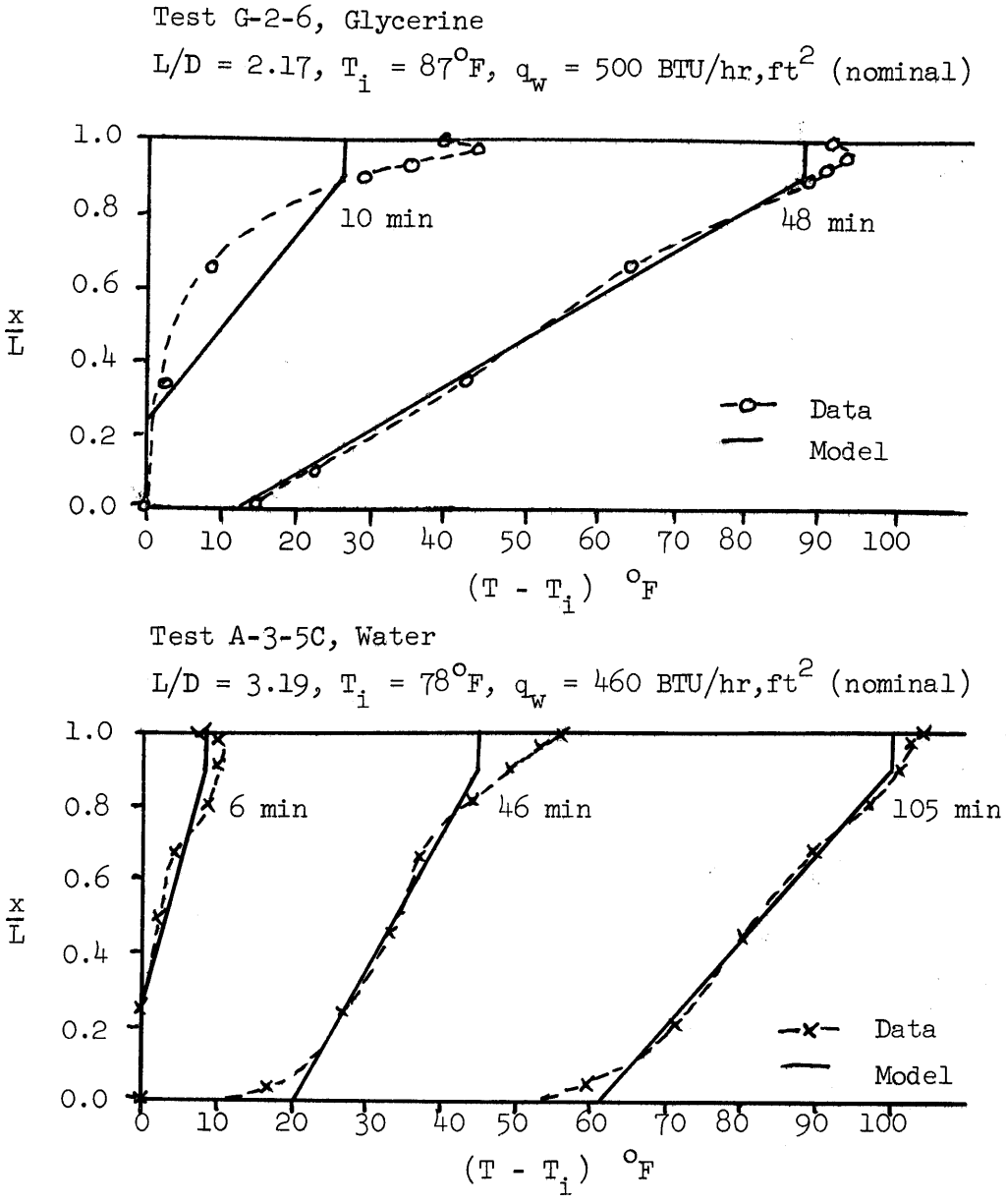

FIGURE 4 - 22

Comparison between Predicted and Observed

Axial Core Temperature Profiles

Limiting Boundary Layer Energy Model

where y is axial distance below surface

T is temperature at y

T_s is surface temperature

T_b is bottom temperature

and $$C = \pi \left[\frac{\pi D^2}{4} \frac{\rho C_p (T_s - T_b)}{2qt} \right]^2$$

based on evaluation of the probability integral for $y = \infty$. Use of an infinite bound is a justifiable assumption if warm fluid has not yet reached the bottom of the vessel.

This model gives a better description of the early temperature distributions than does the linear model, but success of the boundary layer model in predicting temperatures after a core gradient is established, indicates that an improved model could be developed for the initial period also.

In the theoretical analysis, it was shown that the core temperature at the top of the system is determined by the boundary layer energy flux into the core at that point. The core temperature distribution is specified if the energy and the flow rate of boundary layer fluid fed to the top of the core were known. The energy flux gives a temperature level at the top of the core at a specific time and the flow rate can be converted into a core plug flow velocity which describes the position of fluid originally at the surface as it slowly sinks into lower regions while maintaining its original temperature.

The energy and flow can both be expressed in terms of a single variable E^* in the laminar case:

$$\frac{dE^*}{dX} = 1 - 1.543 \, Pr^{1/5} \frac{d\theta_{oo}}{dX} \, E^{*4/5}. \qquad (4\text{-}11)$$

So an iterative calculation is possible in which the system is divided into a number of vertical sections and core temperature variation is assumed linear only over the extent of a single section.

The analytic solution of the preceding equation is given in eq. 3-47, but is in an inconvenient form involving exponents containing difference terms in the E^* and $\frac{d\theta_\infty}{dX}$ variables. A computer solution based on the iterative procedure and the analytic solution would certainly be possible for a specific case.

A further simplification is possible if it is assumed that core gradients are initially small. Then,

$$dX = dE^* \frac{1}{1 - aE^{*4/5}} = dE^* \left[1 + aE^{*4/5} + a^2E^{*8/5} + \cdots\right] \qquad (4\text{-}12)$$

and terms higher than first order in $\underline{a}$ may be neglected.

This leads to:

$$\frac{d\theta_\infty}{dX} = \frac{9}{5} \frac{1}{(1.525)} \frac{1}{Pr^{1/5}} \frac{X - E^*}{E^{*4/5}} \quad . \qquad (4\text{-}13)$$

Initially $\frac{d\theta_\infty}{dX} = 0$, and $E^* = X$, so the equation is valid. The term, $X - E^*$, represents the decrease in boundary layer energy at height X as a result of core gradient effects.

Figure 4-23 presents a temperature profile computed on the basis of this somewhat simplified model. The corresponding experimental profile is shown for purposes of comparison.

Temperature distributions may also be estimated during the initial period on the basis of the data presented in Figures 4-13 and 4-14. Although there is considerable scatter in the results which are presented as normalized temperatures (based on the mixed-mean) at various dimen-

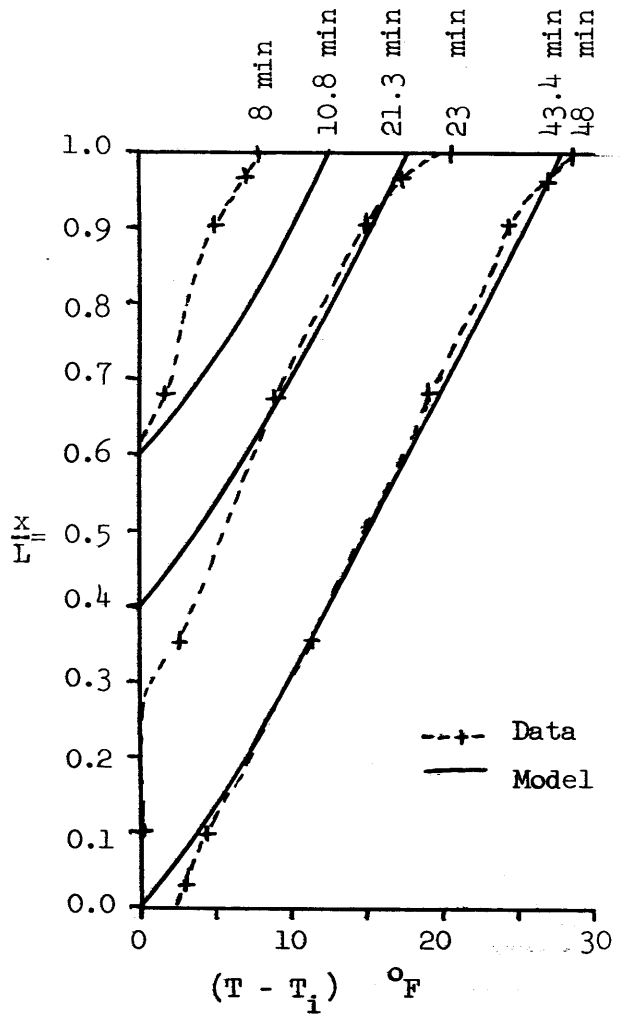

TEST DATA:

Run E-2-3
85% Glycerine
$T_i = 76^{\circ}F$

time (min)	q_w(avg) (BTU/hr,ft^2)
0 to 8	85
8 to 23	160
23 to 48	160

COMPUTED CASE:

85% Glycerine
$T = 82^{\circ}F$ (assumed constant for evaluating properties)
$q_w = 150$ BTU/hr,ft^2

Note that q_w does not build up instantaneously in the experimental case. This explains the over-all lag in the experimental temperature profiles. The shape of the initial experimental profile is probably also influenced by the large initial variation in Prandtl number (Pr=680 at $76^{\circ}F$, Pr=500 at $82^{\circ}F$, Pr=400 at $93^{\circ}F$).

FIGURE 4-23
Comparison between Iterative Boundary Layer Solution for Initial Period and Observed Axial Core Temperature Profiles

sionless heights as functions of dimensionless time, a consistent picture of the core temperature distribution transient is given. At the point where the temperature at $\frac{x}{L} = 0.1$ begins to rise, the previously developed boundary layer model becomes valid. Prior to this time, the temperature values are generated by the sort of complicated exponential boundary layer energy equation which was derived theoretically.

A final area of interest is the effect of the core gradient on the over-all system heat transfer coefficient or Nusselt number. For no core gradient, the equations predict values of Nusselt number equivalent to those estimated from the usual natural convection correlations. For a laminar boundary layer, if wall heat flux is held constant the heat transfer coefficient increases due to presence of a core gradient. In fact, when a steady-state core temperature gradient is established, the laminar Nusselt number becomes a function of the $\frac{1}{3}$ - power of the Rayleigh number rather than the $\frac{1}{4}$ - power function observed for no core gradient. Experimental support of this dependence is provided in a study made by Eckert and Carlson (16). For natural convection between long, closely-spaced, parallel vertical plates with one hot and one cold wall and a linear core temperature distribution, they report a 0.30 power dependence of Nusselt on Rayleigh number for laminar flow. The turbulent Nusselt number also has a steady-state, $\frac{1}{3}$ - power relationship to the Rayleigh number which is the same functional dependence as obtained with no core gradient.

V. ENGINEERING IMPLICATIONS

In this chapter an attempt is made to evaluate the theoretical and experimental findings, described in Chapters III and IV, in the light of application to practical problems. First, some general considerations are presented; then the application of the analysis to a hypothetical liquid hydrogen storage vessel is presented; finally, the calculated temperature profiles are compared with limited experimental data on a similar system. Complete comparison is qualitative since boiling was also occurring in the experimental system.

The design engineer can utilize the correlations developed in this thesis to estimate the time and spatial temperature distribution within a vertical tank of fluid subjected to sidewall heating by:

1. Assuming radial temperature variation is negligible.
2. Using Figs. 4-13 and 4-14 to predict the axial core temperature distribution during the initial period after the start of heating (until the first warm fluid reaches the bottom of the tank).
3. Assuming either laminar or turbulent flow and then using Eqs. 4-3 or 4-8 to predict subsequent axial core temperature gradients, which are assumed constant over the axial system height at any time.
4. Checking the computed values of $\frac{d\theta_\infty}{dX}$ at the known fluid Prandtl number with Fig. 4-18 to see whether the flow regime assumed is correct.
5. Computing the mixed-mean temperature and assuming it is equal to the temperature at $\frac{X}{L} = 0.5$.

6. Checking the assumed values of fluid properties with those that correspond to the mixed-mean temperature and correcting assumed values if necessary.

However, additional conditions are often present in real systems and the engineer must be able to judge the influence of these "non-idealities" on his analysis. The model presented in this thesis has been developed for natural convection flow in systems subjected to a uniform wall heat flux. If other modes of heat transfer are predominant in the system, the model should not be used, other than, perhaps, to estimate possible natural convection contributions to the over-all system behavior. A convenient way to evaluate the relative importance of various heat transfer modes is to compute Nusselt numbers for each mode. Of course the Nusselt number, itself, may be considered as an approximate ratio of actual heat transfer to pure conduction. For example, if a mixer were present in a tank with an internal convective flow, the forced convection Nusselt number could be evaluated, based on the fluid velocity imparted by the mixer to the fluid near the natural convective boundary layer. If the forced convective Nusselt number turned out to be of the same order or larger than the natural convection Nusselt number, a natural convection analysis alone would give poor results. Even if natural convection was found to predominate at the walls, additional consideration would have to be given to alteration of core temperature distribution by the presence of a superimposed mixing field. If considerable axial mixing were produced, then the effect of core temperature distribution on the boundary layer energy would be different from that in an unagitated batch system. Similar reasoning can be applied to systems in which radiative effects or

internal heat generation effects are of concern.

For the constant wall temperature situation, an approximate estimate of temperature distribution can probably be made by computing the equivalent heat flux, q:

$$q = h(T_w - T_o) \tag{5-1}$$

$$\frac{hL}{k} = f(Gr,Pr) \tag{5-2}$$

and using the constant wall flux model. A more rigorous treatment would require using the constant wall temperature equations in Table II and repeating the same procedures used for the constant wall flux case derivation, including numerical solution of the energy and momentum equations.

Estimates for cooling, rather than heating, at the walls are made by reversing the direction of gravity in the basic coordinate system. Consequently cooling may be treated in the same manner as a heating analysis except that the mixing region occurs at the bottom and the sign of the computed core temperature gradient is reversed. Whether the same model is strictly valid for a cooling system is uncertain; however, Stefany (23,99) and others have found no difference in heat transfer coefficients for transient heating and cooling of fluids within tanks, so application of the model developed in this study to the cooling case is probably justified.

Major variation in wall heat flux can also be considered. Either a rigorous iterative computation can be made or else a simplified procedure can be followed to give approximate estimates. As part of the experimental investigation reported in this thesis, a test (E-2-35) was carried out to study this effect. After a period of heating at

one flux level, the wall heat flux was suddenly changed and maintained at a level about three times greater than the original level. Satisfactory agreement between the model and data was obtained only if the time scale used in predicting behavior after the increase in flux level was based on a time scale with an origin intermediate between the initial start of heating and the time of the step increase. Good results were achieved if the time of heating at the lower rate was multiplied by the ratio of the lower to the higher heat flux values, and this scaled time interval was added to actual times after the flux increase to compute modified Fourier numbers for purposes of analysis. A similar starting time value for the second transient could also be obtained by extrapolating the average temperature-versus-time curve for the system back to a time corresponding to the original initial temperature of the system. Had the initial period been considerably longer, this type of initial heating period scaling would not be valid, but a guess at an initial time could be made. At long times after the change in wall flux, errors in choice of the time base would become negligible.

The work of Dickey (14) indicates that natural convection flow is not appreciably modified by small protruberances from the tank walls. This study investigated the possibility of using baffles to reduce stratification in tanks. They found that a one-inch circumferential, annular baffle was required to produce any real diversion of the boundary layer flow up a heated tank wall. They used an 8-in. diameter tank containing glycerin with a wall heat flux of about 600 BTU/hr ft^2. Consequently seams and reinforcing bands inside large tanks probably will not have a significant effect on over-all natural convection system behavior. On the other hand, if baffles are to be used to

reduce stratification, they must be quite wide and perhaps even extend inward to distances of one-quarter of the tank radius.

Example

Consider a vertical cylindrical tank filled with liquid hydrogen and subjected to a constant wall heat flux. A system studied experimentally by Segel (87) will be used as an example since temperature distributions predicted for this system can subsequently be compared with real data. The comparison is not direct since surface vaporization was an important factor in the liquid hydrogen experiments, but qualitative evaluation of the model is possible.

System:

$L = 75$ cm

$D = 26$ cm

$T_o = 20.4°K$

Fluid Properties: Saturated Liquid Hydrogen (1 atm.) (41)

$\rho = 0.071$ gm/cc

$C_p = 1.8$ cal/gm°C

$k = 2.86 \times 10^{-4}$ cal/sec cm°C

$\beta = 0.013$ °C^{-1}

$\mu = 0.013$ cp.

$Pr = 1.8$

$\nu = 0.0018$ cm^2/sec

$\alpha = 0.00224$ cm^2/sec

$\frac{g\beta}{\nu^2} = 3.85 \times 10^6$/°C cm

Case 1. $q = 8 \times 10^{-3}$ k cal/m^2-sec

$t = 20$ minutes

$$RaNu = \frac{3.85 \times 10^{6} \times 8 \times (75)^{4}}{2.86 \times 10^{-4} \times 10^{4}} = 3.4 \times 10^{14}$$

$$Fo = \frac{2.24 \times 10^{-3} \times (1200)}{(75)(26)}$$

$$Pr = 1.8$$

Turbulent Model (Eqn 4-8)

$$\frac{d\theta_{\infty}}{dX} = 11.5\ Fo^{8/15}\ Pr^{7/45}\ (RaNu)^{-2/15}$$

$$\frac{d\theta_{\infty}}{dX} = 11.5\ (.0298)(1.095)/(86.4)$$

$$\frac{d\theta_{\infty}}{dX} = 0.00433$$

$$\frac{dT}{dx} = 0.00433\ \left(\frac{q}{k}\right)$$

$$\frac{dT}{dx} = 4.33 \times 10^{-3} \times \frac{8 \times 10^{-4}}{2.86 \times 10^{-4}} = .0121\ \frac{^{\circ}K}{cm}$$

The temperature at 60 cm. above the bottom should be about 0.7°K higher than that at the bottom. The data presented by Segel indicate a value of about 0.5°K for this difference (A measurement accuracy of 0.15°K is reported). Although this was the lowest heat flux studied, surface vaporization accounted for about 35% of the energy supplied to the system walls. Although the energy loss due to vaporization was fairly high, not much mass was vaporized. Consequently, the residence time of fluid in the core was barely altered. The loss

of energy at the surface probably accounts for the measured axial temperature gradient being somewhat less than that predicted by the model.

Case 2. $q = 60 \times 10^{-3}$ k cal/m^2-sec

$t = 20$ minutes

$RaNu = 2.55 \times 10^{15}$

$Fo = 1.38 \times 10^{-3}$

$Pr = 1.8$

Turbulent Model

$$\frac{d\theta_\infty}{dX} = 4.33 \times 10^{-3} \left(\frac{8}{60}\right)^{2/15} = 3.31 \times 10^{-3}$$

$$\frac{dT}{dx} = 3.31 \times 10^{-3} \left(\frac{60}{2.86}\right) = .0695 \frac{^\circ K}{cm}$$

or for 60 cm:

$$\Delta T \backsim 4.16\ ^\circ K\ .$$

The experimental value is about 2.5°K. However, in this test, 85% of the energy and approximately one-half of the boundary layer mass flow was lost by surface vaporization. Therefore it is not surprising that a model which ignores surface vaporization effects overestimates the core temperature variation. If the model calculation were based on the heat flux actually entering the core region rather than the total wall heat flux, the predicted ΔT value would be reduced by about a factor of 4. In addition, the residence time of fluid in the core is doubled (since half the heated mass of fluid is lost by vaporization) and this effect would tend to double the temperature

differential between the fluid at the top and bottom of the core. The net effect of these two factors is to reduce the predicted value by a half which brings it in the vicinity of the observed value. Although this analysis is certainly rough and oversimplified, the general agreement indicates that good results could be obtained if surface vaporization effects were included in the mixing region model in a quantitative manner.

VI. CONCLUSIONS

An extensive experimental study was made of natural convection temperature fields and circulation patterns generated within a vertical gylinder as a result of a wall heat flux. Although only fluids of Prandtl number greater than unity were investigated, the study included a range of convective flows from weakly laminar to highly turbulent conditions. The height-to-diameter ratio of the system was also varied from one to three.

1. On the basis of experimental observations, a general natural convection system of this type consists of a very thin boundary layer flow up the wall, a rapid turning of the boundary layer into the central region as it approaches the liquid surface, excellent radial mixing of the warm boundary layer fluid near the surface, and gradual plug-flow sinking of the radially-mixed fluid as still warmer fluid displaces it and cool fluid is fed to the boundary layer from below it.

2. During an initial period, defined as the length of time required for the first warm fluid to sink to the bottom of the core, axial temperature distribution in the core region may be estimated by:

a. Iterative Method

The core and boundary layer are divided into increments in the axial direction and it is assumed that the core temperature gradient is constant over each incremental distance. The the differential energy and momentum equations (Table II) are solved iteratively in the boundary layer region to give, based on the axial core gradient distribution, the energy and flow leaving the top of boundary layer region. The solution is advanced in time by an increment corresponding to changing the mixing region (upper 10%) temperature by ΔT_L. Core temperatures are

readjusted by changing the temperature at the bottom of the mixing region to $(T_L)_{t+\Delta t} = (T_L)_t + \Delta T_L$, and by shifting all lower temperature values to the next lower space increment. New core gradient values are then estimated and the iteration continued. A computer program following this method is included in Appendix H.

b. Qualitative Method

Empirical curves, Figs. 4-13 and 4-14, may be used to give an indication of the core temperature distribution during the initial period for the laminar and turbulent cases respectively.

3. After the initial period, the axial core temperature distribution becomes linear with a gradient that varies with time and system parameters according to:

$$\underline{\text{Laminar}} \qquad \frac{d\theta_\infty}{dX} = 4(Fo)^{4/9}/(RaNu)^{1/9} \tag{4-3}$$

$$\underline{\text{Turbulent}} \qquad \frac{d\theta_\infty}{dX} = 11.5\ Fo^{8/15}\ Pr^{7/45}/(RaNu)^{2/15} \tag{4-8}$$

4. The core temperature level, after the initial period, is essentially equal to the mixed-mean fluid temperature (Fig. 4-19):

$$\overline{\Delta T} = T_{\frac{x}{L}=.5} = \frac{4}{\rho C_p D}\int_0^t q\ dt \tag{6-1}$$

5. The presence of a positive axial temperature gradient limits the amount of energy and momentum which can be transported in a natural convection boundary layer flow. This limitation restricts the intensity of boundary layer flow and postpones turbulent transition to a higher Rayleigh number range than the normal 10^8-10^9 range encountered in the absence of core temperature variation. Figure 4-18 can be used to indicate the turbulent transition range when the core temperature gradient

is known. Consequently $\frac{d\theta}{dX}$ may have to be computed by both models and checked with Fig. 4-18 to see which analysis is valid. Both models give essentially the same results in the transition range.

6. The effect of a linear core temperature gradient on a vertical natural convection boundary layer with a constant wall heat flux is to increase the heat transfer coefficient or Nusselt number. It is shown that the Nusselt number would be expected to depend on the $\frac{1}{3}$ - power of the Rayleigh number for both laminar and turbulent flows under these circumstances.

7. The solutions can also be applied to the case where cooling occurs at the wall by the mathematical expedient of changing the direction of the gravitational force--the buoyancy term becomes negative in the original equations. The case of a constant temperature wall can also be treated by boundary layer theory and a partial analysis of this case is presented in Table II.

VII. RECOMMENDATIONS FOR FUTURE WORK

1. Detailed study of surface phenomenon

Although surface temperatures were recorded in this study, surface phenomena are quite complex, especially when interaction with a vapor phase is considered. For a system near saturation temperature, temperature gradients along the surface might even cause vaporization near the wall and condensation near the center surface. Because of the concern about surface temperature in pressurized transfer of cryogens, this area merits further consideration.

An experimental study in which numerous temperature measurements are made in the surface region is probably warranted. For liquids, movement of the surface due to fluid expansion must be considered as part of such an investigation.

Conditions near both a free and a bounded liquid surface should be compared and effects of vaporization should be evaluated under carefully controlled conditions. A comparison between upper region mixing phenomena in gases and liquids would also be of interest.

2. Development of boundary layer theory for generalized wall and core temperature distributions

Many systems have more complex thermal boundary conditions than are considered in the current work. In addition, non-linear core temperature distributions are encountered in systems of other geometries--for example, spherical and conical tanks or even horizontal cylinders. Maahs (50) study of isotherms in horizontal cylinders would provide one interesting experimental check on such a model.

Maahs presented experimental isotherms for both gas and liquid

systems. Boundary layer flow along the curved walls was well-defined only in the liquid systems and the resulting core isotherms show a crowding near the upper region of the horizontal cylinder. Solution of the boundary layer equations using a constant core temperature gradient assumption relative to circumferential distance, which is the boundary layer trajectory, rather than to actual height might provide a model which agrees with Maahs' data.

3. Experimental Study of Natural Convection Boundary Layer on a Vertical Plate with Temperature Variation at Infinity

The model developed in this study assumes that a constant boundary layer flow and temperature profiles are maintained even though fluid is lost to the core as a result of an increasing positive temperature gradient outside the boundary layer. In addition the model indicates that for a particular core gradient, the boundary layer attains a constant total energy and momentum and additional energy input at the wall is completely used to increase the boundary layer average temperature level at the same rate that the core temperature is rising. Experimental evaluation of this phenomenon would be interesting. Such a study might also include development of criteria for complete deceleration of a boundary layer due to edge temperature fields and an analysis of possible boundary layer separation or reversal effects.

In order to actually investigate boundary layer flow and temperature profiles, a viscous fluid should be used to provide as wide a physical boundary layer as possible. For simplicity, a vertical plate study could be made and this would permit use of Schlieren or interferometric techniques for experimental analysis of boundary layer flow. The system would probably be a rectangular box consisting of two

parallel heated walls, quite wide to eliminate end effects, an insulated bottom plate, and transparent, insulated side-walls for viewing.

Nomenclature

a	constant (eq. 2-1)
A	constant (eqs. 3-10 to 3-13)
b	constant (eq. 2-1)
D	diameter (ft)
E	dimensionless boundary layer energy parameter (eq. 3-24)
$C_{subs.}$	dimensionless coefficients (eqs. 3-23, 3-24, 3-25)
C	dimensional factor $\left[gBq/k\nu^2\right]^{1/4}$ (ft^{-1}) (eqs. 3-16 to 18)
C_p	fluid specific heat capacity (BTU/lb, °F)
g	acceleration of gravity or equivalent for other body force fields (ft/hr^2)
h	heat transfer coefficient (BTU/hr, ft^2, °F)
k	thermal conductivity (BTU/hr, ft, °F)
L	length or height (ft)
M	dimensionless boundary layer momentum parameter (eq. 3-25)
P	pressure (lbs/ft^2)
q	heat flux (BTU/hr, ft^2)
r	radial coordinate (ft)
R	dimensionless radial coordinate (eq. 2-13)
t	time (hr)
T	temperature (°F)
u	velocity in x-direction (ft/hr)
v	velocity in y-direction (ft/hr)
V	dimensionless velocity (eq. 2-13)
w	wall thickness (ft)
x	Cartesian coordinate (opposed to direction of gravity or other body force) (ft)

X dimensionless x-coordinate (eq. 2-13)

y Cartesian coordinate (ft)

Dimensionless Groups

Fo Fourier Number, $\frac{\alpha t}{ID}$

Gr Grashof Number, $\frac{g\beta(T_w - T_o)L^3}{\nu^2}$

GrNu Grashof-Nusselt Number, $\frac{g\beta q L^4}{k\nu^2}$

L/D Aspect ratio

Nu Nusselt Number, $\frac{hL}{k}$

Pr Prandtl Number, $\frac{\nu}{\alpha}$

Ra Rayleigh Number, (Gr)(Pr)

Greek letters

α thermal diffusivity (ft^2/hr)

β coefficient of thermal expansion ($^oF^{-1}$)

γ dimensionless factor (eq. 3-47)

δ boundary layer width (ft) (eq. 2-32ff.)

Δ dimensionless boundary layer width (eq. 3-17)

η similarity width parameter for boundary layer (eq. 2-27)

θ angular coordinate (radians)

Θ dimensionless temperature = Ra

Note: $\Theta_s = \frac{T - T_o}{T_w - T_o}$ (eq. 2-28)

Θ_∞ = dimensionless core temperature, $(\frac{kC}{q} T_\infty)$

μ fluid viscosity (lb/ft hr)

ν kinematic viscosity, $\frac{\mu}{\rho}$ (ft^2/hr)

ξ similarity flow potential parameter (eq. 2-27)

ρ density (lb/ft^3)

τ_w shear stress at wall ($lb/ft, hr^2$) (eq. 3-5)

τ dimensionless time (eq. 2-13)

ϕ vorticity

ψ stream function

ω boundary layer velocity scale (ft/hr) (eq. 2-37)

Ω dimensionless boundary layer velocity scale (eq. 3-22)

Subscripts

a asymptotic or limiting value (eq. 3-61)

E boundary layer energy parameter (eq. 3-24)

i initial

L at x = L or in homogeneous mixing region (eq. 3-53)

M boundary layer momentum parameter (eq. 3-25)

o bulk average condition (with properties and T)

or "no core temperature gradient" (with E and M)

r radial direction (cylindrical coordinates)

s similarity solution parameter (eq. 2-28)

w wall

x axial direction (cylindrical coordinates or Cartesian coordinates)

∞ outside the boundary layer, i.e. at $y = \infty$.

boundary layer width parameter (eq. 3-23)

θ angular direction (cylindrical coordinates)

boundary layer velocity parameter (eq. 3-22)

Superscripts

* normalized dimensionless coordinate (eqs. 3-24, 3-25)

BIBLIOGRAPHY

1. Arnett, R. W. and D. R. Millhiser, "A Theoretical Model for Predicting Thermal Stratification and Self Pressurization of a Fluid Container", Proc. Conf. on Propellant Tank Pressurization and Stratification, Jan. 20-21, 1965.

2. Aziz, K., "A Numerical Study of Cellular Convection", PhD Thesis, Rice University, Houston, Texas (1965).

3. Bailey, T., R. Van de Koppel, G. Skartvedt, and T. Jerrerson, "Cryogenic Propellant Stratification Analysis and Test Data Correlation", AIAA Journ., Vol. 1, No. 7, pp. 1657 - 1659 (1963).

4. Barakat, H. Z. and J. A. Clark, "Transient, Laminar, Free-Convection Heat and Mass Transfer in Closed, Partially Filled, Liquid Containers", Univ. of Michigan, Dept. of Mech. Eng., Heat Transfer Lab., Tech. Rep. No. 1, (NASA Contract No. NAS-8-825),(Jan. 1964).

5. Barakat, H. Z. and J. A. Clark, "On the Solution of the Diffusion Equation by Numerical Methods", Heat Transfer Laboratory Publication, Dept. of Mech. Eng., University of Michigan (Also presented to the A.S.M.E. Heat Transfer Division 1964 Winter Annual Meeting).

6. Batchelor, G. K., "Heat Transfer by Free Convection across a Closed Cavity between Vertical Boundaries at Different Temperatures", Quart. Appl. Math., Vol. 12, 209-233 (1954).

7. Bhutani, O. P., "Certain Boundary Value Problem and its Applications", Appl. Sci. Res. A., Vol. 8, No. 6, (1959), pp. 413-424.

8. Bodoia, J. R. and J. F. Osterle, "The Development of Free Convection between Heated Vertical Plates", Trans. ASME J. Heat Transfer, Series C, Vol. 84, pp. 40-44 (1962).

9. Chang, K. S., R. G. Akins and S. G. Bankoff, "Free Convection of Liquid Metal from Uniformly Heated Vertical Plate", Ind. and Eng. Chem. Fundamentals, Vol. 5, No. 1, p. 26 (1966).

10. Cooper, W. W. et al, "Heating of Cylinders of Liquids", MIT Chem. Lab. Report, Dept. of Chem. Eng. (1962).

11. Crawford, L. and R. Lemlich, "Natural Convection in Horizontal Concentric Cylindrical Annuli", Ind. and Eng. Chem. Fundamentals, 260, (1962).

12. Deardorff, J. W. "A Numerical Study of Two-Dimensional Parallel Plate Convection", J. Atmos. Sci., Vol. 21, 419 (1964).

13. DeGraaf, J. G. A., and E. F. M. van der Held, "The Relation between the Heat Transfer and the Convection Phenomena in Enclosed Plane Gas Layers", Appl. Sci. Res. A., Vol. 3, 393 (1954).

14. Dickey, J. W., R. N. Leslie and P. M. Cukor, "Modification of Flow in Cylindrical Vessels", 10.27 Chem. Eng. Lab. Project No. K-3-65, Mass. Inst. of Tech., Cambridge, Mass. (1966).

15. Donaldson, I. G., "Free Convection in Vertical Tubes with Linear Wall Temperature Gradient", Austral. J. Physics, Vol. 14, No. 4, 529-539 (Dec. 1961).

16. Eckert, E. R. G. and W. O. Carlson, "Natural Convection in an Air Layer Enclosed between Two Vertical Plates with Different Temperatures", Intl. J. Heat Mass Trans., Vol. 2, 106-120. (1961).

17. Eckert, E. R. G., J. P. Hartnett, and T. F. Irvine, Jr., "Flow-Visualization Studies of Transition to Turbulence in Free Convection Flow", ASME Paper No. 60-WA-250, (1960).

18. Eckert, E. R. G. and T. W. Jackson, "Analysis of Turbulent Free-Convection Boundary Layer on Flat Plate", NACA Report 1015, Lewis Flight Prop. Lab., (July 1950).

19. Eichhorn, R., "Flow Visualization and Velocity Measurement in Natural Convection with Tellurium Dye Method", ASME Trans. J. Heat Transfer, Series C, Vol. 83, pp. 379-381 (1961).

20. Elder, J. W., "Laminar Free Convection in a Vertical Slot", J. Fluid Mech., Vol. 23, Part 1, 77-98, (1965).

21. Elder, J. W. "Turbulent Free Convection in a Vertical Slot", J. Fluid Mech., Vol. 23, Part 1, 99-112, (1965).

22. Elenbaas, W., "Heat Dissipation of Parallel Plates by Free Convection", Physica, Vol. 9, No. 1, 1-28, (1942).

23. Evans, L. B. and N. E. Stefany, "An Experimental Study of Transient Heat Transfer to Liquids in Cylindrical Enclosures", Chem. Engr. Progr. Symposium Ser. No. 64, Vol. 62 (1966).

24. Faulkenberry, S. T., "Heat Transfer to a Fluid in an Enclosure", S. B. Thesis, Mass. Inst. of Tech., Cambridge, Mass. (1963).

25. Foster, C. V., "Heat Transfer by Free Convection to Fluids Contained in Vertical Tubes", PhD Thesis, Univ. of Delaware, Newark, Del. (1953).

26. Gebhart, B., "Transient Natural Convection from Vertical Elements", Trans. ASME, J. Heat Transfer, Series C, Vol. 83, No. 1, 61-70 (1961).

27. Gershuni, G. Z. and E. M. Zhukhovitskii, "The Closed Convective Boundary Layer", (translation) Sov. Phys. Dokl., Vol. 4, No. 1, 102-104 (1959).

28. Globe, S. and D. Dropkin, "Natural Convection Heat Transfer in Liquids Confined by Two Horizontal Plates and Heated from Below", Trans. ASME J. Heat Transfer, Series C, Vol. 81, 24-28 (1959).

29. Goldstein, R. J. and Eckert, E. R. G., "The Steady and Transient Free Convection Boundary Layer on a Uniformly Heated Vertical Plate", Intl. J. Heat Mass Transfer, Vol. 1, 208-218 (Aug. 1960).

30. Griffiths, E. and A. H. Davis, "The Transmission of Heat by Radiation and Convection", Food Investigation Board, Brit. Dept. Sci. and Ind. Res., Spec. Report No. 9 (1922).

31. Hammitt, F. G., "Modified Boundary Layer Type Solution for Free Convection Flow in a Vertical Closed Tube with Arbitrarily Distributed Internal Heat Source and Wall Temperature", ASME Paper No. 58-SA-30 (June 1958).

32. Hammitt, F. G., "Natural Convection Heat Transfer in Closed Vessels with Internal Heat Sources", ASME Paper No. 58-A-212 (Dec. 1958).

33. Hammitt, F. G., E. M. Brower and P. T. Chu, "Free Convection Heat Transfer and Fluid Flow in Closed Vessels with Internal Heat Source", OTS, NP-9780, Dept. of Commerce, Wash. D. C.

34. Harlow, F. H. and J. E. Fromm, "Dynamics and Heat Transfer in the von Karman Wake of a Rectangular Cylinder", Physics of Fluids, Vol. 7 No. 8, 1147-1156 (1964).

35. Hartnett, J. P. and W. E. Welsh, "Experimental Studies of Free Convection Heat Transfer in a Vertical Tube with Uniform Wall Heat Flux", Trans. ASME, Vol. 79, 1551 (1957).

36. Hellums, J. D., "Finite Difference Computation of Natural Convection Heat Transfer", ScD Thesis, Univ. of Michigan, (1960).

37. Hellums, J. D. and S. W. Churchill, "Transient and Steady State, Free and Natural Convection Numerical Solutions", AIChE Journ., Vol. 8, No. 5, 690 (1962).

38. Hellums, J. E. and S. W. Churchill, "Computation of Natural Convection by Finite Difference Methods", Intl. Dev. in Heat Transfer, Part V, 985-994 (1961).

39. Herring, J. R., "Investigation of Problems in Thermal Convection: Rigid Boundaries", Journ. Atmos. Sci., Vol. 20, 325 (1963).

40. Illingworth, C. R., "Unsteady Laminar Flow of Gas near an Infinite Flat Plate", Proc. Camb. Phil. Soc., Vol. 46, 603 (1950).

41. International Critical Tables, McGraw-Hill, New York (1930).

42. Jakob, M. and P. C. Gupta, "Heat Transfer by Free Convection through Liquids between Two Horizontal Surfaces", Chem. Eng. Prog. Symp. Ser., Vol. 50, 15 (1954).

43. Jakob, M., "Free Heat Convection through Enclosed Plane Gas Layers", Trans. ASME, Vol. 68, 189 (1946).

44. Jeffreys, H., "The Stability of a Layer of Fluid Heated Below", Phil. Mag., Series 7, No. 2, 833-844 (1926).

45. Klei, H. E., "A Study of Unsteady State Natural Convection for a Vertical Plate", S. B. Thesis, Mass. Inst. of Tech., Cambridge, Mass. (1957).

46. Larsen, F. W. and J. P. Hartnett, "Effect of Aspect Ratios and Tube Orientation on Free Convection Heat Transfer to Water and Mercury in Enclosed Circular Tubes", Trans. ASME, J. Heat Transfer, Vol. 83, No. 1, 87 (1961).

47. Lighthill, M. J., "Theoretical Consideration on Free Convection in Tubes", Quart. J. Mech. and Appl. Math., Vol. 6, 398 (Mar. 1953).

48. Liu, C-Y, W. K. Mueller and F. Landis, "Natural Convection Heat Transfer in Long Horizontal Cylindrical Annuli", Intl. Dev. Heat Transfer, Part V (ASME 1961).

49. Liu, V. C. and H. Jew, "On Laminar Free Convection Flows in Cavities", Bull. Amer. Phys. Soc., Vol. 5, No. 2, 130 (1960).

50. Maahs, H. G., "Transient Natural Convection Heat Transfer in a Horizontal Cylinder", PhD Thesis, Univ. of Wash., Seattle, Wash. (1964).

51. Malkus, W. V. R. and G. Veronis, "Finite Amplitude Cellular Convection", J. Fluid Mech., Vol. 4, No. 3, 225-260 (July 1958).

52. Martin, B. W. and H. Cohen, "Heat Transfer by Free Convection in an Open Thermosyphon Tube", Brit. J. Appl. Phys., Vol. 5, 91-96 (1954).

53. Martini, W. R. and S. W. Churchill, "Natural Convection Inside a Horizontal Cylinder", AIChE Journ., Vol. 6, No. 2, 251-257 (1960).

54. McAdams, W. H., "Heat Transmission", 3rd Edition, McGraw-Hill, New York (1954).

55. Menold, E. R. and S. Ostrach, "Natural Convection in a Horizontal Cylinder at Large Prandtl Numbers", Eng. Div. Case Inst. Tech., Report No. AFOSR 65-2239, Cleveland, Ohio (1965).

56. Menold, E. R. and K. T. Yang, "Asymptotic Solutions for Unsteady Laminar Free Convection on a Vertical Plate", Trans. ASME, Journ. Appl. Mech., Vol. E85, 124 (1962).

57. Miner, C. S. and N. N. Dalton, "Glycerol", Am. Chem. Soc. Monograph 117 (1953), as included and augmented in a booklet "Physical Properties of Glycerine and its Solutions", published by Glycerine Producers' Assn., 295 Madison Ave., New York (1963).

58. Mull, W. and H. Reiher, "Der Warmeschutz von Luftschichten", Gesund.-Ing. Beihefte, Vol. 1, No. 28 (1930).

59. Neff, R., "A Survey of Stratification in a Cryogenic Liquid", Adv. in Cryo. Eng., Vol. 5, 460-466 (1960).

60. Noble, J. J., "Interaction between Radiative Convection and Natural Convection", ScD Thesis Proposal, Dept. of Chem. Eng., Mass. Inst. of Tech., Cambridge, Mass. (Feb. 1965).

61. Oshima, M. "Natural Convection Heat Transfer to a Fluid in an Enclosure", SM Thesis, Mass. Inst. Tech., Cambridge, Mass. (1964).

62. Ostrach, S. and D. Pnueli, "The Thermal Instability of Completely Confined Fluids inside some Particular Configurations", ASME Paper No. 62-WA-140 (1962).

63. Ostrach, S., "An Analysis of Laminar Free-Convection Flow and Heat Transfer About a Flat Plate Parallel to the Direction of the Generating Body Force", NACA TR 1111 (1953).

64. Ostrach, S., "Convection Phenomena in Fluids Heated from Below", Trans. ASME, Vol. 79, 299 (1957).

65. Ostrach, S., "Combined Natural and Forced Convection Laminar Flow and Heat Transfer of Fluids with and without Heat Sources in Channels with Linearly Varying Wall Temperatures", NACA TN 3141, (1954).

66. Ostrach, S. and P. R. Thornton, "On the Stagnation of Natural Convection Flows in Closed-End Tubes", Trans. ASME, Vol. 80, 363 (1958).

67. Ostroumov, G. A. and Tetiuev, "On the question of the theory of free thermal convection in cylindrical cavities", (translation) Sov.-Phys.-Tech. Phys., Vol. 3, No. 6, 1173 (1959).

68. Pellew, A. and R. V. Southwell, "On Maintained Convection in a Fluid Heated from Below", Proc. Roy. Soc. (London), Series A, Vol. 176, 312 (1940).

69. Perry, J. H., "Chemical Engineer's Handbook", 3rd Edition, McGraw-Hill, New York (1950).

70. Pohelkin, L. M., "Heat Transfer by Natural Convection in a Vertical Pipe", (abstract) Appl. Mech. Rev., Vol. 14, Abstr. No. 4380 (1961).

71. Pohlhausen, K. "Zur naherungsweisen Integration der Differentialgleichung der Laminaren Reibungsschicht", ZAMM, Vol. 1, 252-268 (1921) - as abstracted in ref. 83.

72. Poots, G., "Heat Transfer by Laminar Free Convection in Enclosed Plane Gas Layers", Quart. J. Appl. Math., Vol. 11, 257-273 (1958).

73. Pustovoit, S. P., "Transient Thermal Convection in a Spherical Cavity", Appl. Mech. Revs., Vol. 13, No. 2, Abstract No. 898, (1960).

74. Rayleigh, Lord, "On Convection Currents in a Horizontal Layer of Fluid when the Higher Temperature is on the Under Side", Phil. Mag., Series 6, Vol. 32, 529-546 (1916).

75. Ruder, J., "Stratification in a Pressurized Container with Sidewall Heating", AIAA Journ., Vol. 2, No. 1, 135 (1964).

76. St. Pierre, C. and C. Tien, "Experimental Investigation of Natural Convection Heat Transfer in Confined Space for Non-Newtonian Fluid", Canad. J. Chem. Eng., Vol. 41, No. 3, 122, (1963).

77. Sandel, Perardi, and Hanson, 10.27 Course Project No. 19-63, Mass. Inst. Tech., Cambridge, Mass., (1964).

78. Saunders, O. A., "Natural Convection in Liquids", Proc. Roy. Soc. (London), Vol. A-172, 55 (1939).

79. Saunders, O. A., "The Effect of Pressure upon Natural Convection in Air", Proc. Roy. Soc. (London), Vol. A-157, 278-291 (1936).

80. Schecter, R. S. and H. S. Isbin, "Natural Convection Heat Transfer in Regions of Maximum Fluid Density", AIChE Journ., Vol. 4, No. 1, 81-89 (1958).

81. Scherberg, M. G., "Natural Convection from Wall Sections of Arbitrary Temperature Distributions by an Integral Method", Intl. Journ. Heat Mass Transf., Vol. 7, 501-516 (1964).

82. Schetz, J. A. and R. Eichhorn, "Unsteady Natural Convection in the Vicinity of a Double Infinite Vertical Plate", Trans. ASME, J. Heat Transfer, Vol. 84, 334, (1962).

83. Schlicting, H., "Boundary Layer Theory", 4th Edition, McGraw-Hill, New York (1960).

84. Schmidt, E. "Versuche zum Warmeubergang bei Naturlicher Konvektion", Chemie. Ing. Techn., Vol. 28, No. 3, 175-180 (1956).

85. Schmidt, E. and W. Beckmann, "Das Temperature und Geswindigkeitsfeld vor einer Warme abgeben sinkrechter Platte bei naturlicher Konvektion", Tech Mech u Thermo., Vol. 1, 341-349, 391-406 (1930).

86. Schwind, R. G. and G. C. Vliet, "Observations and Interpretations of Natural Convection and Stratification in Vessels", Proc. 1964 Heat Transfer and Fluid Mech. Inst., 51, Stanford University Press, Palo Alto, Calif. (1964).

87. Segel, M. P., "Experimental Study of the Phenomena of Stratification and Pressurization of Liquid Hydrogen", Intl. Advances in Cryogenic Engineering, Vol. 10, 308-313 (1964).

88. Sevryk, I. G., "Uniqueness of the Solution of the Fundamental Problem of the Free Thermal Convection of a Liquid", Appl. Mech. Rev., Vol. 14, Abst. No. 2656 (1961).

89. Shaidurov, G. F., "Convective Heat Transfer in a Horizontal Cylinder", Intl. J. Heat Mass Transfer, Vol. 2, No. 4, 280-282 (1961).

90. Sherman, M. and S. Ostrach, "The Thermal Stability of Completely Confined Fluids including Magnetohydrodynamic Effects", Eng. Div., Case Inst. of Tech., AFOSR 65-1455, Cleveland, Ohio (1965).

91. Siefkes, D. "Heat Transfer to a Liquid in a Cylindrical Vessel with an Insulated Bottom", S. B. Thesis, Mass. Inst. Tech., Cambridge, Mass. (1964).

92. Siegel, R. "Transient Free Convection from a Vertical Flat Plate", Trans. ASME, Vol. 80, 347 (1958).

93. Smith, K. A., Personal Communication, Mass. Inst. of Tech., Cambridge, Mass., (1966). Paper submitted to Ind. Eng. Chem., Fundamentals.

94. Soberman, R. K., "Onset of Convection in Liquids Subjected to Transient Heating from Below", Phys. Fluids, Vol. 2, No. 2, 131-138 (1959).

95. Spangenberg, W. G. and W. R. Roland, "Convective Circulation in Water induced by evaporative cooling", Phys. Fluids, Vol. 4, No. 6, 743-750 (1961).

96. Sparrow, E. M., "Laminar Free Convection on a Vertical Plate with Prescribed Non-Uniform Wall Heat Flux or prescribed Non-Uniform Wall Temperature", NACA TN 3508. (also see Sparrow, E. M. and J. L. Gregg, Trans. ASME, Vol. 80, 379 (1958).

97. Sparrow, E. M. and J. L. Gregg, "The Variable Fluid Property in Free Convection", Trans. ASME, Vol. 80, 879-886 (1958).

98. Sparrow, E. M. and J. L. Gregg, "Laminar Free Convection from a Vertical Plate with Uniform Surface Heat Flux", Trans. ASME, J. Heat Transfer., Vol. 78, 435 (1956).

99. Stefany, N., "Transient Heat Transfer to Fluids in Cylindrical Enclosures", S. M. Thesis, Mass. Inst. Tech., Cambridge, Mass., (1964).

100. Sugawara, S. and I. Michiyoshi, "The Heat Transfer by Natural Convection in the Unsteady State on a Vertical Flat Wall", Proc. 3rd Jap. Nat. Cong. Appl. Mech., 501, (1951).

101. Townsend, A. A., "Temperature Fluctuations over a Heated Horizontal Surface", J. Fluid Mech., Vol. 5, 209, (1959).

102. Weinbaum, S., "Natural Convection in a Horizontal Circular Cylinder", J. Fluid Mech., Vol. 18, Part 3, 409, (1964).

103. Wilkes, J. O., "The Finite Difference Computation of Natural Convection in an Enclosed Rectangular Cavity", PhD Thesis, Univ. of Michigan, Ann Arbor, Michigan (1963).

104. Wilkie, D. and S. A. Fisher, "Natural Convection in a Liquid Containing a Distributed Heat Source", Intl. Dev. in Heat Trans., Part V, 995 (1962).

105. Zhukhovitskii, E. M., "Free Stationary Convection in an Infinite Horizontal Tube", Zhur. Tech. Fiz., Vol. 22, 832-835 (1952).

VIII. APPENDIX

A. Details of Experimental Apparatus

1. Enclosure (Figure 4-1, p. 128)

The Pyrex cylinder was deformed slightly in the process of applying the E-C coating, so that it actually was slightly elliptical. The dimensions along the major and minor axes of the cylinder end cross-sections are indicated in Figure 8-1. The spacing of the contact bands is also shown.

The upper and lower end flanges were 11 in. diameter, $\frac{1}{4}$ -in. thick, hot-rolled steel discs. The sealing surfaces were Blanchard ground to provide flat faces. A $\frac{1}{8}$ -in. silicone rubber gasket, covering the entire cross-section cushioned the Pyrex cylinder from each flange. The gasketed flanges were sealed to the main section by means of six tie rods. The threaded, $\frac{3}{8}$ -in. steel rods were inserted through the flanges and end nuts were tightened uniformly to provide an even pressure against the glass. The enclosure stood on three special feet which also served as levelling devices and were screwed onto the bottom of alternating tie rods. The region between the bottom flange and the wooden base table was filled with glass wool insulation. A drain line from the bottom flange consisted of a 3-in. length of $\frac{3}{8}$ -in. copper tubing upstream of a drain valve.

2. Temperature measurement system

A ladder structure, constructed of two main $\frac{3}{8}$ -in. nylon rods and ten short $\frac{1}{8}$ -in. nylon cross rods, was designed to support the grid of thermocouples. Figure 4-3 indicates details of the ladder and its support system. The main rods were 23-$\frac{1}{2}$ in. in length, but $\frac{1}{4}$ -in. sections

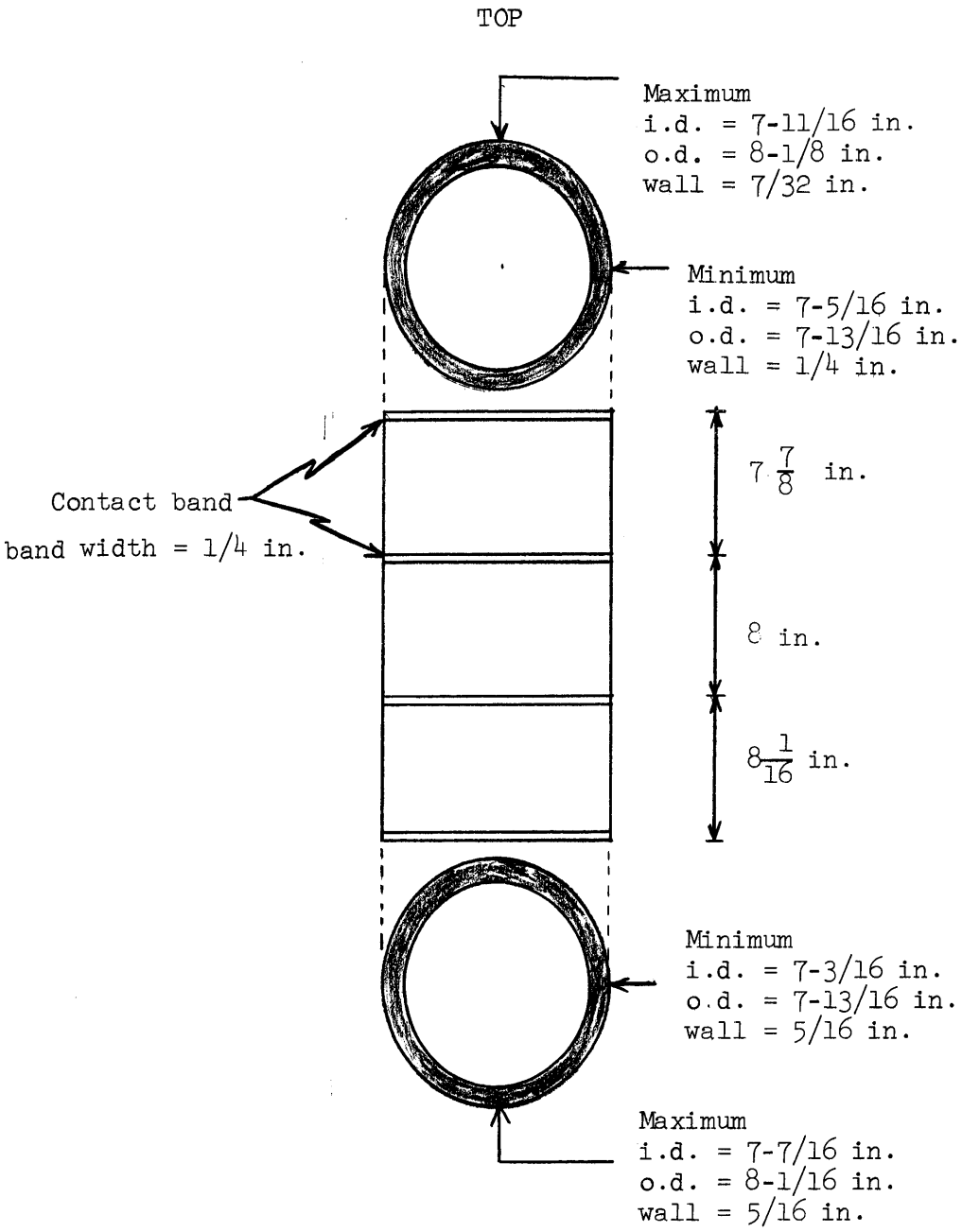

FIGURE 8-1

Enclosure: Details

at the ends of each rod were machined down to a $\frac{1}{8}$ -in. diameter. These ends were inserted into nylon bushings which had been cemented with epoxy resin to the silicone gaskets. The bushings, $\frac{1}{4}$ -in. in length, had bores slightly greater than $\frac{1}{8}$ -in. to allow a sliding fit with the ends of the main ladder rods. The position of the supports, shown in Fig. 4-3, was determined accurately in the following manner. In preparing the end flanges, the center of the steel disc had been located with the flange held securely in a calibrated milling machine. Bolt holes, fill and drain holes, and instrumentation holes were all positioned with respect to the reference point. Next, the gasket was placed over the flange and cut to match. Finally, the support socket positions were measured from the undisturbed original reference point and a center punch was used to hold the supports firmly while they were cemented in place.

The ladder was located parallel to, but $\frac{3}{4}$ -in. behind, the radius lying in the vertical plane where measurements were made. The cross rods were drilled with holes just large enough to allow passage of the 0.010-in. thermocouple beads. The 3-mil copper-constantan thermocouple wires, insulated with a thin baked-on silicone coating, were extended so that the beads lay in the measuring plane. Epoxy cement was used to anchor the wires to the cross rod support. The thermocouple spacing in the radial direction was determined on the basis of a 7 $\frac{3}{8}$ -in. average cylinder diameter (3.69-in. radius) such that dimensionless radial positions from the centerline were determined by: $\left(\frac{r}{R}\right)^2 = 0, \frac{1}{4}, \frac{1}{2}, \frac{3}{4}, 0.97$. This resulted in thermocouple spacings, relative to the wall, of: 0.05 in., 0.50 in., 1.07 in., 1.84 in. and 3.69 in. (centerline). Since the cross rod was about 0.16 in. shorter

than the radius, the thermocouple nearest the wall had to be bent toward the wall from its base support point. A 0.05-in. spacer was used in positioning the thermocouples nearest the wall. The other thermocouples were correctly positioned when they extended straight outward from the cross rod. The minor variations in enclosure radius were compensated for by making sure that all cross rod tips were in contact with the wall. This provided accurate spacing relative to the wall with any errors in position occurring in the central region where temperature gradients are smallest.

Nylon was chosen as a support material because of its low thermal conductivity and its machinability. Although it provided a workable system, nylon tends to swell somewhat in water. This meant that the support system occasionally required some minor modifications to maintain correct thermocouple positions. Hindsight indicates that Pyrex rods might have provided a less troublesome support structure.

A 16-point Brown recorder (Model No. 153x60P16-x-1F, Serial No. 328555) with a 30 sec/point printing rate was used to automatically record thermocouple data. In addition, manual read-out of another 15 thermocouples through a rotary switch could be accomplished using a precision potentiometer: Rubicon, Model No. 2715, calibrated to 0.005 mv.

3. Tracer Injection System

A 24-in., 22 gauge, hypodermic needle was used to inject a mixture of ink and test fluid into the system during a test. To prevent flow disturbance, the needle was positioned prior to the start of the experiment. A special dispenser with a calibrated screw mechanism

actuating the hypodermic syringe allowed minute amounts of dye to be injected slowly.

A second similar system with an 8-in, 15 gauge needle was used for dye injection near the surface.

B. Additional Literature References for Other Geometries (Figure 8-2)

1. Fluid heated from below

A fluid layer lying on top of a heated horizontal plate can exhibit several types of convective flow. Using a characteristic length corresponding to the fluid depth, or to plate spacing if a second horizontal plate forms the upper boundary, a Rayleigh number of about 1700 is required to initiate convection. If the characteristic spacing is about 1 cm. or greater, cellular flow patterns are observed. These "Bénard" cells are hexagonal with length equal to twice the height of the cell. Adjacent cells have opposite rotations. Rayleigh (74) developed the earliest model describing the cell flows. Later, Jeffreys (44) presented a more complete mathematical analysis; more recent analytical studies of Bénard cells include the work of Pellew (68) and Malkus (51). Experimental observations of such flows are presented by DeGraaf (13) who also measured heat transfer coefficients for the system. DeGraaf, as well as Globe (28), Soberman (94) and Jakob (42, 43) report that above Ra $\backsim 10^5$, the Nusselt number depends upon the $\frac{1}{3}$ -power of the Rayleigh number. Jakob's analysis was based on data obtained by Mull (58). The $\frac{1}{3}$ -power relationship is generally assumed to indicate a transition to turbulent flow in these studies at an unusually low Rayleigh value.

Townsend (101) has studied turbulent natural convection of air confined above a heated plate. St. Pierre (76) observed the effects of Non-Newtonian behavior on a horizontal layer of fluid heated from below. A recent numerical study by Aziz (2) is also concerned with this problem. Ostrach (64) gives an excellent summary of studies completed before 1957 on this model.

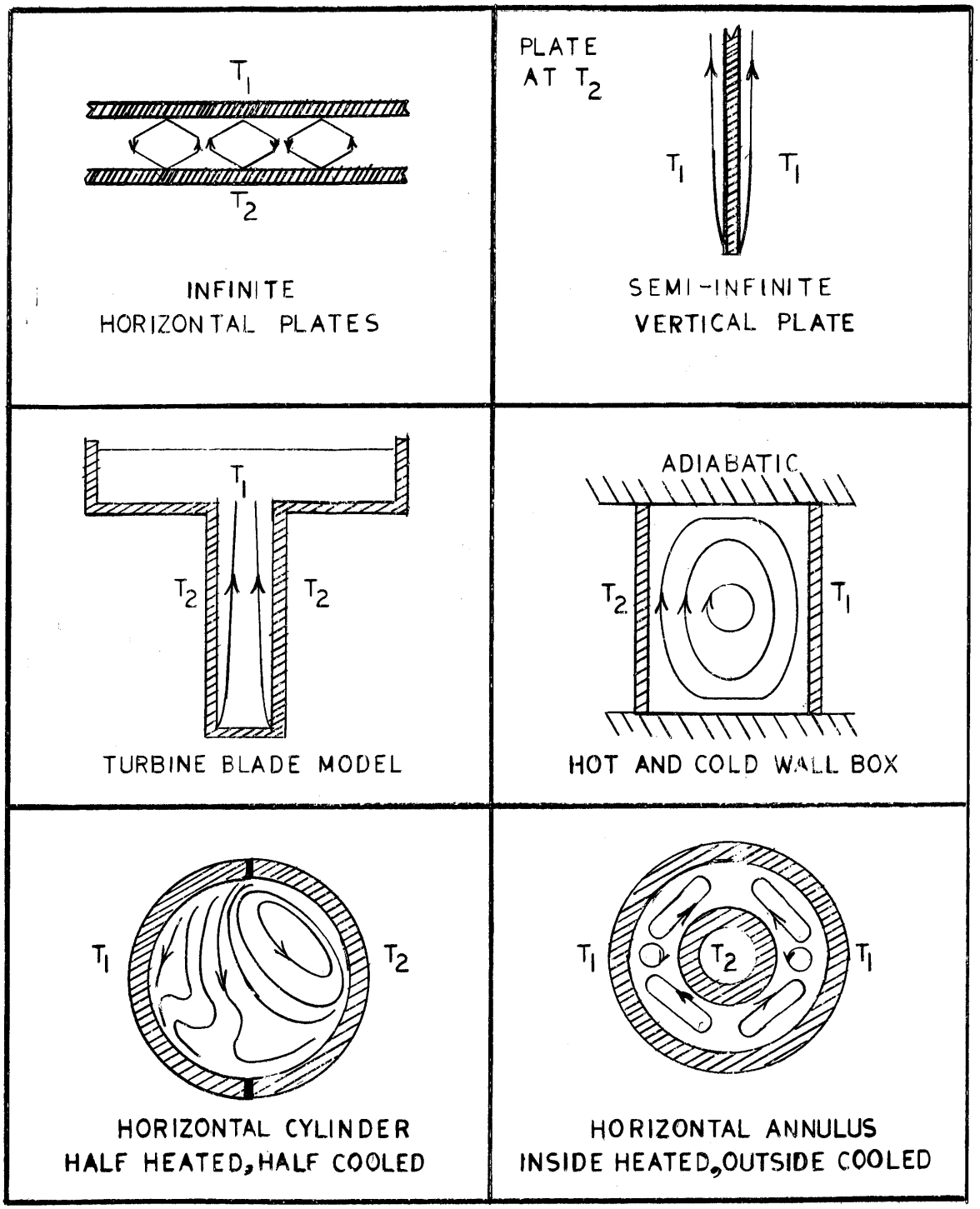

FIGURE 8-2

TYPICAL NATURAL CONVECTION SYSTEMS

APPROXIMATE STREAMLINES ARE SHOWN

$T_2 > T_1$

2. Fluid within Horizontal Cylindrical and Spherical Enclosures

Schmidt (84) measured natural convection heat transfer coefficients for fluids within both horizontal cylinders and spheres, following a step change in wall temperature. For spheres, he found the Nusselt and Rayleigh numbers could be correlated in the usual manner. (Eqn. 2-1). For Rayleigh numbers between 10^8 and 10^{12}, the exponent $b = \frac{1}{3}$, indicating a turbulent flow mechanism. In horizontal cylinder experiments, Schlieren techniques were used to observe initiation of natural convection at Ra = 1700. The transition to turbulence apparently occurred if the Rayleigh number exceeded 24,000.

Stefany (23, 99) studied horizontal cylinders as well as vertical ones. Transient heat transfer was determined by measuring fluid expansion as a function of time after a step change in wall temperature. The Nusselt number was found to remain essentially constant until the bulk average temperature of the enclosed fluid closely approached the wall temperature.

An extensive study on a 6-in. horizontal cylinder system subjected to a constant wall heat flux was conducted by Maahs (50). He found empirical relationships between the Nusselt, Rayleigh and Fourier Numbers. At long times, he found that liquid heat transfer coefficients for this configuration become independent of Fourier number (time). For gaseous systems a time dependent correlation was found which fit all his gas data and also correlated liquid data during the initial period before the time independent relation became valid.

Weinbaum (102) and Menold (55) have made extensive mathematical analyses of fluid convection inside horizontal cylinders with specified circumferential wall temperature distributions. By assuming a constant

vorticity, isothermal core and using a modified Oseen linearization, a number of special cases were solved. Gershuni and Zhukhovitskii (27, 105) have considered the same problem in a similar manner; Shaidurov (89) has measured heat transfer coefficients for the case of an angular temperature variation simulated by embedding the cylinder in a rectangular steel block. One vertical side of the block was heated; the other, cooled. This resulted in a sinusoidal temperature distribution around the cylinder.

A related case in which opposite vertical halves of a horizontal cylinder wall are maintained at different temperatures, has been studied by Hellums, Churchill and Martini (36, 37, 38, 53). Martini and Churchill (53) measured temperature profiles and obtained some local velocity indications using particle tracers. Hellums (36, 37, 38) finite difference computation for the corresponding theoretical system agreed fairly well at steady-state with the measured temperature fields. The velocity measurements were not accurate nor extensive enough to give a meaningful evaluation of the analytical velocity field solution.

Liu (48) has observed flow patterns during natural convection within an annulus formed by two horizontal cylinders, each at a different temperature. He observed cellular flows for certain ratios of inner and outer radius. A theoretical steady-state model for this system has been developed by Crawford (11).

3. Rectangular Enclosures

Oshima (61) measured over-all transient heat transfer coefficients in a rectangular cavity using a liquid expansion method to estimate bulk temperature. Ostrach (62), using bronze powder as a tracer in silicone

oils, observed flow patterns in spaces formed between inner and outer rectangular enclosures. Heat flux, due to a temperature differential across a rectangular cavity, has been studied experimentally by Eckert (16) and Elder (20, 21). This configuration has been treated analytically by Poots (72), Batchelor (6) and Wilkes (103), although none were able to obtain valid solutions for fairly rapid convective circulations.

4. Other Cases

Still another area of interest has evolved from problems associated with convective heat transfer in nuclear reactors (26, 31, 32, 33, 104). A model based on the Kármán-Pohlhausen method with a heat generation term included in the boundary layer energy equation has been developed. The model gives reasonable agreement with heat transfer coefficient data obtained using resistance heating of an aqueous salt solution.

Schecter (80) has considered convective behavior in water at 4°C, the maximum density point. Spangenburg (95) observed effects produced by surface evaporation of water.

C. Tabulation of Experimental Data

The following pages contain a temperature data matrix corresponding to the results obtained during the experimental part of this thesis. At the start of each group of data is a line describing the over-all test conditions. Then a line of time values (minutes) is given. These are the times at which temperature values throughout the matrix were evaluated. The main part of the data consists of a thermocouple location number (corresponding to the points shown on Figure 4-2, p. 135), followed by a listing of temperature rise values ($T - T_i$) for each time listed in the TIMES line.

```
R
R     TEMPERATURE DATA MATRIX,  DEGREES FAHRENHEIT
R     ACTUAL TEMPERATURE MINUS INITIAL TEMPERATURE


R     NFL=1  PURE GLYCERINE
R     NFL=2  85 WT PERCENT GLYCERINE-WATER
R     NFL=3  PURE WATER
R     TINIT IS INITIAL FLUID TEMPERATURE
R     NOMQ  IS NOMINAL WALL HEAT FLUX IN BTU/HR,FT2
R     L  IS FLUID DEPTH IN FEET
R     TIMPTS  IS NUMBER OF TIME READINGS FOR TEST
R     TIMES  ARE TIMES FROM START IN MINUTES
R     TCNO.  IS THERMOCOUPLE LOCATION NUMBER
R
```

NFL =1, TINIT =76.0, NOMQ = 130.0, L = 0.667, TIMPTS = 13.0

TIMES	5.0	14.0	27.0	45.0	60.0	90.0	120.0	150.0	180.0
TCNO.									
0.0	0.7	6.3	14.0	20.0	24.0	34.3	42.3	48.0	56.0
50.0	1.5	9.0	14.8	21.0	25.0	34.5	42.5	50.0	58.0
75.0	2.2	10.7	16.7	22.5	26.7	36.0	44.5	50.7	59.7
95.0	4.7	13.5	19.0	25.0	29.7	39.3	46.3	52.5	61.8
41.0	0.0	10.5	18.5	24.5	30.0	40.0	49.0	57.0	64.5
42.0	4.5	15.0	21.5	27.5	32.5	42.0	51.0	59.0	66.0
43.0	10.0	20.0	25.0	30.5	36.0	45.5	54.0	62.0	69.0
16.0	0.0	3.0	10.5	18.5	24.0	35.0	45.0	54.0	61.5
17.0	0.0	3.0	10.5	18.5	24.0	35.0	45.0	54.0	61.5
18.0	0.0	3.0	10.5	18.5	24.0	35.0	45.0	54.0	61.5
19.0	0.0	5.0	11.5	18.5	24.5	35.0	45.0	54.0	61.5
20.0	0.5	5.0	11.5	18.5	24.5	35.0	45.0	54.0	61.5
44.0	0.0	0.5	5.5	11.0	17.5	28.0	39.0	48.0	57.0
45.0	0.0	0.5	5.5	11.0	17.5	28.0	39.0	48.0	57.0
46.0	0.5	4.5	8.0	13.5	18.5	29.0	39.0	48.0	57.0
47.0	0.0	0.0	1.5	6.0	11.5	22.0	31.5	40.0	49.0
21.0	0.0	0.0	1.0	2.0	4.0	11.0	17.0	21.5	26.5
22.0	0.0	0.0	1.0	2.0	4.0	11.0	17.0	21.5	26.5

TIMES	210.0	240.0	300.0	360.0
TCNO.				
0.0	63.0	71.0	79.0	94.0
50.0	63.2	71.5	79.0	93.0
75.0	63.5	71.8	81.7	95.5
95.0	65.0	72.7	82.0	96.3
41.0	73.5	80.0	92.0	102.0
42.0	74.0	81.0	92.5	102.0
43.0	77.0	84.0	96.0	107.0
16.0	69.5	77.0	90.0	101.0
17.0	69.5	77.0	90.0	101.0
18.0	69.5	77.0	90.0	101.0
19.0	69.5	77.0	90.0	101.0
20.0	69.5	77.0	90.0	101.0
44.0	65.5	74.5	87.5	99.0
45.0	65.5	74.5	87.5	99.0
46.0	65.5	74.5	87.5	99.0

```
47.0    57.5   64.5   78.0   89.0
21.0    32.0   36.0   44.5   51.0
22.0    32.0   36.0   44.5   51.0 *

NFL=1, TINIT =78.0, NOMQ = 375.0, L = 0.667, TIMPTS = 11.0
TIMES    4.0   12.0   21.0   33.0   46.0   56.0   73.0   91.0  106.0
TCNO.
 0.0     0.5   15.5   25.5   40.0   51.5   62.0   78.5   84.0   95.0
50.0     3.0   17.0   28.5   41.0   54.0   62.0   75.0   84.0   98.0
75.0     5.0   21.0   31.0   44.0   56.5   65.0   80.0   86.0  100.0
95.0    11.0   25.5   36.0   49.0   60.5   69.0   82.5   90.0  102.0
41.0     6.0   22.0   34.0   48.0   59.0   69.0   80.5   93.5  104.0
42.0     6.0   28.0   38.0   50.0   61.0   69.0   80.5   93.5  104.0
43.0    14.0   33.0   42.0   51.0   63.0   71.5   84.0   97.0  109.0
16.0     0.0    7.5   21.5   36.0   48.0   58.5   74.0   89.0   99.0
17.0     0.0    7.5   21.5   36.0   48.0   58.5   74.0   89.0   99.0
18.0     0.0    7.5   21.5   36.0   48.0   58.5   74.0   89.0   99.0
19.0     0.5    8.0   21.5   35.0   47.0   58.0   72.0   87.0   96.0
20.0     1.0    8.0   21.5   35.0   47.0   58.0   72.0   87.0   96.0
44.0     0.0    1.0    7.0   19.5   32.0   43.0   59.0   75.0   87.0
45.0     0.0    1.0    7.0   20.5   32.0   43.0   59.0   75.0   87.0
46.0     1.5    3.0    8.0   19.5   32.0   43.0   59.0   75.0   87.0
47.0     0.0    1.0    4.5   14.5   23.5   33.0   48.0   63.5   74.5
21.0     0.0    0.5    1.5    5.0    9.5   15.0   21.0   32.0   38.5
22.0     0.0    0.5    1.5    5.0    9.5   15.0   21.0   32.0   38.5
TIMES  121.0  139.0
TCNO.
 0.0   100.0  106.0
50.0    98.5  107.0
75.0   101.0  110.0
95.0   103.0  113.5
41.0   116.0  126.5
42.0   116.0  126.5
43.0   125.5  140.0
16.0   111.0  125.0
17.0   111.0  125.0
18.0   111.0  125.0
19.0   108.0  120.0
20.0   108.0  120.0
44.0   101.0  113.0
45.0   101.0  113.0
46.0   101.0  113.0
47.0    87.5  102.5
21.0    45.5   55.0
22.0    45.5   55.0  *

NFL =1, TINIT =83.0, NOMQ =  60.0, L = 1.333, TIMPTS = 11.0
TIMES   10.0   30.0   59.0   89.0  120.0  149.0  180.0  211.0  240.0
TCNO.
 0.0     0.0    5.5   10.5   14.7   17.8   20.3   22.5   25.0   27.0
 1.0     1.0    3.5    8.5   14.0   19.0   23.0   25.0   27.5   30.0
 3.0     3.0   10.0   16.0   20.0   24.5   28.0   30.0   33.0   35.0
 4.0     5.0   12.0   17.0   22.0   26.0   29.0   31.0   34.0   35.5
 5.0     9.0   14.0   19.0   24.0   28.0   31.0   33.0   36.0   36.5
 6.0     3.0    8.5   14.0   19.5   25.0   28.0   31.0   34.0   35.0
```

7.0	0.0	7.5	13.0	18.5	24.0	27.0	30.0	33.0	34.5
8.0	0.0	7.5	13.0	18.5	24.0	27.0	30.0	33.0	34.5
9.0	0.0	7.0	13.0	18.5	22.0	26.0	29.0	32.0	34.5
10.0	3.0	9.0	14.0	19.0	23.0	26.5	29.5	32.0	34.5
12.0	0.0	3.5	9.5	14.0	18.5	22.0	25.5	28.5	30.5
13.0	0.0	4.0	9.5	14.0	18.5	22.0	25.5	28.5	30.5
14.0	1.0	4.0	10.0	15.0	20.0	25.0	28.0	31.0	34.0
15.0	1.0	4.5	10.0	15.0	20.0	25.0	28.0	31.0	34.0
16.0	0.0	1.5	5.5	10.0	13.5	17.0	20.5	24.0	26.5
17.0	0.0	2.0	6.0	10.0	14.0	17.0	20.5	23.5	26.5
18.0	0.0	2.0	6.0	10.0	14.0	17.0	20.5	23.5	26.5
19.0	1.0	2.0	6.0	10.0	15.0	19.0	22.0	26.0	29.0
20.0	1.0	3.0	6.0	10.0	15.0	19.0	22.0	26.0	29.0
47.0	0.0	0.5	2.0	5.0	8.5	11.5	14.0	16.5	19.0
21.0	0.0	0.0	1.0	4.0	5.5	7.0	9.5	10.5	12.5
22.0	0.0	0.0	1.0	4.0	6.0	7.0	10.0	11.5	13.0
25.0	0.0	1.0	2.0	5.0	7.0	9.5	11.0	13.0	15.0

TIMES	269.0	300.0
TCNO.		
0.0	29.3	31.5
1.0	32.0	34.5
3.0	38.0	41.5
4.0	38.5	41.5
5.0	41.0	43.0
6.0	39.0	40.0
7.0	38.0	40.0
8.0	38.0	40.0
9.0	37.5	40.0
10.0	38.0	40.0
12.0	33.5	36.0
13.0	33.5	36.0
14.0	35.0	39.0
15.0	35.0	39.0
16.0	29.0	31.5
17.0	29.0	31.5
18.0	29.0	31.5
19.0	32.0	34.5
20.0	32.0	34.5
47.0	21.5	23.5
21.0	13.0	15.0
22.0	14.0	15.5
25.0	16.0	18.0 *

NFL =1, TINIT =85.0, NOMQ = 125.0, L = 1.333, TIMPTS = 9.0

TIMES	6.5	16.0	31.0	46.0	87.0	118.0	149.0	180.0	209.0
TCNO.									
0.0	1.5	12.5	18.5	23.5	35.3	43.5	49.0	54.7	60.0
1.0	2.0	6.0	14.0	19.0	30.5	38.0	46.0	54.0	62.0
3.0	5.0	15.0	23.0	28.0	39.5	47.0	54.0	61.0	65.0
4.0	6.0	16.0	24.0	29.0	40.5	48.0	54.0	61.0	65.0
5.0	12.0	18.0	26.0	30.0	41.5	49.0	55.0	62.0	66.0
6.0	3.0	6.0	13.0	21.0	37.0	44.0	52.0	59.0	64.0
7.0	3.0	10.0	19.0	24.0	37.0	44.0	52.0	59.0	64.0
8.0	4.0	10.0	19.0	24.0	37.0	44.0	52.0	59.0	64.0
9.0	4.0	10.0	19.0	24.0	37.0	44.0	52.0	59.0	64.0

10.0	5.0	12.0	19.0	24.0	37.0	44.0	52.0	59.0	64.0
12.0	0.0	3.5	10.0	16.5	30.0	38.0	45.0	52.5	58.5
13.0	0.1	3.5	10.0	16.5	30.0	38.0	45.0	52.5	58.5
14.0	1.0	5.0	13.0	18.0	32.0	41.0	50.0	57.0	62.0
15.0	2.0	5.0	13.0	18.0	32.0	41.0	50.0	57.0	62.0
16.0	0.0	0.5	3.0	9.5	21.5	29.5	38.5	45.5	52.5
17.0	0.0	0.5	4.5	9.5	22.0	30.5	38.5	45.5	52.5
18.0	0.0	0.5	5.5	9.5	22.0	30.5	38.5	45.5	52.5
19.0	1.0	4.0	8.0	11.0	25.0	35.0	42.0	50.0	55.0
20.0	1.0	4.0	8.0	11.0	25.0	35.0	42.0	50.0	55.0
47.0	0.0	0.0	1.0	4.0	13.0	20.5	28.0	34.0	41.0
21.0	0.0	0.0	1.0	2.5	8.5	12.0	17.5	21.5	25.5
22.0	0.0	0.0	1.0	2.5	8.5	13.5	19.0	23.0	27.5
25.0	1.5	3.0	4.0	5.0	12.0	16.0	22.0	26.5	29.0*

NFL =1, TINIT =82.0, NOMQ = 215.0, L = 1.333, TIMPTS = 8.0

TIMES	5.0	15.0	31.0	46.0	58.0	75.0	91.0	104.0
TCNO.								
0.0	2.5	20.0	31.0	38.5	45.0	53.0	59.0	65.0
1.0	(2.0)	8.5	22.0	33.0	37.0	45.0	50.0	55.0
3.0	(10.0)	25.0	38.0	48.0	53.0	61.0	68.0	73.0
4.0		26.0	39.0	49.0	54.0	61.0	68.0	73.0
5.0		28.0	41.0	50.0	54.0	61.0	68.0	73.0
6.0	(4.0)	20.0	35.0	44.0	48.0	56.0	59.0	63.0
7.0	(4.0)	16.0	33.0	42.5	47.0	57.5	65.0	69.0
8.0		16.0	32.0	42.5	47.0	57.5	65.0	69.0
9.0		16.0	31.0	42.0	47.0	57.5	65.0	69.0
10.0		16.0	31.0	42.0	47.0	57.5	65.0	69.0
12.0	1.0	4.5	18.0	28.5	34.0	43.0	51.0	57.0
13.0	1.0	4.5	18.0	28.5	34.0	43.0	51.0	57.0
14.0	0.0	6.0	20.0	29.0	36.0	44.0	53.0	59.0
15.0	0.0	6.0	20.0	29.0	36.0	44.0	53.0	59.0
16.0	0.0	1.5	7.0	15.5	22.0	30.0	37.5	45.0
17.0	0.0	1.5	7.0	17.0	22.0	31.0	39.0	45.0
18.0	0.0	1.5	8.0	17.0	22.0	31.0	39.0	45.0
19.0	0.0	2.0	10.0	18.0	24.0	32.0	40.0	47.0
20.0	0.0	5.0	11.0	18.0	24.0	32.0	40.0	47.0
47.0	0.0	1.5	3.0	9.5	13.5	21.5	27.5	33.5
21.0	0.0	0.0	1.5	5.5	7.0	12.5	15.0	18.5
22.0	0.0	0.0	2.0	5.5	7.5	12.5	17.5	20.5
25.0	0.0	2.0	5.0	9.0	11.0	14.0	18.0	22.0 *

NFL =1, TINIT =89.0, NOMQ = 520.0, L = 1.333, TIMPTS = 6.0

TIMES	10.0	18.0	26.0	33.0	42.0	48.0
TCNO.						
0.0	41.0	54.0	66.5	77.0	88.0	94.0
1.0	40.0	57.0	67.0	75.0	86.0	93.0
3.0	43.0	58.0	67.0	75.0	86.0	93.0
4.0	45.0	59.0	67.0	75.0	86.0	93.0
5.0	49.0	60.0	68.0	76.0	86.0	93.0
6.0	34.0	52.0	61.5	72.0	83.0	91.0
7.0	30.0	46.0	60.0	70.0	82.0	89.0
8.0	30.0	46.0	60.0	70.0	82.0	89.0
9.0	30.0	46.0	60.0	70.0	82.0	89.0
10.0	28.0	45.0	59.0	70.0	82.0	89.0

12.0	8.5	23.0	33.5	46.5	56.0	63.5
13.0	9.0	23.0	34.0	46.5	56.5	63.5
14.0	10.0	26.0	38.0	47.0	59.0	67.0
15.0	10.0	26.0	38.0	47.0	59.0	67.0
16.0	1.0	8.0	16.5	26.5	35.5	41.5
17.0	1.0	8.0	17.0	26.5	35.5	42.5
18.0	1.0	8.0	17.0	26.5	35.5	42.5
19.0	5.0	13.0	20.0	27.0	38.0	46.0
20.0	5.0	13.0	20.0	27.0	38.0	46.0
47.0	3.5	4.5	9.0	14.5	22.0	26.5
21.0	0.5	3.0	3.5	6.5	10.5	13.5
22.0	0.5	3.0	5.0	7.5	11.5	14.5
25.0	4.0	11.0	14.0	17.0	20.0	23.0 *

NFL =1, TINIT =77.0, NOMQ = 150.0, L = 1.960, TIMPTS = 12.0

TIMES	4.0	10.0	20.0	37.0	56.0	76.0	96.0	122.0	149.0
TCNO.									
0.0	0.0	7.5	18.0	29.0	38.5	49.0	55.3	63.5	71.5
95.0	9.0	15.5	25.0	35.0	42.0	50.5	56.5	63.5	73.0
31.0	3.0	12.0	29.0	40.0	51.0	61.0	63.5	73.0	77.5
32.0	4.0	12.5	27.0	38.0	50.0	59.5	63.0	74.0	79.5
33.0	8.0	11.5	25.0	35.0	47.0	57.5	60.0	72.0	77.0
34.0	3.0	4.0	14.5	25.0	36.0	47.0	53.0	64.0	73.0
35.0	2.0	6.0	16.0	28.0	39.5	48.5	54.0	64.0	71.0
36.0	6.0	10.0	16.5	28.0	38.5	48.5	54.0	64.0	71.0
1.0	3.0	6.5	13.5	24.0	35.0	45.0	48.5	60.0	66.0
4.0	2.0	2.5	12.5	15.5	26.5	38.5	42.0	54.0	63.0
5.0	6.0	8.0	12.5	21.0	29.5	40.5	43.0	55.0	63.0
6.0	0.0	3.5	8.5	17.0	28.0	37.0	41.0	53.0	61.0
9.0	1.0	7.0	11.5	21.5	32.5	43.0	47.0	59.0	67.0
12.0	0.0	1.0	2.0	7.5	15.0	23.0	29.5	38.5	47.5
13.0	0.0	1.0	2.0	8.0	15.0	23.0	29.5	38.5	48.0
15.0	0.0	7.0	9.0	14.0	20.0	28.5	32.0	44.0	54.0
43.0	0.0	6.0	10.0	14.0	19.5	25.5	27.0	37.0	46.0
16.0	0.0	0.5	1.0	4.5	10.0	16.0	23.5	32.5	41.5
17.0	0.0	0.5	1.0	4.5	10.0	16.0	23.5	32.5	41.5
18.0	0.0	0.5	1.0	4.5	10.0	16.0	23.5	32.5	41.5
19.0	0.0	3.0	5.0	8.0	14.0	25.0	28.0	41.0	49.0
20.0	0.0	3.5	5.0	8.0	14.0	21.5	25.0	36.0	46.0
47.0	0.0	0.0	0.5	1.5	5.5	10.5	16.0	23.5	32.0
21.0	0.0	0.0	0.0	1.0	2.5	6.0	9.0	13.0	18.5
22.0	0.0	0.0	0.0	1.0	2.5	6.0	9.0	13.0	18.5

TIMES	180.0	211.0	240.0
TCNO.			
0.0	79.0	88.0	91.5
95.0	80.0	88.5	93.0
31.0	81.0	85.5	92.0
32.0	82.5	86.5	93.0
33.0	83.0	88.5	94.0
34.0	77.5	82.5	89.0
35.0	76.5	80.0	87.0
36.0	77.5	82.5	89.0
1.0	70.0	73.5	84.0
4.0	69.5	77.5	86.0
5.0	69.5	77.5	86.0

6.0	67.5	74.0	80.0
9.0	72.5	78.5	87.0
12.0	57.5	67.5	76.0
13.0	57.5	67.5	76.0
15.0	64.5	75.5	86.0
43.0	55.0	65.0	73.0
16.0	50.0	60.0	69.0
17.0	50.0	60.0	69.0
18.0	50.0	60.0	69.0
19.0	59.0	65.0	71.0
20.0	56.0	63.0	71.0
47.0	40.0	48.5	57.0
21.0	23.5	28.0	32.0
22.0	23.5	28.0	32.0 *

NFL =1, TINIT =77.0, NOMQ = 400.0, L = 1.960, TIMPTS = 9.0

TIMES	3.0	9.0	16.0	25.0	32.0	43.0	53.0	63.0	69.0
TCNO.									
0.0	2.0	20.0	40.0	56.5	69.0	82.5	93.0	104.5	112.5
95.0	15.0	49.0	56.0	69.0	80.0	88.5	97.5	109.0	114.5
31.0	10.0	37.0	64.5	73.0	80.5	84.0	92.0	89.0	88.0
32.0	11.0	36.0	61.0	71.0	80.5	84.0	92.0	89.0	89.0
33.0	12.0	33.0	59.0	70.0	80.5	84.0	92.0	90.0	90.0
34.0	7.0	17.0	38.5	53.5	63.0	73.0	80.5	81.0	82.0
35.0	11.0	22.0	42.5	55.5	64.0	68.0	77.0	76.0	80.0
36.0	10.0	20.0	39.5	52.0	62.0	69.0	76.0	79.0	85.0
1.0	14.0	17.0	32.5	45.5	53.5	60.0	63.0	64.5	66.0
4.0	6.0	7.5	17.5	31.5	42.0	54.0	62.5	66.0	68.5
5.0	10.0	14.0	22.5	33.0	42.0	53.0	59.0	65.5	68.0
6.0	7.0	9.0	19.0	31.0	40.0	50.0	56.0	63.0	61.0
9.0	14.0	16.0	25.5	38.5	49.0	58.0	67.5	75.0	67.0
12.0	0.0	1.0	3.0	12.0	20.0	30.5	40.5	51.0	57.5
13.0	0.0	1.0	3.0	12.0	20.5	30.5	41.0	51.0	57.5
15.0	6.5	10.0	11.5	14.5	22.0	34.0	48.5	65.0	73.5
43.0	8.0	14.0	15.5	17.0	24.0	37.0	47.0	54.0	58.5
16.0	0.0	0.0	1.0	4.5	11.0	19.0	29.0	38.0	43.5
17.0	0.0	0.0	1.0	5.0	11.0	19.0	29.0	38.0	43.5
18.0	0.0	0.0	1.0	5.5	11.5	19.0	29.0	38.0	43.5
19.0	5.0	9.0	8.0	10.0	17.0	26.0	36.0	41.0	46.5
20.0	5.0	8.0	7.5	5.0	11.0	18.0	27.0	36.0	43.0
47.0	0.0	0.0	0.7	1.5	5.0	10.0	17.5	25.0	30.0
21.0	0.0	0.0	0.5	1.0	2.0	4.5	8.5	12.0	15.0
22.0	0.0	0.0	0.5	1.0	2.0	4.5	8.5	12.5	15.0*

NFL =2, TINIT =82.5, NOMQ = 50.0, L = 1.333, TIMPTS = 7.0

TIMES	23.0	71.0	111.0	160.0	204.0	268.0	335.0
TCNO.							
0.0	3.0	10.0	14.5	17.0	21.0	28.0	33.5
50.0	4.5	12.5	17.5	20.0	23.0	29.5	35.0
75.0	5.5	13.5	18.5	21.5	24.0	31.0	37.0
95.0	7.0	14.0	19.0	23.0	26.0	32.0	37.5
1.0	3.5	11.0	16.0	22.0	27.0	34.0	39.0
3.0	8.5	16.0	21.0	27.0	31.0	37.5	41.0
4.0	8.5	16.0	21.0	27.0	31.0	37.5	41.0
5.0	8.5	16.0	21.0	27.0	31.0	37.5	41.0
6.0	6.0	14.0	20.0	26.0	30.0	36.5	41.0
7.0	6.0	14.0	20.0	26.0	30.0	37.0	41.0
8.0	6.0	14.0	20.0	26.0	30.0	37.0	41.0
9.0	6.0	14.0	20.0	26.0	30.0	37.0	41.0
10.0	6.0	14.0	20.0	26.0	30.0	37.0	42.0
12.0	3.5	10.5	16.0	22.5	26.5	35.5	39.5
13.0	3.5	10.5	16.0	22.5	26.5	35.5	39.5
14.0	4.0	12.0	17.0	23.0	29.0	37.0	41.0
15.0	6.0	13.0	17.0	24.0	29.0	37.0	41.0
16.0	0.5	7.5	12.5	18.0	22.5	32.5	36.0
17.0	0.5	7.5	12.5	18.0	22.5	32.5	36.0
18.0	0.5	7.5	12.5	18.0	22.5	32.5	36.0
19.0	2.0	9.0	13.0	20.0	25.0	34.0	38.0
20.0	2.0	9.0	14.0	20.0	25.0	34.0	38.0
47.0	0.0	5.0	8.5	13.5	18.0	26.0	30.0
21.0	0.0	3.5	7.0	11.0	13.0	21.5	23.5
22.0	0.0	3.5	6.5	10.0	12.0	19.5	21.5
25.0	0.5	4.0	7.0	11.0	14.0	19.5	23.0 *

NFL =2, TINIT =76.0, NOMQ = 150.0, L = 1.333, TIMPTS = 8.0

TIMES	8.0	23.0	48.0	71.0	104.0	145.0	173.0	222.0
TCNO.								
0.0	5.0	17.0	26.0	31.5	38.0	44.0	49.5	57.5
50.0	7.5	20.0	28.0	33.0	38.5	44.5	50.0	58.0
75.0	9.0	22.0	29.5	34.0	39.0	45.0	50.5	58.5
95.0	10.0	23.0	31.0	35.0	39.5	45.5	51.0	59.0
1.0	2.0	14.5	26.5	35.0	40.5	52.0	57.0	65.0
3.0	8.0	17.5	27.5	33.5	40.5	52.0	57.0	65.0
4.0	8.0	17.5	27.5	33.5	40.5	52.0	57.0	65.0
5.0	8.0	17.5	27.5	33.5	41.0	52.0	57.0	65.0
6.0	1.0	11.5	24.5	33.0	41.0	52.0	57.0	65.0
7.0	2.5	14.5	24.5	32.5	40.0	52.0	57.0	65.0
8.0	5.0	15.0	24.5	32.5	40.0	52.0	57.0	65.0
9.0	5.0	15.0	24.5	32.5	40.0	52.0	57.0	65.0
10.0	5.5	15.5	24.5	32.5	40.0	52.0	57.0	65.0
12.0	0.0	5.5	18.5	29.5	40.0	42.0	48.0	57.5
13.0	0.0	7.0	19.0	29.5	40.0	42.0	48.0	57.5
14.0	2.0	9.5	19.0	28.5	36.0	46.0	53.0	63.0
15.0	6.5	12.5	20.0	28.5	36.0	46.0	53.0	63.0
16.0	0.0	0.5	10.0	20.0	30.0	36.0	47.5	52.0
17.0	0.0	1.0	10.0	20.0	30.0	36.0	47.5	52.0
18.0	0.0	2.5	11.0	20.0	30.0	36.0	47.5	52.0
19.0	0.0	5.0	12.0	19.5	29.0	38.0	46.0	55.0
20.0	1.0	5.0	12.0	19.5	29.0	38.0	46.0	55.0

47.0	0.0	0.5	4.0	11.5	22.0	26.5	35.5	49.0	
21.0	0.0	0.0	2.5	9.0	15.0	19.0	25.5	45.0	
22.0	0.0	0.5	2.5	8.0	14.0	16.0	24.0	45.0	
25.0	0.0	2.0	4.5	8.5	14.0	21.0	24.0	30.0	*

NFL= 2, TINIT =76.0, NOMQ = 180.0, L = 1.333, TIMPTS = 10.0

TIMES	5.0	19.0	39.0	66.0	93.0	121.0	151.0	182.0	212.0
TCNO.									
0.0	2.5	18.0	26.0	29.0	41.0	49.0	57.0	66.0	70.0
50.0	8.0	22.5	32.0	37.0	43.0	49.5	58.5	66.0	71.0
75.0	10.5	25.5	34.0	39.0	45.0	49.5	59.0	67.5	71.5
95.0	11.5	27.0	34.5	40.0	46.0	51.0	60.0	67.5	72.5
1.0	1.0	11.0	23.0	33.0	44.5	52.5	61.5	68.0	75.0
3.0	4.0	17.5	26.0	35.5	44.5	52.5	61.0	68.0	75.0
4.0	5.0	17.5	26.0	35.5	44.5	52.5	61.0	68.0	75.0
5.0	5.0	17.0	26.0	35.5	44.5	52.5	61.0	68.0	75.0
6.0	1.5	8.0	20.0	34.5	43.5	51.5	60.0	68.0	74.5
7.0	2.0	14.0	23.0	33.5	43.0	51.5	60.0	68.0	74.5
8.0	4.0	14.0	23.0	33.5	43.0	51.5	60.0	68.0	74.5
9.0	4.0	14.0	23.0	33.5	43.0	51.5	60.0	68.0	74.5
10.0	5.5	14.0	23.0	33.5	43.0	51.5	60.0	68.0	74.5
12.0	0.0	6.5	16.5	24.0	36.0	45.5	53.0	61.5	69.0
13.0	0.0	6.5	16.5	24.0	36.0	45.5	53.0	62.0	69.0
14.0	0.5	8.0	17.0	27.5	37.0	46.0	57.0	65.5	73.0
15.0	0.5	13.0	19.5	28.5	38.0	46.0	57.0	65.5	73.0
16.0	0.0	1.5	9.0	15.0	30.5	36.0	45.0	55.5	64.0
17.0	0.0	1.5	10.0	15.0	30.5	36.0	45.0	55.5	64.0
18.0	0.0	2.0	11.5	16.0	30.5	36.5	45.0	55.5	64.0
19.0	0.0	4.0	11.0	20.0	29.0	38.5	49.0	58.0	67.0
20.0	0.5	5.0	11.0	20.0	29.0	38.5	49.0	58.0	67.0
47.0	0.0	0.5	3.0	12.0	22.0	30.5	38.0	45.5	51.0
21.0	0.0	0.5	2.5	4.5	14.0	20.5	27.5	34.0	37.5
22.0	0.0	0.5	3.0	4.5	14.0	19.5	27.5	31.5	36.0
25.0	0.0	1.5	4.0	8.0	14.0	19.5	26.0	31.0	36.5

TIMES	241.0
TCNO.	
0.0	80.0
50.0	80.5
75.0	80.5
95.0	81.0
1.0	83.0
3.0	83.0
4.0	83.0
5.0	82.5
6.0	82.5
7.0	82.5
8.0	82.5
9.0	82.5
10.0	83.0
12.0	77.5
13.0	77.5
14.0	80.0
15.0	80.0
16.0	71.5
17.0	71.5

```
18.0    71.5
19.0    75.0
20.0    75.0
47.0    59.0
21.0    43.0
22.0    43.0
25.0    42.0 *

NFL =2, TINIT =77.5, NOMQ = 200.0, L = 1.333, TIMPTS = 6.0
TIMES   11.0   49.0   75.0 106.0 138.0 150.0
TCNO.
 0.0    15.5   43.0   52.0   63.0   73.5   77.5
 1.0    16.0   42.5   56.5   66.5   78.0   81.5
 3.0    16.0   42.5   56.0   67.0   78.0   81.0
 4.0    16.0   42.0   56.0   67.0   78.0   81.0
 5.0    16.0   42.0   56.0   66.5   78.0   81.0
 6.0    14.0   42.5   55.5   66.0   77.5   80.5
 7.0    12.5   42.0   55.5   66.0   77.5   80.5
 8.0    12.5   41.5   55.5   66.0   77.5   80.5
 9.0    12.5   41.5   55.5   66.0   77.5   80.5
10.0    12.5   41.0   55.5   66.0   77.5   80.5
12.0     5.5   30.0   44.5   56.5   70.5   75.0
13.0     5.5   30.0   44.5   56.5   70.5   75.0
14.0     5.5   32.0   47.0   62.5   73.0   77.0
15.0    12.5   35.0   47.0   62.5   73.0   77.0
16.0     1.0   21.5   35.5   47.0   63.5   67.5
17.0     1.0   21.5   35.5   47.0   63.5   67.5
18.0     1.0   21.5   35.5   47.0   63.5   67.5
19.0     3.0   22.0   37.0   50.0   66.0   70.0
20.0     3.5   22.0   37.0   50.0   66.0   70.0
47.0     0.0   12.0   24.0   36.5   50.5   54.0
21.0     0.0    8.5   16.5   24.5   40.0   40.0
22.0     0.0    7.5   15.0   24.0   37.5   37.5
25.0     0.0    9.0   17.0   26.0   35.0   38.0   *

NFL =2, TINIT =75.5, NOMQ = 260.0, L = 1.333, TIMPTS = 7.0
TIMES    8.0   23.0   42.0   56.0   81.0 108.0 132.0
TCNO.
 0.0     9.0   30.0   41.5   48.5   59.0   73.5   85.0
50.0    11.5   32.0   43.0   49.5   60.0   74.0   85.5
75.0    13.5   34.0   44.5   51.0   62.0   76.0   87.5
95.0    15.0   35.0   46.0   52.5   63.5   77.0   87.5
 1.0    11.5   28.0   42.0   51.0   63.5   77.0   88.5
 3.0    12.5   29.0   42.0   51.0   63.5   77.0   88.5
 4.0    12.5   28.5   41.0   50.5   63.0   76.5   88.5
 5.0    12.5   28.0   40.5   50.5   62.5   76.5   88.0
 6.0     9.0   26.0   39.5   49.5   62.5   76.5   87.0
 7.0     8.5   25.0   38.5   49.5   62.0   76.0   87.0
 8.0     8.5   25.0   38.5   49.5   62.0   76.0   87.0
 9.0     8.5   25.0   38.5   49.5   62.0   76.0   87.0
10.0     8.5   25.0   38.5   49.0   62.0   76.0   87.0
12.0     0.5   13.0   31.5   36.5   50.0   68.5   79.5
13.0     0.5   13.0   31.0   36.5   50.0   68.5   79.5
14.0     2.0   15.0   29.5   38.5   53.0   69.0   82.0
15.0    10.0   20.0   31.0   40.5   53.0   69.0   82.0
```

16.0	0.0	4.5	18.5	26.5	40.5	56.0	70.0
17.0	0.0	5.5	19.0	26.5	40.5	56.0	70.0
18.0	0.0	5.5	19.0	26.5	40.5	56.0	70.0
19.0	0.5	8.5	18.5	28.0	42.0	57.5	73.0
20.0	1.0	9.0	18.0	27.5	42.0	57.5	73.0
47.0	0.0	2.0	12.5	18.0	35.5	49.0	59.0
21.0	0.0	1.5	6.0	12.0	31.0	36.5	44.0
22.0	0.0	1.5	5.5	10.0	29.5	34.5	40.5
25.0	0.5	3.0	6.5	12.5	21.5	29.0	40.5 *

NFL =2, TINIT =80.0, NOMQ = 500.0, L = 1.333, TIMPTS = 7.0

TIMES	6.0	15.0	26.0	36.0	47.0	56.0	65.0
TCNO.							
0.0	19.0	38.5	54.5	63.5	74.5	82.5	90.0
50.0	19.5	40.0	56.0	65.0	75.5	83.5	92.0
75.0	22.0	42.5	57.5	67.5	77.5	85.0	94.0
95.0	25.0	46.0	60.0	70.0	79.0	87.5	96.5
1.0	25.0	44.0	59.0	70.0	80.0	87.0	94.0
3.0	25.0	43.0	59.0	69.5	79.0	86.0	93.5
4.0	23.5	43.0	59.0	69.5	79.0	86.0	93.0
5.0	23.0	43.0	58.0	69.5	78.5	85.5	92.5
6.0	17.0	38.0	55.0	68.0	78.0	84.0	93.0
7.0	16.0	38.0	55.0	67.0	77.0	84.0	92.0
8.0	16.0	37.0	55.0	66.0	76.0	84.0	92.0
9.0	16.0	37.0	55.0	66.0	76.0	84.0	92.0
10.0	16.0	38.0	55.0	65.5	75.5	84.0	92.0
12.0	1.0	19.0	37.5	47.0	58.0	70.0	77.0
13.0	2.0	19.0	37.5	47.0	58.0	70.0	79.0
14.0	6.0	21.5	38.0	50.0	61.0	72.0	81.0
15.0	17.0	28.0	41.0	52.0	61.0	72.0	81.5
16.0	0.0	5.5	20.5	29.0	41.5	53.0	63.0
17.0	0.0	6.0	20.5	29.5	41.5	53.0	63.0
18.0	0.0	7.0	21.5	30.0	41.5	53.0	63.0
19.0	3.5	10.5	23.0	35.0	45.0	54.0	65.0
20.0	3.5	10.0	22.0	34.0	44.0	54.0	65.0
47.0	0.0	1.0	8.0	16.0	28.0	36.5	45.0
21.0	0.0	1.0	4.0	9.0	18.0	27.0	34.0
22.0	0.0	1.0	4.0	9.0	17.0	24.0	30.5
25.0	2.0	3.0	8.0	11.0	17.0	23.0	28.0 *

NFL =2, TINIT =81.0, NOMQ = 800.0, L = 1.333, TIMPTS = 8.0

TIMES	6.0	11.0	17.0	24.0	29.0	37.0	41.0	48.0
TCNO.								
0.0	9.0	16.0	29.5	47.5	56.5	74.0	86.0	102.5
50.0	25.0	37.5	51.0	67.5	79.0	95.5	101.0	110.0
75.0	32.0	47.5	61.0	76.0	85.0	97.5	103.0	111.5
95.0	37.0	54.5	67.5	80.0	87.0	99.5	105.0	114.0
1.0	18.5	45.0	60.0	75.0	83.0	94.0	101.0	112.0
3.0	34.0	48.0	60.0	75.0	83.0	94.0	101.0	112.0
4.0	34.0	48.0	60.0	75.0	82.5	94.0	101.0	112.0
5.0	33.0	48.0	60.0	74.0	82.0	94.0	101.0	112.0
6.0	9.5	29.0	53.0	69.0	77.0	90.0	97.0	109.0
7.0	21.5	38.0	53.0	69.0	77.0	90.0	97.0	109.0
8.0	21.5	38.0	53.0	69.0	77.0	90.0	97.0	109.0
9.0	21.5	38.0	53.0	69.0	77.0	90.0	97.0	109.0

10.0	21.5	38.0	53.0	69.0	77.0	90.0	97.0	109.0
12.0	2.0	15.0	28.0	42.0	55.0	68.0	78.0	89.0
13.0	2.0	15.0	28.0	42.0	55.0	68.0	78.0	89.0
14.0	6.0	20.0	31.0	47.0	57.0	71.0	79.0	93.0
15.0	18.5	27.0	37.0	52.0	60.0	73.0	80.0	94.0
16.0	2.0	3.0	10.0	20.5	32.0	44.5	56.0	66.0
17.0	2.0	3.5	12.5	24.0	34.5	47.0	56.0	66.5
18.0	2.0	3.5	12.5	24.0	35.0	47.5	56.0	66.5
19.0	3.0	5.5	16.0	28.0	35.0	50.0	57.0	70.0
20.0	2.0	5.0	15.0	27.0	34.5	49.0	56.0	69.0
47.0	1.0	1.5	3.0	10.0	18.0	27.0	34.5	44.5
21.0	0.5	1.0	1.5	5.5	11.0	18.0	23.0	29.5
22.0	0.5	1.0	1.5	5.5	11.0	18.0	23.0	28.0
25.0	0.5	1.5	2.0	5.0	11.0	18.0	22.0	28.0 *

NFL =2, TINIT =75.0, NOMQ = 150.0, L = 1.333, TIMPTS = 5.0

TIMES	9.0	23.0	43.0	68.0	85.0
TCNO.					
0.0	1.5	6.0	13.3	22.2	26.4
50.0	4.0	11.5	18.0	25.8	31.2
75.0	8.5	14.5	20.8	29.3	34.0
95.0	11.5	16.3	23.0	31.8	37.0
1.0	2.0	7.0	15.0	26.0	30.5
3.0	10.5	19.0	27.0	36.0	41.0
4.0	10.5	19.0	27.0	36.0	41.0
5.0	10.5	18.0	26.0	35.5	41.0
6.0	3.0	8.5	18.5	29.0	35.0
7.0	7.0	15.0	23.0	32.5	38.5
8.0	7.0	15.0	23.0	32.5	38.5
9.0	7.0	15.0	23.0	33.0	39.0
10.0	7.0	16.0	23.0	33.0	39.0
12.0	1.5	7.5	15.0	24.5	31.0
13.0	1.5	7.5	15.0	24.5	31.0
14.0	2.0	9.0	17.0	27.0	33.0
15.0	8.0	13.0	19.0	28.0	34.0
16.0	0.5	2.0	9.0	17.5	22.5
17.0	0.5	5.0	9.5	17.5	23.0
18.0	0.5	5.0	9.5	17.5	23.0
19.0	1.0	4.5	11.0	19.0	25.0
20.0	1.0	4.5	11.0	19.0	25.0
47.0	0.0	0.0	4.0	11.5	15.5
21.0	0.0	0.0	2.5	7.5	11.0
22.0	0.0	0.0	2.5	7.5	11.0
25.0	0.0	1.5	3.5	8.5	11.0

NFL =2, TINIT =CONT, NOMQ = 400.0, L = 1.333, TIMPTS = 5.0

TIMES ACTUAL	99.0	110.0	121.0	135.0	149.0
TIMES STEP Q	39.0	50.0	61.0	75.0	89.0
TCNO.					
0.0	33.0	42.5	52.5	69.0	92.0
50.0	45.0	54.3	56.0	83.0	97.5
75.0	53.0	62.5	73.0	87.5	98.0
95.0	57.0	65.0	75.5	89.8	99.3
1.0	45.5	64.5	76.5	88.0	97.5
3.0	54.0	66.0	76.0	87.0	97.0
4.0	54.0	66.0	76.0	87.0	97.0

5.0	53.0	65.0	75.0	86.0	96.5
6.0	40.0	59.0	71.5	85.0	95.0
7.0	49.0	62.0	73.0	85.0	95.0
8.0	49.0	62.0	73.0	85.0	95.0
9.0	49.0	62.0	73.0	85.0	95.0
10.0	49.0	62.0	73.0	85.0	95.0
12.0	37.0	48.5	59.0	73.5	84.0
13.0	37.0	48.5	59.0	73.5	84.0
14.0	41.0	51.0	62.5	75.0	88.0
15.0	45.0	53.5	64.0	76.5	89.0
16.0	29.0	37.0	45.0	59.5	71.5
17.0	29.0	38.5	47.0	60.3	72.0
18.0	29.0	38.5	47.0	60.3	72.0
19.0	33.0	41.0	51.0	62.0	75.0
20.0	32.0	40.0	50.0	61.5	74.0
47.0	21.5	29.0	35.5	47.0	57.5
21.0	14.5	22.0	27.0	34.0	41.5
22.0	14.0	20.0	25.0	33.5	38.0
25.0	15.0	21.0	26.5	33.0	41.0 *

NFL =3, TINIT = 75.0,NOMQ = 100.0, L = 0.667, TIMPTS =13.0

TIMES	7.0	16.0	32.0	59.0	88.0	121.0	153.0	181.0	213.0
TCNO.									
0.0	2.5	6.0	10.7	17.0	25.5	33.0	39.5	45.0	50.3
50.0	3.0	7.0	11.5	18.5	26.5	33.5	40.0	45.5	51.0
75.0	3.5	7.7	12.5	19.7	27.5	34.5	40.2	46.0	51.5
95.0	4.5	8.5	13.5	20.4	28.3	36.0	41.0	47.0	52.3
41.0	3.0	6.0	12.0	19.5	27.0	35.0	41.5	48.0	54.0
42.0	3.0	6.0	12.0	19.5	27.0	35.0	41.5	48.0	54.0
43.0	3.0	6.0	12.0	19.5	27.0	35.0	41.5	48.0	54.0
16.0	0.0	4.0	9.0	17.5	25.5	34.0	40.5	46.0	51.5
17.0	0.0	4.0	9.0	17.5	25.5	34.0	40.5	46.0	51.5
18.0	0.0	4.0	9.0	17.5	25.5	34.0	40.5	46.0	51.5
19.0	0.0	4.0	9.0	17.5	25.5	33.5	40.5	46.0	52.0
20.0	0.0	4.0	9.0	17.5	25.5	33.5	40.5	46.0	52.0
44.0	0.0	1.0	7.0	15.0	23.0	32.0	39.0	45.0	51.0
45.0	0.0	1.0	7.0	15.0	23.0	32.0	39.0	45.0	51.0
46.0	0.0	1.0	7.0	15.0	23.0	32.0	39.0	45.0	51.0
47.0	0.0	1.0	5.0	13.0	20.5	28.5	36.0	41.5	47.5
21.0	0.0	0.0	1.0	5.0	11.0	16.5	22.0	25.5	30.0
22.0	0.0	0.0	1.0	5.0	11.0	16.5	22.0	25.5	30.0

TIMES	245.0	272.0	301.0	329.0
TCNO.				
0.0	55.0	59.5	61.0	64.5
50.0	55.5	59.5	59.5	64.0
75.0	56.0	59.5	61.5	65.0
95.0	56.7	60.0	63.5	67.3
41.0	58.0	62.0	66.0	69.0
42.0	58.0	62.0	66.0	69.0
43.0	58.0	63.0	68.0	71.5
16.0	56.0	61.0	64.5	66.5
17.0	56.0	61.0	64.5	66.5
18.0	56.0	61.0	64.5	66.5
19.0	56.0	61.0	64.5	67.0
20.0	56.0	61.0	64.5	67.0
44.0	55.0	60.0	64.0	67.0
45.0	55.0	60.0	64.0	67.0
46.0	55.0	60.0	64.0	67.0
47.0	53.0	57.5	61.0	63.5
21.0	34.0	37.0	40.0	43.5
22.0	34.0	37.0	40.0	43.5 *

NFL =3, TINIT =76.0, NOMQ = 400.0, L = 0.667, TIMPTS =11.0

TIMES	5.0	10.0	20.0	30.0	41.0	50.0	60.0	76.0	91.0
TCNO.									
0.0	7.5	12.5	20.5	28.0	36.0	41.0	48.0	58.0	66.5
50.0	7.5	13.0	21.5	29.0	36.0	41.5	49.0	59.0	67.0
75.0	9.0	14.5	23.0	30.0	36.0	42.5	50.0	60.0	68.5
95.0	11.5	17.0	25.0	31.0	38.0	44.0	51.5	61.0	69.5
41.0	8.0	13.5	23.5	29.5	38.5	43.5	50.5	61.0	68.0
42.0	8.0	13.5	23.5	29.5	38.5	43.5	50.5	61.0	68.5
43.0	10.0	15.5	24.5	30.5	40.0	46.0	55.0	66.0	75.0
16.0	4.0	9.5	18.0	25.5	33.5	41.0	47.5	58.0	67.0
17.0	4.0	9.5	18.0	25.5	33.5	41.0	47.5	58.0	67.0
18.0	4.0	9.5	18.0	25.5	33.5	41.0	47.5	58.0	67.0

19.0	4.0	10.0	18.0	25.0	34.0	41.0	47.5	58.0	67.0
20.0	4.0	10.0	18.0	25.0	34.0	41.0	47.5	58.0	67.0
44.0	0.0	5.0	14.0	20.5	30.5	36.0	43.5	55.0	64.0
45.0	0.0	5.0	14.0	20.5	30.5	36.0	43.5	55.0	64.0
46.0	1.0	5.0	14.0	20.5	30.5	36.0	43.5	55.0	64.0
47.0	0.7	3.0	10.5	18.0	25.5	31.5	38.5	50.0	59.5
21.0	0.5	1.0	3.0	9.5	13.0	16.0	21.0	29.0	35.5
22.0	0.5	1.0	3.0	10.0	13.5	19.0	24.0	30.0	36.0

TIMES	120.0	150.0
TCNO.		
0.0	76.0	92.5
50.0	76.5	91.0
75.0	77.0	92.5
95.0	80.5	94.0
41.0	82.0	97.0
42.0	82.0	97.0
43.0	88.0	102.0
16.0	81.5	96.0
17.0	81.5	96.0
18.0	81.5	96.0
19.0	81.5	96.0
20.0	81.5	96.0
44.0	79.5	94.5
45.0	79.5	94.5
46.0	79.5	94.5
47.0	76.0	91.5
21.0	47.5	59.5
22.0	48.0	59.5 *

NFL =3, TINIT =80.5, NOMQ = 65.0, L = 1.333, TIMPTS = 6.0

TIMES	12.0	38.0	86.0	137.0	167.0	202.0
TCNO.						
1.0	3.0	7.0	13.5	18.5	22.0	25.0
2.0	3.0	7.0	13.5	18.5	22.0	25.0
3.0	3.0	7.0	13.5	18.5	22.0	25.0
4.0	3.0	7.0	13.5	18.5	22.0	25.0
5.0	3.5	7.0	13.5	18.5	22.0	25.0
6.0	2.5	7.0	13.5	18.5	22.0	25.0
7.0	2.0	7.0	13.5	18.5	22.0	25.0
8.0	2.0	7.0	13.5	18.5	22.0	25.0
9.0	2.5	7.0	13.5	18.5	22.0	25.0
10.0	2.5	7.0	13.5	18.5	22.0	25.0
12.0	0.5	5.0	11.0	17.0	21.0	24.5
13.0	0.5	5.0	11.5	17.5	21.0	24.5
14.0	1.0	5.5	12.0	18.0	21.5	25.0
15.0	1.0	5.5	12.0	18.0	21.5	25.0
16.0	0.0	3.5	9.5	15.5	19.0	22.0
17.0	0.0	3.5	9.5	15.5	19.0	22.0
18.0	0.0	3.5	9.5	15.5	19.0	22.0
19.0	0.5	4.0	10.0	16.0	19.5	23.0
20.0	0.5	4.0	10.0	16.0	19.5	23.0
21.0	0.0	2.0	6.0	10.0	12.5	14.5
22.0	0.0	2.0	6.0	10.0	12.5	14.5
23.0	0.0	2.0	6.0	10.0	12.5	14.0
24.0	0.0	2.0	6.0	10.0	12.0	14.0

25.0 0.0 2.0 6.5 11.0 12.5 15.0 *

NFL =3, TINIT =87.0, NOMQ = 125.0, L = 1.333, TIMPTS = 8.0

TIMES	32.0	56.0	92.0	122.0	154.0	182.0	214.0	247.0
TCNO.								
1.0	12.5	19.0	27.0	36.5	38.5	44.5	49.0	53.0
2.0	12.5	19.5	27.0	36.5	38.5	44.5	49.0	53.0
3.0	12.5	19.5	27.0	36.5	38.5	44.5	49.0	53.5
4.0	12.5	19.5	27.0	36.5	38.5	44.5	49.0	53.5
5.0	12.5	19.5	28.0	36.5	39.0	44.5	49.0	54.0
6.0	12.5	19.0	27.0	36.0	38.5	44.0	49.0	53.0
7.0	12.5	19.0	27.0	36.0	38.5	44.0	49.0	53.0
8.0	12.5	19.0	27.0	36.0	38.5	44.0	49.0	53.0
9.0	12.0	19.0	27.5	36.0	38.5	44.0	49.0	53.0
10.0	12.0	19.0	28.0	36.0	38.5	44.0	49.0	53.0
12.0	7.5	15.0	25.0	33.0	38.0	44.0	48.0	53.0
13.0	8.0	15.0	25.0	33.0	38.0	44.0	49.0	53.0
14.0	9.0	16.0	25.5	33.5	38.0	44.0	48.5	53.0
15.0	9.0	16.0	25.5	35.5	38.0	44.0	48.5	53.0
16.0	6.0	11.0	22.5	31.0	37.0	43.0	48.0	52.5
17.0	6.0	11.0	22.5	31.0	37.0	43.0	48.0	52.5
18.0	6.0	11.0	22.5	31.0	37.0	43.0	48.0	52.5
19.0	6.5	13.0	22.0	30.5	37.0	43.0	48.0	53.0
20.0	6.5	13.0	22.0	30.5	37.0	43.0	48.0	53.0
21.0	3.5	6.0	14.0	20.0	24.0	27.0	31.0	33.5
22.0	3.0	6.0	14.0	20.0	24.0	27.0	31.0	33.5
23.0	3.0	6.0	14.0	20.0	24.0	27.0	31.0	33.5
24.0	3.0	6.0	13.5	20.0	24.0	27.0	30.5	33.5
25.0	3.0	7.0	14.0	19.5	24.0	27.0	30.5	34.0 *

NFL =3, TINIT =81.5, NOMQ = 225.0, L = 1.333, TIMPTS = 8.0

TIMES	17.0	35.0	52.0	70.0	98.0	108.0	147.0	178.0
TCNO.								
1.0	15.0	24.0	31.0	38.5	49.0	52.0	63.5	71.5
2.0	15.0	24.0	31.0	38.0	49.0	52.0	63.5	71.5
3.0	15.0	24.0	31.0	39.0	49.0	52.3	63.5	71.5
4.0	15.0	24.0	31.0	38.5	49.0	52.5	63.5	72.0
5.0	15.0	24.0	31.0	38.5	50.0	53.5	65.0	73.0
6.0	13.5	23.0	30.5	38.0	49.5	52.5	64.0	72.0
7.0	13.5	22.5	30.5	38.0	49.0	52.3	63.5	72.0
8.0	13.5	22.5	30.5	38.0	49.0	52.0	63.5	72.0
9.0	13.0	22.5	30.5	38.0	49.0	52.0	63.5	72.0
10.0	13.0	23.0	31.0	39.0	51.0	55.0	65.0	75.0
12.0	8.5	16.5	24.5	33.0	44.5	49.5	61.5	69.5
13.0	8.5	17.0	24.5	33.5	44.5	49.5	61.5	69.5
14.0	9.0	18.5	26.0	35.0	46.0	50.5	63.0	72.0
15.0	9.0	18.5	26.0	34.5	46.0	50.5	64.0	73.0
16.0	5.5	12.5	20.0	28.5	40.0	44.5	58.0	67.5
17.0	5.5	12.5	20.0	28.5	40.0	44.5	58.0	67.5
18.0	5.5	12.5	20.0	28.5	40.0	44.5	58.0	67.5
19.0	6.0	14.0	22.0	29.5	41.5	46.0	59.0	69.5
20.0	6.0	14.0	21.5	29.0	41.0	45.5	59.0	70.0
21.0	1.5	6.0	11.0	16.0	24.0	27.0	36.0	41.0
22.0	2.0	6.0	11.0	16.0	24.0	27.0	36.0	41.0
23.0	2.0	6.5	11.0	16.0	24.0	27.0	36.0	42.0

24.0	2.0	6.0	10.5	16.0	23.5	27.0	35.5	40.5
25.0	3.0	7.0	12.0	17.0	24.5	28.0	36.0	42.5 *

NFL =3, TINIT =83.5, NOMQ = 225.0, L = 1.333, TIMPTS = 3.0

TIMES	41.0	70.0	94.0
TCNO.			
1.0	25.0	36.0	43.0
2.0	25.0	36.0	43.0
3.0	25.0	36.0	43.0
4.0	25.0	36.0	43.0
5.0	25.0	36.0	43.0
6.0	24.0	35.5	43.0
7.0	24.0	35.5	43.0
8.0	24.0	35.5	43.0
9.0	24.0	35.5	43.0
10.0	24.0	35.5	43.0
12.0	18.0	31.5	40.5
13.0	19.0	31.5	40.5
14.0	20.0	32.0	42.0
15.0	20.0	32.0	42.0
16.0	16.0	27.0	37.5
17.0	16.0	27.0	37.5
18.0	16.0	27.5	37.5
19.0	16.5	29.0	38.0
20.0	16.5	28.0	38.0
21.0	9.5	16.5	23.0
22.0	9.0	16.5	23.0
23.0	9.0	16.5	23.0
24.0	9.0	16.5	23.0
25.0	10.0	17.0	23.0 *

NFL =3, TINIT =82.0, NOMQ = 225.0, L = 1.333, TIMPTS = 8.0

TIMES	11.0	29.0	45.0	59.0	77.0	93.0	121.0	138.0
TCNO.								
1.0	9.0	19.0	26.0	32.0	39.0	45.5	55.0	61.0
3.0	11.0	20.5	27.5	33.5	40.5	45.0	55.0	63.0
4.0	10.0	20.0	28.0	33.0	41.0	45.0	56.0	63.0
5.0	12.5	20.0	27.5	33.0	41.0	45.0	55.5	63.0
6.0	9.0	19.0	26.0	32.0	40.0	45.0	55.5	62.0
7.0	9.0	18.0	26.5	32.0	40.0	45.0	55.5	62.0
8.0	8.0	18.0	26.0	32.0	40.0	45.0	55.5	62.0
9.0	8.0	18.0	26.0	32.0	40.0	45.0	55.5	62.0
10.0	9.0	18.0	26.0	32.0	40.0	45.0	55.0	62.0
12.0	5.0	15.0	21.5	29.0	36.0	41.0	51.0	58.0
13.0	5.0	15.0	21.5	29.0	36.0	41.0	51.0	58.0
14.0	6.0	15.5	22.5	29.5	37.0	43.5	54.0	61.0
15.0	6.0	15.5	22.5	29.5	37.0	43.5	54.0	61.0
16.0	3.0	11.0	18.0	25.0	32.0	37.5	47.5	54.0
17.0	3.0	11.0	18.0	25.0	32.0	37.5	47.5	54.0
18.0	3.0	11.0	18.0	25.0	32.0	37.5	47.5	54.0
19.0	4.5	12.5	19.5	25.5	33.5	40.0	51.0	58.0
20.0	4.5	12.5	19.5	25.5	33.5	40.0	51.0	58.0
47.0	1.5	6.0	13.5	19.5	27.0	36.5	41.0	47.0
21.0	0.5	5.0	7.5	13.0	18.0	26.0	28.0	32.0
22.0	0.5	5.0	7.5	13.5	18.5	26.5	30.0	34.5

25.0	2.0	6.0	10.0	14.0	19.0	23.0	30.0	34.0 *

NFL =3, TINIT =86.0, NOMQ = 400.0, L = 1.333, TIMPTS = 7.0

TIMES	2.0	15.0	31.0	50.0	60.0	69.0	76.0
TCNO.							
1.0	2.0	18.0	31.5	43.5	51.0	56.0	60.0
3.0	2.0	20.0	31.5	45.0	52.0	57.0	62.0
4.0	2.0	19.5	31.0	44.5	52.0	57.0	62.0
5.0	2.0	19.0	31.0	44.5	52.0	57.0	62.0
6.0	1.5	17.5	30.0	43.5	50.5	56.5	61.5
7.0	1.5	17.0	29.0	43.5	50.0	56.0	61.0
8.0	1.5	17.0	29.0	43.5	50.0	55.5	60.0
9.0	1.5	16.5	29.0	43.5	49.5	55.0	59.5
10.0	1.5	16.3	29.0	43.5	50.5	57.0	62.0
12.0	1.0	11.0	24.0	37.5	45.0	49.5	55.0
13.0	1.0	11.0	24.0	37.5	45.0	49.5	55.0
14.0	1.5	12.5	25.0	40.0	47.0	53.0	58.0
15.0	1.5	12.5	25.0	40.0	47.0	53.0	58.0
16.0	0.5	8.0	21.5	32.0	38.0	44.0	49.0
17.0	0.5	8.0	21.5	32.0	38.0	44.0	49.0
18.0	0.5	8.0	21.5	32.0	38.0	44.0	49.0
19.0	0.5	9.5	20.0	33.5	40.5	46.5	51.5
20.0	0.5	9.5	20.0	33.5	40.5	46.5	51.5
47.0	0.0	5.0	14.5	27.0	32.5	37.0	41.0
21.0	0.0	2.0	9.0	15.5	21.0	25.0	27.5
22.0	0.0	2.5	9.0	17.5	22.0	26.0	30.0
25.0	0.5	4.5	9.0	17.0	20.5	25.0	28.0 *

NFL =3, TINIT =82.5, NOMQ = 800.0, L = 1.333, TIMPTS = 6.0

TIMES	2.0	10.0	17.0	23.0	31.0	37.0
TCNO.						
0.0	12.5	28.0	39.0	48.0	59.0	66.5
1.0	6.5	26.0	38.5	48.0	58.0	65.0
3.0	5.5	26.0	40.5	47.5	58.5	66.0
4.0	5.5	25.5	38.5	47.0	58.0	65.0
5.0	4.0	25.5	38.5	47.0	60.0	68.5
6.0	4.0	22.0	35.5	45.0	56.5	63.5
7.0	4.0	22.0	35.5	45.0	56.5	64.0
8.0	4.0	22.5	36.0	45.5	56.5	63.5
9.0	4.0	22.5	36.0	45.5	57.0	64.0
10.0	4.0	22.0	35.0	45.0	58.0	67.0
12.0	0.5	15.5	25.5	36.5	46.5	55.5
13.0	0.5	15.5	25.5	36.5	46.5	55.5
14.0	0.5	15.5	28.5	38.5	50.5	58.0
15.0	0.5	16.0	28.5	38.0	49.5	57.0
16.0	0.0	8.5	18.5	27.5	37.0	45.5
17.0	0.0	8.5	18.5	27.5	37.0	45.5
18.0	0.0	8.5	18.5	27.5	37.0	45.5
19.0	0.0	9.5	20.0	29.0	40.0	47.5
20.0	0.0	9.0	19.5	28.5	39.5	47.0
47.0	0.0	5.0	14.0	21.0	29.0	37.0
21.0	0.0	2.0	8.0	11.0	19.0	21.5
22.0	0.0	2.0	8.0	13.5	19.5	23.0
25.0	0.0	3.0	7.5	12.5	19.0	23.0 *

NFL =3, TINIT =75.0, NOMW =1000.0, L = 1.333, TIMPTS =10.0

TIMES	3.0	7.0	12.0	17.0	21.0	27.0	34.0	41.0	47.0
TCNO.									
0.0	10.0	24.0	38.0	48.0	53.5	64.0	77.0	87.5	96.5
50.0	12.0	28.0	40.0	49.5	56.5	66.0	77.0	87.5	97.0
75.0	18.0	32.0	43.0	52.0	59.0	66.0	77.5	87.5	97.0
95.0	21.0	35.0	44.0	53.5	60.5	70.5	79.5	89.5	98.5
1.0	14.0	31.0	41.5	50.0	58.0	69.0	80.0	91.0	98.0
4.0	15.0	32.0	41.5	51.0	59.0	71.0	81.0	91.0	98.0
5.0	16.0	32.0	42.0	55.0	67.0	80.0	93.0	103.0	109.0
6.0	8.0	28.0	37.0	50.0	57.0	68.0	80.0	92.0	99.5
7.0	8.0	24.0	35.0	48.0	56.0	66.0	79.0	88.0	96.0
9.0	9.0	24.0	35.0	48.0	56.5	67.0	78.0	89.0	97.0
12.0	0.0	11.0	22.0	32.5	41.5	52.0	64.0	76.0	87.5
13.0	0.0	11.0	22.0	32.5	41.5	52.0	64.0	76.0	87.5
15.0	1.0	11.0	25.0	35.0	43.0	56.0	71.0	83.0	98.0
41.0	0.0	10.0	19.0	28.0	39.0	48.0	58.0	73.0	83.0
42.0	0.0	10.0	19.0	28.0	39.0	48.0	58.0	73.0	83.0
16.0	0.0	3.5	15.0	23.0	29.5	39.0	52.0	65.0	75.0
17.0	0.0	3.5	15.0	23.0	29.5	39.0	52.0	65.0	75.0
18.0	0.0	3.5	15.0	23.0	29.5	39.0	52.0	65.0	75.0
19.0	0.0	4.0	15.0	23.0	30.0	40.0	54.0	66.0	77.0
20.0	0.0	4.0	15.0	24.0	30.0	40.0	54.0	66.0	77.0
44.0	0.0	4.0	12.0	19.0	27.0	37.0	49.0	61.0	70.0
45.0	0.0	4.0	12.0	19.0	27.0	37.0	49.0	61.0	70.0
46.0	0.0	4.0	12.0	19.0	27.0	37.0	49.0	61.0	70.0
47.0	0.0	1.0	6.0	12.0	20.0	28.5	40.0	51.5	62.5
21.0	0.0	0.0	2.5	5.0	7.5	13.0	21.0	28.0	35.0
22.0	0.0	0.0	2.5	5.0	7.5	13.0	21.0	28.0	35.0

TIMES	53.0
TCNO.	
0.0	104.0
50.0	104.0
75.0	104.5
95.0	106.5
1.0	106.5
4.0	106.5
5.0	118.0
6.0	107.0
7.0	104.0
9.0	105.0
12.0	96.5
13.0	96.5
15.0	106.0
41.0	93.0
42.0	93.0
16.0	85.0
17.0	85.0
18.0	85.0
19.0	86.0
20.0	86.0
44.0	80.0
45.0	80.0
46.0	80.0
47.0	70.5

21.0 40.0
22.0 40.0 *

NFL =3, TINIT =75.0, NOMQ =1650.0, L = 1.333, TIMPTS = 7.0

TIMES	3.0	7.0	11.0	16.0	22.0	27.0	32.0
TCNO.							
0.0	8.5	39.0	53.0	71.0	89.0	103.0	117.5
50.0	12.0	41.0	56.0	74.0	91.5	105.0	120.0
75.0	17.0	43.0	59.0	75.0	93.0	108.0	121.0
95.0	22.0	46.0	62.5	78.0	96.0	109.0	122.0
1.0	6.0	24.0	40.0	52.0	73.0	88.0	103.0
4.0	20.0	37.0	49.0	61.0	79.0	92.0	106.0
5.0	22.0	38.0	55.0	77.0	97.0	109.0	119.0
6.0	23.0	37.0	54.0	75.0	95.0	107.0	118.0
7.0	6.0	19.0	36.0	47.0	70.0	85.0	103.0
9.0	8.0	19.0	36.0	48.0	71.0	86.0	103.0
12.0	2.0	19.0	33.0	49.0	69.0	85.5	103.0
13.0	2.0	19.0	33.0	49.0	69.0	85.5	103.0
15.0	5.0	22.0	39.0	51.0	73.0	88.0	103.0
41.0	2.0	17.0	33.0	45.0	63.0	79.0	94.0
42.0	2.0	16.0	32.0	44.0	62.0	79.0	94.0
43.0	7.0	25.0	33.0	45.0	63.0	79.0	95.0
16.0	1.0	8.0	22.5	35.5	54.0	67.0	85.0
17.0	1.0	8.0	22.5	35.5	54.0	67.0	85.0
18.0	1.0	8.0	22.5	35.5	54.0	67.0	85.0
19.0	0.0	9.0	22.5	36.0	56.0	68.0	86.0
20.0	0.0	9.0	22.5	36.0	56.0	68.0	86.0
44.0	0.0	8.0	21.5	31.0	49.0	62.5	78.0
45.0	0.0	8.0	21.5	31.0	49.0	62.5	78.0
46.0	0.0	8.0	21.5	31.0	49.0	62.5	78.0
47.0	0.0	3.5	12.0	23.0	37.5	51.5	67.0
21.0	0.0	2.0	3.5	9.5	16.5	25.0	34.0
22.0	0.0	2.0	3.5	9.5	16.5	25.0	34.0 *

NFL =3, TINIT =77.0, NOMQ = 160.0, L = 1.960, TIMPTS.=11.0

TIMES	6.0	16.0	30.0	47.0	63.0	89.0	120.0	150.0	181.0
TCNO.									
0.0	9.0	15.5	22.5	30.0	34.5	43.5	51.5	60.0	67.5
95.0	11.0	17.5	24.0	31.0	36.0	44.5	52.5	61.5	69.0
31.0	8.5	13.0	19.5	26.0	32.0	40.0	49.0	56.5	66.0
32.0	9.0	14.0	20.5	27.0	32.0	41.0	49.5	57.5	66.5
33.0	11.5	15.5	23.0	29.0	34.5	42.5	52.0	60.0	68.0
34.0	6.0	13.0	18.0	23.5	29.0	36.5	47.0	56.0	65.0
36.0	10.0	16.5	22.5	28.5	34.0	43.5	53.0	63.0	73.0
1.0	4.0	8.0	12.0	18.0	23.0	31.0	41.0	50.0	60.0
3.0	3.5	8.0	13.0	19.5	24.0	31.0	41.0	50.0	60.0
4.0	3.5	8.0	13.0	19.5	23.0	31.0	41.0	50.0	60.0
5.0	3.5	8.0	13.0	19.0	23.0	31.0	41.0	50.0	60.0
6.0	3.0	7.0	11.5	17.0	21.0	30.0	39.0	48.0	56.0
12.0	2.0	4.0	9.5	14.0	19.5	26.5	36.0	45.0	53.0
13.0	2.0	4.5	9.5	14.5	19.5	26.5	36.0	45.0	53.0
15.0	6.0	9.5	13.5	18.0	21.5	28.5	38.0	47.0	56.0
16.0	2.0	3.5	7.5	12.0	16.5	23.5	32.0	41.0	50.5
17.0	2.0	3.5	7.5	12.0	16.5	23.5	32.0	41.0	50.5
18.0	1.5	3.5	7.5	12.0	16.5	23.5	32.0	41.0	50.5

19.0	1.5	4.0	7.8	12.5	16.5	23.5	32.0	41.0	50.0
20.0	1.5	4.0	7.8	12.5	16.5	23.5	32.0	41.0	50.0
47.0	0.0	1.5	4.5	9.5	13.0	19.5	27.0	34.5	42.5
21.0	0.0	1.0	2.5	6.0	8.5	12.5	18.5	23.0	28.5
22.0	0.0	1.0	2.5	6.0	8.5	12.5	18.5	23.0	28.5

TIMES	210.0	240.0
TCNO.		
0.0	73.5	78.5
95.0	75.0	80.0
31.0	71.0	77.5
32.0	72.0	78.5
33.0	75.5	82.0
34.0	72.0	79.0
36.0	81.0	85.5
1.0	67.5	76.0
3.0	67.5	76.0
4.0	67.5	76.0
5.0	67.5	76.0
6.0	65.5	73.0
12.0	62.5	69.5
13.0	62.5	69.5
15.0	66.0	74.0
16.0	57.5	66.0
17.0	57.5	66.0
18.0	57.5	66.0
19.0	58.0	66.0
20.0	58.0	66.0
47.0	49.0	55.5
21.0	32.0	36.5
22.0	32.0	36.5 *

NFL =3, TINIT =81.0, NOMQ = 450.0, L = 1.960, TIMPTS = 9.0

TIMES	6.0	11.0	21.0	31.0	46.0	61.0	76.0	91.0	105.0
TCNO.									
0.0	6.0	13.0	34.0	47.0	60.5	74.5	85.5	96.0	105.0
95.0	7.0	16.0	37.0	48.0	62.0	78.0	88.0	97.5	106.0
31.0	9.5	18.0	29.0	38.0	53.0	66.0	79.5	91.0	101.5
32.0	9.5	18.0	29.0	38.0	54.0	68.0	81.0	93.0	103.5
33.0	13.0	20.0	31.0	41.0	56.0	70.0	82.0	94.0	104.0
34.0	10.0	15.5	25.0	32.0	48.0	62.5	76.5	90.0	101.5
36.0	13.0	20.0	29.0	36.5	55.0	64.0	80.0	92.5	105.0
1.0	7.0	12.0	19.0	25.0	39.0	51.0	66.5	77.5	90.0
3.0	5.5	11.0	18.5	25.0	36.0	53.0	68.0	82.0	93.0
4.0	4.5	10.0	18.5	25.0	36.0	53.0	68.0	82.0	93.0
5.0	2.5	8.0	16.0	22.0	35.0	47.0	61.0	74.0	85.0
6.0	1.5	7.0	14.0	21.0	34.0	46.0	58.0	72.0	83.0
12.0	0.5	5.5	12.0	19.5	32.0	43.0	56.0	68.0	78.5
13.0	0.5	5.5	12.0	19.5	32.0	43.0	56.0	68.0	78.5
15.0	4.0	8.5	16.0	23.0	36.0	47.0	61.0	74.0	86.0
16.0	0.5	3.0	8.0	15.0	26.5	37.0	49.5	60.5	71.5
17.0	0.5	3.0	8.0	15.0	26.5	37.0	49.5	60.5	71.5
18.0	0.5	3.0	8.0	15.0	26.5	37.0	49.5	60.5	71.5
19.0	1.0	4.0	9.0	16.0	27.0	39.0	52.5	63.0	74.0
20.0	1.0	4.0	9.0	16.0	27.0	39.0	52.5	63.0	74.0
47.0	0.0	1.0	5.5	11.5	20.5	31.5	42.0	52.5	61.5

21.0	0.0	0.0	1.5	5.0	12.0	19.0	26.0	34.0	40.0
22.0	0.0	0.0	1.5	5.0	12.0	19.0	26.0	34.0	40.0 *

D. Sample Calculations

The procedures used for data analysis can best be presented by showing a typical detailed computation for a specific test. A test, designated E-II-7CV, was arbitrarily selected for this purpose.

General test conditions are described by the designation:

Fluid (E)	85% by weight glycerin and water
Aspect ratio (II)	L/D = 2.17
Wall heat flux (7)	Nominal current through resistive coating on outer wall was 7 amps.
Operational mode (C)	Power level was increased during course of run in an attempt to maintain constant heat flux to the fluid
Surface condition (V)	A thin film of stearic acid was present on the liquid surface to prevent excessive vaporization of water.

Before considering the data from this test, some general observations about the system are pertinent.

1. System Geometry: The enclosure was a vertical cylinder

outer diameter	8 in.
wall thickness	$\frac{5}{16}$ in.
inner diameter	$7\frac{3}{8}$ in.
liquid depth	16 in.
enclosure volume filled with liquid	0.4 ft.^{3} (3.0 gal.)
outer wall surface area (heated section)	2.8 ft.^{2}

inner wall surface area

(heated section) 2.6 ft.^{2}

Heat Capacity of system:

a. Walls

Data for Pyrex 7740

$\rho = 139$ lb/ft^3

$C_p = 0.2$ BTU/lb°F

$$\frac{\text{Wall heat capacity}}{\text{unit surface area}} = \frac{Q_w}{A_w \Delta T} = \rho C_p (\text{wall thickness})$$

$$\frac{Q_w}{A}\frac{1}{\Delta T} = 139(0.2)\left(\frac{5}{16 \times 12}\right) = 0.725 \frac{\text{BTU}}{\text{ft}^2\ °\text{F}}$$

b. End flange and gasket

Flange: $\frac{1}{4}$-in. thick steel, 11 in. diameter

Gasket: $\frac{1}{8}$-in. thick silicone rubber, 11 in. diameter

Data:	Steel	Silicone Rubber
ρ	500 lb/ft^3	80 lb/ft^3
C_p	0.11 BTU/lb°F	0.2 BTU/lb°F

End flange and gasket heat capacity =

$$\frac{\pi D_f^2}{4}\left\{\left[\rho C_p(\text{thickness})\right]_{\text{steel}} + \left[\rho C_p(\text{thickness})\right]_{\substack{\text{silicone}\\\text{rubber}}}\right\}$$

$$\frac{Q_{end}}{\Delta T} = \frac{\pi}{4}\left(\frac{11}{12}\right)^2\left[(500)(0.11)\left(\frac{1}{48}\right) + (80)(0.2)\left(\frac{1}{96}\right)\right]$$

$$\frac{Q_{end}}{\Delta T} = 0.865 \frac{\text{BTU}}{°\text{F}}$$

c. Fluid heat capacity

$$(\rho C_p)_{\substack{85\% \\ \text{glycerin}}} \sim 48.0 \frac{BTU}{ft^3\ ^\circ F}$$

In the temperature range from 70°F to 150°F, the value of (ρC_p) ranges from 47.0 to 49.0.

$$\frac{Q_{fluid}}{\Delta T} = \frac{\pi D^2}{4} L \rho C_p$$

$$\frac{Q_{fluid}}{\Delta T} = \frac{\pi}{4}\left(\frac{7.375}{12}\right)^2\left(\frac{16}{12}\right)(48) = 19.0 \frac{BTU}{^\circ F}$$

d. Ratio of enclosure heat capacity to fluid heat capacity

Enclosure heat capacity = walls and end

Enclosure $\frac{Q}{\Delta T} = 0.725(2.7) + 0.865$

$= 2.83$ BTU/°F

Fluid: $\frac{Q}{\Delta T} = 19.0$ BTU/°F

For a given temperature increase:

$$\frac{Q_{enclosure}}{Q_{enclosure + fluid}} = \frac{2.83}{21.8} = 0.13 \quad \text{(13\% loss to enclosure)}$$

2. Other system heat losses:

a. To air outside cylinder

Heat transfer is by natural convection and the formula given by McAdams (54) for heat transfer to air outside heated vertical cylinders may be used.

$$h_o = 0.29 \left(\frac{\Delta T_o}{L}\right)^{1/4}$$

where L = height of cylinder (ft)

T_o = outer wall temperature--ambient temperature

For a test with a 16-in. heated vertical cylindrical section:

$$\frac{Q}{A}_o = 0.29\left(\frac{1}{1.33}\right)^{1/4} \Delta T_o^{5/4} = 0.27 \Delta T_o^{5/4}$$

Since the heat flux of interest is that at the inner wall, all heat flux values are based on the inside wall area.

$$\left(\frac{Q}{A_i}\right)_{ambient} = 0.27\ \Delta T_o^{5/4} \left(\frac{2.8}{2.6}\right)$$

$$= 0.29\ \Delta T_o^{5/4} \quad \frac{BTU}{ft^2}$$

In order to estimate the ambient heat loss, the outer wall temperature of the enclosure must be known. Because of the constant wall heat flux boundary condition, a vertical temperature distribution in the wall existed. Sparrow and Gregg (98) have shown that use of a midpoint temperature in constant wall temperature natural convection correlations for heated vertical plates closely approximates the results of a constant wall heat flux analysis in prediction of heat transfer coefficients. Consequently, the outside wall temperature was assumed constant and equal to the average fluid temperature (which has been found to be nearly equal to the vertical midpoint fluid temperature) plus the temperature differential across the wall.

$$\Delta T_{wall} = \left(\frac{Q}{A}\right)_{fluid} \frac{(\text{wall thickness})}{k_{wall}}$$

Data: $k = 0.65 \frac{BTU}{hr\ ft\ ^oF}$ Pyrex #7740

$$\Delta T_{wall} = \left(\frac{Q}{A}\right)_{fluid} \cdot \frac{5}{12 \times 16} \quad \frac{1}{(0.65)}$$

$$\Delta T_{wall} = 0.04 \left(\frac{Q}{A}\right)_{fluid} \quad ^{o}F$$

Therefore $$\Delta T_{o} = \Delta T^{*} + 0.04 \left(\frac{Q}{A}\right)_{fluid}$$

ΔT^{*} = average fluid temperature increase

b. Initial heating of enclosure wall

Before full heat transfer to the fluid can occur, the necessary temperature differential across the wall must be established. This differential was computed in the preceding analysis. Assuming a linear wall temperature gradient, the average wall temperature is just one-half of the over-all gradient.

Initial wall heating = (total wall heat capacity) x (0.5) x (ΔT_{wall})

$$\text{Initial wall heating} = (0.725 \times 2.7)(0.5)(0.04)\left(\frac{Q}{A}\right)_{fluid}$$

$$= 0.0392 \left(\frac{Q}{A}\right)_{fluid} \quad \text{BTU}$$

The time required to establish the initial wall gradient may be estimated if $\left(\frac{Q}{A}\right)_{fluid}$ is assumed constant

$$t_{\substack{\text{initial} \\ \text{wall heating}}} \gtrsim \frac{0.0392 \left(\frac{Q}{A}\right)_{fluid}}{\left(\frac{Q}{A}\right)_{fluid} A}$$

$$t_{\substack{\text{initial} \\ \text{wall heating}}} \gtrsim \frac{0.0392}{2.7} = .0145 \text{ hr} = 0.87 \text{ min.}$$

c. Vaporization of fluid from liquid surface

For a test in which the liquid depth is 16 in., the volume of the vapor space over the liquid is 0.2 ft^3. The volume is enclosed although not sealed. Openings in the upper flange were packed with woven asbestos tape to permit gradual release of vapor and prevent internal pressure build-up. If it is assumed that saturation pressure is maintained in the vapor as the liquid is warmed, and that no condensation occurs on the walls, then the energy loss by vaporization may be estimated.

Data: Fluid	T °F	saturation P(mm. Hg)	specific Volume of Vapor ft^3/lb
Water	70°	18.8	868
	170°	311	62
Glycerin	70°	2×10^{-4}	
	170°	3.3×10^{-2}	
	270°	2	2100

Because of the very low vapor pressure of glycerin throughout the range of temperatures which were investigated, the effects of glycerin vaporization are negligible in comparison to those for water. An estimate of the mass of water vaporized in the vapor space of the enclosure when the liquid is heated from room temperature to about 170°F is (assuming initial vapor concentration is negligible):

$$\text{Mass water vaporized} = \frac{311}{760} \times 0.2 \times \frac{1}{62} = 0.0013 \text{ lbs.}$$

The latent heat of vaporization at 170°F is 996 BTU/lb for water, so

$$(\text{Energy loss})_{170^\circ} \backsim 1.3 \text{ BTU}$$

The energy required to heat the bulk liquid by 100°F is:

$$Q_{liquid} \backsim \rho C_p \left(\frac{\pi}{4} D^2 L\right) \Delta T$$

$$Q_{liquid} \backsim 48\ (0.4)(100) = 1920\ \text{BTU}$$

The fraction of energy lost by vaporization is negligible <u>if</u> no condensation occurs in the vapor space. Condensation was observed in initial tests with water, so a surface film of stearic acid was used to reduce surface vaporization. Condensation was not observed when the surface film was present.

In the few tests in which condensation occurred, only a rough estimate of the amount of condensate was possible. The actual surface loss could have been increased by as much as a factor of 100. Although this still would have been only 5% of the total energy input, obviously the energy loss occurs from the surface regions only and the behavior of the surface fluid could be severely affected by this loss.

d. <u>Heat loss by conduction to unheated portion of wall</u>

An approximate estimate of the magnitude of wall conduction losses was made by assuming the wall was an 8 in. long fin, $\frac{5}{16}$ -in. thick, and 8π in. wide with a constant heat transfer coefficient to air on both sides.

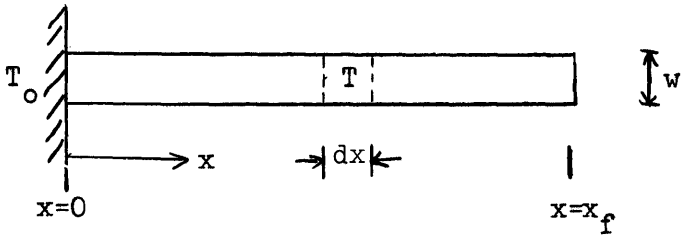

Let $\theta_o = T_o - T_a$ $\qquad\qquad$ $\theta = T - T_a$

where T_a = ambient temperature

The conduction equation is

$$\frac{d^2\theta}{dx^2} - \left(\frac{2h}{kw}\right)\theta = 0$$

and the solution is

$$\frac{\theta}{\theta_o} = \frac{\cosh\left[\left(\frac{2h}{kw}\right)(x_f - x)\right]}{\cosh\left[\left(\frac{2h}{kw}\right)x_f\right]}$$

The mean temperature for heat loss to ambient is described by

$$\frac{\theta_m}{\theta_o} = \frac{\tanh\left[\left(\frac{2h}{kw}\right)x_f\right]}{\left(\frac{2h}{kw}\right)x_f}$$

For typical values of:

$$(T_o - T_a) = \theta_o = 50^\circ F$$

$$k = 0.65 \frac{BTU}{hr\ ft\ ^\circ F} \qquad \text{Pyrex} \qquad 7740$$

$$w = \frac{5}{16}\text{-in.}$$

$$h_o = 0.29\ \theta_m^{1/4}$$

Then $\left(\frac{2h}{kw}\right) = \frac{2(.29)(16)(12)}{(.65)(5)}\ \theta_m^{1/4} = 34\ \theta_m^{1/4}$

By trial and error, assume $\theta_m = 1^\circ F$

$$\text{then } \frac{\theta_m}{\theta_o} = \frac{\tanh\left[(34)\left(\frac{8}{12}\right)\right]}{(34)\left(\frac{8}{12}\right)} = \frac{1}{34\ \left(\frac{8}{12}\right)}$$

$$\frac{\theta_m}{\theta_o} = .044$$

Or $\theta_m = 2.2°F.$

Since the correct value of θ_m would lie between 1.0 and 2.2°F, an approximate estimate of the energy loss can be made by assuming a 2°F heat-up of the fin for a 50°F heat-up at its base. This amount turns out to be about 1 BTU which is negligible relative to total energy input to the main heated section. The energy loss from the fin to the surrounding air is also negligible.

3. Energy flux to fluid

The reduced temperature data, as presented in Appendix C, are used to compute the average fluid temperature, which can then be used to estimate the average heat flux to the fluid during a specified time interval. In Figure 8-3 temperature profiles are plotted for three time points during the test: 17, 24, and 29 min. Radial temperature variations are neglected and an arithmetic average of radial temperatures is used at each data level. The validity of this procedure is indicated by the dotted and dashed lines shown which represent the center line and outer core temperatures respectively at 29 min. The area under each profile was measured using a planimeter. If the volumetric heat capacity of the liquid is assumed constant, then the measured area is proportional to the energy added to the fluid since the beginning of the test.

As a basis, consider a square (Fig. 8-3) representing a uniform 50°F increase in liquid temperature. The energy represented for an 85% glycerin test with L = 16 in. is:

FIGURE 8-3
AXIAL TEMPERATURE PROFILES

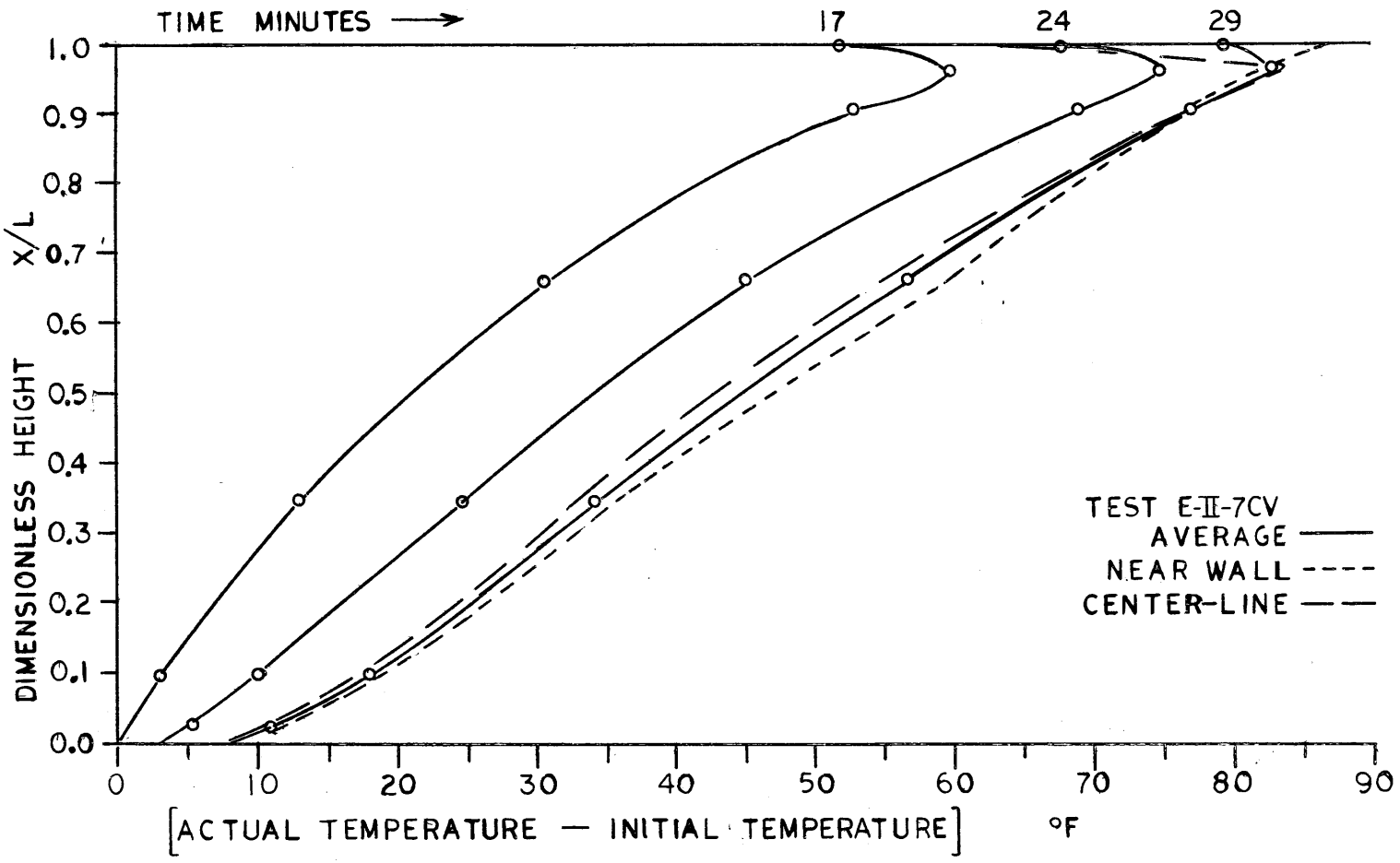

$$Q = \frac{\pi D^2}{4} L \rho C_p \Delta T$$

$$= (0.4)(48)(50) = 960 \text{ BTU}$$

The area of the square equivalent to this energy input, as measured from the original set of profile graphs was 15.6 in^2.

Therefore each square inch of area under the profile represented 61.5 BTU of energy input. On the basis of the inside wall area, this is equivalent to an average wall energy input of:

$$\overline{\left(\frac{Q}{A}\right)}_{t\ \text{fluid}} = \frac{61.5}{2.6} \quad \text{(planimeter measurement)}$$

$$= 23.7 \quad \text{(planimeter measurement)} \ \frac{\text{BTU}}{ft^2}$$

By subtracting the total energy at a given time from the total energy at the next recorded time, a net increase in energy during the time interval can be found and converted to an average heat flux value. This heat flux is assumed to be the actual heat flux at the midpoint of the time interval (Another procedure was to plot the total energy as a function of time and graphically find the slope of the energy curve at the time points of interest. The values computed in both manners agreed quite well (2 to 5% error), but only the incremental method is presented here for simplicity)

From Run E-II-7CV

t Time (min.)	Measured Area under curve (in^2)	$\int_0^t \left(\frac{Q}{A}\right)dt$ (BTU/ft^2)	$\Delta\left[\int_0^t \left(\frac{Q}{A}\right)dt\right]$ (BTU/ft^2)	Δt (min.)	$\bar{t}$ average time (min.)	average $\frac{Q}{A}$ $\frac{BTU}{hr\ ft^2}$
17	7.63	181	95	7	20.5	812
24	11.64	276	67	5	26.5	805
29	14.47	343				

The values of $\frac{Q}{A}$ were plotted versus time using the $\bar{t}$ values. The values for $(\frac{Q}{A})$ at the particular times of interest, e.g. 17, 24 and 29 minutes in the above example since data were obtained at these times, were then read off the curve drawn through these points.

4. Electrical Energy Input

Two sections of the system were heated in test E-II-7CV. The power was increased during the test to compensate for increased losses to the surroundings. The voltages below are the sum of the voltage drops across each of the two sections.

Time (min.)	Current (amps)	Voltage (volts)	Power (watts)
0-10	7.0	112	785
10-20	7.3	117	854
20-35	7.4	118.5	876
35-50	7.6	122.5	930

Note that the resistance of each section was measured to be 8 ohms. The above values agree well with a two-section series resistance of 16 ohms.

Following the convention of basing all heat flux values on the inside wall area of 2.6 ft^2 and noting that 3.413 BTU/hr = 1 watt:

$$\left(\frac{Q}{A}\right)_{\substack{\text{elect}\\ \text{input}}} = (\text{watts})\,\frac{3.413}{2.6}\quad\frac{\text{BTU}}{\text{hr ft}^2}$$

t min	$\left(\frac{Q}{A}\right)_{\text{elect. input}}$ BTU/hr ft^2
0-10	1030
10-20	1120
20-35	1150
35-50	1220

5. Average Bulk Fluid Temperature

Using the value to total energy input to the fluid computed in part 3, the average temperature rise of the fluid can be estimated.

$$\Delta T^* = \frac{A_i \int_o^t \frac{Q}{A}\, dt}{(\text{Vol})\, \rho\, c_p} = \frac{2.6}{(0.4)(48)} \int_o^t \frac{Q}{A}\, dt$$

For the typical test, E-II-7CV, which had an initial temperature of 81°F:

time min	$\int_o^t \frac{Q}{A}\, dt$ BTU/ft^2	ΔT^* °F	$T^* = T_i + \Delta T^*$ °F
17	181	24.5	105.5
24	276	37.4	118.4
29	343	46.4	127.5

The temperature, T^*, is used as a basis for computing all physical properties of the liquid at a particular time.

6. Over-all Energy Balance

Figure 8-4 presents the results of an energy balance for E-II-7CV. The electrical energy flux should equal the sum of the energy input to the fluid, the losses to the surroundings and the losses in heating the enclosure. The agreement is within less than 3%. Energy balances for other runs are presented in Appendix F.

7. Computation of Normalized Temperature Rise

The values of temperature at $\frac{X}{L}$ = 0.9, 0.7, 0.5, 0.3, and 0.1 are read from the profiles in Figure 8-3 and are normalized by dividing by ΔT^*.

At t = 24 min.:

$\frac{X}{L}$	ΔT	$\frac{\Delta T}{\Delta T^*}$
.9	68.5	1.83
.7	48.0	1.285
.5	34.7	0.93
.3	22.0	0.59
.1	10.0	0.27

These values were plotted against a dimensionless time parameter as in Figure 4-13 in Section IV to give an idea of the temperature distribution within the fluid.

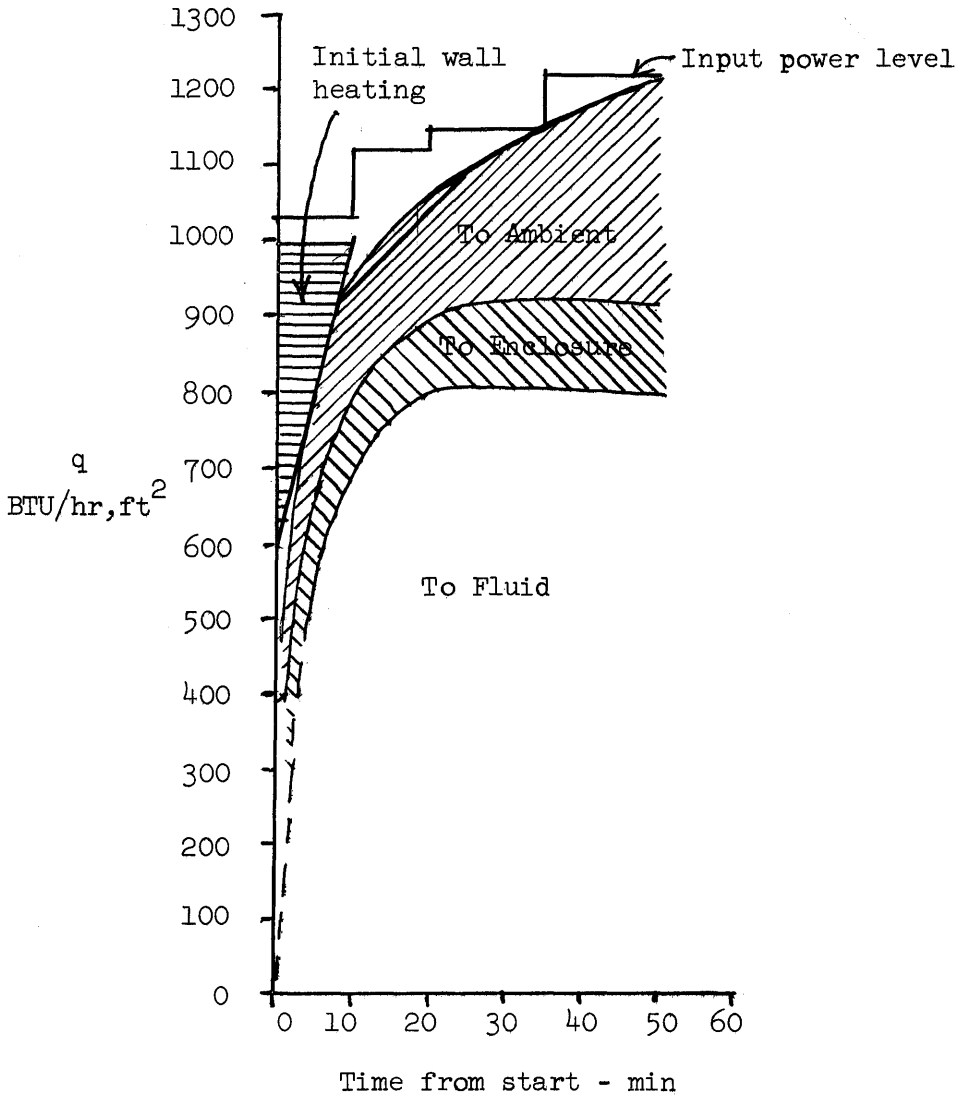

FIGURE 8-4

Energy Balance

Test E-2-7CV

85% glycerine, L = 1.33 ft, T_i = 81°F, q_w = 800 BTU/hr,ft^2 (nominal)

8. Computation of Core Temperature Gradient

The core temperature gradient is defined as

$$\frac{d\theta_\infty}{dX} = \frac{k}{q}\frac{dT}{dx}$$

or in terms of actual data

$$\frac{d\theta_\infty}{dX} = \frac{k}{\left(\frac{Q}{A}\right)} \frac{(\Delta T_{.9} - \Delta T_{.1})}{(.8)L}$$

Again at 24 minutes in E-II-7CV, at $T^* = 118.4^\circ F$,

$k = 0.179 \frac{BTU}{hr\ ft\ ^\circ F}$, $\left(\frac{Q}{A}\right) \backsim 800 \frac{BTU}{hr\ ft^2}$, $\left[\Delta T_{.9} - \Delta T_{.1}\right] = 58.5^\circ F$

and $L = 1.33$ ft.

$$\frac{d\theta_\infty}{dX} = \frac{(.179)}{(800)} \frac{(58.5)}{(.8)(1.33)} = 0.0123$$

9. Computation of dimensionless parameters

Fluid properties used to compute various dimensionless parameters are evaluated, for the example, at $T^* = 118.4^\circ F$. At this temperature:

$C_p = 48.2$ BTU/lb °F

$k = 0.179$ BTU/ft hr °F

$\nu = 0.737$ ft^2/hr

$\frac{g\beta}{k\nu^2} = 1.03 \times 10^6$ $1/BTU\ ft^2$

Also,

$L = 1.33$ ft

$\frac{Q}{A} = 800$ $BTU/hr\ ft^2$

$D = 0.614$ ft.

$t = 24$ min $= 0.4$ hr.

a. Prandtl number

$$Pr = \frac{\gamma}{a} = \frac{\nu}{\frac{k}{\rho C_p}} = 219$$

b. Grashof-Nusselt number

$$GrNu = \frac{g\beta}{k\gamma^2} \left(\frac{Q}{A}\right) L^4 = 2.61 \times 10^9$$

c. Rayleigh-Nusselt number

$$RaNu = GrNuPr = 5.71 \times 10^{11}$$

d. Nusselt number (nominal, using empirical correlation from Section IV, eqn 4-1)

Assume turbulent flow:

$$Nu = 0.13\ (Ra)^{1/3}$$

$$Nu^{4/3} = 0.13\ (RaNu)^{1/3}$$

$$Nu = (0.13)^{3/4}\ (RaNu)^{1/4}$$

$$Nu = 0.217\ (8.7 \times 10^2)$$

$$Nu = 189$$

e. Rayleigh Number

$$Ra = \frac{RaNu}{Nu} = 3.02 \times 10^9$$

, based on usual criterion, (turbulent or nearly so)

f. Grashof Number

$$Gr = \frac{Ra}{Pr} = 1.4 \times 10^7$$

g. Fourier Number

$$Fo = \frac{\alpha t}{ID} = \frac{(0.179)}{(48.2)} \frac{(0.4)}{(1.33)(0.614)}$$

$$Fo = 0.0018$$

10. Correlation for Core Temperature Gradient

Use laminar model (transition retarded by presence of core temperature gradient)

$$\frac{d\theta_\infty}{dX} = 4.0\ (Fo)^{4/9} \frac{1}{(RaNu)^{1/9}}$$

$$\frac{d\theta_\infty}{dX} = \frac{4.0\ (0.0596)}{(20.2)} = 0.0118$$

The corresponding experimental value was 0.0123 (about 4% agreement).

E. Summary of Reduced Data

The following pages contain a listing of the values of various dimensionless groups, based on average fluid properties at a given time, for each time point when the temperature matrix values were recorded.

```
R
   R     REDUCED DATA IN DIMENSIONLESS FORM
R
   R     N=1  PURE GLYCERINE
   R     N=2  85 WT PERCENT GLYCERINE-WATER
   R     N=3  PURE WATER
   R     L  IS HEIGHT IN FT
   R     M IS TIME FROM START IN MINUTES
   R     Q  IS WALL HEAT FLUX IN BTU/HR-FT2
   R     P  IS PRANDTL NUMBER
   R     RN  IS RAYLEIGH-NUSSELT PRODUCT
   R     F  IS FOURIER NUMBER  (ALPHA)(TIME)/(L)(D)
R
```

```
N=1,L=0.67,M=  5.0,Q= 130.0,P=7999.0,RN=1.34E08,F=0.00074*
N=1,L=0.67,M= 14.0,Q= 160.0,P=6957.0,RN=2.09E08,F=0.00208*
N=1,L=0.67,M= 27.0,Q= 150.0,P=4873.0,RN=2.78E08,F=0.00399*
N=1,L=0.67,M= 45.0,Q= 150.0,P=3493.0,RN=4.05E08,F=0.00660*
N=1,L=0.67,M= 60.0,Q= 145.0,P=2867.0,RN=5.01E08,F=0.00877*
N=1,L=0.67,M= 90.0,Q= 140.0,P=1910.0,RN=7.52E08,F=0.0130 *
N=1,L=0.67,M=120.0,Q= 130.0,P=1362.0,RN=1.04E09,F=0.0172 *
N=1,L=0.67,M=150.0,Q= 120.0,P=1028.0,RN=1.36E09,F=0.0212 *
N=1,L=0.67,M=180.0,Q= 120.0,P= 814.0,RN=1.77E09,F=0.0252 *
N=1,L=0.67,M=210.0,Q= 110.0,P= 655.0,RN=2.05E09,F=0.0293 *
N=1,L=0.67,M=240.0,Q= 100.0,P= 548.0,RN=2.35E09,F=0.0333 *
N=1,L=0.67,M=274.0,Q= 100.0,P= 463.0,RN=2.87E09,F=0.0376 *
N=1,L=0.67,M=300.0,Q=  95.0,P= 404.0,RN=3.24E09,F=0.0410 *
N=1,L=0.67,M=330.0,Q=  85.0,P= 355.0,RN=3.41E09,F=0.0448 *
N=1,L=0.67,M=360.0,Q=  80.0,P= 320.0,RN=3.58E09,F=0.0486 *
N=1,L=0.67,M=  4.0,Q= 260.0,P=7285.0,RN=3.06E08,F=0.00060*
N=1,L=0.67,M= 12.0,Q= 350.0,P=5089.0,RN=6.15E08,F=0.00178*
N=1,L=0.67,M= 21.0,Q= 430.0,P=2867.0,RN=1.44E09,F=0.00307*
N=1,L=0.67,M= 33.0,Q= 415.0,P=1721.0,RN=2.53E09,F=0.00475*
N=1,L=0.67,M= 46.0,Q= 390.0,P=1162.0,RN=3.86E09,F=0.00655*
N=1,L=0.67,M= 56.0,Q= 375.0,P= 838.0,RN=5.33E09,F=0.00788*
N=1,L=0.67,M= 73.0,Q= 355.0,P= 562.0,RN=8.20E09,F=0.01013*
N=1,L=0.67,M= 91.0,Q= 340.0,P= 395.0,RN=1.01E10,F=0.01244*
N=1,L=0.67,M=106.0,Q= 340.0,P= 320.0,RN=1.55E10,F=0.0144 *
N=1,L=0.67,M=121.0,Q= 335.0,P= 250.0,RN=2.00E10,F=0.01625*
N=1,L=0.67,M=139.0,Q= 325.0,P= 230.0,RN=3.52E10,F=0.01845*
N=1,L=1.33,M= 10.0,Q=  20.0,P=5554.0,RN=5.00E08,F=0.00074*
N=1,L=1.33,M= 30.0,Q=  66.0,P=4970.0,RN=1.92E09,F=0.00221*
N=1,L=1.33,M= 59.0,Q=  63.0,P=4114.0,RN=2.29E09,F=0.00436*
N=1,L=1.33,M= 89.0,Q=  62.0,P=3493.0,RN=2.66E09,F=0.00656*
N=1,L=1.33,M=120.0,Q=  60.0,P=2980.0,RN=3.02E09,F=0.00882*
N=1,L=1.33,M=180.0,Q=  45.0,P=2332.0,RN=3.06E09,F=0.0132 *
N=1,L=1.33,M=240.0,Q=  43.0,P=1880.0,RN=3.76E09,F=0.01755*
N=1,L=1.33,M=300.0,Q=  32.0,P=1607.0,RN=3.32E09,F=0.0219 *
N=1,L=1.33,M=  6.5,Q= 110.0,P=4873.0,RN=3.23E09,F=0.00048*
N=1,L=1.33,M= 16.0,Q= 120.0,P=4475.0,RN=3.89E09,F=0.00118*
N=1,L=1.33,M= 31.0,Q= 130.0,P=3637.0,RN=5.35E09,F=0.00229*
N=1,L=1.33,M= 46.0,Q= 130.0,P=3100.0,RN=6.38E09,F=0.00339*
N=1,L=1.33,M= 87.0,Q= 125.0,P=1910.0,RN=1.08E10,F=0.00636*
N=1,L=1.33,M=118.0,Q= 110.0,P=1503.0,RN=1.25E10,F=0.00860*
```

```
N=1,L=1.33,M=149.0,Q= 110.0,P=1126.0,RN=1.80E10,F=0.01080*
N=1,L=1.33,M=180.0,Q=  97.0,P= 887.0,RN=2.04E10,F=0.0130 *
N=1,L=1.33,M=209.0,Q=  82.0,P= 770.0,RN=2.00E10,F=0.01503*
N=1,L=1.33,M= 15.0,Q= 170.0,P=4475.0,RN=5.51E09,F=0.00111*
N=1,L=1.33,M= 31.0,Q= 240.0,P=2990.0,RN=1.18E10,F=0.00228*
N=1,L=1.33,M= 46.0,Q= 230.0,P=2166.0,RN=1.69E10,F=0.00338*
N=1,L=1.33,M= 58.0,Q= 215.0,P=1811.0,RN=1.90E10,F=0.00424*
N=1,L=1.33,M= 75.0,Q= 200.0,P=1340.0,RN=2.54E10,F=0.00546*
N=1,L=1.33,M= 91.0,Q= 195.0,P=1059.0,RN=3.38E10,F=0.00660*
N=1,L=1.33,M=104.0,Q= 190.0,P= 900.0,RN=3.96E10,F=0.00753*
N=1,L=1.33,M= 10.0,Q= 440.0,P=3224.0,RN=2.06E10,F=0.00073*
N=1,L=1.33,M= 18.0,Q= 550.0,P=1979.0,RN=4.55E10,F=0.00131*
N=1,L=1.33,M= 26.0,Q= 520.0,P=1426.0,RN=6.23E10,F=0.00189*
N=1,L=1.33,M= 33.0,Q= 510.0,P=1012.0,RN=8.30E10,F=0.00239*
N=1,L=1.33,M= 42.0,Q= 480.0,P= 770.0,RN=1.19E11,F=0.00303*
N=1,L=1.33,M= 48.0,Q= 460.0,P= 665.0,RN=1.40E11,F=0.00344*
N=1,L=1.96,M=  4.0,Q= 180.0,P=7633.0,RN=1.45E10,F=0.00020*
N=1,L=1.96,M= 10.0,Q= 190.0,P=7285.0,RN=1.58E10,F=0.00051*
N=1,L=1.96,M= 20.0,Q= 170.0,P=6957.0,RN=1.51E10,F=0.00101*
N=1,L=1.96,M= 37.0,Q= 165.0,P=5315.0,RN=2.00E10,F=0.00187*
N=1,L=1.96,M= 56.0,Q= 160.0,P=3947.0,RN=2.33E10,F=0.00281*
N=1,L=1.96,M= 76.0,Q= 150.0,P=2867.0,RN=3.68E10,F=0.00378*
N=1,L=1.96,M= 96.0,Q= 145.0,P=2205.0,RN=4.85E10,F=0.00474*
N=1,L=1.96,M=122.0,Q= 140.0,P=1607.0,RN=6.74E10,F=0.00593*
N=1,L=1.96,M=149.0,Q= 120.0,P=1199.0,RN=8.03E10,F=0.00721*
N=1,L=1.96,M=180.0,Q= 110.0,P= 887.0,RN=1.06E11,F=0.00865*
N=1,L=1.96,M=211.0,Q= 110.0,P= 673.0,RN=1.48E11,F=0.0100 *
N=1,L=1.96,M=240.0,Q= 110.0,P= 548.0,RN=1.86E11,F=0.0113 *
N=1,L=1.96,M=  3.0,Q= 420.0,P=7633.0,RN=3.39E10,F=0.00015*
N=1,L=1.96,M=  9.0,Q= 420.0,P=7285.0,RN=3.61E10,F=0.00046*
N=1,L=1.96,M= 16.0,Q= 420.0,P=6645.0,RN=3.99E10,F=0.00081*
N=1,L=1.96,M= 25.0,Q= 420.0,P=4475.0,RN=6.10E10,F=0.00126*
N=1,L=1.96,M= 32.0,Q= 400.0,P=3100.0,RN=8.82E10,F=0.00160*
N=1,L=1.96,M= 43.0,Q= 350.0,P=2126.0,RN=1.22E11,F=0.00212*
N=1,L=1.96,M= 53.0,Q= 330.0,P=1503.0,RN=1.85E11,F=0.00258*
N=1,L=1.96,M= 63.0,Q= 310.0,P=1092.0,RN=2.29E11,F=0.00304*
N=1,L=1.96,M= 69.0,Q= 310.0,P= 887.0,RN=2.84E11,F=0.00331*


N=2,L=1.33,M= 23.0,Q=  60.0,P=488.2, RN=1.66E10,F=0.00176*
N=2,L=1.33,M= 71.0,Q=  60.0,P=394.9, RN=2.05E10,F=0.00541*
N=2,L=1.33,M=111.0,Q=  59.0,P=342.1, RN=2.54E10,F=0.00845*
N=2,L=1.33,M=160.0,Q=  55.0,P=290.3, RN=2.78E10,F=0.01217*
N=2,L=1.33,M=204.0,Q=  50.0,P=261.4, RN=3.08E10,F=0.01544*
N=2,L=1.33,M=268.0,Q=  45.0,P=204.2, RN=3.32E10,F=0.02025*
N=2,L=1.33,M=335.0,Q=  35.0,P=194.9, RN=2.93E10,F=0.02533*
N=2,L=1.33,M=  8.0,Q=  85.0,P=653.8, RN=1.74E10,F=0.00062*
N=2,L=1.33,M= 23.0,Q= 160.0,P=536.7, RN=4.08E10,F=0.00177*
N=2,L=1.33,M= 48.0,Q= 160.0,P=431.8, RN=6.05E10,F=0.00368*
N=2,L=1.33,M= 71.0,Q= 150.0,P=332.7, RN=6.32E10,F=0.00542*
N=2,L=1.33,M=104.0,Q= 140.0,P=261.4, RN=8.10E10,F=0.00792*
N=2,L=1.33,M=145.0,Q= 120.0,P=214.2, RN=7.72E10,F=0.01100*
N=2,L=1.33,M=173.0,Q= 100.0,P=177.9, RN=9.45E10,F=0.01307*
N=2,L=1.33,M=222.0,Q=  90.0,P=150.0, RN=1.05E11,F=0.01673*
N=2,L=1.33,M= 11.0,Q= 230.0,P=525.0, RN=6.30E10,F=0.00085*
```

```
N=2,L=1.33,M= 49.0,Q= 250.0,P=282.7, RN=1.30E11,F=0.00373*
N=2,L=1.33,M= 75.0,Q= 230.0,P=202.0, RN=1.79E11,F=0.00567*
N=2,L=1.33,M=106.0,Q= 200.0,P=156.0, RN=2.19E11,F=0.00797*
N=2,L=1.33,M=138.0,Q= 180.0,P=114.0, RN=3.02E11,F=0.01032*
N=2,L=1.33,M=150.0,Q= 160.0,P=106.0, RN=3.08E11,F=0.01118*
N=2,L=1.33,M=  8.0,Q= 165.0,P=632.0, RN=3.54E10,F=0.00062*
N=2,L=1.33,M= 23.0,Q= 300.0,P=473.0, RN=8.51E10,F=0.00177*
N=2,L=1.33,M= 42.0,Q= 270.0,P=319.0, RN=1.21E11,F=0.00320*
N=2,L=1.33,M= 56.0,Q= 260.0,P=258.0, RN=1.50E11,F=0.00426*
N=2,L=1.33,M= 81.0,Q= 255.0,P=182.0, RN=2.31E11,F=0.00613*
N=2,L=1.33,M=108.0,Q= 250.0,P=130.0, RN=3.50E11,F=0.00812*
N=2,L=1.33,M=132.0,Q= 250.0,P=104.0, RN=5.20E11,F=0.00987*
N=2,L=1.33,M=  6.0,Q= 425.0,P=504.0, RN=1.14E11,F=0.00046*
N=2,L=1.33,M= 15.0,Q= 550.0,P=362.0, RN=2.14E11,F=0.00114*
N=2,L=1.33,M= 26.0,Q= 550.0,P=245.0, RN=3.37E11,F=0.00197*
N=2,L=1.33,M= 36.0,Q= 460.0,P=195.0, RN=3.80E11,F=0.00273*
N=2,L=1.33,M= 47.0,Q= 460.0,P=150.0, RN=5.40E11,F=0.00353*
N=2,L=1.33,M= 56.0,Q= 460.0,P=125.0, RN=6.99E11,F=0.00418*
N=2,L=1.33,M= 65.0,Q= 460.0,P=106.0, RN=9.00E11,F=0.00484*
N=2,L=1.33,M=  6.0,Q= 590.0,P=476.0, RN=1.67E11,F=0.00046*
N=2,L=1.33,M= 11.0,Q= 710.0,P=380.0, RN=2.66E11,F=0.00084*
N=2,L=1.33,M= 17.0,Q= 780.0,P=294.0, RN=3.82E11,F=0.00128*
N=2,L=1.33,M= 24.0,Q= 800.0,P=219.0, RN=5.71E11,F=0.00180*
N=2,L=1.33,M= 29.0,Q= 800.0,P=161.0, RN=8.36E11,F=0.00218*
N=2,L=1.33,M= 37.0,Q= 800.0,P=128.0, RN=1.17E12,F=0.00277*
N=2,L=1.33,M= 41.0,Q= 800.0,P=112.0, RN=1.46E12,F=0.00305*
N=2,L=1.33,M= 48.0,Q= 800.0,P= 92.0, RN=1.98E12,F=0.00356*
N=2,L=1.33,M=  9.0,Q= 135.0,P=654.0, RN=2.77E10,F=0.00070*
N=2,L=1.33,M= 23.0,Q= 140.0,P=563.0, RN=3.90E10,F=0.00177*
N=2,L=1.33,M= 48.0,Q= 150.0,P=459.0, RN=4.45E10,F=0.00366*
N=2,L=1.33,M= 68.0,Q= 155.0,P=352.0, RN=6.15E10,F=0.00516*
N=2,L=1.33,M= 85.0,Q= 155.0,P=306.0, RN=7.19E10,F=0.00642*
N=2,L=1.33,M= 39.0,Q= 350.0,P=251.0, RN=1.98E11,F=0.00292*
N=2,L=1.33,M= 50.0,Q= 400.0,P=195.0, RN=3.23E11,F=0.00370*
N=2,L=1.33,M= 61.0,Q= 400.0,P=159.0, RN=4.20E11,F=0.00449*
N=2,L=1.33,M= 75.0,Q= 390.0,P=118.0, RN=6.30E11,F=0.00544*
N=2,L=1.33,M= 89.0,Q= 390.0,P=102.0, RN=7.85E11,F=0.00640*
N=-1*
FORTRAN PM  (MAIN)(ENTIRE),ALL


N=3,L=0.67,M=  7.0,Q= 140.0,P=6.43,  RN=1.47E10,F=0.00160*
N=3,L=0.67,M= 16.0,Q= 150.0,P=6.08,  RN=2.86E10,F=0.00364*
N=3,L=0.67,M= 32.0,Q= 160.0,P=5.68,  RN=3.58E10,F=0.00732*
N=3,L=0.67,M= 59.0,Q= 155.0,P=5.05,  RN=4.24E10,F=0.0137 *
N=3,L=0.67,M= 88.0,Q= 130.0,P=4.57,  RN=4.38E10,F=0.0207 *
N=3,L=0.67,M=121.0,Q= 130.0,P=4.16,  RN=5.00E10,F=0.0289 *
N=3,L=0.67,M=153.0,Q= 120.0,P=3.84,  RN=5.18E10,F=0.0369 *
N=3,L=0.67,M=181.0,Q= 110.0,P=3.64,  RN=5.02E10,F=0.044  *
N=3,L=0.67,M=213.0,Q=  90.0,P=3.41,  RN=4.60E10,F=0.0523 *
N=3,L=0.67,M=245.0,Q=  85.0,P=3.27,  RN=4.52E10,F=0.0605 *
N=3,L=0.67,M=272.0,Q=  80.0,P=3.11,  RN=4.36E10,F=0.0675 *
N=3,L=0.67,M=301.0,Q=  65.0,P=3.00,  RN=3.67E10,F=0.0753 *
N=3,L=0.67,M=321.0,Q=  60.0,P=2.94,  RN=2.94E10,F=0.0805 *
N=3,L=0.67,M=  5.0,Q= 410.0,P=6.00,  RN=8.10E10,F=0.00115*
```

```
N=3,L=0.67,M= 10.0,Q= 450.0,P=5.53,  RN=1.02E11,F=0.00229*
N=3,L=0.67,M= 20.0,Q= 420.0,P=4.98,  RN=1.14E11,F=0.00465*
N=3,L=0.67,M= 30.0,Q= 415.0,P=4.51,  RN=1.38E11,F=0.00705*
N=3,L=0.67,M= 41.0,Q= 400.0,P=4.11,  RN=1.46E11,F=0.00980*
N=3,L=0.67,M= 50.0,Q= 390.0,P=3.80,  RN=1.71E11,F=0.0121. *
N=3,L=0.67,M= 60.0,Q= 375.0,P=3.52,  RN=1.76E11,F=0.01465*
N=3,L=0.67,M= 76.0,Q= 340.0,P=3.18,  RN=1.84E11,F=0.0189 *
N=3,L=0.67,M= 91.0,Q= 310.0,P=2.91,  RN=1.87E11,F=0.0230 *
N=3,L=0.67,M=120.0,Q= 290.0,P=2.54,  RN=2.07E11,F=0.0310 *
N=3,L=0.67,M=150.0,Q= 280.0,P=2.29,  RN=2.17E11,F=0.0396 *
N=3,L=1.33,M= 12.0,Q=  35.0,P=5.92,  RN=1.08E11,F=0.00137*
N=3,L=1.33,M= 38.0,Q=  80.0,P=5.60,  RN=2.26E11,F=0.00435*
N=3,L=1.33,M= 86.0,Q=  70.0,P=5.18,  RN=2.16E11,F=0.00992*
N=3,L=1.33,M=136.0,Q=  62.0,P=4.80,  RN=2.16E11,F=0.0159 *
N=3,L=1.33,M=167.0,Q=  60.0,P=4.63,  RN=2.98E11,F=0.01965*
N=3,L=1.33,M=202.0,Q=  55.0,P=4.46,  RN=2.96E11,F=0.0238 *
N=3,L=1.33,M= 32.0,Q= 140.0,P=4.98,  RN=6.32E11,F=0.00372*
N=3,L=1.33,M= 56.0,Q= 150.0,P=4.63,  RN=7.70E11,F=0.00657*
N=3,L=1.33,M= 92.0,Q= 140.0,P=4.16,  RN=8.11E11,F=0.0109 *
N=3,L=1.33,M=122.0,Q= 130.0,P=3.76,  RN=9.06E11,F=0.01475*
N=3,L=1.33,M=154.0,Q= 120.0,P=3.56,  RN=8.90E11,F=0.01874*
N=3,L=1.33,M=182.0,Q= 110.0,P=3.34,  RN=9.00E11,F=0.0223 *
N=3,L=1.33,M=214.0,Q= 100.0,P=3.18,  RN=8.56E11,F=0.0265 *
N=3,L=1.33,M=247.0,Q=  90.0,P=3.05,  RN=8.24E11,F=0.0308 *
N=3,L=1.33,M= 17.0,Q= 240.0,P=5.32,  RN=9.25E11,F=0.00195*
N=3,L=1.33,M= 40.0,Q= 270.0,P=4.63,  RN=1.34E12,F=0.00469*
N=3,L=1.33,M= 70.0,Q= 250.0,P=4.02,  RN=1.57E12,F=0.00837*
N=3,L=1.33,M=108.0,Q= 220.0,P=3.45,  RN=1.71E12,F=0.0132 *
N=3,L=1.33,M=130.0,Q= 200.0,P=3.10,  RN=1.76E12,F=0.0161 *
N=3,L=1.33,M=178.0,Q= 180.0,P=2.76,  RN=1.78E12,F=0.0226 *
N=3,L=1.33,M= 41.0,Q= 240.0,P=4.57,  RN=1.23E12,F=0.00486*
N=3,L=1.33,M= 70.0,Q= 225.0,P=4.00,  RN=1.42E12,F=0.00850*
N=3,L=1.33,M= 94.0,Q= 205.0,P=3.64,  RN=1.48E12,F=0.01160*
N=3,L=1.33,M= 11.0,Q= 240.0,P=5.46,  RN=8.95E11,F=0.00127*
N=3,L=1.33,M= 29.0,Q= 260.0,P=4.95,  RN=1.16E12,F=0.00336*
N=3,L=1.33,M= 45.0,Q= 250.0,P=4.51,  RN=1.31E12,F=0.00527*
N=3,L=1.33,M= 59.0,Q= 240.0,P=4.16,  RN=1.43E12,F=0.00692*
N=3,L=1.33,M= 77.0,Q= 230.0,P=3.84,  RN=1.55E12,F=0.00936*
N=3,L=1.33,M= 93.0,Q= 210.0,P=3.64,  RN=1.52E12,F=0.01147*
N=3,L=1.33,M=121.0,Q= 210.0,P=3.27,  RN=1.74E12,F=0.01504*
N=3,L=1.33,M=138.0,Q= 205.0,P=3.05,  RN=1.84E12,F=0.0175 *
N=3,L=1.33,M=  2.0,Q= 235.0,P=5.53,  RN=8.52E11,F=0.00023*
N=3,L=1.33,M= 15.0,Q= 425.0,P=4.63,  RN=2.13E12,F=0.00176*
N=3,L=1.33,M= 31.0,Q= 400.0,P=4.25,  RN=2.27E12,F=0.00368*
N=3,L=1.33,M= 50.0,Q= 390.0,P=3.67,  RN=2.64E12,F=0.00606*
N=3,L=1.33,M= 60.0,Q= 380.0,P=3.41,  RN=2.86E12,F=0.00735*
N=3,L=1.33,M= 69.0,Q= 370.0,P=3.21,  RN=3.11E12,F=0.00855*
N=3,L=1.33,M= 76.0,Q= 370.0,P=3.05,  RN=3.36E12,F=0.00952*
N=3,L=1.33,M=  2.0,Q= 360.0,P=5.76,  RN=1.19E12,F=0.00023*
N=3,L=1.33,M= 10.0,Q= 810.0,P=4.92,  RN=3.64E12,F=0.00116*
N=3,L=1.33,M= 17.0,Q= 900.0,P=4.30,  RN=5.08E12,F=0.00201*
N=3,L=1.33,M= 23.0,Q= 800.0,P=3.93,  RN=5.19E12,F=0.00277*
N=3,L=1.33,M= 31.0,Q= 770.0,P=3.48,  RN=5.74E12,F=0.00380*
N=3,L=1.33,M= 37.0,Q= 750.0,P=3.21,  RN=6.32E12,F=0.00458*
N=3,L=1.33,M=  3.0,Q= 700.0,P=6.43,  RN=1.83E12,F=0.00034*
```

```
N=3,L=1.33,M=  7.0,Q= 950.0,P=5.53,   RN=3.49E12,F=0.00080*
N=3,L=1.33,M= 12.0,Q=1200.0,P=4.80,   RN=5.62E12,F=0.00141*
N=3,L=1.33,M= 17.0,Q=1280.0,P=4.21,   RN=7.57E12,F=0.00202*
N=3,L=1.33,M= 21.0,Q=1050.0,P=3.80,   RN=7.36E12,F=0.00253*
N=3,L=1.33,M= 27.0,Q= 980.0,P=3.41,   RN=7.84E12,F=0.00331*
N=3,L=1.33,M= 34.0,Q= 970.0,P=3.02,   RN=8.75E12,F=0.00425*
N=3,L=1.33,M= 41.0,Q= 960.0,P=2.70,   RN=9.75E12,F=0.00523*
N=3,L=1.33,M= 47.0,Q= 900.0,P=2.43,   RN=1.02E13,F=0.00612*
N=3,L=1.33,M= 53.0,Q= 850.0,P=2.26,   RN=1.04E13,F=0.0070 *
N=3,L=1.33,M=  3.0,Q=1470.0,P=6.25,   RN=4.06E13,F=0.00034*
N=3,L=1.33,M=  7.0,Q=1900.0,P=4.98,   RN=8.32E13,F=0.00081*
N=3,L=1.33,M= 11.0,Q=1710.0,P=4.21,   RN=1.01E14,F=0.00131*
N=3,L=1.33,M= 16.0,Q=1670.0,P=3.52,   RN=1.27E14,F=0.00195*
N=3,L=1.33,M= 22.0,Q=1660.0,P=2.88,   RN=1.58E14,F=0.00277*
N=3,L=1.33,M= 27.0,Q=1630.0,P=2.47,   RN=1.80E14,F=0.0035 *
N=3,L=1.33,M= 32.0,Q=1600.0,P=2.15,   RN=2.04E14,F=0.00426*
N=3,L=1.96,M=  6.0,Q= 220.0,P=6.00,   RN=3.18E12,F=0.00047*
N=3,L=1.96,M= 16.0,Q= 190.0,P=5.84,   RN=2.93E12,F=0.00124*
N=3,L=1.96,M= 30.0,Q= 180.0,P=5.46,   RN=3.12E12,F=0.00235*
N=3,L=1.96,M= 47.0,Q= 160.0,P=5.11,   RN=3.18E12,F=0.00371*
N=3,L=1.96,M= 63.0,Q= 160.0,P=4.80,   RN=3.50E12,F=0.00502*
N=3,L=1.96,M= 89.0,Q= 160.0,P=4.41,   RN=4.00E12,F=0.00714*
N=3,L=1.96,M=120.0,Q= 160.0,P=3.93,   RN=4.79E12,F=0.00981*
N=3,L=1.96,M=150.0,Q= 160.0,P=3.56,   RN=5.51E12,F=0.01245*
N=3,L=1.96,M=181.0,Q= 160.0,P=3.27,   RN=6.21E12,F=0.0152 *
N=3,L=1.96,M=210.0,Q= 150.0,P=2.99,   RN=6.43E12,F=0.0179 *
N=3,L=1.96,M=240.0,Q= 140.0,P=2.80,   RN=6.44E12,F=0.0207 *
N=3,L=1.96,M=  6.0,Q= 430.0,P=5.84,   RN=6.44E12,F=0.00047*
N=3,L=1.96,M= 11.0,Q= 430.0,P=5.46,   RN=7.48E12,F=0.00086*
N=3,L=1.96,M= 21.0,Q= 430.0,P=5.05,   RN=8.60E12,F=0.00166*
N=3,L=1.96,M= 31.0,Q= 430.0,P=4.57,   RN=1.00E13,F=0.00248*
N=3,L=1.96,M= 46.0,Q= 460.0,P=3.97,   RN=1.37E13,F=0.00378*
N=3,L=1.96,M= 61.0,Q= 470.0,P=3.52,   RN=1.66E13,F=0.00506*
N=3,L=1.96,M= 76.0,Q= 470.0,P=3.08,   RN=1.91E13,F=0.00645*
N=3,L=1.96,M= 91.0,Q= 450.0,P=2.75,   RN=2.06E13,F=0.00787*
N=3,L=1.96,M=105.0,Q= 430.0,P=2.50,   RN=2.22E13,F=0.00925*
N=3,L=0.75,M=  1.0,Q= 192.0,P=6.25,   RN=5.38E10,F=0.00044*
N=3,L=0.75,M=  2.0,Q= 426.0,P=6.17,   RN=1.24E11,F=0.00089*
N=3,L=0.75,M=  3.0,Q= 492.0,P=6.00,   RN=1.52E11,F=0.00134*
N=3,L=0.75,M=  4.0,Q= 486.0,P=5.88,   RN=1.57E11,F=0.00180*
N=3,L=0.75,M=  1.0,Q= 237.0,P=6.53,   RN=6.00E10,F=0.00044*
N=3,L=0.75,M=  2.0,Q= 900.0,P=6.34,   RN=2.44E11,F=0.00089*
N=3,L=0.75,M=  3.0,Q= 890.0,P=6.00,   RN=2.74E11,F=0.00134*
N=3,L=0.75,M=  4.0,Q= 810.0,P=5.76,   RN=2.73E11,F=0.00180*
N=3,L=0.75,M=  1.0,Q= 576.0,P=5.84,   RN=1.89E11,F=0.00045*
N=3,L=0.75,M=  2.0,Q=1670.0,P=5.39,   RN=6.42E11,F=0.00091*
N=3,L=0.75,M=  3.0,Q=1625.0,P=4.92,   RN=7.37E11,F=0.00138*
N=3,L=0.75,M=  4.0,Q=1660.0,P=4.57,   RN=8.55E11,F=0.00185*
N=3,L=0.75,M=  0.5,Q=1300.0,P=5.92,   RN=4.13E11,F=0.00022*
N=3,L=0.75,M=  1.0,Q=2230.0,P=5.60,   RN=7.93E11,F=0.00045*
N=3,L=0.75,M=  1.5,Q=3100.0,P=5.11,   RN=1.31E12,F=0.00068*
N=3,L=0.75,M=  2.0,Q=4650.0,P=4.68,   RN=2.31E12,F=0.00092*
N=3,L=0.56,M=  1.0,Q= 600.0,P=5.96,   RN=5.98E10,F=0.00025*
N=3,L=0.56,M=  1.5,Q=1100.0,P=5.87,   RN=1.13E11,F=0.00037*
N=3,L=0.56,M=  2.0,Q=1118.0,P=5.84,   RN=1.17E11,F=0.00050*
```

```
N=3,L=0.56,M=   3.0,Q=1240.0,P=5.68,   RN=1.37E11,F=0.00075*
N=3,L=0.56,M=   4.0,Q=1390.0,P=5.53,   RN=1.62E11,F=0.00100*
N=3,L=0.56,M=   5.0,Q=1435.0,P=5.32,   RN=1.81E11,F=0.00125*
N=3,L=0.56,M=   6.0,Q=1445.0,P=5.18,   RN=1.92E11,F=0.00149*
N=3,L=0.56,M=   7.0,Q=1500.0,P=5.05,   RN=2.08E11,F=0.00178*
N=3,L=0.56,M=   8.0,Q=1420.0,P=4.86,   RN=2.11E11,F=0.00204*
N=3,L=0.56,M=   9.0,Q=1330.0,P=4.74,   RN=2.07E11,F=0.00227*
N=3,L=0.56,M=  10.0,Q=1300.0,P=4.63,   RN=2.10E11,F=0.00259*
N=-1*
FORTRAN PM  (MAIN)(ENTIRE),ALL
```

F. Energy Balances

Figures 8-5 to 8-7 show energy balances for typical tests in a graphical form. In Fig. 8-6, the energy balance for the test in which the power level was changed suddenly during the course of the run is presented. Techniques for computing the various contributions to the energy balances are given in D. Sample Calculations.

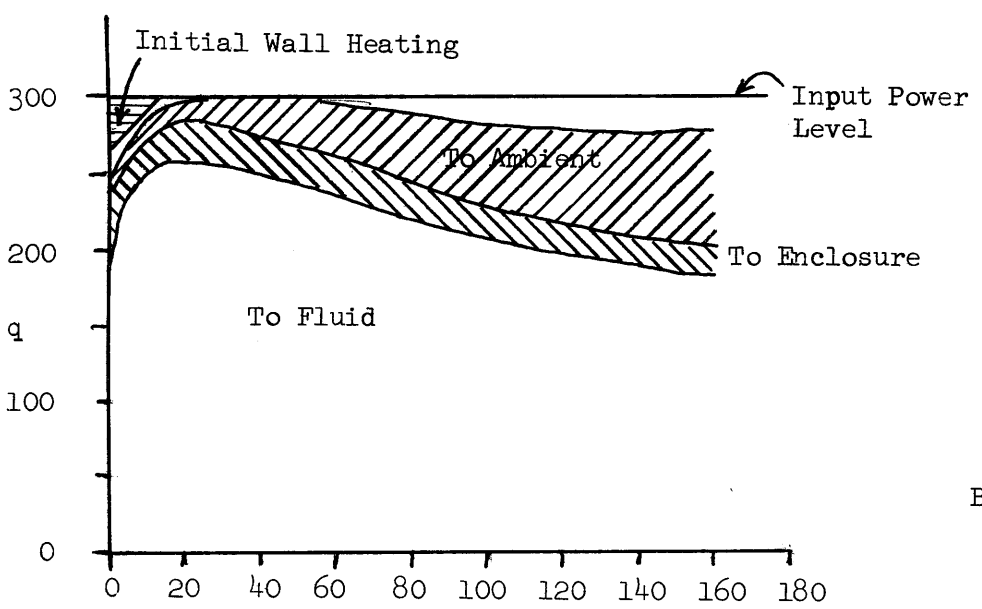

Test A-2-4, Water, L=1.33ft, T_i=81°F

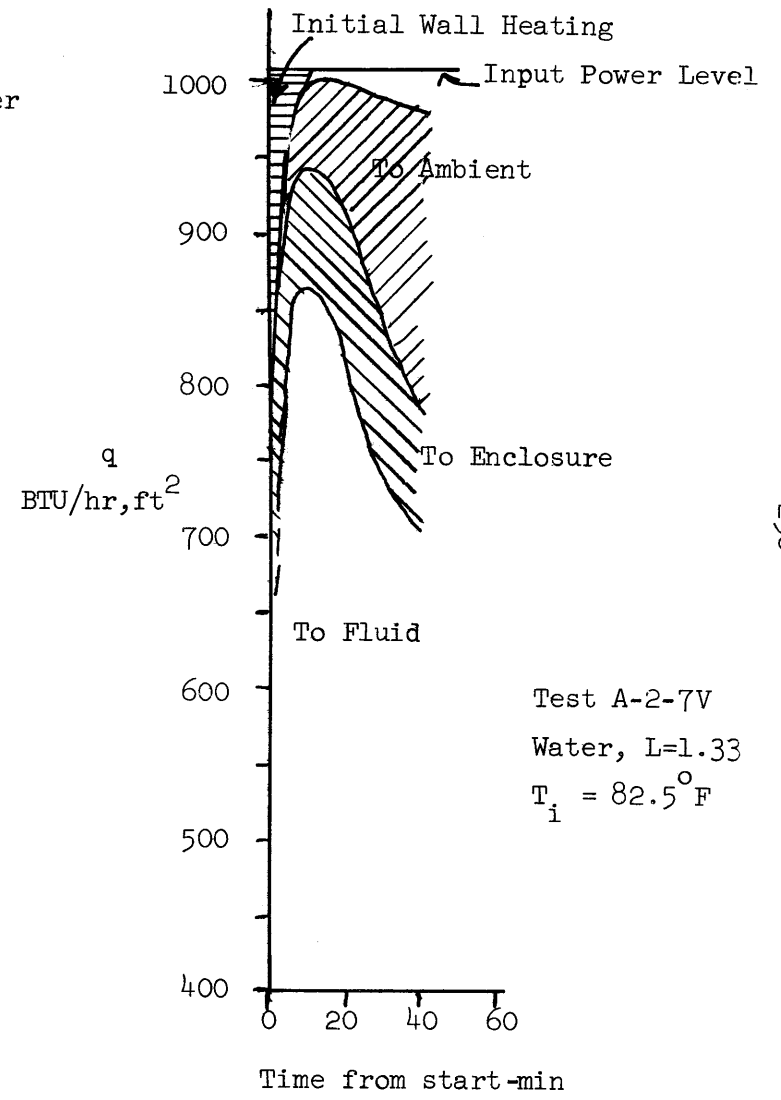

FIGURE 8 - 5

Energy Balances

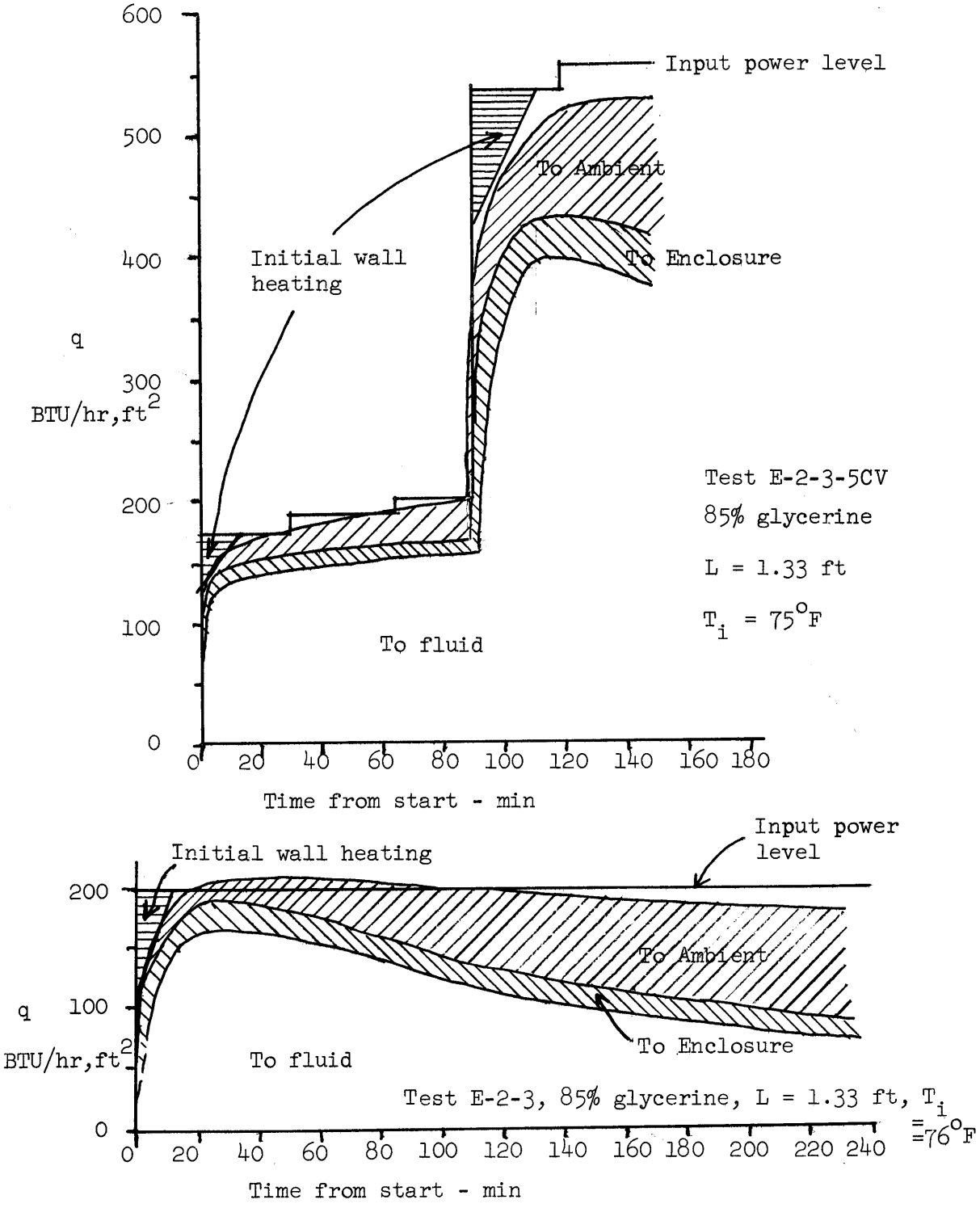

FIGURE 8-6

Energy Balances

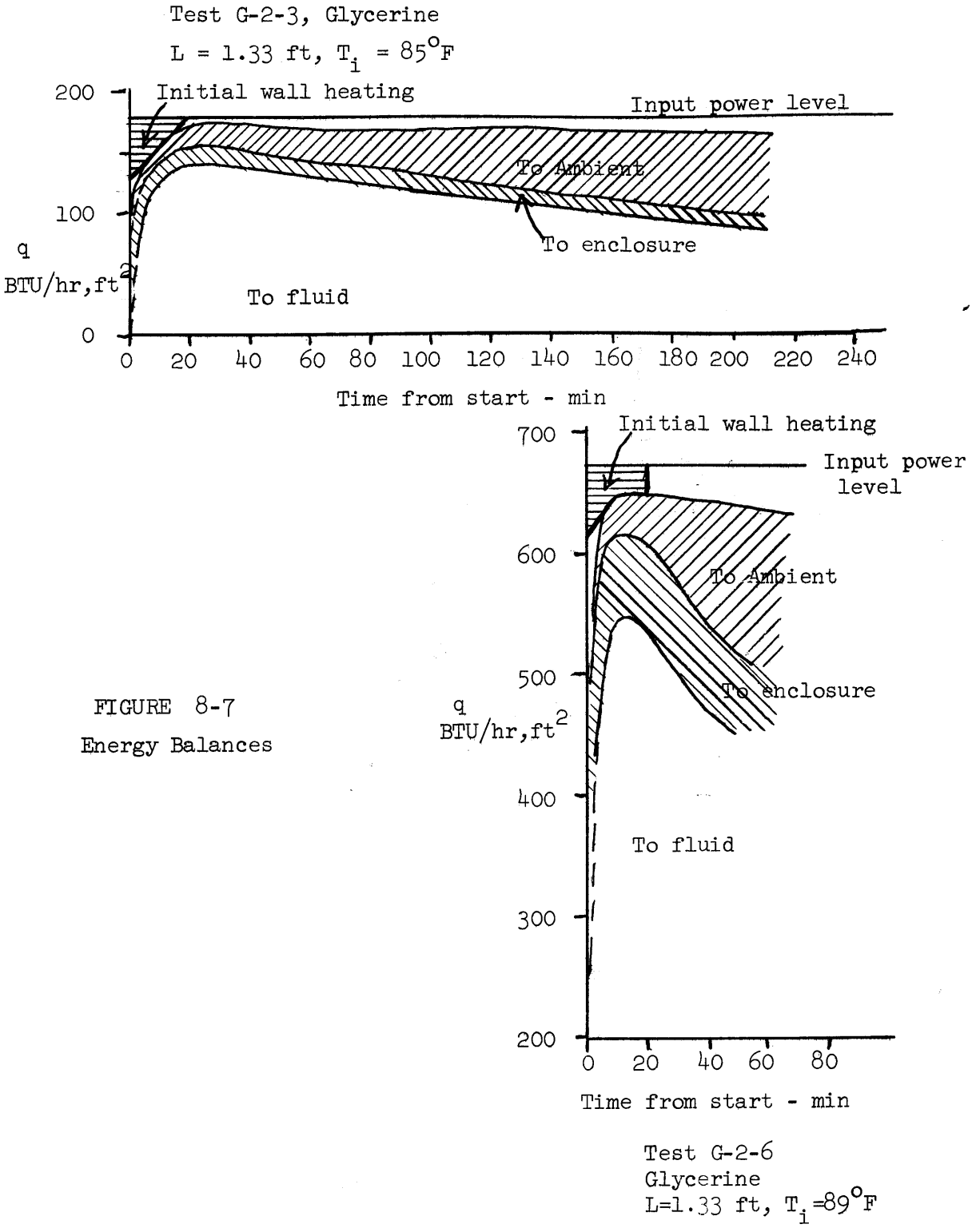

FIGURE 8-7
Energy Balances

G. Physical Properties of Fluids

The fluid property values used in this study were obtained by a three-point Lagrangian interpolation scheme using reference values for each property at 20°C, 40°C, and 70°C. (57)

TABLE III

Reference Points for Evaluation of Physical Properties

Fluid	Glycerine			85% Glycerine			Water		
Temperature	20°C	40°C	70°C	20°C	40°C	70°C	20°C	40°C	70°C
ρ (liq) gm/cc	1.261	1.249	1.229	1.222	1.209	1.190	0.998	0.992	0.978
C_p (liq) kcal/kgm,°C	0.57	0.59	0.64	0.61	0.64	0.68	1.0	1.0	1.0
μ (liq) cp.	1410	284	51.6	109	33.5	10.0	1.005	0.656	0.4061
k (liq) kcal/m,hr,°C	0.245	0.245	0.245	0.267	0.266	0.266	0.508	0.536	0.576
β (liq) x10^4/°C	3.8	4.5	5.2	4.9	4.9	6.66	2.0	4.0	5.9

H. Computer Programs

Three programs are included in this section. The first program permits computation of the functions E^* and M^* using the laminar, constant wall heat flux boundary layer model for the laminar case. The value of the constant core temperature gradient and the Prandtl number must be specified. The curves shown in Fig. 3-1 were generated by this program.

The second program is similar to the first except that the turbulent flow temperature and velocity profiles are used in formulating the model. Figure 3-2 was obtained from this program.

Finally, a program for calculation of core temperature distribution during the initial period is presented. In this method, the boundary layer and core regions are divided into N vertical increments and the constant core temperature gradient assumption is made over individual increments only. Starting with an isothermal core, the boundary layer flow and exit temperature are computed using the energy function for the laminar case. It is assumed that the topmost core increment will be filled with a constant flow of boundary layer fluid at the computed T_L in a certain length of time DELTAU. During the next time increment, the effect of the change in temperature at the top of the core is considered in computing a new DELTL and DELTAU. Because of plug flow in the core, the core temperatures are moved down one level after each time increment. Results of this iteration up the boundary layer and in time are shown to generate core temperature profiles like those in Fig. 4-23.

```
*       MAD
            R
            R     TRANSIENT NATURAL CONVECTION WITH CORE GRADIENT
            R     ENERGY AND MOMENTUM KARMAN FORMULATION
            R     LAMINAR CASE, CONST Q
            R
             DIMENSION F(2), Y(2)
             INTEGER N, MAXN, I, RKSUB., NFL, Z
START        READ AND PRINT DATA NFL, TINIT, Q, PR, MODGR,
            1COREGR, K, L, Z, MAXN, XINIT
             WHENEVER NFL.L.0, EXECUTE EXIT.
             C=MODGR.P.0.25
             H=C*L/MAXN
             X = XINIT
             ESTAR =  X
             MSTAR =  X.P.1.400
             Y(1)=ESTAR
             Y(2)=MSTAR
             HPRINT = Z*H
             XPRINT = X-H
ST1          WHENEVER X.G.XPRINT-H/2.0
                EXECUTE PRINT.
                XPRINT = X + HPRINT
             END OF CONDITIONAL
             W'R X.GE.L*C,  T'O ST3
ST2          I = RKSUB. (2,Y,F,X,H)
             W'R Y(1).L.0.0, T'O START
             W'R Y(2).L.0.0, T'O START
             W'R I.E.2, T'O ST1
             EXECUTE DERIV.
             T'O ST2
             INTERNAL FUNCTION
             ENTRY TO DERIV.
             F(1) = 1.0 - (5.0*((PR/60.0).P.0.4)*((10.0/(0.8+PR)).P.0.2)
            1*((Y(1)*Y(2)).P.0.333)* COREGR)
             F(2) = (7.0/4.0) * (((0.8 +PR)*(Y(1)*Y(1)/Y(2) ).P.0.667)
            1-(PR*Y(2)/Y(1)))
             FUNCTION RETURN
             END OF FUNCTION
             INTERNAL FUNCTION
             ENTRY TO PRINT.
             EXECUTE DERIV.
             PRINT RESULTS  X, Y(1), Y(2), F(1), F(2)
             FUNCTION RETURN
             END OF FUNCTION
ST3          CONTINUE
             CM = ((60.0/PR).P.0.8)*((10.0/(0.8+PR)).P.0.6)
             CE = 60.0/PR
             E = CE*Y(1)
             M = CM * Y(2)
             ESTARL = Y(1)
             MSTARL = Y(2)
             DIMFLO = (E*M).P.0.333
             DELTA = (E*E/M).P.0.333
             NUSSL = 2.0*C*L/DELTA
```

```
 DTBARL = Q*DELTA/(5.0*C*K)
 DTCOR = Q* COREGR / K
 TCORL = TINIT + (L*DTCOR)
 PRINT RESULTS  TINIT, PR,  Q, MODGR,  COREGR, K, L,
1C, CE, CM, ESTARL,MSTARL,E, M, DIMFLO, DELTA
2, NUSSL, DTBARL, DTCOR, TCORL
 T'O START
 END OF PROGRAM
```

```
*       MAD
            R
            R     TRANSIENT NATURAL CONVECTION WITH CORE GRADIENT
            R     ENERGY AND MOMENTUM KARMAN FORMULATION
            R     TURBULENT CASE, CONST Q
            R
             DIMENSION F(2), Y(2)
             INTEGER N, MAXN, I, RKSUB., NFL, Z
START        READ AND PRINT DATA NFL, TINIT, Q, PR, MODGR,
            1COREGR, K, L, Z, MAXN, XINIT
             WHENEVER NFL.L.0, EXECUTE EXIT.
             C=MODGR.P.0.25
             H=C*L/MAXN
             X = XINIT
             ESTAR = X
             MSTAR =  X.P.( 11.0 / 7.0 )
             Y(1)=ESTAR
             Y(2)=MSTAR
             A1 =7.0*(3.0/8.0+3.0/11.0+1.0/36.0-1.0/9.0-2.0/15.0
            1 -6.0/23.0-4.0/29.0-1.0/37.0)
             A2 = 7.0*(1.0/8.0+3.0/11.0+1.0/36.0-4.0/15.0-4.0/29.0)
             A3 = 7.0*(1.0/9.0+28.0/23.0+70.0/37.0+28.0/51.0+1.0/65.0
            1 -1.0/2.0-28.0/15.0-14.0/11.0-4.0/29.0)
             A4 = 0.1250
             A5 = 0.02250
             CE =  A5 / ( A1 * (PR.P.0.667 ) )
             CM =  ( CE.P.(13.0/14.0)) * (( A4 / ( A5*A3*(PR.P.0.333)
            1  * (( 11.0/7.0 ) + (A1 * (PR.P.0.667) / A3)))).P.(9.0/14.0))
             HPRINT = Z*H
             XPRINT = X-H
ST1          WHENEVER X.G.XPRINT-H/2.0
                EXECUTE PRINT.
                XPRINT = X + HPRINT
             END OF CONDITIONAL
             W'R X.GE.L*C,  T'O ST3
ST2          I = RKSUB. (2,Y,F,X,H)
             W'R Y(1).L.0.0, T'O START
             W'R Y(2).L.0.0, T'O START
             W'R I.E.2, T'O ST1
             EXECUTE DERIV.
             T'O ST2
             INTERNAL FUNCTION
             ENTRY TO DERIV.
             F(1)  = 1.0 - (A2 * PR * ( CE.P.(8.0/7.0)) * (( A4 /
            1 ( A5 * A3 * (PR.P.0.333) * (( 11.0 / 7.0 ) + (A1 *
            2 ( PR.P.0.667) / A3 )))).P.(2.0/7.0)) * (( Y(1) * Y(2))
            3 .P.(4.0/9.0)) * COREGR )
             F(2) = (((11.0/7.0) + ( A1 * (PR.P.0.667) / A3)) *
            1 ( Y(1).P.(13.0/9.0)) / ( Y(2).P.(5.0/9.0)))
            2 - ( A1 * (PR.P.0.667) * Y(2) / ( A3 * Y(1)))
             FUNCTION RETURN
             END OF FUNCTION
             INTERNAL FUNCTION
             ENTRY TO PRINT.
             EXECUTE DERIV.
```

```
      PRINT RESULTS  X, Y(1), Y(2), F(1), F(2)
      FUNCTION RETURN
      END OF FUNCTION
ST3   CONTINUE
      E = CE*Y(1)
      M = CM * Y(2)
      ESTARL = Y(1)
      MSTARL = Y(2)
      DIMFLO = ( E * M ).P.(4.0/9.0)
      DELTA =  E.P.(8.0/9.0) / ( M.P.(1.0/9.0) )
      DTCOR = Q * COREGR / K
      TCORL = TINIT + (L*DTCOR)
      NUSSL =  A5 * C * L * (PR.P.0.333) *
     1  ( M.P.(4.0/9.0 )) / ( E.P.(5.0/9.0) )
      DTBLL = Q * L / ( K * NUSSL )
      DTBARL = A1 * DTBLL / A2
      TW = TCORL + DTBLL
      PRINT RESULTS  TINIT, PR,  Q, MODGR,  COREGR, K, L,
     1C, CE, CM, ESTARL,MSTARL,E, M, DIMFLO, DELTA
     2, NUSSL, DTBARL, DTCOR, TCORL, TW, DTBLL
     3, A1, A2, A3, A4, A5
      T'O START
      END OF PROGRAM
```

MAC PROGRAM LISTING ... ...

```
                PROGRAM TO CALCULATE INITIAL PERIOD
                CORE TEMPERATURE PROFILES, VERTICAL CYLINDER
                LAMINAR MODEL,  QWALL

              DIMENSION T(10), ES(10), FINEES(100)
              INTEGER M,N,S,MAXM,MAXN,MAXS,NFL
START         READ AND PRINT DATA NFL, MODGR, PR, Q, K, NU,
             1  L, R, MAXM, MAXN, MAXS
              WHENEVER NFL.L.0, EXECUTE EXIT.
              TIME = 0.0
              THROUGH SET, FOR N=0,1,N.G.MAXN
SET           T(N) = 0.0
              DELTAU = 0.0
              C = MODGR.P.0.25
              CE = 60.0/PR
              DELCX = C*L/(MAXN*MAXS)
              PRINT RESULTS C, CE, DELCX
              THROUGH ST4, FOR M=1,1,M.G.MAXM
              ES(0) = 0.0
              ES(1) = C*L/MAXN
              THROUGH ST2, FOR N=2,1,N.G.MAXN
              THROUGH ST1, FOR S=1,1,S.G.MAXS
              COREGR = K*MAXN*(T(N)-T(N-1)) / (Q * L)
              FINEES(0) = ES(N-1)
              FINEES(S) = FINEES(S-1) + (( 1.0 - 1.543 * (PR.P.0.20)
             1  * COREGR * (FINEES(S-1).P.0.80)) * DELCX)
ST1           CONTINUE
              ES(N) = FINEES(MAXS)
              PRINT RESULTS M, ES(N), T(N), COREGR
ST2           CONTINUE
              DELTAU = 6.0*L*R / (MAXN*NU*(CE*ES(MAXN)).P.0.80)
              DELTL = C*NU*CE*ES(MAXN)*MAXN*DELTAU
             1  / (30.0*K*C*R*L)
              TIME = TIME + DELTAU
              THROUGH ST3, FOR N=1,1,N.G.MAXN-1
              T(N) = T(N+1)
ST3           CONTINUE
              T(MAXN) = T(MAXN) + DELTL
              PRINT RESULTS M, TIME, DELTAU, DELTL
ST4           CONTINUE
              TRANSFER TO START
              END OF PROGRAM

 THE FOLLOWING NAMES HAVE OCCURRED ONLY ONCE IN THIS PROGRAM.
 COMPILATION WILL CONTINUE.

MAXM
MODGR
NFL
```

I. Biographical Note

Elisabeth (Mertz) Drake is the daughter of Ruth Johnson Mertz and John Martin Mertz of Tarrytown, New York. She was born in New York City on December 20, 1936, and attended public schools in Mount Vernon, New York. In September 1954 she entered the Massachusetts Institute of Technology where she was President of the Association of Women Students, a member of the Institute Committee, and Chairman of the Freshman Co-ordinating Committee. In June 1958, she was awarded the degree S.B. in Chemical Engineering.

During the next six years, she worked as an engineer in the Cryogenic Process Design Group, Division "500", at Arthur D Little, Inc. in Cambridge, Massachusetts. In June 1964, she returned to the Massachusetts Institute of Technology to begin a program of full-time graduate study. She expects to receive the degree Sc.D. in Chemical Engineering in June 1966.

She was married in 1957 to Alvin William Drake. Her husband is presently an Assistant Professor of Electrical Engineering at M.I.T. and is affiliated with the Operations Research Center there.

She is a member of Sigma Xi, and an associate member of the American Institute of Chemical Engineers and the American Chemical Society.